POLYSACCHARIDE-BASED NANOPARTICLES FOR NUCLEIC ACID DELIVERY

Dissertation

zur Erlangung des Grades

"Doktor der Naturwissenschaften"

im Promotionsfach Pharmazie

am Fachbereich Chemie, Pharmazie und Geowissenschaften

der Johannes Gutenberg-Universität in Mainz

Vorgelegt von

Denise Nadine Bamberger

geboren am 01. Dez. 1986 in Wiesbaden

Mainz im Juli 2016

D77 – Mainzer Dissertation

[redacted]

[redacted]

[redacted]

Datum der mündlichen Prüfung: 26.08.2016

EIDESSTATTLICHE ERKLÄRUNG

Die vorgelegte Dissertation wurde am Institut für Pharmazie und Biochemie der Johannes Gutenberg-Universität in Mainz zur Erlangung des Grades „Doktor der Naturwissenschaften“ angefertigt.

Erstgutachter: [redacted]

Zweitgutachter: [redacted]

Hiermit versichere ich eidesstattlich:

1. Ich habe die jetzt als Dissertation vorgelegte Arbeit selbst angefertigt und alle benutzten Hilfsmittel (Literatur, Apparaturen, Material) in der Arbeit angegeben.
2. Ich habe oder hatte die jetzt als Dissertation vorgelegte Arbeit nicht als Prüfungsarbeit für eine staatliche oder andere wissenschaftliche Prüfung eingereicht.
3. Ich hatte / werde die jetzt als Dissertation vorgelegte Arbeit noch Teile davon bei einer anderen Fakultät bzw. einem anderen Fachbereich als Dissertation eingereicht / einreichen.

Ort, Datum Denise N. Bamberger

"Everything is theoretically impossible, until it is done."

Robert A. Heinlein

“I don't want to believe. I want to know.”

Carl Sagan

DANKSAGUNG

[redacted]

[redacted]

„In jedem Ende liegt ein neuer Anfang."
(Miguel de Unamuno y Yugo)

ABSTRACT

Nanocarriers gained great importance in the medical field since their first definition over 40 years ago. Besides the application as diagnostic markers, nanoparticles can be designed to deliver a wide range of various high potent drugs. The ability to choose between different shapes, sizes, and basic materials forms a huge tool box for scientists to design the perfect nanocarrier for nearly every application. Especially the delivery of nucleic acids requires a safe and highly efficient packaging material due to their sensitivity to plasma nucleases, high manufacturing costs, and their potency to induce unwanted immune responses. Up until now, only a few nucleic acid nano-formulations have entered clinical phases and none is approved by the FDA yet. Most existing nanoparticle systems are complexes of simple cationic lipids and nucleic acids. But these cationic complexes often lack of biocompatibility due to toxic effects in high doses and non-targeted delivery of the active drug. Biodegradable nanoparticles protect the encapsulated nucleic acid from nucleases and can be tuned on the particle surface with targeting moieties or shielding groups to increase the biocompatibility. For systemic delivery, a biocompatible and targeted transport of active agents is required to enhance the therapeutic effect and limit the undesired side effects.

Herein we present the development of a new class of advanced, biocompatible, and acid-sensitive polysaccharide-based nanocarriers for the delivery of siRNA and DNA. The introduction of a hydrophilic PEG layer on the surface of the particles prevents unwanted aggregation under physiological conditions and decreases unspecific cell uptake in different cell lines. The opposite effect can be observed with a parallel performed DEXylation of the particle surface that encourages the nanoparticle uptake by antigen-presenting cells like macrophages and dendritic cells and that can be used as an active targeting agent. First *in vitro* and *in vivo* studies show that the particles are preferred taken up by liver macrophages, so that the possibility for the treatment of liver diseases is opened using dextran-based nanocarriers. PEGylation hinders the particle accumulation in the lungs due to less aggregation and improves the particle biocompatibility. We also introduced targeting moieties on the PEGylated nanoparticles to control their *in vivo* distribution, but further experiments are needed to evaluate the targeted delivery of these nanoparticles.

In addition, we also developed a new lipid dextran-based nanoparticle system using a microfluidic technology. The system features high encapsulation efficiency of siRNA and promising knockdown results. This lipid-dextran nanoparticle system stands out with its quick preparation and low *in vitro* and *in vivo* toxicity. Next experiments will include further targeted transfection trials to improve the selectivity and efficiency of the nanoparticles.

Both developed dextran-based particle systems represent promising candidates for successful *in vivo* applications in the delivery of therapeutic nucleic acids due to high nucleic acid binding capacity and low toxicity. Further studies will focus on targeted delivery of nucleic acids and efficient knockdown *in vivo*.

ZUSAMMENFASSUNG

Seit ihrer ersten Beschreibung vor über 40 Jahren gewinnen Nanopartikel stetig an Bedeutung in der Medizin. Neben ihrer Anwendung in der Diagnostik können Nanopartikel für den Transport von einer Vielzahl an hochpotenten Wirkstoffen konzipiert werden. Verschiedene Formen, Größen und Ausgangsmaterialien bieten Naturwissenschaftlern einen riesigen Baukasten für die Synthese des perfekten Transportsystems für nahezu jede Anwendung. Besonders Nukleinsäuren erfordern ein sicheres und hoch effizientes Verpackungsmaterial, da sie leicht durch Nukleasen abgebaut werden und ihr Wirkpotential auf genetischer Ebene entfalten. Doch bis heute haben nur wenige Nukleinsäure-Nanopartikelformulierungen klinische Phasen erreicht und keine Einzige ist bisher von der FDA zugelassen worden. Die meisten Systeme in der klinischen Forschung sind einfache Komplexe von kationischen Lipiden und anionischen Nukleinsäuren. Durch Toxizität in hohen Konzentrationen und ungerichteten Wirkstofftransport sind diese kationische Komplexe jedoch wenig biokompatibel. Bioabbaubare Nanopartikel hingegen schützen die eingeschlossenen Nukleinsäuren vor Degradation und zeigen erhöhte Bioverträglichkeit durch abschirmende Gruppen oder Targetstrukturen auf der Partikeloberfläche. Für eine systemische Anwendung wird ein bioverträglicher und zielgerichteter Wirkstofftransport vorausgesetzt, um die therapeutische Wirksamkeit zu erhöhen und gleichzeitig unerwünschte Nebenwirkungen zu vermeiden.

Hier wird ein säurelabiles, bioabbaubares und biokompatibles Polysaccharid-basiertes Nanopartikelsystem für den Transport von siRNA und DNA beschrieben. Die hydrophile PEG-Schicht der Nanopartikel verringert Aggregation in wässrigen Medien und vermindert gleichzeitig die unspezifische Aufnahme in diversen Zelllinien. Die Funktionalisierung der Partikeloberfläche mit hydrophilem Dextran hingegen fördert die Aufnahme besonders in Antigen-präsentierenden Zellen wie Makrophagen und Dendritischen Zellen, was für einen zielgerichteten Transport genutzt werden kann. Erste *in vitro* und *in vivo* Experimente zeigten eine bevorzugte Aufnahme Dextran-basierter Nanopartikel von Lebermakrophagen, woraus sich ein therapeutisches Potential der Partikel speziell für Lebererkrankungen ergibt. PEGylierung senkt zudem die Ansammlung der Partikel in der Lunge durch weniger Agglomeratbildung und erhöht somit die Bioverträglichkeit der Partikel. Erste Ergebnisse für die Anbringung von Targetstrukturen an die PEG-Hülle bedürfen weiterer Untersuchungen, um einen zielgerichteten Transport der Partikel zu fördern.

Zusätzlich wurde ein neuer Dextran-basierter Lipidnanopartikel mittels einer Mikrofluidiktechnik formuliert, der hohe siRNA Einschlusseffizienzen und vielversprechende Knockdown-Ergebnisse zeigt. Dieses Lipid-DEX Nanopartikelsystem besticht durch eine einfache Herstellung und geringe Toxizität *in vitro* als auch *in vivo*. Weitere Experimente sollen die Selektivität und Effizienz der Partikel durch den Einsatz von Targetstrukturen verbessern.

Beide hier entwickelten Dextran-basierten Partikelsysteme zeichnen sich durch hohen Nukleinsäureeinschluss und geringe Toxizität aus und sind daher vielversprechende Kandidaten für eine erfolgreiche *in vivo* Anwendung. Nächste Experimente fokussieren sich daher auf einen zielgerichteten Transport und effizienten *in vivo* knockdown.

CONTENTS

1 INTRODUCTION

1.1 Nanoparticles as Delivery Vehicles in Medicine

Micro- and nanoparticles are promising delivery vehicles in the pharmaceutical and medicinal research area. Besides pills, capsules, pellets, suspensions, solutions, and other well established administration forms, nanoparticles gain great advantages in drug safety and effectivity. Encapsulating drugs, biomolecules or genetic material in a particle delivery vehicle protects the drug from degradation and therefore enhances its bioavailability. A particle formulation can help to increase the solubility of a hydrophobic drug which results in an enhanced bioavailability and applicability of the active compound.[1] Furthermore, particles can enhance the pharmacokinetics by prolonging the blood-circulation and the drug release. This increased bioavailability affects the applied dose. If the drug generates more activity in lower doses the side effects and toxicity will be reduced.[2] Depending on the formulation, more effectiveness can be reached by targeted drug delivery and tuning of the type of application. In comparison to microparticles, nanoparticles stand out with better uptake properties due to their smaller size that favors endosomal uptake mechanisms, explained in chapter 1.2.2. This chapter introduces in common particle materials, especially polysaccharides, different particle designs and manufacturing methods for medical applications, in particular for nucleic acid delivery.

1.1.1 Common Materials and Manufacturing Methods for Nanocarriers

General Types of Nanocarriers

In 1994, Kreuter characterized nanocarriers as particles with sizes of 1 nm to 1000 nm.[3] Since the preparation of the first nanoparticles in the late 1960s many different shapes of nanoparticle formulations were developed.[4] **Figure 1** gives an overview of the most common types of nanoparticle formulations used for medical applications.

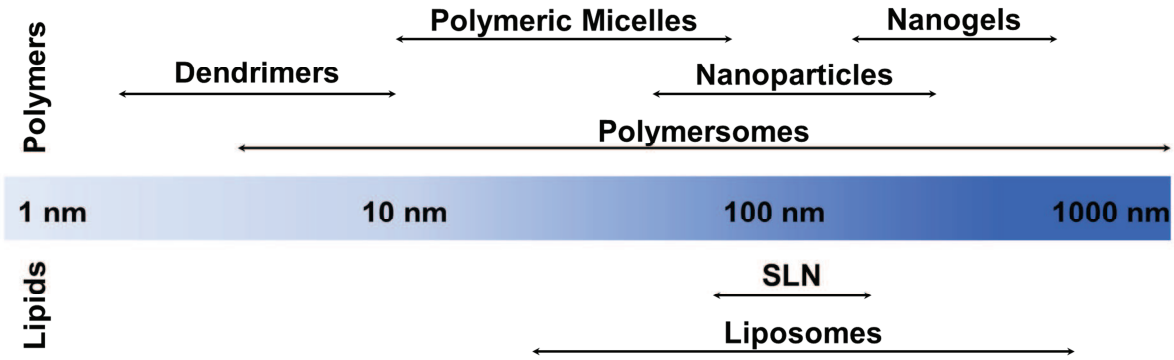

Figure 1: Overview of different nanoparticle shapes and their common sizes (Nicolas *et al.* (2013))[5].

Nanocarriers can be roughly divided into two main basic materials, namely lipids and polymers. Lipid nanoparticles include solid lipid nanoparticles (SLN) and liposomes. Up to

now these two systems present the most efficient carriers for drug delivery *in vitro* and *in vivo*.[6] The best known and FDA-approved liposomal vehicles in the clinic are Doxil®, a doxorubicin liposomal formulation, and AmBisome, an amphotericin B liposomal formulation.[7] Nevertheless, especially cationic lipid formulations can induce systemic toxic effects and the production of pro-inflammatory cytokines which prevents the *in vivo* application of high doses.[8] Furthermore, long-term stability of liposomal formulations indicates some disadvantages including aggregation or bacterial contamination when stored in aqueous buffers. Instead, lyophilization can lead to a destabilizing of the lipid bilayer and leakage of the encapsulated drug. The water-replacement method or addition of high amounts of cryoprotectants can stabilize the liposomes during the freeze-drying process but the methods are time-consuming and the liposomal formulations are mixed with a large proportion of a foreign material. Cryoprotectants can also fuse with liposomal membranes depending on the used concentrations. For example, high mass ratios of trehalose as a cryoprotectant (8:1 cryoprotectant/liposome) are needed to prevent this fusion.[9]

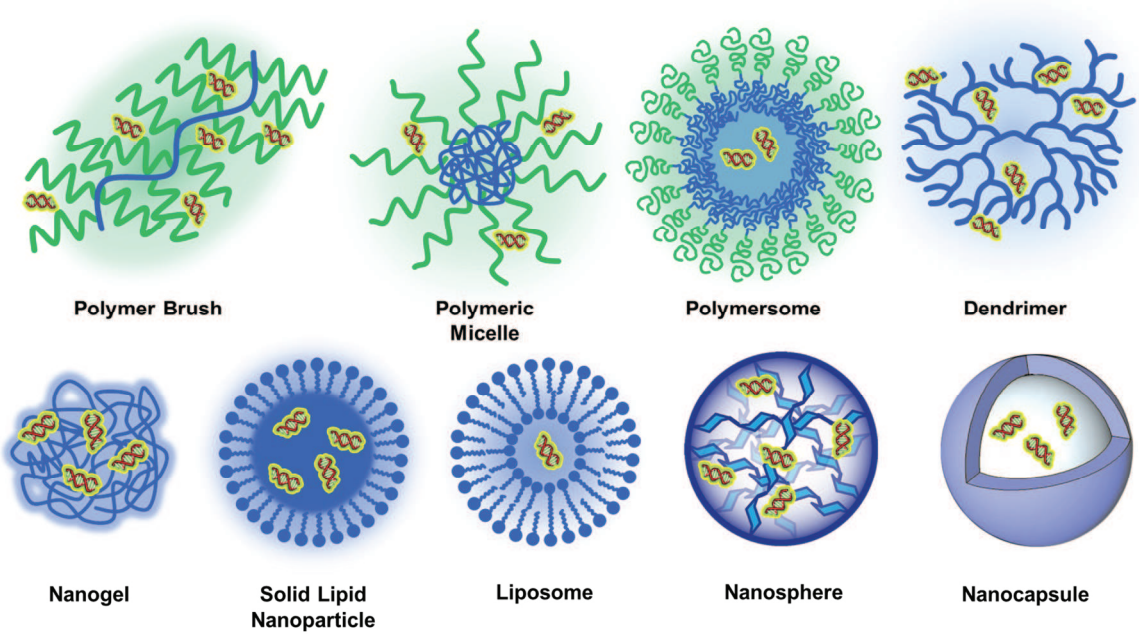

Figure 2: Nanocarrier types for nucleic acid delivery.

Besides lipid formulations, many different polymer particles were investigated to enhance the transfection potential of active drugs. Cationic polymer brushes, polymeric micelles, and dendrimers form polyplexes for example with the negatively charged nucleic acids. Although these formulations can impress with their small and uniform particle sizes, polymersomes, nanogels, and nanoparticles show greater potential in the drug safety.[10-12] In contrast to polyplex formulations where the active compound is attached to the particle surface due to electrostatic interactions, drugs are encapsulated inside of polymersomes, nanogels, and nanoparticles which leads to a shielding of the drug from the external environment. Polymersomes consist of hydrophilic and hydrophobic block copolymers similar to liposomal formulations and form a core-shell structure.[13] Instead, nanogels consist of cross-linked polymers that swell due to their high water-binding capacity.[14] The last group is formed by

solid nanoparticles in which the active drug can be dissolved or dispersed. The class of nanoparticles can be divided into nanospheres and nanocapsules. Nanospheres consist of a matrix-like system in which the active drug is homogenously distributed, whereas nanocapsules consist of a core-shell structure with a cavity in which the drug is dissolved.[15]

The following chapters will primarily focus on nanospheres and their potential for efficient nucleic acid delivery.

Materials for the Preparation of Nanocarriers

In general, drug delivery vehicles can be divided in viral and non-viral carrier systems. Although viral delivery forms are known to be very efficient, they suffer from several disadvantages, including safety risks like severe immune responses and unintended gene transfer as well as limited encapsulation efficiency.[16] Non-viral delivery vehicles can be categorized in non-biodegradable and biodegradable polymers. In medicine, established non-biodegradable materials are poly(methyl methacrylate) (PMMA), polyacrylamide, polystyrene, polyacrylates, and polyethylenimine (PEI).[17] Especially PEI shows high transfection efficiency for genetic materials.[18] Overall, non-biodegradable particles bear several toxicity risks. Due to their non-biodegradability, particles can accumulate in the body which may lead to severe immune reactions. Therefore, these particles need a precise formulation so that they can be cleared by the kidneys or liver after a defined time.[17] A safer method to prevent accumulation of non-biodegradable polymers in the body is the use of biodegradable materials for the preparation of nanoparticles.

Biodegradable polymers can be divided in synthetic compounds, like poly(lactide) (PLA), poly(lactide-co-glycolide) copolymers (PLGA), poly (ε-caprolactone) (PCL), and poly(amino acids), and natural occurring polymers, like polysaccharides and proteins.[19] The next chapter (1.1.2) focusses on the formation of nanocarriers based on polysaccharides which are characterized by great biodegradability and biocompatibility.

1.1.2 Polysaccharides as Material for Nanocarriers

Polysaccharides are constructed from single D-glucose units or other monosaccharides connected via glycosidic bonds. The basic carbohydrate structure can form linear or branched polymer chains with different molecular weights and solubilities. Due to the high number of hydroxyl groups as well as occurring aldehydes, amines, and carboxyl groups, polysaccharides are highly interesting for chemical modification strategies. Furthermore, only low immunogenicity of polysaccharides is described and they are well established in the clinical use for years.[20] Polysaccharides can be obtained by diverse natural resources at low costs including algae (*e.g.* alginate), plants (*e.g.* pectins, cellulose, cyclodextrin), microorganisms (*e.g.* dextran, pullulan), and animals (*e.g.* chitosan, hyaluronan).[21]

Preparation Methods for Polysaccharide-based Nanospheres

The main mechanisms used for the preparation of polysaccharide-based nanospheres include cross-linking, polyelectrolytes, self-assembling, and polysaccharide drug conjugates.

Particles can be formed by covalent cross-linking of the single polysaccharide chains using glutaraldehyde or by ionic cross-linking using charged polysaccharides. Cross-linking with glutaraldehyde showed toxic effects and should be replaced by non-toxic coupling agents like EDC.[22-23] Typical ionic crosslinking agents are tripolyphosphate (TPP) for chitosan particles[24] and Ca^{2+} for alginate particles.[25] A great advantage of the ionic cross-linked particles is pH sensitivity which leads to the disaggregation of the particles in the acidic environment of cells and the release of the entrapped payload.[26] Similar to the ionic cross-linking method are polyelectrolyte complexes (PEC) formed by two opposite charged compounds with high molecular weight. Typical polysaccharide-based PECs consist of cationic chitosan and anionic alginate, dextran-sulfate, heparin, peptides or nucleic acids.[27-28]

When hydrophilic polysaccharides are conjugated to hydrophobic moieties, like fatty acids, cholesterol or hydrophobic drugs, an amphiphilic compound is formed. Certain concentrations of the amphiphilic compound in aqueous buffers lead to the formation of micelle-like structures with a hydrophobic core and hydrophilic corona.[29] These formulations are specifically described with a prolonged circulation time *in vivo*.[15] Polysaccharide-drug conjugates consist of a hydrophilic polysaccharide conjugated via a degradable linker to the hydrophobic active compound. The pro-drug like formulation should be stable in the blood stream and release the active drug at the target site by degradation of the linker moiety.[30]

Two important methods for the preparation of nanoparticles comprise the emulsion evaporation method and the nanoprecipitation. In both methods the hydrophobic polymer is dissolved in an organic solvent. In contrast to nanoprecipitation, the organic solvent is not miscible with water using the solvent evaporation method. Bachelder *et al.* (2008) described an emulsion method for the preparation of acetalated dextran particles.[31] Therefore, the hydrophobic polymer was dissolved in dichloromethane and an aqueous solution of poly(vinyl alcohol) as surfactant was added to perform particles by ultrasonication or mixing. The organic solvent can be removed with a rotary evaporator or by evaporation via stirring of the emulsion. Particles can be obtained then in an aqueous suspension. Purification of the particles is mandatory since the suspension contains high amounts of surfactant.

Nanoprecipitation is often used for the formation of polyplexes consisting of a hydrophobic cationic polymer and a negatively charged siRNA or DNA. The hydrophobic polymer is dissolved in an organic solvent which is miscible with water, like ethanol or acetonitrile. Afterwards, the polymer is added to an aqueous solution by rapidly mixing leading to fine precipitation of the assembled polymer in the water-phase.[32] Disadvantages of the emulsion evaporation methods are often higher polydispersities of the prepared particle samples compared to controllable sizes with the microfluidic mixing systems for nanoprecipitation.[33] Another advantage of the nanoprecipitation is the waiver of surfactants during the preparation process. Similar to the nanoprecipitation is the dialysis method. Therefore, the hydrophobic polymer is dissolved in a water miscible organic solvent and loaded into a dialysis chamber.

The organic solvent is slowly replaced by the outer aqueous phase leading to the assembly and precipitation of polymer particles in the solvent. This method is hardly controllable and can lead to high polydispersity of the particle sample.[34]

Chitosan

Chitosan is a linear polysaccharide consisting of D-glucosamine and *N*-acetyl-D-glucosamine units which are linked via β-(1,4) glycosidic bonds. Chitosan can be obtained by alkaline deacetylation of chitin which can be found in the exoskeletons of crustaceans and the cell walls of fungi. As most of the polysaccharides, chitosan is known to be non-toxic, biodegradable, and biocompatible. Furthermore, wound-healing and anti-ulcer properties are described. Therefore, chitosan has high potential in the medical field as a biocompatible drug carrier.[35]

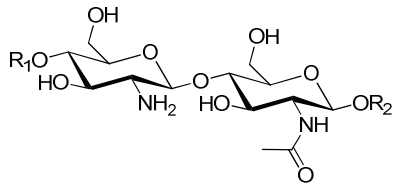

Figure 3: Structure of the polysaccharide chitosan and its building blocks glucosamine and *N*-acetyl-D-glucosamine.

A great disadvantage of chitosan is its limited solubility. Chitosan cannot be dissolved in common organic solvents or aqueous buffers. A preparation of acidic aqueous buffers with a pH lower 6 is the only possibility to dissolve chitosan. Chemical modifications of chitosan are therefore challenging.[36] But the amines of chitosan can be used to form electrostatic complexes with negatively charged siRNA or DNA so that a further introduction of a positive charge is not necessary for this polysaccharide to deliver genetic material.[37] Due to the cationic properties of chitosan, affinities to the negative charged mucus and cell membranes are described.[38]

Corbet *et al.* (2016) described a nano-formulation of PEGylated chitosan particles obtained by ionic gelation. The chitosan particles were loaded with a mixture of two different siRNAs encoding for the lactate transporter MCT1 and the glutamine transporter ASCT2. RGDp, a peptidomimetic arginine-glycine-aspartic acid motif, was introduced as a target structure for $\alpha_v\beta_3$ integrin. This integrin is especially overexpressed on endothelial cells of the tumor vessels and on the surface of some tumor cells. The efficient knockdown of the two transporters MCT1 and ASCT2 was shown *in vitro*. Further *in vivo* studies led to an inhibited tumor growth compared to untreated mice after peritumoral administration of the particles.[39]

Alginate

Alginate is a linear polysaccharide consisting of two different alternating blocks, namely β-(1,4)-D-mannuronic acid and α-L-guluronic acid. The polysaccharide can be obtained from algae, mainly the brown seaweed. Depending on the origin, the molecular weight and the composition of the two blocks in the polysaccharide can differ extremely. This composition

leads to a high swelling property of alginate and usual delivery forms are therefore nanohydrogels obtained by ionic gelation. In contrast to chitosan, alginate contains negative charges but shows also muco-adhesive properties like chitosan.[40-41]

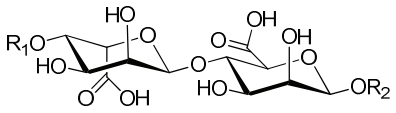

Figure 4: The structure of alginate consists of β-(1,4)-D-mannuronic acid (left) and α-(1,4)-L-guluronic acid (right) building blocks.

Jain *et al.* (2015) showed the successful transfection of a plasmid DNA with alginate nanoparticles in rats. The DNA encoded for the anti-inflammatory cytokine IL-10 and should lead to a re-polarization of macrophages in rheumatoid arthritis. The specificity of the intraperitoneal administered nanoparticles was enhanced by the introduction of a target group for macrophages, the tuftsin peptide. The group showed a reduction in pro-inflammatory cytokines and an improved general condition of the animals after the therapy without the occurrence of toxic side effects.[42]

Dextrin and Amylopectin

Dextrin is a linear polysaccharide consisting of linked α-(1,4)-D-glucose units which can be obtained by partial hydrolysis of starch resembling its characteristics. Dextrin chains are shorter than starch chains and less cross-linked which leads to better solubility and less gelation properties in water. Nonetheless, dextrins are often used for the formation of hydrogels and are also popular among the food industry due to their great biodegradability.[43]

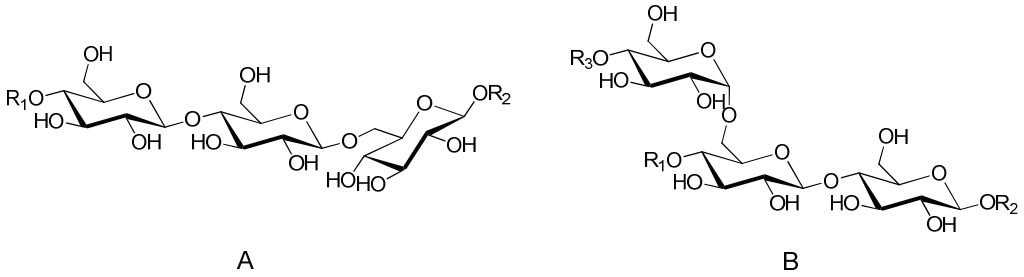

Figure 5: Structures of the polysaccharides dextrin (A) and amylopectin (B).

Manchun *et al.* (2015) reported the preparation of a dextrin nanogel for the delivery of doxorubicin to treat colorectal cancer. The nanogel led to a pH-dependent drug release with less cytotoxicity compared to free doxorubicin *in vitro*. First *in vivo* studies showed inhibited tumor growth in mice after treatment with the doxorubicin-loaded dextrin nanogels.[44]

The polysaccharides amylopectin and amylose form the polysaccharide starch which can be obtained in huge amounts from plants. In normal starches, the amount of amylopectin is around 65%–80%. Amylopectin consists of about 95% α-(1,4)-glucose and 5% α-(1,6)-glucose units with an average molecular weight of 10,000 kDa to 1,000,000 kDa. Due to the rich branching properties amylopectin has a high gelation potential and can be used for the

formation of medicinal gels. Up to now, amylopectin is used as a thickener and stabilizer in the food and pharmaceutical industry.[45-46]

Zhou *et al.* (2012) reported the conjugation of different polyamines to the polysaccharide amylopectin followed by the complexation with a pDNA encoding for eGFP (green fluorescent protein). The complex showed good blood compatibility with low toxicity and first promising results in gene knockdown in 293T and A549 cells.[18]

Hydroxyethyl Starch

Hydroxyethyl starch (HES) is a semi-synthetic polysaccharide which can be obtained from the biological starch by ethoxylation. Due to the amount of contained amylopectin, HES is a branched polymer with linked α-(1,4)- and α-(1,6)-glucose units. The degree of branching can reach from 0.5 to 0.7 depending on the composition of the starch and its molecular weight. HES is used in the clinic for years as a plasma volume expander and known as non-toxic.[20] Nevertheless, several hypersensitivity side effects and kidney injuries in the plasma expander therapy of sick patients led to a precautious use of HES as a plasma substitute.[47-48] Immunogenic effects could not be detected which can be explained by the similarity of the structures of HES and glycogen, the storage form of glucose in humans.[49] The chemical modification of starch resulting in HES led to an improvement in the solubility of the polysaccharide which opens up new functionalization strategies for the formation of new drug carrier systems. Furthermore, the functionalization led to a more stable product in the blood and enhanced *in vivo* circulation since the degradation of HES via amylases is hindered.[50]

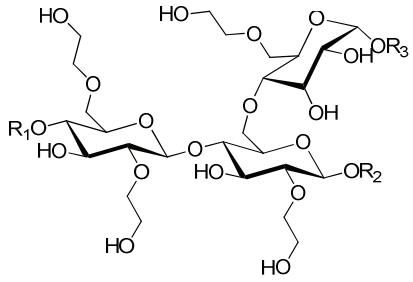

Figure 6: Structure of branched hydroxyethyl starch (HES).

Paleos *et al.* (2015) described carboxylated HES particles encapsulating the anti-cancer drug doxorubicin. Doxorubicin was efficiently delivered *in vitro* to the cytosol of human prostate cancer cells and the cell viability decreased slowly due to controlled release of the drug from the particles.[50] Fichter *et al.* (2013) reported the successful delivery of HES capsules encapsulating dexamethasone to non-parenchymal murine liver cells followed by the reduction of inflammatory cytokines.[51] Successful delivery of siRNA or DNA by pure HES nanoparticles is not described so far. Noga *et al.* (2014) described the formation of polyplexes of a HES-polyethylenimine compound with DNA which promises high delivery efficiency and low toxicity.[52]

Dextran

Dextran is a promising polysaccharide for the formation of nanoparticles since it is known for medical applications as a plasma expander, treating anti-thrombogenesis and haemodilution, or in eye drop formulations in humans for years.[53-55] The synthesis of dextran is mainly based on the transformation of sucrose by the lactic-acid bacteria *Leuconostoc mesenteroides* and *Streptococcus mutans*.[56] Dextran itself is a linear polysaccharide consisting of α-(1,6)-linked glucopyranose units with a normally low degree of (1,3)-branching. The degree of branching depends on the bacteria used for the synthesis of the dextran and is around 5% for the most common dextrans used in the biomedical research.[57] Low branching of dextran results in high water solubility, whereas a (1,3)-branching of about 43% and higher yields in an insoluble dextran polymer. Most commercially available dextrans show a degree of branching of only 0.5%. Depending on the degree of hydrolysis followed by fractionation, dextran is commercially available in low (1 kDa) and high (200 kDa) molecular weights.[58]

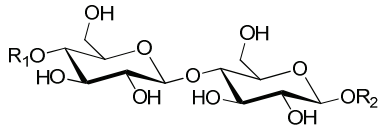

Figure 7: Structure of dextran consisting of α-(1,6)-linked glucopyranose units.

Clinical used dextrans have molecular weights of 40 kDa and 70 kDa and are used as plasma expanders since 1947.[55] Typical concentrations of the applied dextran solutions are 10% for dextran 40 kDa and 6% for dextran 70 kDa with post-operative doses of 750 to 1000 mL.[53, 59] Although dextran is known to be biocompatible and non-toxic, some reports of allergic reactions arose since the 1960s when used as a plasma expander.[60-61] These severe dextran-induced anaphylactic reactions (DIARs) led to bronchospasms, severe hypotension, cardio-respiratory arrest, and in the worst case to death of the treated patients. It is presumed that the main effect is caused by an immune-complex-mediated (type III) anaphylactic reaction where the infused dextran binds to endogenous IgG antibodies and forms big aggregates.[62] The application of Promit®, an infusion of dextran 1 kDa, as a hapten, can reduce the risk of anaphylactic reactions when administered shortly before the use of dextran 40 kDa and 70 kDa.[63] Since the adverse effects occurred all in the first 60 minutes and most of them (approx. 60%) within the first 5 minutes after the start of the infusion, it seems that the reactions are more size dependent and not dose dependent.[64]

The elimination of the parenteral administered dextran from the human organism is also size dependent. Dextrans of lower molecular weights (<40 kDa) have shorter circulation times and are filtered by the kidneys.[65] Whereas dextrans with high molecular weights show longer blood circulation times and are cleared by the mononuclear phagocytic system in the spleen and liver.[66] The risk of an accumulation of dextran in the human body is very low due to the presence of dextranases, α-1-glucosidases, in several different organs like liver, spleen, kidneys, and the lower gastrointestinal tract.[58]

Besides the long tradition of dextran in humans, the polysaccharide is highly interesting for chemical modifications due to the large number of hydroxyl groups in each dextran chain.

Cross-linking of the dextrans leads to a gel that is known as Sephadex and can be used for purification or buffer exchange.[67] Reactive compounds containing carboxylic acids or alcohols can be conjugated to the hydroxyl groups of the dextran leading to the formation of ester or ether linkages. Oxidation of the dextran introduces a new functional group named aldehydes and can also lead to ring opening of the anhydrous glucose units. One single aldehyde is already available for functionalization at each reducing chain end.[68] Moreover, dextran is attractive for chemical modifications because of its high solubility in water and also several common organic solvents, like DMSO and formamide.[69]

De Backer *et al.* (2015) showed the efficient pulmonary delivery of siRNA *in vivo* to murine alveolar macrophages. The group used a cationic nanogel for the delivery based on dextran conjugated to 2-hydroxyethyl methacrylate (HEMA).[70] Afterwards, they loaded the gel with siRNA targeting the protein tyrosine phosphatase receptor type C (CD45) and coated the particles with the pulmonary surfactant Curosurf®. After pulmonary inhalation, they showed an efficient knockdown of the target gene in alveolar macrophages of mice with a siRNA dose of 1 $mg \cdot kg^{-1}$. Only low activation of inflammatory cytokines could be detected but toxicity studies need to be evaluated in further experiments.[71] Tiyaboonchai *et al.* (2007) described a dextran sulfate based nanoparticle system for the encapsulation of amphotericin B. The negative dextran sulfate formed complexes with the positive chitosan which enhanced the encapsulation efficiency of the antifungal agent. The nanoparticle formulation could efficiently reduce nephron-toxicity in mice and is a promising particle system for the encapsulation of sensitive drugs due to its mild preparation technique using polyelectrolyte complexation.[72]

In summary, dextran is proven to be biocompatible and biodegradable so that it seems to be a suitable candidate for the delivery of bioactive compounds in the medical use.[73-74] Immunological side effects were described when high molecular weight dextrans were used in the plasma expander therapy. But the amount and formulation of dextran in the nanoparticle therapy is not comparable to the dextran in the plasma expander formulations. Nevertheless, toxic or immunologic events of particle formulations *in vivo* should be always monitored. The next chapter (1.1.3) describes a hydrophobic acetalated dextran system with promising results for the delivery of small hydrophobic biomolecules as well as hydrophilic siRNA or DNA.

1.1.3 A Hydrophobic Dextran System for Drug Delivery

The group of Jean Fréchet developed a biocompatible, biodegradable, and non-toxic particle system for the encapsulation of small biomolecules, proteins or nucleic acids. The hydrophobic particle material can be obtained by acetalation of dextran (Ac-DEX) which was first described by Bachelder *et al.* in 2008.[31] Due to the acetalation and the chemical switch to a hydrophobic material, the dextran becomes water insoluble but is still soluble in common organic solvents. Therefore, the formation of stable particles in aqueous buffers using a single or double emulsion method is possible. In the first paper, they described the stability of the particles at the physiological pH 7.4, whereas the incubation of the particles in slightly acidic buffers at pH 5 leads to a degradation of the particles. Acidic buffers hydrolyze the acetal linkages so that the original dextran and small, non-toxic amounts of the by-products,

methanol and acetone, are generated.[31] In a following paper, the composition of the acetalated dextran was described more exactly. Broaders *et al.* (2009) showed the time-dependent composition of acyclic and cyclic acetals in the Ac-DEX formulation. With increased reaction time acyclic acetals were transformed to cyclic acetals. A prolonged reaction time enhanced the amount of cyclic acetals but not the total degree of acetalation of the dextran (~80%). The increased ratio of cyclic to acyclic acetals led to a reduced hydrolyzation of Ac-DEX in acidic buffers. An Ac-DEX with a reaction time of 10 minutes was almost totally degraded (90%) after incubation in acidic buffer for 10 hours, whereas only 10% of a 60 minutes Ac-DEX was hydrolyzed after the same time.[75]

As mentioned before in this chapter, particles based on the Ac-DEX material can be prepared by a standard emulsion method. Depending on the preparation method, small hydrophobic biomolecules can be encapsulated with a single emulsion method and hydrophilic compounds with high molecular weights via a double emulsion method. Moreover, the size of the particles during the emulsion process is tunable using sonication methods for nanoparticles (~100–200 nm) and homogenization with an ultra-turrax for microparticles (~4–7 μm).[76] As described in chapter 1.1.2, polysaccharides contain various functional groups that can be further modified. The aldehyde at the reducing end of the polysaccharide chain can be functionalized with alkoxyamine structures leading to stable oxime linkages. Successful labeling of Ac-DEX particles with alkoxyamine fluorescent dyes[76] or with cell penetrating peptides[77] was shown. Regarding the pH sensitivity of Ac-DEX, it is important to mention that modification strategies can only be performed in neutral or slightly basic environment. Moreover, further functionalization of Ac-DEX particles can only be carried out in aqueous buffers due to the dissolving properties of Ac-DEX in organic solvents.

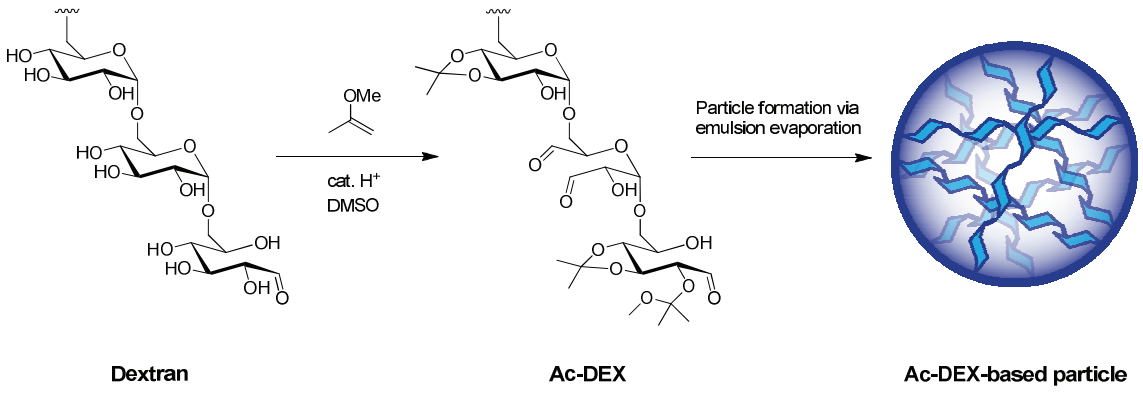

Figure 8: Preparation of an acetalated dextran (Ac-DEX) followed by the formation of particles with an emulsion evaporation method.

Bachelder *et al.* (2008) described the encapsulation of the protein ovalbumin (OVA) in Ac-DEX particles for the first time. The presentation of SIINFEKL, a $CD8^+$ T cell epitope, by MHC class I proteins could be increased after incubation with OVA-Ac-DEX particles in RAW macrophages compared to the effect of free OVA. MHC class I activation is an important tool for possible cancer vaccination by increasing the proliferation of $CD8^+$ T cells.[31] Furthermore, it could be shown that not only MHC class I but also MHC class II presentation could be enhanced by OVA-Ac-DEX particles in murine bone marrow derived

dendritic cells (BMDC).[75] The co-encapsulation of a CpG DNA adjuvant and OVA led to an increased immune reactivity *in vitro* and *in vivo* due to the stimulation and maturation of antigen-presenting cells (APC).[78] An increased Ac-DEX particle uptake in specific cells could be obtained by modification of the particles surface with mannose using biorthogonal click-reactions. Dendritic cells (DC) are known to carry mannose receptors on their surface. The active targeting of these receptors with OVA-loaded mannosylated particles led to enhanced endocytosis of the Ac-DEX particles and enhanced MHC I antigen presentation on the cell surface compared to non-modified particles.[79]

Regarding the stimulation of the immune system, dextran microparticles could be used as a potent delivery vehicle for the Toll-like receptor (TLR) agonist imiquimod. Successful activation of macrophages and BMDCs after the treatment with imiquimod-loaded Ac-DEX particles was shown by measuring activation markers (iNOS and NO) and inflammatory cytokines (IL-1β and IL-6).[80]

The group of Kristy Ainslie focused on the successful delivery of small active biomolecules with single emulsion Ac-DEX microparticles. They showed that incubation of RAW macrophages with rapamycin-loaded Ac-DEX particles, an immunosuppressive drug, led to reduced nitric oxide production and decreased pro-inflammatory response.[81] In further studies they showed that encapsulation of the vaccine adjuvants poly I:C and CpG in Ac-DEX microparticles led to enhanced immune activity in RAW macrophages.[82] First vaccination studies in mice showed promising results to treat infectious diseases caused by bacteria like *Burkholderia pseudomallei*[83] or parasites like *Leishmania donovani*[84].

Ac-DEX nanoparticles prepared by single emulsion encapsulating silver carbene complexes (SCC) were developed by Ornelas-Megiatto *et al.* (2012). Besides small and uniform particle sizes around 140 nm, high encapsulation of the silver carbene complexes (~65%) was obtained. The Ac-DEX-SCC nanoparticles showed promising antibacterial properties against Gram-negative and Gram-positive bacteria with the possibility to be applied *in vivo* as an aerosol.[85]

In first gene delivery studies using the Ac-DEX system, plasmid DNA (pDNA) was successfully encapsulated in Ac-DEX microparticles leading to an increased uptake after labeling the particle surface with cell penetrating peptides.[76] To enhance the encapsulation of pDNA and trigger the endosomal release of the particles, Ac-DEX particles were modified with tertiary amine-containing poly(β-amino ester) polymers (PBAE). Enhanced *in vitro* transfection of the luciferase encoding pDNA could be shown for fast degrading Ac-DEX particles modified with PBAE compared to non-modified particles in RAW macrophages and HeLa cells.[77] Cohen *et al.* (2011) worked on an Ac-DEX-based nanoparticle system for the successful encapsulation of siRNA. For the increase of siRNA encapsulation into the particles, Ac-DEX was functionalized with a polyamine, spermine, before particle preparation (Sp-Ac-DEX). Sp-Ac-DEX showed a high binding capacity (>75%) of encapsulated anti-luciferase siRNA (siLuc*)*. After the incubation of siLuc-loaded Sp-Ac-DEX nanoparticles with HeLa-*luc* cells for 48 hours, a successful knockdown of luciferase (up to 60%) was shown. No cytotoxic effects were detectable after the determination of the cell viability with a MTT assay.[86]

In summary, the Ac-DEX system is a highly tunable particle material for the delivery of active small hydrophobic or huge hydrophilic drugs. High encapsulation efficiencies were obtained for proteins or big pDNAs and also for smaller siRNAs after the functionalization of Ac-DEX with cationic amine groups. A great advantage is the large biocompatibility of the Ac-DEX particles due to their *in vivo* degradation into harmless and biological by-products. *In vitro* experiments showed promising results for example for the treatment of bacterial infections and for the tumor therapy so that further development of the Ac-DEX system for *in vivo* application seems promising.

1.2 Challenges of Drug Delivery

The first chapter describes the different particle formulation strategies and basic materials for drug delivery focused on biodegradable carriers, especially polysaccharide-based carriers. In this chapter, the challenges of drug delivery and the fate of nanoparticles in the human body will be described. An efficient delivery system requires a physically stable formulation which is not easily degradable during storage or right after administration before reaching the target site and shows no self-aggregation of the nanoparticles. The nanocarrier system improves the pharmacokinetic and biodistribution properties of the encapsulated compound, protects it, and reduces its toxicity. Despite many promising characteristics, most nanoparticle formulations still lack of reproducibility with polydisperse particles and varying encapsulation efficiencies and long-term stability. Especially, intravenous administration routes request low contamination and high purity of the nanoparticle formulation. First promising results were obtained after the introduction of targeting groups, prolonging blood circulation, enhancing the encapsulation of the drugs or formation of smaller nanoparticles but none of the existing nanoparticle systems can combine all requirements. Therefore, the need for the development of a perfect nanocarrier which respects the following requirements is urgent.

1.2.1 Administration

Different Routes of Administration

The encapsulated active compound, the location of the target site in the human organism, and the composition of the nanoparticle determine the application route of the nanoparticulary delivery vehicles. Different routes are well investigated for the delivery of pharmaceutical active compounds. In general, dermal, ocular, oral, buccal, nasal, pulmonary, vaginal, rectal, and intravenous application systems are available for drug delivery. Each administration route provides advantages and disadvantages. Many physical and cellular barriers need to be overcome before the entrapped drug reaches its active site. First external barriers, like the skin or mucus, have to be passed with appropriate formulations, like microneedles[87] for dermal delivery or aerosols for pulmonary delivery[88], in which the nanoparticles are included. Up to now, the most common and promising delivery route for nanoparticle delivery is the intravenous administration. Nonetheless, some insight should be given in various possible administration routes.

As mentioned before, microneedle systems can be used to deliver nanoparticles through the skin. The skin is the biggest organ of a human body and consists of four different layers with a total thickness of around 60 to 120 μm. The hydrophobic stratum corneum builds the outer layer and forms the main barrier of the skin. It consists of a crosslinked network of cells and lipids which retards a diffusion of particles. Only compounds with a molecular weight below 500 Da can passively diffuse through this layer.[89] Followed by the stratum corneum, the immunological layer of the skin is formed by the epidermis and dermis which consist of high numbers of phagocytic Langerhans and dendritic cells. The subcutis forms the last layer and

the connection to the systemic route with a widespread network of blood vessels. This complex system of different layers needs chemical enhancers or specific active delivery methods for the particles so that they can cross the membrane and reach the systemic circulation.[90] An advantage of subcutaneously and also intramuscular injections is the formation of a particle-drug depot from where the active compound is slowly released over a longer time and clearance mechanisms like the first pass effect of the liver are prevented until the particles reach the systemic route.[91]

Many administration routes have to deal with mucus which is characterized by a viscoelastic hydrogel. The composition can differ depending on the organ and health status of the patient. The pH of the mucus in the lungs and nose for example is neutral, whereas the eye mucus is slightly basic (pH 7.8) and the vaginal mucus is acidic with a pH of 3.5 to 4.5. Mucus can be found in the gastrointestinal tract (GIT), eyes, nose, rectal or vaginal cavities, and lung airways. Due to sialic acids and sulfate groups of the monosaccharides which are part of the mucus, the mucosal environment is negatively charged and therefore cationic particles can have adhesive properties.[92] Nonetheless, nanoparticle delivery is challenging due to high enzymatic activity and steric hindrance of the viscous network of carbohydrates in the mucus. The addition of mucolytic agents like acetylcysteine can improve the delivery of particles through the mucus. Due to the addition of these mucolytic agents the compact network of mucus can be loosened so that the diffusion of nanoparticles is facilitated.[93]

Oral delivery is very challenging due to rough and changing conditions. The pH varies from 1–3 in the stomach to pH 5–7 in the small intestines and becomes nearly neutral in the large intestines with pH 6–7.5.[94] Especially, the digestive enzymes of the stomach are crucial for the type of the delivery vehicles.[95] Besides the safe transport of the drug by nanoparticles, most drugs have to reach the systemic route to arrive at their target sites. Chitosan was described to be able to loose tight junctions so that small nanoparticles can cross the epithelial barrier paracellular and finally reach the systemic blood stream.[96]

The easiest way to spread the particles in the whole body is the administration of the nanoparticle formulation via direct injection into the blood stream. Up to now, it is the most common way to administer high amounts of nanoparticles, especially in cancer therapy. Intravenously injections request high stability, sterility, and need qualified personnel for the treatment. Nonetheless, barriers like the skin or the mucosa of the GIT need not to be overcome before particles reach the systemic blood vessels. In general, the systemic circulation is not the target area of the particles so that the uptake of the particles by specific cells or organelles is required. Therefore, the particles have to be physically stable in the blood stream and should circulate for a long time to increase the chance of the uptake by the target cells.[97]

Interactions of Nanoparticles with Blood Proteins: The Protein Corona

Since nanoparticles are in the size range of viral or microbial pathogens, defense mechanisms like the mononuclear phagocytic system (MPS) try to clear the particles from the blood stream which is described in detail later. When nanoparticles enter the systemic route they encounter

a medium that contains a high amount of circulating cells, electrolytes, and proteins. The human blood consists mainly of erythrocytes (45%–55%) and lower amounts of leukocytes and thrombocytes (1%). The rest of the blood is filled with proteins, small molecules, and water. Leukocytes are phagocytic cells but need to be activated to be able to recognize nanoparticles.[98] Instead, proteins interact directly and strongly with charged nanoparticles and form a so called protein corona around the particle surface. Depending on the surface charge, hydrophobicity or size of the particles the composition of the protein corona can vary.[99] In general, plasma proteins can be divided into two groups. Opsonins, like the apolipoproteins Apo A-1 and Apo B-100, immunoglobulins or the complement factor C3b, are proteins which mark particles for the MPS so that they are recognized by the immune system and cleared rapidly from the blood stream. Instead, dysopsonins (albumin or clusterin) hide particles from the immune cells and prolong circulation in the blood system which is preferred due to increased uptake of the particles at the target sites.[100-102]

The majority of the plasma proteins consists of albumin, which has a molecular weight of 67 kDa and a long half-life of 19 to 22 days before it is cleared from the blood stream. Albumin owes the long circulation time to the recognition of neonatal Fc receptors (FcRn) which lead to a reabsorption after glomerular filtration and hinders the renal clearance of the protein.[103] A medicinal product Abraxane® uses this mechanism to deliver the cytostatic drug paclitaxel which is bound to albumin.[104] Besides albumin, lipoproteins, apolipoproteins or chylomicrons, macromolecular complexes of lipoproteins, with sizes from 3.5 nm up to 6 μm can interact with the hydrophobic surface of nanoparticles.[105] Whereas albumin forms the biggest population of plasma proteins, lipoproteins represent only 6% of the total plasma protein content.[106] Apolipoproteins which are responsible for the lipid transport can replace other proteins like albumin on the particle surface and therefore mark the particles for elimination by the immune cells and transport to the liver.[107-108] It was shown *in vitro* that nanoparticles labeled with Apo E were taken up by hepatocytes to a higher amount than the unlabeled particles.[109] Whereas a labeling of particles with Apo A-1, Apo B-100, and also Apo E showed an enhanced uptake of the nanoparticles by cells of the central nervous system (CNS).[110]

A third fraction of proteins in the blood is presented by the complement system, which is part of the innate immune system. An activation of the complement system leads to opsonization of the particles followed by the recognition of the particles by the MPS and clearance of the particles from the blood stream by phagocytosis. The activation of the complement system is triggered by high positive or negative charges of the particles and leads to the release of pro-inflammatory cytokines (C3a, C5a) which can induce systemic reactions and adaptive immunity.[111] The adsorption of the immunoglobulins IgM and IgG can also enhance the clearance of particles from the blood circulation.[112]

Challenges for Nanoparticles Entering the Systemic Circulation

Besides the recognition of the particles by the MPS, the particle size is also important to prevent a rapid clearance of the particles and improve their safety. After intravenous injection, all particles are first delivered to the heart and follow the systemic circulation to enter the

pulmonary circulation. From there, particles are delivered via the systemic circulation to the rest of the body.[98] Lung capillaries are the smallest blood vessels with diameters around 2 to 13 μm. Particles which are smaller than 3 μm pass the lung circulation and can directly enter the systemic circulation. Bigger particles with diameters around 3 to 6 μm are first stuck but can be cleared over time from the lung capillaries, whereas particles which are larger than 10 μm are tightly plugged in the small blood vessels and can induce severe dyspnea or heart failure due to insufficient oxygen supply.[113] When particles have entered the systemic circulation they can be eliminated by renal clearance which has a molecular weight cut off of 48 kDa corresponding to a size of around 10 nm. Hepatic clearance of bigger particles is introduced by the recognition of the MPS as described before or by passive diffusion through the fenestrations of the sinusoids with diameters of about 110 nm.[114] Furthermore, particle size is important for the tissue uptake. Blood capillaries have an average size of 5 to 40 μm with pore sizes of around 5 nm. Instead, tumors can have pore sizes in the blood vessels of around 200 nm.[115]

Improvement in Blood Circulation: The Stealth Effect

The adsorption of plasma proteins which normally have sizes bigger than 7 nm and the formation of a protein corona can enhance the hepatic clearance of the particles and the activation of the immune system.[116] This activation can lead to a destabilization of the particles so that the encapsulated cargo is released prematurely before the particles can reach the target sites. Furthermore, the activation of the immune system can induce severe cytotoxic reactions like inflammation or hypersensitivity reactions due to enhanced cytokine production. Since hydrophobicity and surface charge are the main reasons for an activation of the immune system, a cover of the particle surface with a neutral, hydrophilic shell is favored. This hiding of the particles from the immune system with a hydrophilic layer is often called "stealth" effect.[117] The most common compound used for the coating of the particles is poly(ethylene glycol) (PEG). The formation, called PEGylation, leads to a reduced adsorption of plasma proteins and decreased recognition by the MPS so that the blood circulation of the particles can be prolonged.[118] However, in the last years pseudoallergic reactions were observed in clinics due to activation of the complement system by PEG itself and the formation of IgM antibodies against PEG.[119] A further huge drawback of PEG is its lack of biodegradability. Therefore, molecular weights below 20 kDa should be used to favor a renal clearance and avoid accumulation in cell organelles.[120] A further advantage of PEGylation comprises its ability to reduce cytotoxic effects which are normally caused by charged nanoparticles. These cytotoxic effects can occur when phagocytic cells from the liver and spleen interact with particles consisting of a negative surface charge which resembles the characteristics of bacteria and leads to an activation of the immune system.[121] Instead, cationic particles have cytotoxic effects due to interaction with and destabilizing of cell membranes. Therefore, the need of a sufficient, non-toxic, hydrophilic stealth compound is urgent to shield charged nanoparticle surfaces and prevent unspecific protein interactions.[122]

Potential PEG alternatives are the synthetic polymers poly(glutamic acid) (PGA), poly-(hydroxyethyl-L-asparagine (PHEA), and poly(hydroxyethyl-L-glutamine) (PHEG). These

polymers are cleaved into amino acids and can be further metabolized *in vivo*. All of them showed similar increase in the blood circulation times when conjugated to particle surfaces but can induce complement activation as previously described for PEG.[123] Natural alternatives to PEG are polysaccharides like chitosan[124], heparin[125], and dextran[126-127]. Besides well described biocompatibility and biodegradability of polysaccharides in *in vivo* applications, polysaccharides consist of several functional groups which can be used for further functionalization of the particles, like introducing target moieties.[128]

1.2.2 Uptake and Targeting

Uptake Routes for Nanoparticles

After the successful administration of the particles and the improvement of their toxicity and blood circulation via surface decoration, particles have to be taken up by target cells. Particles can be included by passive mechanisms like diffusion through the cell membrane using cell-penetrating peptides or active mechanisms using specific cell surface receptors for the uptake.[129]

Endocytosis describes the invagination of the plasma membrane with extracellular fluid and compounds resulting in the formation of intracellular vesicles. In general, three different mechanisms of endocytosis are described, phagocytosis, micropinocytosis, and receptor-mediated endocytosis (see **Figure 9**). The emerged vesicles are called phagosomes, macro-pinosomes, and endosomes, respectively. These are all mechanisms for the uptake of extracellular material into cells. Exocytosis is the opposite transport mechanism when intra-cellular compounds are encapsulated in exosomes and delivered to the outside of the cells.

Phagocytosis is the uptake of extracellular compounds into the cytosol of macrophages and dendritic cells. The mechanism is part of the innate and adaptive immune system and should remove pathogens from the organism. Phagocytosis is normally activated by the addressing of specific cell surface receptors (opsonization) and leads to phagosomes with sizes up to several micrometers.[130-131]

Instead, macropinocytosis can be found in almost every cell and describes the invagination of huge amounts of extracellular fluid and molecules. The formed vesicles can vary in their diameter and extend to several micrometers (0.5 to 10 μm) in size.[131] In contrast to the receptor-mediated endocytosis pathways, pinocytosis is very unspecific and is responsible for the uptake of apoptotic cell fragments, viruses or bacteria.[132] After entering the cytosol, macropinosomes merge with lysosomes leading to the degradation of the encapsulated material.[133]

Receptor-Mediated Endocytosis

The receptor-mediated endocytosis can be divided in clathrin-mediated endocytosis, caveolae-mediated endocytosis, and clathrin/caveolae-independent endocytosis. Clathrin-mediated endocytosis is the main mechanism for the uptake of small extracellular compounds in intracellular endosomes. These endosomes can fuse with lysosomes or plasma membrane with

the goal to recycle the incorporated compounds. Cationic nanoparticles with an average diameter of 100 nm are preferentially taken up via the clathrin-mediated endocytosis.[134-135] Clathrin-independent endocytosis is described for the uptake of bacterial toxins and cell-surface proteins so that the uptake of anionic particles may be favored by this pathway. The clathrin-independent pathway is also involved in plasma membrane repair mechanisms and intracellular signaling. The occurred early endosomes transform to late endosomes and finally fuse with lysosomes.[136]

Compared to the lysosomal pathways, internalization of proteins via the caveolae-mediated endocytosis leads to neutral caveosomes with sizes of around 60–80 nm which avoid lysosomal fusion processes. Negatively charged particles are preferentially taken up by this pathway and are delivered to the Golgi apparatus or endoplasmic reticulum which are organelles of the signal transduction and are responsible for the metabolism of proteins.[137]

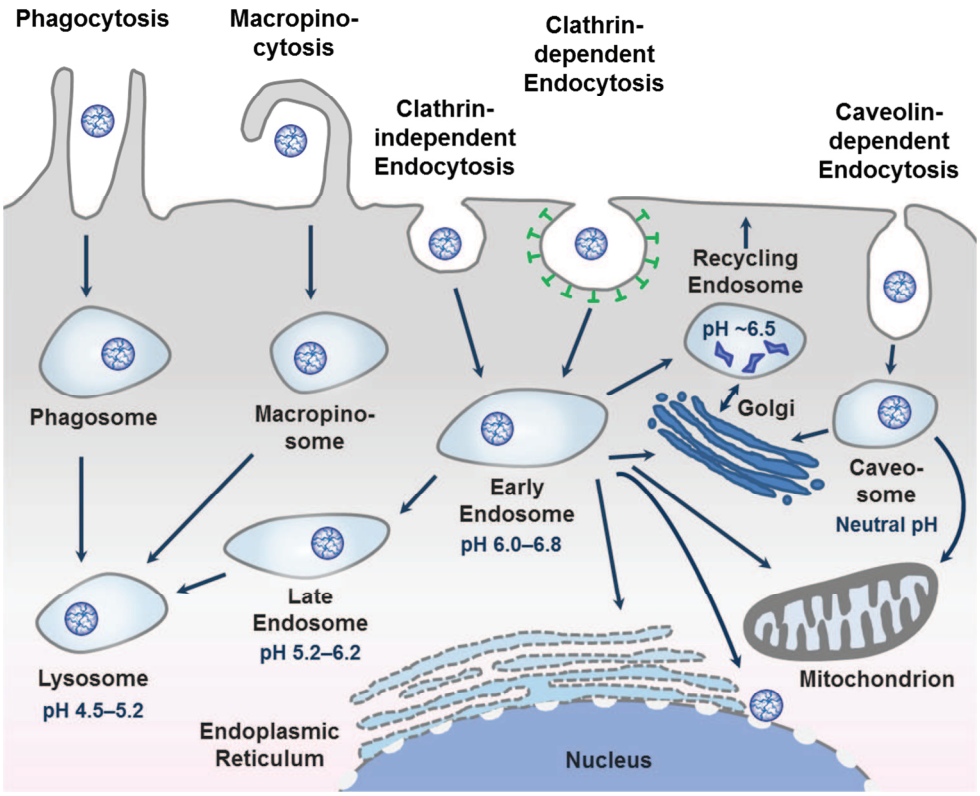

Figure 9: Possible cellular uptake mechanisms for nanoparticles can be divided into phagocytosis, macropinocytosis, and endosomal pathways.[138]

The described endocytic uptake mechanisms can help nanoparticles to cross the cell membrane and reach the inner of the cells where possible target organelles, like mitochondria, lysosomes, intracellular proteins, and the nucleus, are located. Especially for nucleic acid delivery, an efficient transport and uptake of nanoparticles inside the cytosol or cell nucleus is needed. The final destination of siRNA is the cytosol[139], whereas DNA[140] has to be delivered to the inside of the nucleus. Nuclear pores have only sizes of 45–70 nm and nanoparticles can hardly cross their membranes.[141] But passive diffusion of small molecules with diameters of around 9 nm into the nucleus was observed. Larger particles or molecules (>40 kDa or

>39 nm) need active transport mechanisms to reach the nucleus.[140] Another method for targeting the nucleus might work with using the caveolin-mediated endocytosis which avoids lysosomal fusion and delivers the encapsulated compounds to the endoplasmic reticulum (ER) which is located around the nucleus. The active drug can diffuse then from the ER to the inner of the nucleus.[142]

Passive Diffusion via the Enhanced Permeability and Retention Effect

Compared to normal blood vessels, the vasculature of tumor tissue is very leaky and is characterized by a highly increased angiogenesis to supply the strong tumor growth with nutrients. This specific structure of the tumor tissue can be used to deliver nanoparticles passively in size ranges of 20–100 nm to the tumor cells via the enhanced permeability and retention effect (EPR). Due to the increased blood circulation and the leaky vasculature, the accumulation of nanoparticles inside the tumor tissue is enhanced compared to healthy tissue.[143-145] Since this passive delivery is very unspecific and healthy tissue will also be targeted by these nanoparticles specific targeting groups should be added to the nanoparticle surface to specify the final uptake of the particles leading to a higher and faster accumulation of the nanoparticles inside the target cells.

Specific Delivery with Targeting Moieties

Active targeting of tumors is possible due to an overexpression of a variety of receptors on the surface of tumor cells. Most of these receptors are also expressed on healthy cells but only to a minimal amount so that labeled particles will be mainly taken up by cells with high density of receptors on their surface. Specific targeting can decrease the cytotoxicity of highly active drugs in healthy tissue and minimize off-target effects due to selective delivery of the active drug.

Many receptors are known to be overexpressed in tumor tissue. One of the most familiar is the folate receptor which is overexpressed on many ordinary tumor cells like ovarian, lung, brain, and colorectal cancer cells. Folic acid is an essentially needed vitamin and therefore highly biocompatible. Further advantages are high stability and the possibility for chemical modifications so that an activation of the vitamin for the conjugation to the surface of nanoparticles is possible. Another widespread receptor is the transferrin receptor. The function of this cell membrane glycoprotein receptor which is expressed on all cell surfaces is the cellular uptake of iron. In contrast to healthy cells, 100-times higher concentrations of the receptor were found on cancer cells.[146] A cyclodextrin-based PEG-adamantane carrier for the delivery of a functional siRNA with transferrin as a targeting moiety entered phase I clinical trials. The cyclodextrin particles were administered intravenously in melanoma patients and promising results regarding tumor accumulation as well as protein and mRNA repression were obtained.[147] Epidermal growth factor receptors (EGFR, HER1) belong to the family of the tyrosine kinase receptors. These receptors are overexpressed in solid tumor cells which include colorectal, breast, brain, ovarian, pancreatic, and prostate cancer cells. Some small molecules, like the tyrosine kinases erlotinib and lapatinib, and monoclonal antibodies, like cetuximab or panitumumab, are in use for targeting of these receptors.[148] Integrins can be used to target the

transmembrane receptor $\alpha_v\beta_3$ which is overexpressed in endothelial cells during angiogenesis. Targeting of the neonatal Fc-receptor (FcRn) can enhance the uptake of orally delivered nanoparticles by epithelial cells.[149-152]

Besides tumor targeting several other cells or tissues are interesting for a specific delivery of nanoparticles. Uptake in hepatocytes can be enhanced by targeting the asialoglycoprotein receptor (AGPR) which belongs to the C-type lectin superfamily and recognizes carbohydrate structures, especially galactose and *N*-acetylglucosamine.[153] A second receptor which can recognize carbohydrates is the scavenger receptor family on Kupffer cells in the liver and endothelial cells.[154] A further receptor family has great impact in the stimulation of immune cells, namely the mannose receptor family. The mannose receptor (CD206) can be found on macrophages, whereas DEC-205 is mainly expressed on dendritic cells. Both receptors consist of high amounts of cysteine-rich regions which can bind to glycoproteins.[155] Vitamin A is often used to target hepatic stellate (Ito) cells in connection with the treatment of liver fibrosis.[156]

Requirements on the Nanoparticle Design

The character of the nanoparticle surface as well as the nanoparticle stability, aggregation behavior, size, and shape are critical factors for the extent of the uptake and the chosen mechanism described above. The optimal particle size for cell uptake was described between 20 nm and 100 nm. These particles are big enough to avoid the renal clearance and small enough for endosomal uptake mechanisms and to avoid opsonization (>1 μm).[157] Besides the size, the surface charge of particles is a critical factor regarding self-assembling of nanoparticles during storage in buffers, after lyophilization or after *in vivo* administration. Increasing particle sizes due to aggregation or also protein adsorption enhance the accumulation of the particles in small capillaries which are located in the lungs for example. Therefore, the concentration of the particles and the active compounds at the target sites are reduced and less therapeutic outcome is obtained. Especially particles with high cationic surface charges are known for enhanced aggregation behavior which can be prevented by the addition of a hydrophilic surface layer.[158] Furthermore, the hydrophilic surface layer can prevent recognition of the particles by the MPS during systemic circulation and prevents a rapid clearance from the blood stream. The prolonged circulation time of the particles in the blood enhances the uptake by the target cells or tumor tissue due to higher interaction with target receptors or due to the EPR effect which is described previously in this chapter.

Barua *et al.* (2013) studied different shapes of nanoparticles and figured out that small cylindrical nanoparticles showed longer circulation times and higher cellular uptake than spheric nanoparticles.[159] Active targeting requires a multiple activation of receptors on the cell surface.[152] Therefore, flexible shapes of particles that can interact with many adjacent receptors are favored than stiff particles which can only interact with single receptors. This might be challenging regarding *in vivo* use since the chemical designed surface of the particles will be covered by a protein corona directly after administration into the blood stream. If target structures are bound too close to the particle surface, the plasma proteins will prevent an efficient interaction with the target receptors. Due to the change in the surface character,

the particles can be delivered to areas where they normally have no access to. For example, some apolipoproteins are known for their potential to cross the blood brain barrier.[160] But in general the transport of nanoparticles to the brain is not welcome since little is known about the consequences. These non-specific uptake mechanisms are not desired because of non-predictable side effects and toxicities.

1.2.3 Liberation and Elimination

Release of Cargo from Nanoparticles

The chapters 1.2.1 and 1.2.2 described the requirements on the particle characteristics regarding administration and uptake into the targeted tissues, organelles or cells. The next challenge of the particle system is its degradation and release of the entrapped drug. The different environment of tumor cells, inflamed tissues or cell organelles benefits various release mechanisms which can be used to trigger the particle degradation. These mechanisms include pH or temperature responsiveness, reductive or oxidative potential, and enzymatic degradation. Particle responsiveness to the pH is the most common way for a specific degradation of the nanocarriers. Tumor cells are characterized by an increased metabolism which consumes more oxygen than the blood can deliver. Therefore, tumor tissue consists of a hypoxic environment with increased glycolysis leading to acidic metabolic products which decrease the pH of the tissue environment.[146]

After the uptake of the particles by cells, the particles are located in endosomal vesicles. Early endosomes have a slightly acidic pH of 6 to 6.5 and are the sorting organelles. They can fuse with late endosomes which contain small concentrations of hydrolases and introduce first degradation mechanisms. Finally, late endosomes fuse with lysosomes where the pH drops to 5. Lysosomes contain high amounts of enzymes like hydrolases and are responsible for the total degradation and recycling of the encapsulated compounds.[161] Therefore, nanoparticles must escape the endosomes or release their encapsulated cargo to the cytosol before the endosomal vesicles fuse with lysosomes in which the active drug will be degraded and inactivated. The most common mechanism for the endosomal escape is the proton sponge effect. Cationic particles with high buffering capacities will be protonated in slightly acidic environment. Consequently, the influx of protons leads to an increased influx of chloride ions followed by water due to osmotic gradients. The immense penetration of water induces swelling and finally disruption of the endosomal vesicles with a release of the nanoparticles into the cytosol.[162] Ideally, the nanoparticles are degraded in the slightly acidic environment of the endosomes before the disruption so that the entrapped cargo is released. Acetals, ketals, and hydrazones are pH-responsive linkers that can be hydrolyzed easily in slightly acidic buffers.[163] Besides acid-cleavable linkers, pH-responsive polymers consisting of weak acids or bases, like carboxylic acids or amines, can be used to disrupt the particle by swelling of the polymers due to altered pH.[164] Since high concentrations of cationic compounds can induce toxic effects a compromise between endosomal escape and biocompatibility has to be found.[165] A further challenge might occur when cationic particles are coated with a stealth corona so that the protonation in the endosomes to induce the proton sponge effect is not

adequate for the endosomal disruption. The attachment of stealth compounds via acid-labile linkers, like acetals, hydrazones or imines, might be a solution to evade this problem.[163]

Further degradation methods for nanoparticles include the interaction of cationic micelles and liposomes with the negatively charged cell membrane of endosomes followed by a destabilizing and disruption of the vesicles.[166] Fusogenic peptides, like GALA or haemagglutinin, are also known to induce a destabilizing effect of endosomal vesicles and release of the nanoparticles or their degradation products. Viral, bacterial or synthetic peptides are available and can be attached on the particle surface.[167]

An alternative strategy is the attachment of cell penetrating peptides to avoid the entrapment in lysosomal compartments due to direct diffusion of nanoparticles from the extracellular matrix inside the cytosol.[168] A great challenge is then the degradation of particles inside the cytosol to allow the release of the cargo from the particles. One method is the formation of particles by crosslinking techniques using thiol groups to form disulfide bonds. These disulfide bonds can be cleaved by oxidative and reductive active compounds like glutathione which are located in the cytosol. [169]

Disposal and Recycling of Nanoparticles

Besides the efficient delivery of the active compounds to their target sites, the elimination of the drug carrier is essential to avoid undesired side effects like cytotoxicity. A general risk of non-biodegradable particles is the accumulation inside specific organelles which can lead to severe maladies like Alzheimer's disease.[170] The focus here should lie on biodegradable nanomaterials which are disassembled by hydrolysis or enzymatically processes in the lysosomes or cytosol.[171] Afterwards, the obtained monomers, like amino acids, fatty acids or glucose units, can be included in biochemical pathways. By-products like PEG which were used to functionalize the particles and are not biodegradable can be delivered back to the blood circulation via lymphatic circulation.[172] Small non-biodegradable polymers (<10 nm) are then eliminated by renal clearance, whereas bigger polymers are opsonized and metabolized in the liver. Since PEG is non-biodegradable, sizes below 30 kDa should be used to allow renal clearance of the degraded carriers.[173]

Tumor tissue can lead to the degradation of nanoparticles due to acidic pH as well as increased enzyme concentration and activity. Matrix metallo-proteases and cathepsin are known to be enzymes that are overexpressed in tumor environment.[174] Increased oxidative stress in tumor tissue enhances the production of reactive oxygen species (ROS). Hydrogen peroxide, which can also be found in inflamed tissue, results as by-product from the oxidative phosphorylation of the reactive oxygen species and can split ester linkers.[175]

The organs of elimination are the kidneys, liver, and spleen. Some of their functions were described before and will be summarized here. Small molecules are filtered directly by the glomeruli in the kidney when they are smaller than 10 nm or 48 kDa. Bigger molecules (1–3 μm) are opsonized by the MPS and phagocytosed by Kupffer cells which are the macrophages of the liver.[115] Phagosomes start the digestion of encapsulated material by enzymatic cleavage and acidic pH.[130] The liver is the organ with the main metabolism which

takes place in the hepatocytes. Hepatocytes form the main cell population (70%–85%) in the liver and have several functions including degradation of proteins, synthesis of glycogen and lipids, and the excretion of foreign material or cell waste.[176] A second organ for the filtration of pathogens is the spleen. The spleen is a lymphatic organ which is responsible for the storage of red blood cells and the proliferation of lymphocytes which are part of the immune system (B and T cells).[177] Therefore, an enhanced accumulation of nanoparticles in the spleen can induce immunogenic reactions.[178] Some groups observed an increased clearance of particles from the blood after the administration of the second dose. This can be explained by the ABC effect (accelerated blood clearance). After the first administration of particles, B cells are activated and induce a memory effect which leads to the secretion of specific antibodies into the blood. When particles are administered the second time they are opsonized by these antibodies (IgM, IgG) and cleared by the MPS.[179]

1.3 Nucleic Acid Delivery

Over the last few years, the research for personalized medicine grew steadily. Up to now several highly active drugs for the treatment of severe diseases like Alzheimer's disease, Parkinson disease, diabetes, metabolic disorders or cancer conquered the medical market. But they all suffer from dangerous side effects or result in adaptation and ineffectiveness. The greatest disadvantage of all therapeutics, especially to treat cancer, is their non-specificity. Cancer drugs cannot difference between normal healthy and degenerated cancer cells. Personalized and targeted medicine may be a perfect solution to decrease the severe side effects as well as enhance the activity of the pharmaceutical drugs. Therefore, the need for efficient therapeutic carriers is urgent. One new alternative to small molecule therapeutics is nucleic acid therapy which will be described in this chapter.

1.3.1 The Mechanism of RNA Interference

RNA interference (RNAi) was first described by Fire and Mello in the nematode *Caenorhabditis elegans* in 1998.[180] This high efficient cellular mechanism leads to post-transcriptional gene silencing in most eukaryotic cells.[181] In general, RNAi leads to the cleavage or suppression of a target mRNA and the decrease of the associated protein that is related to the disease. Three types of active RNAs are known to be related to the RNAi mechanism, namely micro-RNA (miRNA), short hairpin RNA (shRNA), and small interfering RNA (siRNA).[182]

miRNAs, small (about 22 nucleotides) non-coding, single stranded RNAs, are produced in the nucleus by the enzymes RNA polymerase II and a ribonuclease leading to the formation of a precursor miRNA (pre-miRNA).[183] Afterwards, the pre-miRNA, with a hairpin structure of about 70 to 100 nucleotides, is delivered to the cytosol and processed into small double-stranded duplexes by the RNase Dicer.[184-185] This mature miRNA consists of only 18 to 25 nucleotides and binds after strand separation by the Argonaute protein to an RNA-induced silencing complex (RISC). The activated, mature miRNA in the RISC complex is able to bind the target mRNA.[183] Since miRNAs are non-coding small RNAs the binding of the target mRNA is not totally complementary in the 3' UTR (untranslated region) region so that the binding leads only to a suppression of the mRNA translation and not to its degradation.[186] Affected pathways of this degradation can be found in cell proliferation, differentiation, apoptosis, and cell death.[187] Besides miRNAs, also shRNAs are first processed in the nucleus by polymerases and nucleases followed by the delivery to the cytoplasm where they bind as a single RNA strand to the RISC complex leading to the degradation of a complementary mRNA.[188-189]

The third group of RNAs that bind to the RISC complex and lead to mRNA cleavage are siRNAs. These small (about 19–30 nucleotides) double-stranded RNA molecules can bind directly to the RISC complex in the cytosol. The protein Argonaute 2 (Ago2) in the RISC complex cleaves the double-stranded siRNA and leads to one single, active RNA strand (guide siRNA) which binds the complementary mRNA. The inactive, passenger strand leaves the

RISC complex and is degraded in the cytoplasm of the cell.[190] Ago2 proteins are also responsible for the degradation of the targeted mRNA.[182] The great advantage of artificially designed siRNAs in contrast to shRNAs and miRNAs is their perfect, complementary binding to the target mRNA while miRNAs can have multiple binding sites. Another benefit for the transportation of siRNAs is that they are active in the cytosol of cells and must not be delivered into the nucleus.[139, 191] The siRNA activated RISC complex can repress the translation of the target mRNAs for 3 to 7 days or sometimes up to weeks depending on the cell type and target.[192] Afterwards, the degraded mRNA is transcribed and translated so that the protein causing the disease is present again and the therapeutic effect lasts only for several days before a new dose has to be administered. Nonetheless, siRNA therapy seems to be a promising tool to fight severe diseases. More information about the delivery and current strategies can be found in chapter 1.3.2.

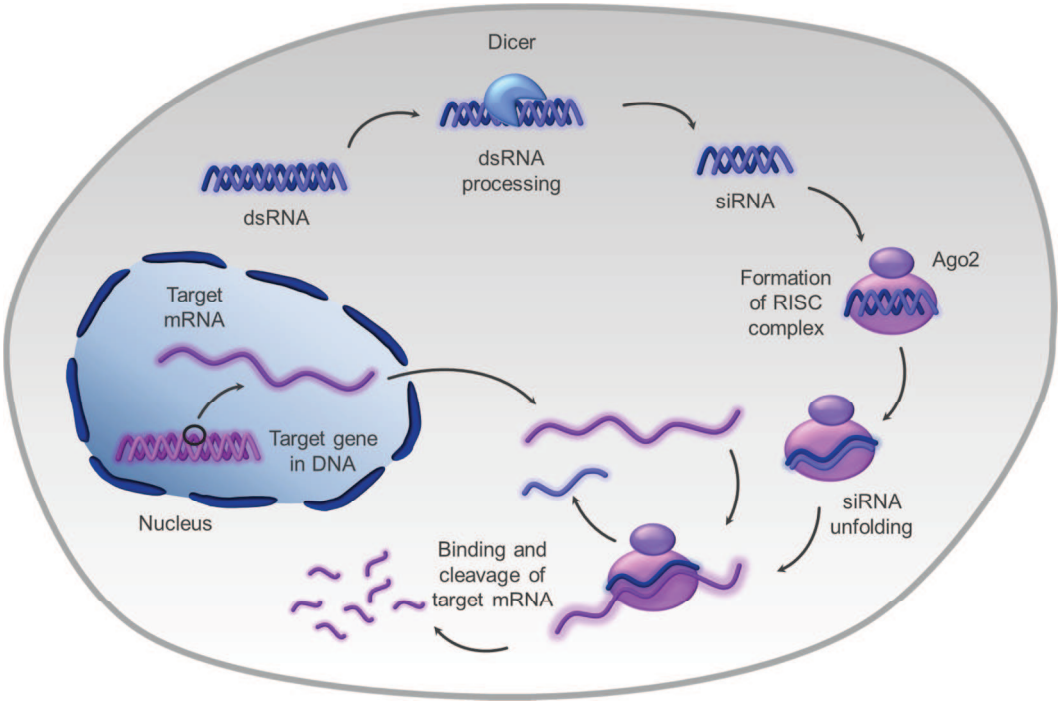

Figure 10: RNAi mechanism adapted from Stevenson *et al.* (2003). The RNase III protein Dicer cleaves long double-stranded RNA (dsRNA) in the cytosol of mammalian cells. The cleavage results in small interfering RNAs (siRNA) which can be synthesized *ex vivo* and applied via delivery vectors into the cells. The activated siRNA forms a complex with the proteins helicase and ribonuclease which build the RNA-induced silencing complex (RISC) together with the Argonaute protein (Ago2). The siRNA is unfolded by the RISC and binds the target mRNA which leads to its degradation.[193]

It should be mentioned that RNAi is a mechanism to control the expression of proteins which are related to severe diseases. The targeted genes are not knocked out or replaced during the therapy but knocked down for a certain time. Further therapeutic approaches using gene delivery can be made by the transfection of DNA which is described in chapter 1.3.3 or with new CRISPR systems. CRISPR stands for "clustered, regularly interspaced, short palindromic repeat system" and can be used for gene therapy together with the protein Cas9. CRISPR

contains a short single RNA strand of about 20 nucleotides which can bind a complementary DNA sequence in the nucleus of eukaryotic cells. After the specific binding of the target DNA, the nuclease Cas9 cleaves the target DNA sequence which leads to the knockout of target genes.[194] Besides gene knockout, CRISPR can be used to repair gene mutations which was shown by Yin *et al.* (2016) using a mouse model with a mutation of fumarylacetoacetate hydrolase in the liver and the delivery of a Cas9 mRNA by lipid nanoparticles.[195] Gene therapy with CRISPR systems shows great potential in successful treatment of diseases but needs further thoroughly investigation.

1.3.2 siRNA Delivery and Knockdown

Administration of siRNA

One big obstacle that has to be overcome for the implementation of siRNA as a therapeutic system is its delivery. In first approaches, siRNA was administered locally to introduce a high concentration of the siRNA at the target site. For example, naked, modified or encapsulated siRNA can be delivered via aerosols to the lungs to cure cancer, pulmonary infections or inflammatory diseases. Nevertheless, the siRNA has to be taken up into the target cells, need to cross mucosal barriers in the lungs, and has to fight the degradation by alveolar macrophages.[196] Furthermore, intratumoral injections can be used to increase the concentration of siRNA at the target site. Disadvantages of this administration route are that only larger, primary tumors can be reached and minimal metastases will be not targeted.[197] Therefore, the systemic application of siRNA should be preferred. The main obstacle of intravenous injection of naked siRNA is its fast degradation by plasma nucleases followed by the clearance via the kidneys. Further, huge siRNA complexes can be recognized by the immune system (MPS) or bound to serum proteins before the final degradation by nucleases.[198-200] Chemical modifications of the siRNA can increase its stability and the plasma circulation due to less degradation by nucleases. Since the modifications should not influence the silencing mechanisms mostly the passenger strand is modified. The addition of unnatural nucleotides at the 5'-end of the passenger strand can increase its stability. Another common modification strategy is the substitution of an oxygen atom by a sulfur atom leading to stable phosphorthioates but lack of toxic side effects.[201] The modification of the 2'-position of the ribose with a methyl group or substitution with a fluor atom also increased the stability against nucleases.[202]

Besides the rapid degradation of naked siRNAs, unmodified siRNAs show only a low uptake by target cells. As described before in chapter 1.2.2, cell membranes are negatively charged which leads to a repulsion of the negatively charged phosphate backbones of the siRNAs. Furthermore, siRNAs are too big to diffuse through the cell membranes or extracellular matrix and need active uptake mechanisms like receptor-mediated endocytosis. The uptake of siRNA can be enhanced by conjugation to a lipid compound like cholesterol.[203] A disadvantage of the endocytic uptake is the fusion of endosomes with lysosomes. The acidic pH and nucleases in the lysosomes lead to a total degradation of the siRNA before it can

reach the active target site in the cytosol. Therefore, endosomal escape mechanisms are needed.[204]

The above described disadvantages of the administration of naked siRNA lead to the development of efficient delivery vehicles like nanoparticles. Nanoparticles can encapsulate the labile siRNA and protect it from degradation by nucleases, enhance the plasma circulation time and increase the uptake in specific target cells. The challenges of these delivery vehicles were described before in chapter 1.2. Lipid-based nanoparticles like liposomes and SNALPs (stable nucleic acid-lipid particles) are the most promising delivery vehicles due to their high knockdown potential (>90%).[205] But also biodegradable, cationic polymers like chitosan or cyclodextrin are used for the efficient delivery of nucleic acids.[206-207] Current nanoparticle delivery systems in clinical development for siRNA delivery are described later in this chapter.

Safety of siRNA Therapy

Advantages of siRNA delivery with efficient carriers are lower costs due to the specific transport of the genetic drugs and the need for less administered material to gain a therapeutic effect. This can be important regarding the toxic effects of pure siRNA, like activation of the immune system or off-target effects. The activation of the innate immune system was first described only for longer (>30 nucleotides) dsRNAs but can be found also in the therapy with smaller double or single stranded RNAs.[208-209] An explanation for siRNAs acting as Toll-like receptor (TLR) agonists may be their original role in fighting viral infections via RNAi mechanisms.[210] TLR3 is known for the recognition of dsRNAs whereas TLR7 and TLR8 recognize ssRNAs.[211] Especially, uridine- and guanosine-enriched regions of siRNAs are known to enhance the production of interferons and inflammatory cytokines which can lead to toxic effects.[199]

The activation of the innate immune system by various siRNA sequences can be one reason for off-target effects which could be observed using non-sense sequences of siRNAs as negative controls. Another reason for off-target events can be explained by the flexibility of the long target mRNA. Although the siRNA binding to the target mRNA is highly specific, off-target effects are often reported. These false positive knockdown results can be explained by mismatch binding of the short siRNA to a long mRNA or wobble pair binding. Wobble pair binding occurs when the long mRNA strand is not stretched but folds itself and a binding to a non-specific siRNA is possible. Mismatching can be avoided by using a second specific siRNA with a different coding to avoid random matches with a non-target mRNA.[191] The potential risks for side effects must be taken into consideration applying siRNAs in medical therapy.

SiRNA Therapeutics in Clinical Trials

Although potent delivery vehicles are still in development, some pharmaceutical companies have worked on successful RNAi therapeutics to start first clinical trials. Acuity Pharmaceuticals started the first clinical trial with siRNA for the treatment of age-related macular degeneration.[212]

Followed by the first clinical trials, Alnylam Pharmaceuticals is one of the leading companies that focus on the treatment of several severe diseases with RNAi therapeutics. Alnylam showed a successful reduction of LDL (low-density lipoprotein) in a phase I clinical study by targeting the pro-protein convertase subtilisin/kexin type 9 (PCSK9) with a lipid particle-based siRNA formulation (ALN-PCSSC).[213-214] Other promising formulations from the Alnylam company target the C5 component of the complement system (ALN-CC5) which is correlated to severe blood disorders like paroxysmal nocturnal hemoglobinuria (PNH) and atypical hemolytic-uremic syndrome (aHUS).[215] First studies showed a safe and well tolerated formulation that led to the start of a phase I clinical trial study.[216] Leading RNAi therapeutics by Alnylam are patisiran and revusiran, two lipid particle formulations that target the liver for the treatment of transthyretin (TTR) amyloidosis (hereditary ATTR amyloidosis). Both therapeutic products are at the moment in phase III clinical trials.[217-218] Besides the genetic medicine for cancer and cardio-metabolic diseases Alnylam also started to develop RNAi vaccine therapeutics for hepatic infectious diseases like hepatitis.[219]

Apeiron Biologics has a running phase I clinical trial study regarding the drug safety, tolerability, and dose with their RNAi vaccine APN401 which targets the E3 ubiquitin ligase Cbl-b. This enzyme plays a fundamental role in blocking the immune system. With the knockdown of Cbl-b the anticancer immune system should be activated to decrease tumor growth of melanoma, kidney or pancreatic cancer.[220] A further promising RNAi therapeutic is TKM-PLK1 from Arbutus Biopharma. This lipid based particle system delivers mRNA to target the polo-like kinase 1 (PLK1) and treat gastrointestinal neuroendocrine tumors, adrenocortical carcinoma, and hepatocellular carcinoma. Phase I and II clinical studies are ongoing.[221]

Promising clinical trials with ASOs (small single stranded antisense oligonucleotides) are reported by Isis Pharmaceuticals. In 2013, their drug mipomersen (Kynamro®) was approved by the FDA. Similar to siRNAs the single strand of mipomersen binds to the complementary mRNA coding for Apo B which leads to the reduction of cholesterol.[222-223] A second promising delivery vehicle was developed in the group of Ugur Sahin using therapeutic RNA-lipoplexes for the targeting of cancer cells. Their liposomal delivery vehicle can be used for vaccination with any specific RNA and is tested in phase I clinical trials at the moment. After intravenous injection, the lipoplex encapsulating a specific mRNA is delivered to the lymphoid organs (spleen) of melanoma patients using the slightly negative charge of the lipoplexes for targeting. In the lymphoid organs, the lipoplexes were taken up by dendritic cells (DC) and macrophages. Thus, the release of IFNα was triggered leading to a maturation of DCs and an inflammatory-related immune response due to T cell priming which was used to fight the cancer cells. The group uses promising vaccination strategies and activation of the immune system in clinical trials to treat cancer.[224]

Targeting Immune Cells with siRNA

As the group of Sahin showed, the immune system plays a fundamental role in the development and treatment of cancer. The primary function of the immune system comprises the recognition and disposal of intruders. The innate immune system consists of phagocytic

cells like macrophages, dendritic cells (DC), natural killer (NK) cells, and neutrophils which present antigens to the cells of the adaptive immune cells in the lymphatic tissue.[225] NK cells can kill tumor cells directly after migration to tumor tissue and recognizing specific receptors on tumor cells. This recognition activates the production of IFNγ which leads to cell death. The adaptive immune system includes immature B and T cells which can be stimulated by antigen-presenting cells (APC). B cells are responsible for the release of specific antibodies, whereas T cells need to bind to major histocompatibility complexes (MHC) for the recognition of antigens.[226-228]

Normally, immature DCs capture pathogenic factors and present them on their surface after maturation releasing interleukins. These interleukins (IL-1β) activate T cells which produce IL-17 leading to the activation of cytotoxic $CD8^+$ T lymphocytes (CTL). CTLs migrate then to tumor tissue due to released chemokines and start to produce interferons (IFNγ) which can directly kill tumor cells.[229-230]

Although the tumor environment consists of inflamed tissue in which immune cells should be accumulated tumor cells developed mechanisms to evade recognition by immune cells. These include the loss of MHC class receptors on the tumor surface so that cytotoxic T cells cannot bind to tumor cells. A second mechanism includes downregulation of the immune system by regulatory cells like myeloid-derived suppressor cells and T regulatory (T_{Reg}) cells which are increased in tumor tissue and prevent the release of IFNγ. Furthermore, macrophages in the tumor environment excessively produce growth factors and immunosuppressive compounds leading to the proliferation of tumor cells.[230-231]

Possible targeting strategies using siRNA in cancer-related tumor therapy include the silencing of immune checkpoints and the activation of Toll-like receptors (TLR) to activate the antitumor response. STAT3 (signal transducer and activator of transcription 3) is a transcription factor acting as an immune checkpoint due to the production of immunosuppressive factors like VEGF, IL-10, and IL-6. These factors inhibit the release of IL-12 and tumor necrosis factor (TNF) which are immune stimulating agents. Therefore, an inhibition of STAT3 can induce an anti-tumor immune response.[232] Toll-like receptors are proteins of the innate immune response and are expressed on the surface of macrophages and DCs. TLR can be targeted directly by the delivery of specific agents like unmethylated CpG oligodeoxynucleotide DNA for TLR-9 leading to an immune response.[231] A further targeting strategy can be the shutdown of $FOXP3^+$ (forkhead box P3) T_{Reg} and myeloid-derived suppressor cells which inhibit the function of CTL.[233]

1.3.3 DNA Transfection

The siRNA activated RISC complex can repress the translation of the target mRNAs for 3 to 7 days or sometimes up to weeks depending on the cell type and target.[192] Afterwards, the degraded mRNA is transcribed and translated so that the protein causing the disease is present again and the therapeutic effect lasts only for several days before a new dose has to be administered.

In contrast to siRNA therapy where the target genes are knocked down or silenced, DNA transfection corrects mutated genes or introduces new genes permanently. A huge challenge of DNA transfection is the efficient transport of the genetic material into the nucleus where the active site is located.[234]

As for RNA therapeutics, the goal of DNA vaccination is to cure severe diseases like cancer or metabolic diseases by replacing or repairing a missing or mutated gene. Two different gene therapies are accessible, germ line or somatic gene therapy. Germ line therapy face many limits regarding safety and ethical problems, since the genes of reproductive cells are affected which leads to the change of the genome of the patient. The most serious problem will be the inheritance of the modified genes to next generations. Therefore, the somatic gene therapy is preferred in which only genes of non-reproductive cells are modified so that the genetic change is limited to the treated patient.[235] A less invasive alternative would be protein therapy where the missing or deformed protein is directly administered. Limitations of this therapy are poor bioavailability due to rapid elimination of the proteins by the kidney or liver or fast degradation by plasma enzymes and opsonization. For a therapeutic effect high doses and multiple injections of the proteins need to be administered leading to enhanced toxic effects. Gene therapy is therefore more efficient, easier and probably cheaper due to less injections than protein therapy.[236]

As mentioned before, the challenge of gene therapy using DNA is its active site and the delivery to the nucleus. DNA is even bigger with several thousand base pairs (up to 1 μm) than siRNA which consists only of about 21 to 23 nucleotides (~7 nm in length) and cannot diffuse through the cell membrane or the nucleic pores.[237] Efficient delivery vehicles are therefore needed which shall also protect the labile DNA from degradation by plasma DNases. First delivery vehicles that were used, and which are up to now the most efficient ones, are viral vectors. The nature of viruses is to include their pathogenic DNA or RNA inside the host genome. Viruses have developed therefore a highly active delivery vehicle which is able to penetrate cell and nucleus membranes and avoid elimination mechanisms like the MPS or renal clearance. The pathogenic gene is replaced by a therapeutic gene so that the infectious character of viruses is not transferred to the viral vectors. Although viral vectors show promising results in gene therapy, huge drawbacks are severe immune responses, high preparation costs and limited amounts of encapsulated DNA. The development of safer and cheaper non-viral vectors is therefore ongoing.[238] Physical delivery methods show great transfection results *in vitro* but their *in vivo* use is limited due to safety reasons or inefficient results. Physical methods induce membrane instability so that the DNA can diffuse inside the cells and nucleus. Well-known methods include electroporation, gene guns, and ultrasound. All methods work well in the cell culture but reach their limits in complex *in vivo* models where the targeted organ or cells lie often deep inside the body and are surrounded by healthy tissue. This may lead to the need of more invasive methods like surgeries.[239] Chemical vectors have several advantages like protection of the DNA from degradation, high encapsulation efficiencies, and better safety due to less invasive application methods. Common vectors are lipo- and polyplexes which form particles with the DNA due to electrostatic interaction between the cationic polymer and negatively charged DNA. Further vehicles are based on

biodegradable polymers and form liposomes, micelles, hydrogels, nanospheres or nanocapsules. The advantages of these delivery vehicles were described earlier in chapter 1.1.[240]

Up to now, none of all gene therapeutics is approved by the American Food and Drug Administration (FDA) but some promising therapeutics reached clinical trials phase II and III. BioCancell completed phase II clinical trials for their DNA drug BC-819 to treat pancreatic and bladder cancer. Phase III clinical trials are currently running. The pDNA consists of a H19 promotor and a Diphtheria toxin sequence. Since the H19 gene is only expressed in tumor cells, the transcription of the Diphtheria toxin is only activated in tumor cells and not in healthy cells which leads to targeted cell death.[241-242] Astellas Pharma also completed phase II clinical trials with their vaccines ASP0113 and VCL-CB01 against CMV (cytomegalovirus). Phase III clinical trials for ASP0113 are ongoing and should be completed in September 2017. The DNA is delivered via a poloxamer CRL1005-benzalkonium chloride which is administered intramuscularly.[243-245] A third vaccination strategy using a PEI-mannose-dextrose complex of DNA (DermaVir/LC002) for the treatment of HIV was developed by Genetic Immunity with ongoing phase II clinical trials.[246-247]

The described examples of DNA therapeutics in clinical trials consist only of simple delivery vehicles or are applied directly as a naked pDNA as it was described for RNA delivery before. Viral vectors can induce strong immune responses so that polymeric carriers gain in importance. Polyplexes and lipoplexes of DNA with cationic polymers showed promising transfection results *in vitro* and *in vivo*. But huge drawbacks are their toxicity and unspecific *in vivo* diffusion so that the complexes have to be administered directly into the target sites by injection. Small or deep areas and metastasized tumors are hard to treat with direct injection so that systemic application with targeted carriers should be favored. Requirements on these nanocarrier systems were described previously in chapter 1.2 and include efficient encapsulation of DNA, targeted delivery, and sufficient release of the DNA at the target site. Since almost all carriers in clinical phases contain very simple delivery vehicles without targeting moieties, the market for the development of safe, complex, and efficient delivery vehicles is great.

2 MOTIVATION AND OBJECTIVES

As described in chapter 1, nanoparticles represent new promising delivery vehicles for high potent drugs compared to the established and FDA approved administration forms like macroscopic capsules, tablets or solutions. Nanoparticles can protect the encapsulated drug from degradation or undesired reactions with plasma proteins which leads to a safe transport of the drug. Moreover, nanoparticles can prevent or reduce unwanted side effects due to specific delivery of the drug to the target organs. Especially nucleic acid delivery applications need high efficient and targeted delivery vehicles since RNA and DNA are easily degradable via plasma nucleases. Furthermore, application systems targeting genes should be handled carefully because of their great potency to interact with the human genome. Specific and targeted delivery is therefore highly desired. Since nucleic acid delivery gains in importance due to its versatile application in miscellaneous diseases the development of efficient delivery vehicles grows constantly. Most promising delivery vehicles, which reached clinical trials due to great transfection potential, comprise adenoviruses or simple lipid-based formulations like liposomes, lipoplexes or SNALPs (stable nucleic acid-lipid particles). However, both systems lack of biocompatibility due to toxicity in higher doses and show unwanted side effects due to non-targeted delivery. Especially viral transfection vectors are known to induce severe undesired immunogenic side reactions. Therefore, there is the need for biocompatible and biodegradable polymers as safe new delivery vectors.

The main goal of this work should comprise the further modification of a dextran-based particle system, initially developed by the Fréchet group, for an efficient nucleic acid delivery *in vivo*. Promising *in vitro* results were obtained for the delivery of small hydrophobic biomolecules, proteins, and DNA with dextran microparticles. The introduction of the cationic polyamine spermine to the basic particle material allowed the formation of nanoparticles encapsulating high amounts of siRNA for the first time which was described by Cohen *et al.* (2011). This spermine-modified acetalated dextran (Sp-Ac-DEX) particle system showed promising *in vitro* knockdown results in HeLa cells with nearly no cytotoxicity and should be therefore used here as the basic particle formulation for further development.[86]

In parallel to the advanced evolution of a more complex and improved dextran-based particle system, the acetalation reaction should be transferred to additional biocompatible polysaccharides followed by the formation of particles using the emulsion evaporation method to obtain smaller and less polydisperse particles with improved biocompatibility or even different *in vitro* and *in vivo* qualities. The prepared polysaccharide particles should be characterized in size, toxicity, encapsulation efficiency, and uptake behavior. Afterwards, the obtained results should be compared to the existing dextran particle formulation and scanned for improved characteristics like higher encapsulation of small biomolecules or better *in vitro* uptake behavior. For example, hydroxyethyl starch (HES) might have stealth properties itself when used as a nanocarrier which was described by Baier *et al.* (2012) before and should be analyzed here.[248]

Since Sp-Ac-DEX particles are highly cationic and can therefore interact with various anionic cell membranes, the first objective should be the introduction of a hydrophilic layer to prevent non-specific reactions of the particles with cell membranes and proteins. After the successful attachment of a hydrophilic stealth layer (described in section 3.2.3), the *in vitro* and *in vivo* behavior of the modified particles should be analyzed in comparison to non-modified particles.

Ideally, the aggregation behavior of the modified particles under physiological conditions is improved due to less interaction between the single particles and less interaction with plasma proteins after systemic administration. Therefore, the change of the particle size should be monitored in protein-free and protein-containing medium to get more information about the different behavior of the particles in complex media before first *in vivo* applications (described in section 3.2.5). When particles enter the systemic circulation, they encounter directly a great number of various plasma proteins including proteins of the MPS. Since the surface characteristics of the particles can be totally changed after the adsorption of proteins the composition and thickness of this protein layer should be analyzed for a predicted behavior of the particles *in vivo* (section 3.2.6).

Furthermore, the shielding of the surface amines should lead to improved biocompatibility due to less cationic surface charges which can induce toxic effects in high concentrations. Therefore, the biocompatibility of the modified particles should be compared first in HeLa cells followed by more sensitive cells obtained from mice and finally *in vivo*.

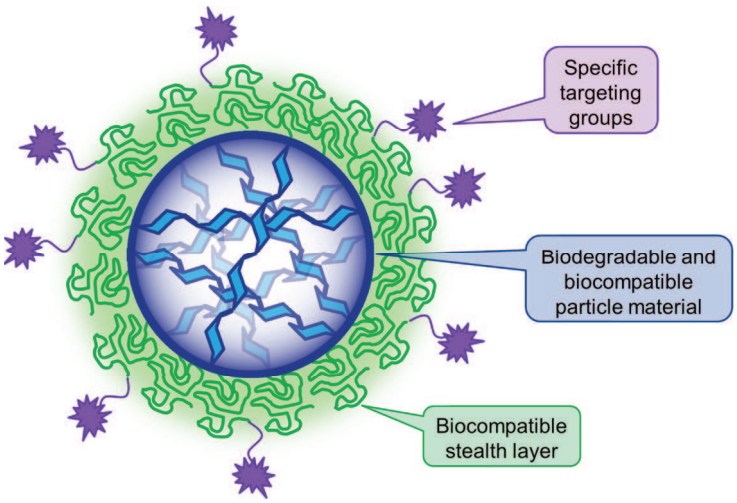

Figure 11: Requirements on the optimal nanocarrier including a basic biocompatible and biodegradable particle material with high encapsulation efficiency of the active compounds, a biocompatible, hydrophilic layer which prolongs systemic circulation, and specific targeting moieties for a focused delivery and high accumulation of the particles at the target site.

The efficient knockdown in HeLa cells described by Cohen *et al.* (2011) required a high particle uptake in the target cells which can be achieved using cationic particles. The shielding of this cationic charge by the hydrophilic layer can reduce the particle uptake into cells. Therefore, the different uptake potential of the modified and non-modified particles should be analyzed in *in vitro* experiments. First *in vivo* biodistribution studies are planned for the

modified particles as well as further *in vivo* uptake studies of the particles after systemic application.

Since non-modified dextran particles show a high unspecific uptake in several cell lines, which was described previously in section 1.1.3, the attachment of specific targeting moieties is planned to focus the particle uptake on target cells or tissues. Here, a targeting strategy should be developed which comprises the attachment of the target moieties on the surface of shielded particles. This targeting strategy will combine the advantages of the hydrophilic particle layer with specific and targeted delivery of the particles (chapter 3.3).

Regarding *in vivo* studies, high amounts of siRNA are needed but the encapsulation efficiency of siRNA in Sp-Ac-DEX particles is limited due to increased aggregation behavior of the particles and rising particle sizes which was described by Cohen *et al.* (2011). Since lipid-based particles are described as highly potent regarding nucleic acid delivery and knockdown effects but often fail in biocompatibility studies due to toxic effects, a new lipid-dextran particle system should be developed. Ideally, the formation of cationic lipids and Sp-Ac-DEX will combine the promising transfection efficiency of cationic lipids with the high encapsulation efficiency of nucleic acids and low toxicity of the Sp-Ac-DEX. *In vitro* knockdown and biocompatibility studies as well as *in vivo* biodistribution of this new lipid-dextran system should be used to describe the improved particle formulation (chapter 3.4).

In summary, the formation of a perfect nanocarrier for the delivery of nucleic acids should be the focus of this work. The main work comprises the improvement and further development of the acetalated dextran particle system described by the Fréchet group. Therefore, all single characteristics which are described in chapter 1 for high efficient delivery vehicles should be combined in one new complex nanoparticle system. This second generation particle system should consist of a biocompatible and biodegradable particle material which shows high encapsulation efficiencies and low toxicity. The encapsulated nucleic acids must be protected from early degradation during the systemic circulation but need to be sufficiently released at the target sites. For this it is planned to attach a biodegradable and hydrophilic layer as well as specific targeting moieties to the nanoparticle surface which should lead to enhanced accumulation of the particles at the target site. The final goal is the development of a complex nanoparticle system for the efficient delivery of nucleic acids consisting of improved biocompatibility, high encapsulation efficiency as well as stealth and targeting properties.

3 RESULTS AND DISCUSSION

3.1 General Aspects of Acetalated Polysaccharides

In this chapter, the acetalation and partial oxidation as well as reductive amination of the different polysaccharides, dextran, hydroxyethyl starch, dextrin, and amylopectin are described. Afterwards, the preparation and characterization of the nanoparticles based on the modified polysaccharides is outlined with the emphasis on advantages of the polysaccharide nanoparticles compared to the already established dextran nanoparticles. Therefore, the particle size and zeta potential were determined as well as the *in vitro* toxicity in HeLa cells. First *in vitro* uptake experiments of the particles will give more information about the differences of the polysaccharide particles. The chapter ends with optimization strategies for the purification and lyophilization of the performed nanoparticles, using dextran-based nanoparticles as an example.

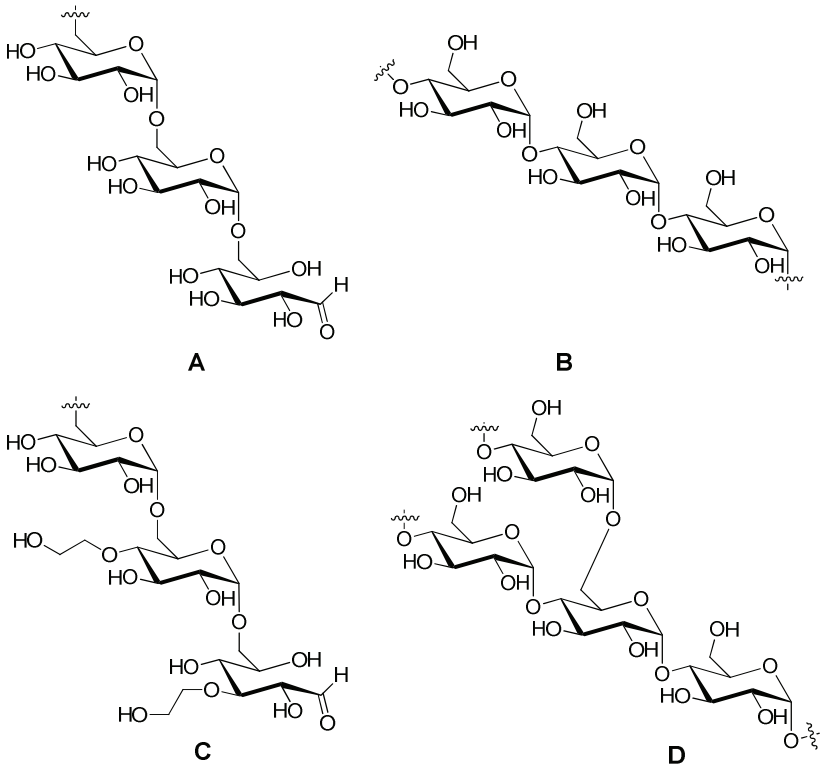

Figure 12: Polysaccharides for the modification with acetals followed by particle preparation; (A) dextran, (B) dextrin (C) hydroxyethyl starch, and (D) amylopectin.

3.1.1 Modification Strategies of Polysaccharides

Acetalation of Polysaccharides

Polysaccharides seem to be optimal starting materials for the preparation of nanoparticles which can be used as carriers in the medical field (as described in chapter 1.1.2). But almost all polysaccharides are well soluble in water. Thus, a preparation of particles made out of natural

polysaccharides, that are stable in aqueous buffers, for storage, and the human blood system, for therapeutic administration, is extremely challenging. A soluble switch, described by Bachelder *et al.* (2008)[31], was used to prepare modified, water-insoluble polysaccharides. Therefore, the polysaccharides were dissolved in dimethyl sulfoxide (DMSO) and 2-methoxypropene was added under acidic catalysis with pyridinium *p*-toluenesulfonate to form acetals using the hydroxyl groups of the polysaccharides. In general, all polysaccharides were incubated with 2-methoxypropene for 10 minutes, unless otherwise noticed, followed by quenching of the acetalation reaction with triethylamine. The modified polysaccharides were precipitated in basic water, purified by centrifugation and rinsing the pellet with basic water until all DMSO was removed followed by freeze-drying of the pure product. After lyophilization, the Ac-polysaccharides were obtained as a colorless powder.

The preparation of acetalated dextran (Ac-DEX), described before elsewhere, was now transferred to the polysaccharides hydroxyethyl starch (HES), dextrin (DIX), and amylopectin (AMY). In contrast to dextran and HES, amylopectin and dextrin were acetalated for 10 minutes or 60 minutes to produce polysaccharides with different hydrolytic stabilities in acidic buffers (described in chapter 1.1.3). The characterization of the obtained hydrophobic Ac-polysaccharides should help to investigate if the acetalation is universal transferable to various polysaccharides with probably new characteristics compared to the acetalated dextran system. The molecular weight of the used polysaccharides is shown in **Table 1**. Hydroxyethyl starch was soluble in DMSO after stirring at room temperature for 30 minutes. In contrast to HES, amylopectin and dextrin had to be dissolved using a sonication bath for a total dissolution in DMSO. Furthermore, the dissolution of amylopectin needs a higher amount of organic solvent to prevent gelation of the polysaccharide.

Table 1: Molecular weights of the modified polysaccharides

Polymer	Molecular Weight
Dextran	10 kDa
Hydroxyethyl starch	70 kDa, 130 kDa, 200 kDa
Amylopectin	*n.a.*
Dextrin	*n.a.*

As described by Broaders *et al.* (2009)[75] longer reaction times of the acetalation with 2-methoxypropene leads to more cyclic than acyclic acetals. This ratio can be important for the stability of the Ac-polysaccharides in aqueous buffers since cyclic acetals are more stable than acyclic. Especially in slightly acidic buffers a higher number of cyclic acetals can lead to a slower degradation of the Ac-polysaccharides. The degree of substitution (DS) of the acetalated polysaccharides was determined by ^{1}H-NMR spectroscopy. Therefore, the Ac-polysaccharides were dissolved in DCl/D_2O according to the method described by Broaders *et al.* (2009).[75] The acidic environment led to the degradation of the Ac-polysaccharides into the original polysaccharides as well as methanol and acetone as by-products of the acetal degradation. Cyclic acetals disintegrated in acetone, whereas acyclic acetals

disintegrated in acetone and methanol. The obtained original polysaccharide backbone, acetone, and methanol peaks of the measured ^{1}H-NMR were integrated and the following formulas were used to calculate the DS.

$$DS(cyclic) = \int 1\,H\ MeOH \div \int 1\,H\ Polysaccharide\ Backbone$$

$$DS(acyclic) = \left[\left(\int 1\,H\ Acetone - \int 1\,H\ MeOH\right) \times 2\right] \div \int 1\,H\ Polysaccharide\ Backbone$$

$$Total\ DS = (DS(cyclic) + DS(acyclic)) \div Number\ Hydroxyl\ Groups\ per\ AGU$$

The molecular weights of dextrin and amylopectin were not indicated by the supplier due to their polydispersity and dextran and HES are also slightly branched. Hence, the DS was related to the anhydrous glucose units (AGU) of the polysaccharides with a molecular weight of 162 g·mol^{-1} for non-modified glucose units.

Table 2: The degree of substitution (DS) of acetalated polysaccharides was determined by ^{1}H-NMR spectroscopy. Approx. 10 mg of acetalated polysaccharide was dissolved in 700 μL D_2O together with one drop DCl to degrade the samples obtaining the original polysaccharide and the by-products acetone and methanol.

Acetalated Polysaccharide	DS (Acyclic Acetals)	DS (Cyclic Acetals)	Total Degree of Substitution	AGU_{new} / g·mol^{-1}
Ac-DEX	0.963	1.196	72.0%	255.4
Ac-HES 70 kDa	1.480	0.330	60.3%	275.3
Ac-HES 130 kDa	1.510	0.130	54.7%	273.4
Ac-HES 200 kDa	1.560	0.430	66.3%	283.0
Ac-AMY 10 min.	1.327	0.755	69.4%	272.8
Ac-AMY 60 min.	1.176	0.320	49.9%	253.2
Ac-DIX 10 min.	1.339	0.304	54.8%	264.6
Ac-DIX 60 min.	0.858	1.239	69.9%	248.7

It is shown in **Table 2** that the highest degree of substitution is obtained with the acetalation of dextran (72.0% of the hydroxyl groups are acetalated). But also the other polysaccharides, Ac-HES, Ac-AMY, and Ac-DIX show a sufficient substitution over 60%. Only Ac-HES 130 kDa, Ac-AMY (60 min.), and Ac-DIX (10 min.) show a lower total degree of substitution. This can be explained by a reduced solubility of the polysaccharides and maybe undissolved or gelation of the starting material. It is remarkable that all acetalated polysaccharides show a higher degree of acyclic than cyclic acetals except Ac-DEX and Ac-DIX (60 min.). Ac-DIX (60 min.) might be an exception but for the other modified polysaccharides it can be explained by their reduced solubility and gelation behavior in DMSO. Furthermore, the DMSO solution of the dissolved dextran was less viscous so that a formation of cyclic acetals might be favored compared to the other polysaccharides.

The formation of particles and their characterization using the acetalated polysaccharides is described in chapter 3.1.2.

Partial Oxidation of Polysaccharides

The above described polysaccharides were partially oxidized with sodium periodate to introduce a second functional group besides the naturally occurring hydroxyl groups. Thus, the oxidized polysaccharides have new opportunities for further modification. Cohen *et al.* (2011)[86] described the synthesis of partially oxidized dextran (ox-DEX) with sodium (meta)periodate. The oxidation of vicinal diols of the anhydrous glucose units (AGU) leads to a ring opening in the polysaccharide chains. This synthesis protocol was now transferred to the oxidation of amylopectin and dextrin without major changes. Due to their poor solubility in water, the mixture of AMY or DIX with water had to be heated up to 50 °C until total dissolution of the polysaccharides. The clear solution was cooled down to room temperature before adding the oxidizing agent sodium (meta)periodate. Otherwise, sodium periodate could disintegrate due to the heat as it was observed in first experiments.

For the oxidation of HES, the amount of sodium periodate had to be reduced so that a following sufficient acetalation and particle preparation were possible. If too many aldehyde groups were introduced by oxidation of HES the oxidized HES would have been hardly soluble in aqueous or organic solvents afterwards. First experiments showed that the ratio of AGU and sodium periodate was responsible for different oxidation grades but not the reaction time (see **Table 3**). Furthermore, it can be shown that HES with different molecular weights but comparable molar masses result in similar oxidation grades during the reaction with sodium periodate.

Table 3: Reaction conditions for the partially oxidation of HES. Shown are the changes in the aldehyde content obtained by modifying reaction times or ratios of the oxidizing agent sodium periodate.

Ratio AGU:$NaIO_4$	Reaction time / h	Aldehyde functions / mol per 100 mol AGUs	M_W HES / kDa
Changing reaction times			
6:1	1	8.2	200
6:1	5	7.4	200
Changing reaction ratios			
1:1	5	23.5	70
6:1	5	8.6	70
1:1	5	26.3	130
6:1	5	9.5	130
1:1	5	25.2	200
6:1	5	9.0	200

It is shown that the degree of oxidation did not change much after one hour of incubation. Nonetheless, the oxidation time of HES was adjusted to the protocol of ox-DEX but the reaction was stopped after 5 hours by adding high amounts of glycerol yielding in ox-HES. The described adaption of oxidizing agent can be seen in the obtained amount of aldehyde

functions. The degree of functionalization was determined by using Roti®-Quant universal (Carl Roth, Germany), a modified PCA assay. In short, this assay kit is a colorimetric reagent that was originally used for the quantification of proteins. As the BCA (bicinchoninic acid) protein assay, the Roti®-Quant universal assay is based on a biuret reaction but further contains a specific colorimetric enhancer reaction. During the biuret reaction copper Cu^{2+}-ions of the Roti®-Quant reagent are reduced to Cu^{+} ions. The intensity of this blue colored complex corresponds to the amount of aldehydes in the sample. To enhance the blue color, a chelate complex is formed between the Cu^{+}-ions and PCA, which ends in a green complex with a strong absorption maximum at 503 nm. Dextran (10 kDa) was used for the calibration and the obtained aldehydes were related to the AGU (M_W 162 g·mol^{-1}) so that a comparison between the different polysaccharides was possible.

The results shown in **Table 4** verify the observations described before that less amounts of used sodium periodate lead to lower yields of aldehydes in the oxidized polysaccharides. Oxidized HES with molecular weights of 130 kDa and 200 kDa had to be reduced with less sodium periodate and less aldehyde functions were obtained (5.4 mol aldehydes per 100 mol AGU). A lower yield of aldehydes for ox-AMY compared to ox-DEX (6.3 mol aldehydes per 100 mol AGUs) can be explained by a more viscous solution and therefore a less reactivity of the hydroxyl groups with sodium (meta)periodate. In contrast to ox-AMY, ox-DIX contains more aldehyde functions (12.4 mol aldehydes per 100 mol AGUs). Maybe the different linkages (α-(1→4) or α-(1→6)) of the AGUs in the dextrin chains facilitated the reaction with sodium periodate and led therefore to a higher amount of aldehydes.

Table 4: Aldehyde content of the partially oxidized polysaccharides and the finally used ratios of sodium periodate compared to AGU (anhydrous glucose unit)

Partially oxidized polysaccharide	Aldehyde functions per 100 mol AGUs	Ratio AGU:$NaIO_4$
Dextran	9.5 mol	6:1
HES 70 kDa	9.1 mol	12:1
HES 130 kDa	5.4 mol	20:1
HES 200 kDa	5.4 mol	20:1
Amylopectin	6.3 mol	6:1
Dextrin	12.4 mol	6:1

It should be noted that the obtained mass yields for ox-DIX were much lower with 59% than for the other oxidized polysaccharides that were obtained with a yield from 70%–90% compared to the initially used polysaccharide. Unfortunately, the provider Sigma-Aldrich gives no information about the chain size and polydispersity of amylopectin and dextrin. Lower yields of ox-DIX can be explained by using a dialysis membrane for the purification with too high MWCO so that small chains were washed out. Nonetheless, the oxidation was transferred to all polysaccharides yielding in partially oxidized compounds.

Acetalation of Partially Oxidized Polysaccharides

The acetalation of the partially oxidized polysaccharides was performed as described in the beginning of this chapter. Compared to ox-DEX, all other used oxidized polysaccharides were less soluble in DMSO so that the amount of solvent had to be enhanced for a total dissolution of the polysaccharides. Furthermore, the reaction time to acetalate ox-HES had to be increased to 2 hours. Otherwise, a sufficient amount of acetals to precipitate a stable product in water was not possible.

As shown in **Table 5**, longer reaction times for the acetalation of ox-HES lead to higher modified Ac-ox-HES (~72%–75%) with an enhanced amount of cyclic acetals compared to Ac-ox-DEX (~66%) which was incubated with the acetalation agents only for 10 minutes. As described previously, longer reaction times result in higher amounts of cyclic than acyclic acetals, as it can be shown for example for the acetalation of ox-AMY and ox-DIX. Therefore, longer reaction times for the acetalation lead to a decrease of the ratio of acyclic to cyclic acetals from 3.69 (10 min.) to 0.81 (60 min.) for Ac-ox-AMY and from 2.63 (10 min.) to 0.89 (60 min.) for Ac-ox-DIX.

Table 5: The degree of substitution of the partially oxidized and acetalated polysaccharides was determined by ^{1}H-NMR spectroscopy. It can be differentiated in acyclic and cyclic acetals (Ac.). The obtained yields of the acetalated polysaccharides are calculated with the new AGU listed below.

Acetalated Polysaccharide	DS (Acyclic Ac.)	DS (Cyclic Ac.)	Total Degree of Substitution	AGU_{new} / g·mol^{-1}	Yield
Ac-ox-DEX	1.25	0.74	66.3%	266.9	87.7%
Ac-ox-HES 70 kDa	1.06	1.10	72.0%	260.4	56.0%
Ac-ox-HES 130 kDa	1.21	0.95	72.0%	268.2	84.8%
Ac-ox-HES 200 kDa	1.11	1.15	75.3%	265.0	75.5%
Ac-ox-AMY 10 min.	1.44	0.39	61.0%	273.6	68.5%
Ac-ox-AMY 60 min.	0.91	1.12	67.7%	250.0	83.4%
Ac-ox-DIX 10 min.	1.29	0.49	59.5%	264.8	92.0%
Ac-ox-DIX 60 min.	1.03	1.16	73.1%	259.5	86.3%

Acetalated partially oxidized polysaccharides gain in weight compared to the initial weight of the oxidized polysaccharides used for the synthesis due to the introduction of acetal groups to the polysaccharide backbone. High yields of about 70% to 90% can be obtained for all modified polysaccharides except for the acetalation of partially oxidized HES 70 kDa. The low yield of the Ac-ox-HES 70 kDa can be explained by the method of purification. After precipitation in basic water the polysaccharides were centrifuged and the pellet washed until nearly all removal of the organic solvent DMSO. Ac-ox-HES 70 kDa was a fine powder and hard to form a solid pellet. The loss of material occurred by removing the supernatant from the pellet. Overall, a successful acetalation of all partially oxidized polysaccharides is described.

Functionalization of Acetalated Polysaccharides with Spermine

The introduced aldehydes can be used to react with primary amines in the formation of imines (Schiff base). Since these imine bonds can easily be hydrolyzed by acids, the reductive amination to an amine bond results in a stable product. Here, the polyamine spermine was used for the further functionalization of the acetalated, partially oxidized polysaccharides. Regarding to the following particle formation with negatively charged nucleic acids, the cationic spermine can help to increase the encapsulation efficiency by forming complexes with these nucleic acids. Furthermore, the primary amine of the unbound end of the spermine can be used for further highly specific reactions, *e.g.* fluorescent dye-labeling using NHS (*N*-hydroxysuccinimide) chemistry.

The Ac-ox-polysaccharides (DEX and HES) were dissolved in DMSO and incubated with spermine overnight to form imine bonds with the aldehydes of the modified polysaccharides. Afterwards, sodium borohydride was added to reduce the imine bond to form more stable amine bonds. The obtained spermine-functionalized, acetalated polysaccharides (Sp-Ac-) were purified by precipitation in water and rinsing the pellet with basic water after centrifugation as described before for the acetalation. The degree of functionalization was determined by measuring the amount of nitrogen atoms by elemental analysis and comparison of this ratio to the amount of spermine (molar mass) per 100 mol AGUs. Due to the lower number of aldehydes of Ac-ox-HES 130 kDa and 200 kDa, the amount of spermine per AGU is also lower compared to Sp-Ac-DEX. The lower degree of functionalization for the smallest HES 70 kDa can be explained by a more viscous solution compared to Ac-ox-DEX and therefore a decreased reactivity of the polysaccharide with spermine. But in summary, the reductive amination with spermine was successfully transferred to Ac-ox-HES. If the synthesis is also transferrable to Ac-ox-AMY and -DIX will have to be studied in further experiments.

Table 6: The amount of spermine per modified polysaccharide was calculated by using the data of the elemental analysis shown below.

Modified Polysaccharide	C	H	N	Amount spermine per 100 mol AGU	AGU_{new} / g·mol^{-1}
Sp-Ac-DEX	54.1%	8.7%	1.5%	7.6 mol	280.9
Sp-Ac-HES 70 kDa	53.0%	8.2%	1.9%	5.4 mol	270.4
Sp-Ac-HES 130 kDa	53.8%	8.8%	1.4%	3.9 mol	275.4
Sp-Ac-HES 200 kDa	53.0%	9.1%	1.4%	4.2 mol	272.8

3.1.2 Preparation of Nanoparticles with Acetalated-Polysaccharides

After the successful functionalization of the polysaccharides with acetals, the formation of particles is possible. Due to the fact that the main focus should lay on the encapsulation of hydrophilic nucleic acids, a double emulsification method described by Cohen *et al.* (2011)[86], adapted for these materials, was used to form nanoparticles (**Figure 13**).

Therefore, the acetalated polysaccharides were dissolved in dichloromethane (DCM) and stored on an ice bath until the end of the particle synthesis. For the first experiments, only empty nanoparticles were prepared and instead of nucleic acids PBS was added to prepare a primary emulsion by sonicating the sample for a few seconds. Afterwards, a high amount of poly(vinyl alcohol) (3% PVA in PBS) was added and a secondary emulsion was prepared by further sonication of the sample. The milky, colorless double emulsion was stirred overnight to evaporate all DCM and an opaque particle solution was obtained the next day. PVA was needed as a surfactant to prepare stable particles but it had to be removed for an efficient application or functionalization. In general, the particles were purified by ultracentrifugation and rinsing with water followed by lyophilization with PVA (0.3% in *dd*-H_2O) as cryo-protectant.

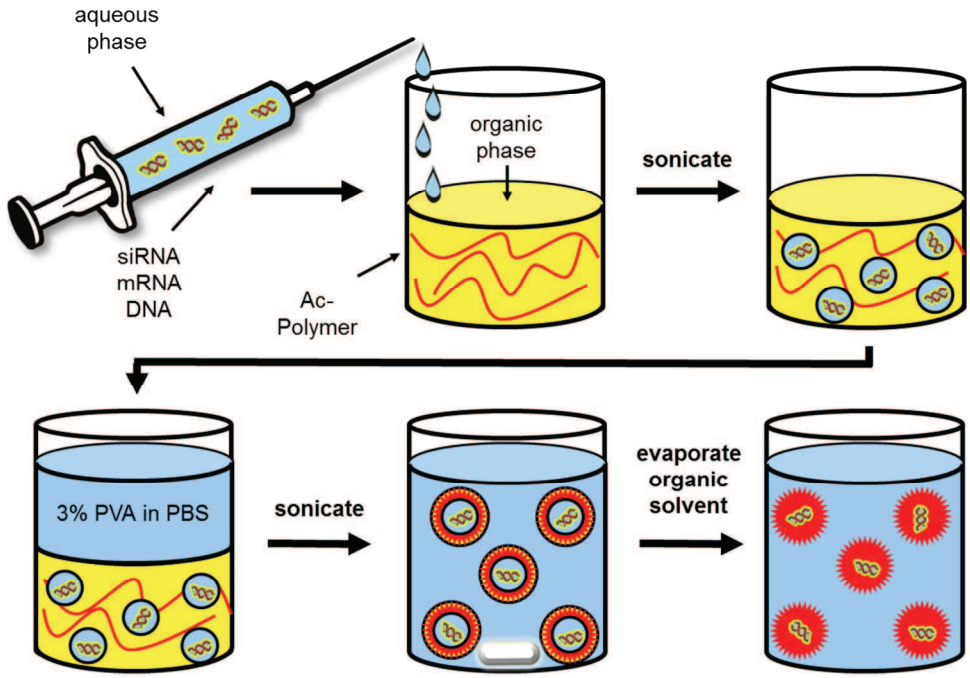

Figure 13: Double emulsion particles are prepared by sonication of the acetalated polysaccharides dissolved in DCM with an aqueous nucleic acid phase. Afterwards, this first emulsion is sonicated with an aqueous solution of poly(vinyl alcohol) (PVA) and a second emulsion is obtained. Particles can be isolated by centrifugation after evaporation of the solvent.

Determination of the Nanoparticle Size and Zeta Potential

In general, the size of the particles was measured at two different time points to characterize the particle size exactly. The first measurement was performed after the evaporation of the solvent DCM before purification of the particles. The second size determination was performed after purification and lyophilization of the particles. Therefore, particles were resuspended and diluted in PBS and treated thoroughly by sonication and vortexing to obtain a homogenous particle suspension without aggregates.

Table 7 shows the sizes of the prepared polysaccharide particles measured by dynamic light scattering (DLS) with a Zetasizer Nano ZS by Malvern. Particle sizes in diameter are described

by the Z-average, number, and PDI. The Z-average describes the mean size of all particles in the sample, whereas the number value describes the mean size of the particles forming the biggest population in the sample. Comparing these two sizes can give a first hint of the polydispersity of the whole particle sample. The third number PDI describes the polydispersity of the sample more exactly. The PDI of 0 normally characterizes a monodisperse particle sample in contrast to the PDI of 1 which characterizes a highly polydisperse sample.

Table 7: Particle sizes and zeta potentials were measured by DLS with a Zetasizer Nano ZS from Malvern. The measurement results of the particles based on the modified polysaccharides before purification (pur.) or after lyophilization (lyo.) are shown below. Z-Average (Z-Av.) is the mean size of all particles in the sample; number is the size of the particles forming the biggest population in the particle sample.

Material	Size before pur.			Size after lyo.			Zeta Potential (mV)
	Z-Av. (d.nm)	Number (d.nm)	PDI	Z-Av. (d.nm)	Number (d.nm)	PDI	
Acetalated Polysaccharides							
Ac-DEX	189.4	139.5	0.108	268.4	142.5	0.238	-2.24 ± 12.1
Ac-HES 70 kDa	200.8	143.9	0.132	276.3	116.6	0.275	-12.1 ± 7.72
Ac-HES 130 kDa	246.2	187.6	0.309	426.8	93.4	0.490	-16.4 ± 6.36
Ac-HES 200 kDa	197.3	139.6	0.170	263.9	197.8	0.156	-3.91 ± 5.82
Ac-AMY 10 min.	320.1	199.2	0.373	318.9	286.8	0.159	-3.60 ± 2.89
Ac-AMY 60 min.	181.3	167.7	0.104	177.6	143.7	0.092	-1.69 ± 3.92
Ac-DIX 10 min.	182.4	139.9	0.144	200.2	126.7	0.220	-6.61 ± 6.01
Ac-DIX 60 min.	201.8	177.6	0.025	214.7	130.2	0.193	-1.98 ± 7.43
Partially Oxidized and Acetalated Polysaccharides							
Ac-ox-DEX	166.1	116.6	0.122	213.7	124.3	0.231	-3.39 ± 4.64
Ac-ox-HES 70 kDa	252.0	235.1	0.869	242.4	199.7	0.167	-4.37 ± 3.66
Ac-ox-HES 130 kDa	295.1	274.2	0.244	216.7	162.3	0.119	-4.61 ± 5.65
Ac-ox-HES 200 kDa	274.3	255.4	0.263	228.4	187.9	0.133	-3.87 ± 3.87
Ac-ox-AMY 10 min.	905.4	306.8	0.759	799.0	266.6	0.739	-12.4 ± 4.64
Ac-ox-AMY 60 min.	602.3	296.4	0.574	1515	295.2	1.000	-3.87 ± 3.66
Ac-ox-DIX 10 min.	168.8	129.9	0.093	191.0	132.2	0.140	-8.3 ± 10.0
Ac-ox-DIX 60 min.	199.0	165.9	0.087	229.9	186.9	0.096	-1.97 ± 5.92
Spermine-functionalized Ac-Polysaccharides							
Sp-Ac-DEX	130.6	69.11	0.200	173.6	74.2	0.267	13.3 ± 7.51
Sp-Ac-HES 70 kDa	219.8	180.3	0.290	263.4	178.2	0.360	0.78 ± 4.22
Sp-Ac-HES 130 kDa	221.9	199.8	0.058	201.5	173.9	0.051	0.85 ± 4.40
Sp-Ac-HES 200 kDa	246.6	233.6	0.076	291.1	228.6	0.231	0.51 ± 4.18

The prepared nanoparticles made out of acetalated polysaccharides are usually characterized by a low polydispersity of around 0.1 to 0.15 and an overall size of about 200 nm before lyo-

philization. The only exceptions are Ac-HES 130 kDa and Ac-AMY (10 min.) with a PDI of about 0.3 and average sizes of 250–300 nm. Longer sonication of the sample might help to form more uniform particles for these materials. The PDI increases slightly after lyophilization which is an indicator for the formation of aggregates during the freeze drying process that cannot easily be separated by resuspension. The PDI ranges from 0.09 for Ac-AMY (60 min.) up to 0.49 for Ac-HES 130 kDa. Furthermore, the formation of aggregates during the freeze drying process can be seen by a slightly increase of the average sizes of the particles (~200–300 nm), whereas the particle sizes described by number is in the same area as for the samples before the lyophilization (~150 nm).

After the partial oxidation and acetalation of the polysaccharides, particles were formed and compared in sizes and zeta potentials. It can be noted that the particle sizes for Ac-ox-DEX and Ac-ox-DIX are in the same area as for the Ac-DEX and Ac-DIX samples with slightly smaller sizes before the lyophilization. Particle sizes for Ac-ox-HES increase up to 250–300 nm before lyophilization but are decreased after lyophilization. This can be explained by the gelation effect of HES. Particles before freeze drying are stirred in aqueous buffers for about 24 hours and can form a huge hydrophilic layer around the particles so that they can swell to bigger sizes. Particle samples measured after lyophilization are prepared right before the measurements and have only about 15 minutes to form a hydrophilic layer. The oxidation and followed acetalation of amylopectin lead to very high particle sizes that cannot be called nanoparticles anymore. A further application of amylopectin for nanocarriers with the double emulsion method like it is described here is therefore not suitable. Ac-ox-AMY can be used for the preparation of microparticles but this has to be proven in further studies. Best results regarding small and uniform particles are obtained for particles based on Ac-ox-DEX and -DIX.

Since HES is described as a stealth compound[249] in the literature it was used for further functionalization with spermine as a potentially stealth particle system. Particles formed by Sp-Ac-HES (~200–300 nm) have about twice the size as Sp-Ac-DEX particles (~130–170 nm). It is remarkable that Sp-Ac-DEX forms much smaller particle sizes (number 70–74 nm) compared to Ac-DEX (~140 nm) or Ac-ox-DEX (120 nm). The introduction of the polyamine spermine helps to form more compact and therefore smaller particles. This can be explained by the smaller molecular weight and no gelation potential of spermine compared to the polysaccharides. Overall, particles with diameters of around 100–200 nm were formed. Amylopectin can be used only in an acetalated formulation for the preparation of nanoparticles, whereas partially oxidation leads to microparticles.

The composition of the particle surface has a high impact on the particle behavior *in vivo* and in cell uptake processes as described before in detail in section 1.2.2. The particle charge determined by the zeta potential can give some additional information to predict the particle behavior *in vitro* and *in vivo*. Due to the negatively charged cell membrane, cationic particles probably have a higher affinity to interact with the cell membrane than negatively charged particles. This affinity can then lead to enhanced cell uptake of the particles. In summary, all acetalated and partially oxidized and acetalated polysaccharides have a slightly negative zeta

potential when measured in HEPES buffer pH 7.4 (25 mM). Due to the fluctuation of the measurements and the sporadically higher standard deviations no differences were observed between the modified polysaccharides. In contrast to these particle formulations the Sp-Ac-DEX particles increase in their zeta potential due to the introduction of amines that can be protonated. Here, a difference between dextran and HES can be described. Whereas the zeta potential increases up to ~13 mV for Sp-Ac-DEX particles, the zeta potential of all three different Sp-Ac-HES particle formulations stays neutral (~0.5–0.8 mV). These differences in the net charge and particle sizes might have an impact on the uptake of the Sp-Ac-HES particles in contrast to Sp-Ac-DEX particles which is determined later in this section.

In Vitro Toxicity of Polysaccharide-based Nanoparticles in HeLa Cells

Before particles can be used as a therapeutic delivery vehicle, their biocompatibility must be proven. Therefore, the particles were incubated with HeLa cells, a cervical carcinoma cell line, and the cell viability was determined by using the MTT assay.[250]

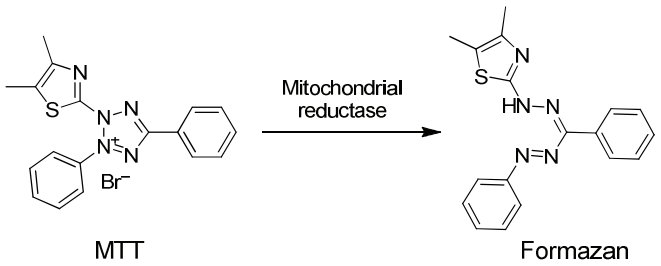

Figure 14: Reduction of a water soluble MTT salt to a purple, water insoluble formazan by mitochondrial reductases of HeLa cells.

MTT (3-(4,5-dimethylthiazol-2-yl)-2,5-diphenyltetrazolium bromide), is a bright yellow, water soluble salt, that can be reduced by cellular oxidoreductase enzymes. The reduction of MTT leads then to a water insoluble purple formazan compound that can be quantified by absorbance measurements (**Figure 14**). The amount of reduced MTT depends on the activity of the metabolism of the HeLa cells and correlates with the number of living cells. If particles are toxic, the cell viability of the HeLas will decline due to a decreased number of cells per well (cell death) or a decreased metabolism of the cells under toxic conditions.

Therefore, HeLa cells were incubated with particle concentrations up to 1 mg·mL^{-1} for 48 hours before the MTT assay was performed (described in detail in section 5.3.10). The obtained cell viabilities were compared to HeLa cells containing no particle samples. As shown in **Figure 15**, there is no change in the cell viability of HeLa cells detectable after incubation with the modified polysaccharide particles made out of dextran, amylopectin, and dextrin. Slightly higher viabilities than 100% can be explained by the use of the polysaccharides as an additional food and energy source for the HeLa cells that leads to an increased growth.

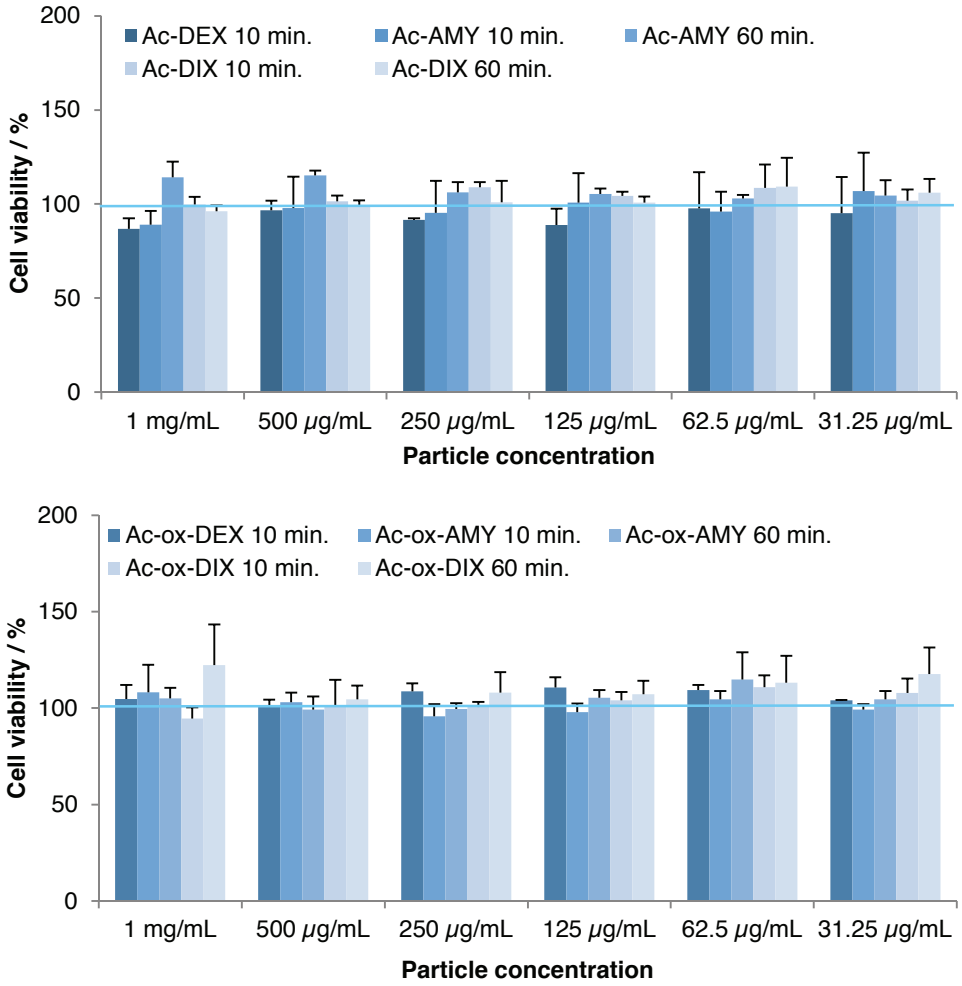

Figure 15: Shown are the cell viabilities of HeLa cells determined after the incubation with different concentrations of acetalated (upper image) or partially oxidized and acetalated polysaccharide nanoparticles (lower image).

Figure 16 shows the results of the MTT assay comparing Ac-DEX and Ac-HES as well as Sp-Ac-DEX and Sp-Ac-HES nanoparticles. As it was shown in **Figure 15** before, incubation with acetalated polysaccharide particles shows no change in the cell viability of HeLa cells and the polysaccharide nanoparticles can be therefore called as non-toxic regarding the first experiments. Instead, the introduction of spermine leads to decreased cell viability for high particle concentrations (~50%–80% viability for 1 mg·mL^{-1} samples). Particle concentrations of 250 µg·mL^{-1} and lower concentrations show no change in the cell viability and are comparable to polysaccharide modifications without spermine. Cationic polymers are known for their possibility to show toxic effects already in *in vitro* experiments.[251] But since all particle formulations still show cell viabilities of around 100%, further cell studies and *in vitro* use should be possible using lower particle concentrations. All functionalized polysaccharides, dextran, amylopectin, dextrin or HES, seem to be suitable regarding the toxicity for further particle formulations with the final goal of *in vivo* applications.

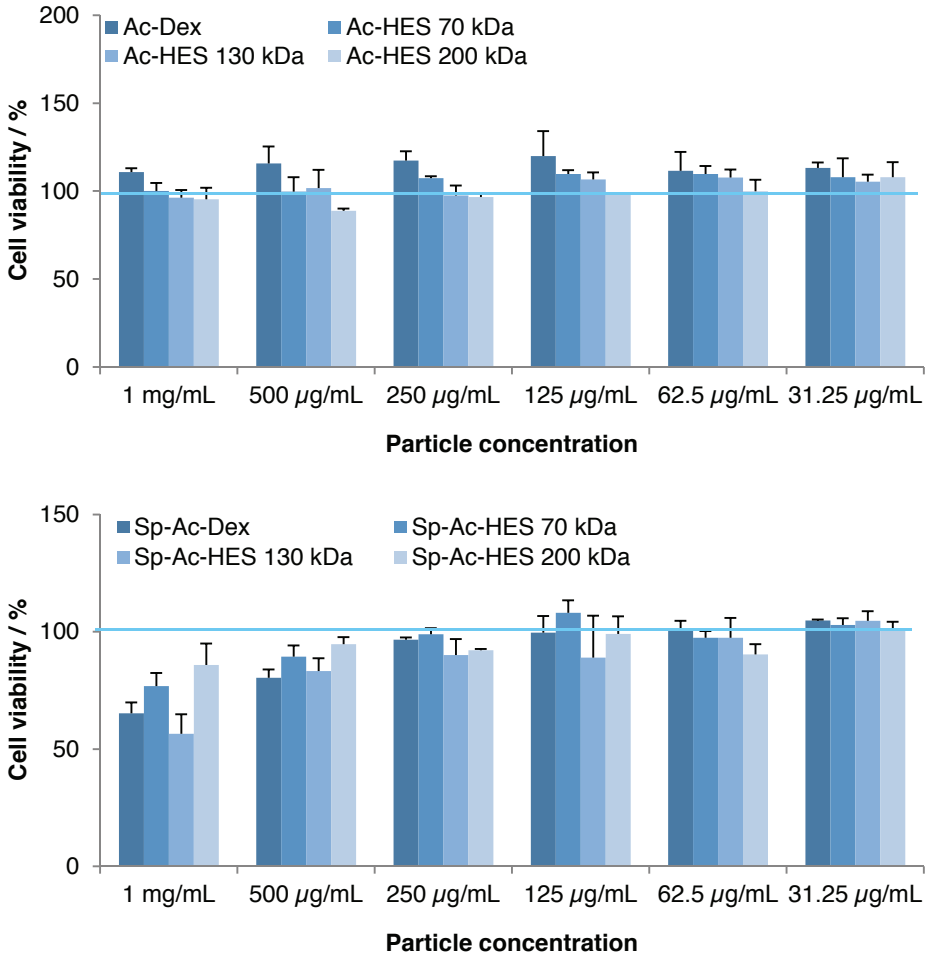

Figure 16: Shown are the cell viabilities of HeLa cells determined after the incubation with different concentrations of acetalated (upper image) or spermine-functionalized and acetalated HES nanoparticles (lower image) compared with the modified dextran nanoparticles.

Encapsulation of Dextran-Oregon Green® 488 in Dextran and HES Nanoparticles

The promising results regarding different particle sizes, zeta potentials, and high cell viabilities led to first encapsulation studies comparing DEX and HES particles. Therefore, a negatively charged dextran (10 kDa) labeled with Oregon Green® 488 (dex-OG488), which is commercially available, was encapsulated in the particles by a double emulsion method as described in the beginning of this chapter. Dex-OG488 was chosen since its size and charge are comparable to siRNA but less expensive than siRNA for the first experiments. The encapsulation efficiency was determined by dissolving the particles in acetate buffer at pH 5 overnight. The emission of the encapsulated dex-OG488 was then correlated to a standard curve prepared with the dissolved pure dex-OG488. Particles were dissolved to avoid quenching effects that can occur when a fluorescent dye is encapsulated in a particle system or is located close to other fluorescent dyes.[252]

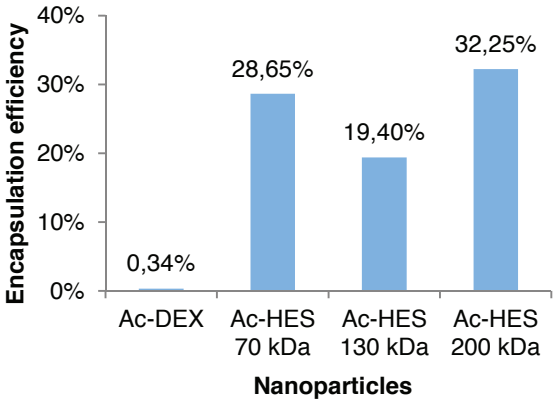

Figure 17: Shown is the encapsulation efficiency of dextran-Oregon Green® 488 in acetalated DEX and HES nanoparticles determined by fluorescence measurements.

As shown in **Figure 17**, there is a huge difference in the encapsulation efficiency of dex-OG488 between Ac-DEX and Ac-HES particles. The measured zeta potential of the acetalated polysaccharide particles was negative. It can therefore be presumed that an encapsulation of a small negatively charged compound might not be efficient using acetalated polysaccharides. This is shown by a very low encapsulation efficiency of around 0.3% dex-OG488 in Ac-DEX particles, whereas Ac-HES particles show relatively good encapsulation efficiencies of around 20% to 30%. HES tends to form viscous solutions and has a gelation effect when dissolved in water. This gelation effect of HES in the particle formulation can help to increase the encapsulation of the negative dex-OG488.

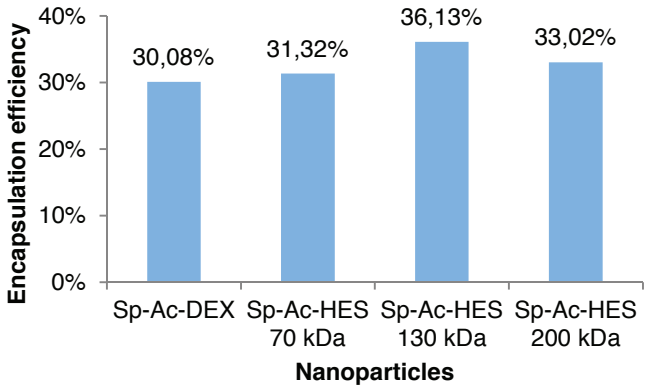

Figure 18: Shown is the encapsulation efficiency of dextran-Oregon Green® 488 in acetalated and spermine-functionalized DEX and HES nanoparticles determined by fluorescence measurements.

Cationic polysaccharides, which were obtained after functionalization with spermine, show relatively high encapsulation efficiencies of dex-OG488 of about 30%. Especially for the spermine-modified dextran, the cationic charge has a huge impact regarding the encapsulation efficiency compared to the Ac-DEX particles. This effect is likely based on electrostatic interactions between the cationic spermine chains of the polysaccharides and the anionic dex-OG488. In contrast to the negatively charged acetalated dextran that might introduce a repulsion of dex-OG488, the cationic parts of Sp-Ac-DEX help to increase the encapsulation. In this case no differences between Sp-Ac-DEX and Sp-Ac-HES are detectable regarding the

encapsulation efficiency. Furthermore, there is no effect of the different molecular weights of HES detectable in both experiments.

Therefore, Ac-HES particles might be promising delivery vehicles for small and negatively charged compounds when cationic spermine chains for further functionalization are not needed or not wanted due to toxic effects when used in high particle concentrations.

In Vitro Uptake of Nanoparticles in HeLa Cells

As previously described in this chapter, acetalated polysaccharides show no toxic effects *in vitro*. Thus, the uptake of the dex-OG488-loaded polysaccharide particles in HeLa cells was determined. A protocol by [redacted][253] was slightly adapted for this experiment. HeLa cells were incubated with particle suspensions at a concentration of 10 $\mu g \cdot mL^{-1}$ for 4 hours or 24 hours. Afterwards, cells were rinsed with PBS to remove particles which were not taken up by the cells and finally lysed with Triton™ X-100 in PBS. The cell lysate containing all particles that were taken up and several cell fragments was divided in two fractions. One part was used to measure the emission of dex-OG488 to determine the amount of particles that were taken up by cells. The other part was used to determine the total protein content with the Roti®-Quant universal assay that was described before. The protein amount correlates with the number of cells per well and therefore considered possible toxic effects. In the end, the measured amount of dex-OG488 was related to the proteins per well to get a more precise statement of the number of particles that were taken up by HeLa cells.

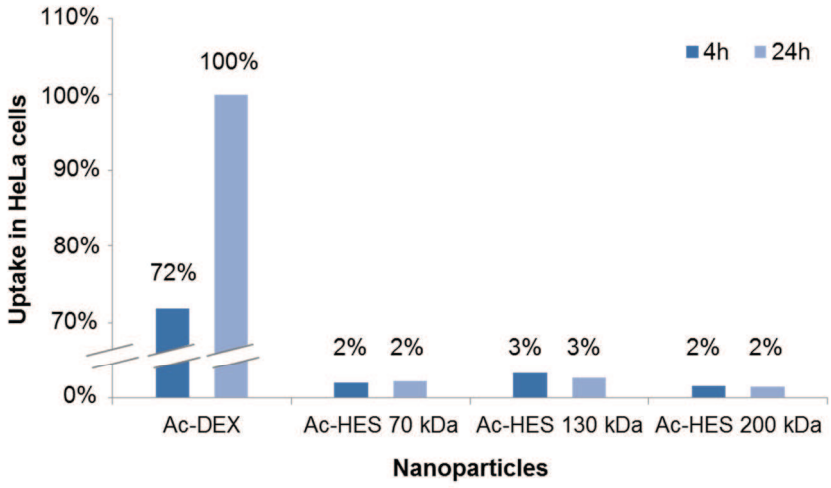

Figure 19: Uptake of acetalated DEX and HES nanoparticles in HeLa cells. The uptake was quantified by measuring the fluorescence of the encapsulated dextran-Oregon Green® 488.

As shown in **Figure 19**, Ac-HES particles are hardly taken up by HeLa cells after 4 hours or 24 hours compared to Ac-DEX particles.

Spermine-functionalized Ac-HES particles are taken up in higher amounts by HeLa cells (**Figure 20**). This is caused probably due to their slightly positive zeta potential so that an interaction with the negatively charged cell membrane is favored. As it was shown for the

acetalated particles before, Sp-Ac-HES particles are taken up less by HeLa cells compared to Sp-Ac-DEX particles.

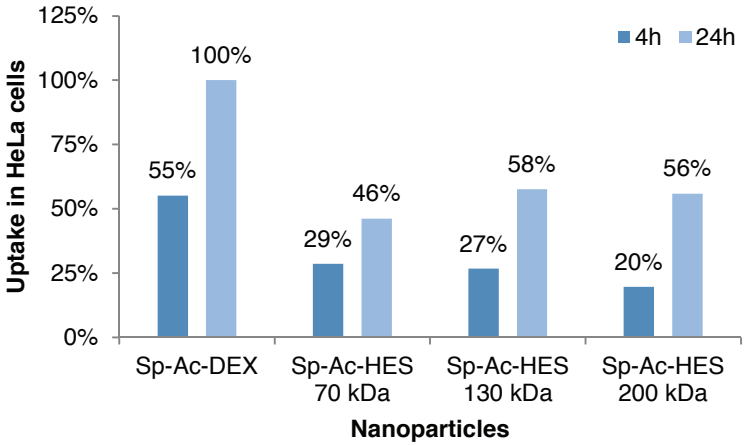

Figure 20: The uptake of spermine-functionalized and acetalated DEX and HES nanoparticles in HeLa cells was quantified by measuring the fluorescence of the encapsulated dextran-Oregon Green® 488.

In conclusion, Sp-Ac-HES particles are a potential new delivery system to avoid unspecific cell uptake. Therefore, the particle uptake should be tested in further cell lines. Targeting groups on the particle surface can enhance a specific uptake and improvement of efficient delivery vehicles. Furthermore, the encapsulation and release of siRNA has to be tested as well as an efficient transfection and knockdown of the nucleic acids before the system can be used *in vivo*.

Encapsulation of siRNA in Sp-Ac-DEX Nanoparticles

In vivo application of siRNA-loaded Sp-Ac-DEX particles requires higher amounts of encapsulated siRNA than described before for *in vitro* experiments by Cohen *et al.* (2011)[86]. Doses of 2.5 mg·kg^{-1} siRNA were described elsewhere for a successfully *in vivo* gene knockdown.[254] This means that 50 μg siRNA are administered for a mouse with a body weight of approx. 20 g. Since particles are only the delivery vehicle for the siRNA their mass should be as low as possible in comparison to the active compound. Therefore, three different amounts of siRNA-*luc* were encapsulated in Sp-Ac-DEX particles by double emulsion with a following particle characterization by size and encapsulation efficiency. **Table 8** shows the calculated volumes needed for *in vivo* application that result from the encapsulated siRNA amounts. The maximal particle concentration used *in vivo* should not exceed 1 mg·mL^{-1} due to high viscous particle samples. Hence, particle volumes of 500 to 800 μL will be needed for the administration in mice. These volumes outstrip the recommended injection volumes for i.v. applications of 5 mL·kg^{-1} used in mice described by Turner *et al.* (2011).[255] An enhanced siRNA encapsulation is therefore strongly needed to reduce dose volumes of the particles.

Table 8: Shown are the calculated dextran particle (NP) masses and volumes encapsulating siRNA for *in vivo* application in mice. It is assumed that 2.5 mg·kg^{-1} siRNA will be needed for a successful gene knockdown (see chapter 3.4).

Amount siRNA per mg NP	Mass NP for the delivery of 50 μg siRNA	Volume NP with a max. NP conc. of 1 mg·mL^{-1}
60 μg	833 μg	833 μL
80 μg	625 μg	625 μL
100 μg	500 μg	500 μL

The sizes of the prepared siRNA Sp-Ac-DEX particles are shown in **Figure 21**. The upper image depicts particle sizes measured before lyophilization with average diameters around 100 nm for the main population of the particles in the sample. The particle size slightly increases with the encapsulation of higher siRNA amounts. Huge particle sizes of 250–750 nm obtained for the intensity and volume values are indicators for a strong aggregation tendency of the particles. This aggregation potency rises enormously for lyophilized particles with stronger aggregation effects for higher siRNA encapsulation efficiencies. The size described by number shows that the main population of empty particles has sizes of about 100 nm which increase with higher amounts of encapsulated siRNA up to 1.2 μm (number).

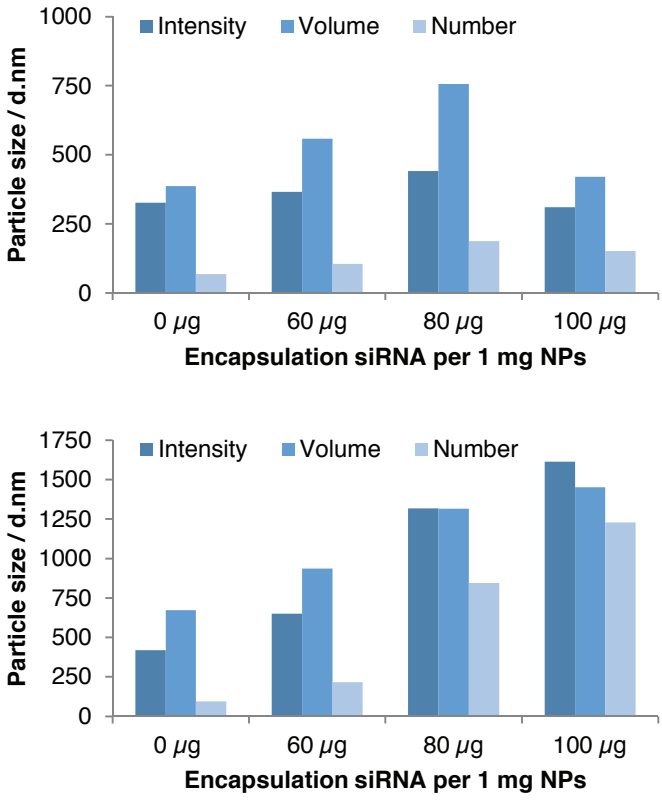

Figure 21: The size of Sp-Ac-DEX particles encapsulating siRNA was determined by DLS with a Zetasizer Nano ZS. Upper image: particles before lyophilization; lower image: particles after lyophilization.

Particles with average sizes from 400 nm to 1.7 μm described by the intensity cannot be described as nanoparticles anymore but result in micrometer sizes due to aggregate formation.

Encapsulation efficiencies of the incorporated siRNA were determined by Quant-iT™ RiboGreen® assay and detection of the free siRNA. Therefore, the particles were centrifuged after preparation and evaporation of the solvent followed by removal of the supernatant from the particle pellet. The free siRNA in the supernatant was determined by incubation with the Quant-iT™ RiboGreen reagent leading to a fluorescent product. Since the amount of used siRNA is known, the amount of encapsulated siRNA can be calculated by determine the free siRNA. All performed particles show a high siRNA binding and encapsulation efficiency of 99%.

In first quantification experiments, the particles were dissolved in acidic buffer and the amount of encapsulated siRNA was tried to determine by the Quant-iT™ RiboGreen® assay. But this procedure led only to low encapsulation efficiencies due to the high siRNA binding potential of Sp-Ac-DEX. The RiboGreen reagent cannot react sufficiently with the siRNA so that too little siRNA amounts are detectable. Hence, the quantification of encapsulated siRNA is performed via an indirect method measuring the free siRNA in the supernatant of the particle suspension.

In summary, Sp-Ac-DEX particles show highly promising results for the successful encapsulation of high amounts of siRNA but a disappointing outcome regarding particle sizes. Therefore, an optimization of the Sp-Ac-DEX particles for siRNA delivery is described in chapter 3.4.

3.1.3 Purification of Ac-DEX Nanoparticles

Purification of the Nanoparticles by Centrifugation

The standard purification method of the Sp-Ac-DEX nanoparticles synthesized by a double emulsion evaporation method is performed by ultracentrifugation. Therefore, the particles are transferred to special centrifugal tubes (Nalgene® Oak Ridge Centrifuge Tubes, Polypropylene Copolymer, Thermo Scientific) and centrifuged at 45,000 x *g* for 20 minutes. The supernatant is removed and the particle pellet rinsed two times with basic *dd*-H_2O before lyophilization. This purification method leads to a low yield of only 34.7% particle mass compared to the initial weight.

The centrifuge *Heraeus*™ *Megafuge*™ *8 R* with a rotor for VWR® SuperSpin™ microcentrifuge tubes can be used if only small volumes of particles are needed. But it needs to be evaluated if the size and yield of particles are comparable to particles that are purified by ultracentrifugation with the *Beckman AvantiTM J-25* centrifuge because the possible maximum speed of the *Heraeus*™ *Megafuge*™ exceeds not 30,000 x *g* for the VWR® SuperSpin™ micro-centrifuge tubes. Particles were resuspended in *dd*-H_2O pH 8 (1 mg·mL^{-1}) after lyophilization and centrifuged at 30,000 x *g* for 20 minutes with the *Heraeus*™ *Megafuge*™ *8 R*. The supernatant was removed and particles rinsed twice with 1 mL *dd*-H_2O pH 8 before they were lyophilized again. The yield (56.4%) was determined by comparing the initial mass and the

obtained mass of the lyophilized particles after the purification steps. These results are comparable to particles that are purified with the large volume ultracentrifuge. As a result, smaller batches of nanoparticles can be purified by using the centrifuge *Heraeus™ Megafuge™ 8 R* for VWR® SuperSpin™ microcentrifuge tubes.

Purification of the Nanoparticles by Centrifugal Filter Units

Many experiments require fluorescent-labeled particles so that a tracking is possible, *e.g. in vitro* uptake measured by FACS. Therefore, free fluorescent dyes should be totally eliminated from the particle samples to avoid false positive signals. Different centrifugal filter membranes (Centrisart®I, Vivaspin 2 PES, Vivaspin 2 CTA, and Vivaspin 2 Hydrosart®, Sartorius) were tested to optimize the particle yield as well as the duration and efficiency of the purification. Two different NHS-activated fluorescent dyes (Sulfo-Cy5, Oregon Green® 488) were conjugated to Sp-Ac-DEX particles in PBS (pH 8) protected from light for 2 hours. Afterwards, the same amount of particles was transferred to the different centrifugal filter membranes and particles were rinsed with *dd*-H_2O pH 8 after each centrifugation step.

Table 9: Shown are the yields of the purified particle samples (NPs) described by the initially used mass of the particles for the functionalization with fluorescent dyes and the finally obtained mass of particles after lyophilization. The amount of conjugated dye after functionalization of the particle surface with sulfo-Cy5 or Oregon Green® 488 was determined by the emission of the fluorescent dyes using the free dyes as standard.

Centrifugal Unit	*Sulfo-Cy5*			*Oregon Green® 488*		
	End Weight[a] NPs (mg)	Recovery Rate of NPs (%)	Dye/NPs (pmol·mg^{-1})	End Weight[b] NPs (mg)	Recovery Rate of NPs (%)	Dye/NPs (nmol·mg^{-1})
Centrisart®I	5.97	165.8	8.38	4.75	135.7	0.48
Vivaspin 2 PES	3.70	102.8	17.94	3.43	98.0	0.38
Vivaspin 2 CTA	0.53	14.7	16.75	0.83	23.7	1.20
Vivaspin 2 Hydrosart®	0.39	10.8	19.16	0.52	14.9	0.74

[a]Starting weight of Cy5-labeled Sp-Ac-DEX nanoparticles before purification with the centrifugal filter membranes: 3.6 mg; [b]Starting weight of Oregon Green® 488-labeled Sp-Ac-DEX nanoparticles: 3.4 mg. The recovery rate describes the percentage of labeled-particles collected after the purification with the centrifugal membranes compared to the starting weight of the particles.

Only small amounts of particles were used to test the purification with the different centrifugal filter units. The precision of the analytical balance is probably not high enough to determine the exact recovery rate of the purified particles with weights beyond 0.5 mg after lyophilization but trends are obvious. The weight of the conjugated dye can be ignored when the recovery rate of the particles is calculated since the additional weight is beyond the detection range of the analytical balance. High particle amounts are obtained with Vivaspin 2 PES filter units, whereas only low amounts of lyophilized particles are obtained using the centrifugal units consisting of cellulose triacetate and regenerated cellulose membranes (Vivaspin 2 CTA and Hydrosart®). The obtained mass of the particles after purification with Centrisart®I filter membranes consisting of a PES (polyethersulfone) membrane is almost

doubled compared to the initial weight of the particles. The increase in the particle mass can be explained by insufficient removal of the PBS salts using the Centrisart®I filter units. Low amounts of particles obtained after the purification with Vivaspin 2 CTA or Hydrosart® can be explained by sticking of the particles on or in the cellulose membranes so that the particles are hardly removable and resuspendable.

The measured amount of dye per sample is comparable for all membranes. It seems that all membranes are qualified to remove free fluorescent dyes from the particles. Only the Centrisart®I unit shows less dye per particle sample when used for the purification of sulfo-Cy5. It is possible that the particles stick in the membrane of the Vivaspin units in which the samples are applied on the membrane, whereas the particles are located under the membrane in the Centrisart®I units. The pores of the Centrisart®I membrane had about 3-times the size of the Vivaspin units. These results lead to the conclusion that all types of membranes were suitable for removing unconjugated dyes from the particle samples. But regarding the yield, Vivaspin 2 PES units are favored. Membranes like the Centrisart®I unit consisting of a high MWCO and in which the sample is applied under the membrane give the best results in removing the free dye. The Centrisart®I units are probably the best filters to recover high amounts of particles due to their high MWCO but they are not suitable for the removal of salts from the particle sample. In summary, Vivaspin 2 units with a PES membrane should be used for the purification of Sp-Ac-DEX particles to remove unconjugated fluorescent dyes.

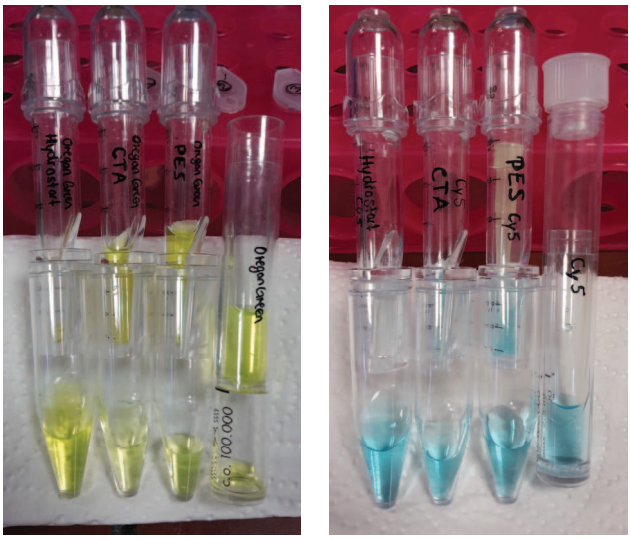

Figure 22: Centrifugal filter units are used for the removal of non-conjugated fluorescent dyes after the coupling to Sp-Ac-DEX nanoparticles. Units from left to right: Vivaspin 2 Hydrosart®, Vivaspin 2 CTA, Vivaspin 2 PES, and Centrisart®I. Left side: particles labeled with Oregon Green® 488; right side: particles labeled with sulfo-Cy5.

3.1.4 Screening of Different Cryoprotectants for Sp-Ac-DEX Particles

Aqueous solutions are only stable for a short time before the risk of a bacterial contamination increases rapidly. Therefore, preserving stabilizers should be added for a long-term storage to prevent bacterial growth in aqueous solutions or suspensions. Since preserving compounds are known to trigger allergic reactions and nanoparticles tend to aggregate over time when stored in aqueous suspensions, lyophilization for long-term storage is a useful tool. But lyophilization can lead to a strong aggregation of particles due to the high energy that is used for removing all water from the particle sample as it can be seen in section 3.1.2. To facilitate the dispersion of the particles after lyophilization the use of cryoprotectants is inevitable. Common cryoprotectants are poly(vinyl) alcohol (PVA), glucose, sucrose, trehalose, lactose, mannitol, fructose, dextran, and gelatine. Furthermore, these additives help to protect the particles from damage by ice-crystals that can be formed during the freezing process.[256-259]

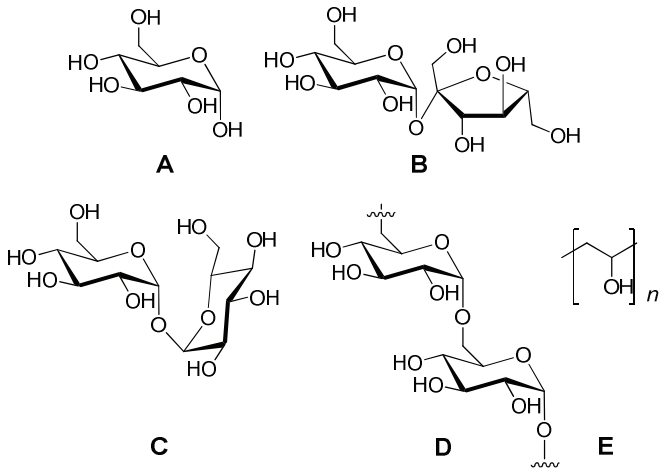

Figure 23: Structures of the scanned cryoprotectants; glucose (A), sucrose (B), trehalose (C), dextran 1 kDa (D), and PVA (E).

Since PVA is used as a stabilizer forming the nanoparticles with a double emulsion method it is used as a cryoprotectant to avoid further contamination of the particles with a second compound. Freshly prepared and purified Sp-Ac-DEX particles were lyophilized with 3% PVA and resuspended in PBS before the size determination by DLS. In **Figure 24**, the sizes of particles without and with cryoprotectant are shown. Particles without cryoprotectant show a smaller particle population at 100 nm and a big population of aggregated particles at about 500 nm. The addition of PVA leads only to a little improvement of the aggregation behavior of the particles. The particle population with a size of 100 nm is more separated from bigger aggregates and increased in the number of particles for this population but big particle aggregates of about 1 μm are still detectable in high amounts. Consequently, PVA seems not to be the optimal cryoprotectant for dextran nanoparticles since strong particle aggregation after redispersion is still detectable. Furthermore, it is very time-consuming to redisperse the lyophilized particles in buffer and a lot of energy using the vortexer and sonication bath is needed to disaggregate the lyophilized particles.

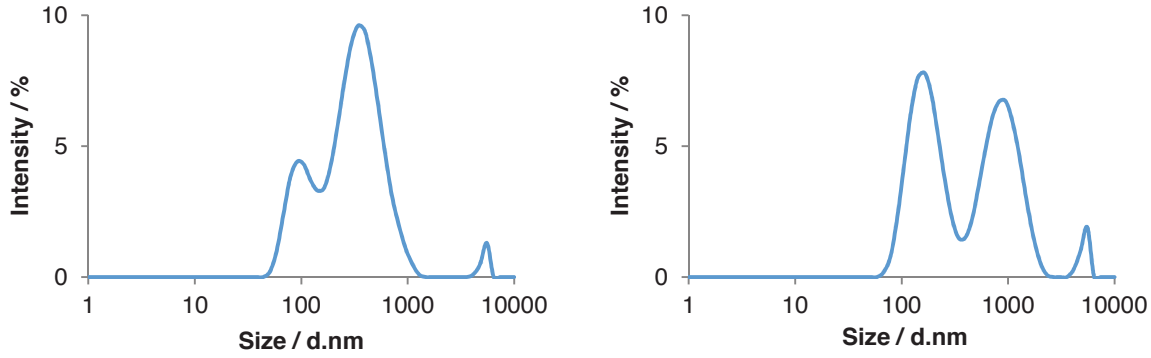

Figure 24: DLS measurements of lyophilized and resuspended Sp-Ac-DEX particles in PBS. Left side: particles without the addition of cryoprotectants; right side: addition of 3% PVA (mass of PVA compared to the mass of particles).

Here, different cryoprotectants (glucose, sucrose, trehalose, and dextran 1 kDa) are compared to lyophilized particles with the addition of the standard cryoprotectant 3% PVA and without the addition of an extra compound. The size of the particles was measured after a strict protocol of redispersion to keep the same reaction conditions for all samples. Typical concentrations of the cryoprotectants were published before elsewhere and used to start the screening.[260]

Empty Sp-Ac-DEX particles were prepared with a double emulsion evaporation method and the above mentioned cryoprotectants were added in different concentrations (1%, 5%, 10%, 20%, and 40% mass ratio) before particles were lyophilized overnight. For example, the addition of 1% cryoprotectant means that 1 mg Sp-Ac-DEX particle sample contains 10 μg cryoprotectant. The effect of the cryoprotectants was determined by measuring the size and zeta potential (Nano Zetasizer ZS, Malvern) of the redispersed particles in PBS or HEPES buffer. Particles were redispersed by vortexing and sonication using an exact time protocol to guarantee the comparability between the different particle batches.

The average particle size before lyophilization is around 146.9 ± 12.4 nm (number 88.2 ± 19.4 nm). First experiments showed that the addition of 1% (m/m) cryoprotectant is not sufficient to prevent aggregation of the particles. The addition of 40% (m/m) cryoprotectant prevents aggregation of the particles during lyophilization but leads to a high addition of a foreign material to the particles. High amounts of cryoprotectant in the particle sample can change the original particle characteristics regarding uptake or toxicity effects in *in vitro* experiments which should be avoided. In conclusion, only the concentrations of 5%, 10%, and 20% cryoprotectant were analyzed in further experiments. An overview for all tested cryoprotectants and the resulting size of the Sp-Ac-DEX particles after resuspension can be found in **Table 34** (section 6.5.1).

Best results in size and reproducibility (n = 3) are obtained for the addition of 10% and 20% sucrose or 20% trehalose (**Figure 25**). All particle samples show an average size around 150 nm with one main peak determined by DLS. Little aggregation can be still found in all samples showing a peak around 5000 nm. The goal should be to use a minimum of additives

in a particle sample so that the addition of 10% sucrose as a cryoprotectant seems to be the optimal solution. With this amount of sucrose the particles are easy to resuspend and show a good size distribution with low polydispersity measured by DLS.

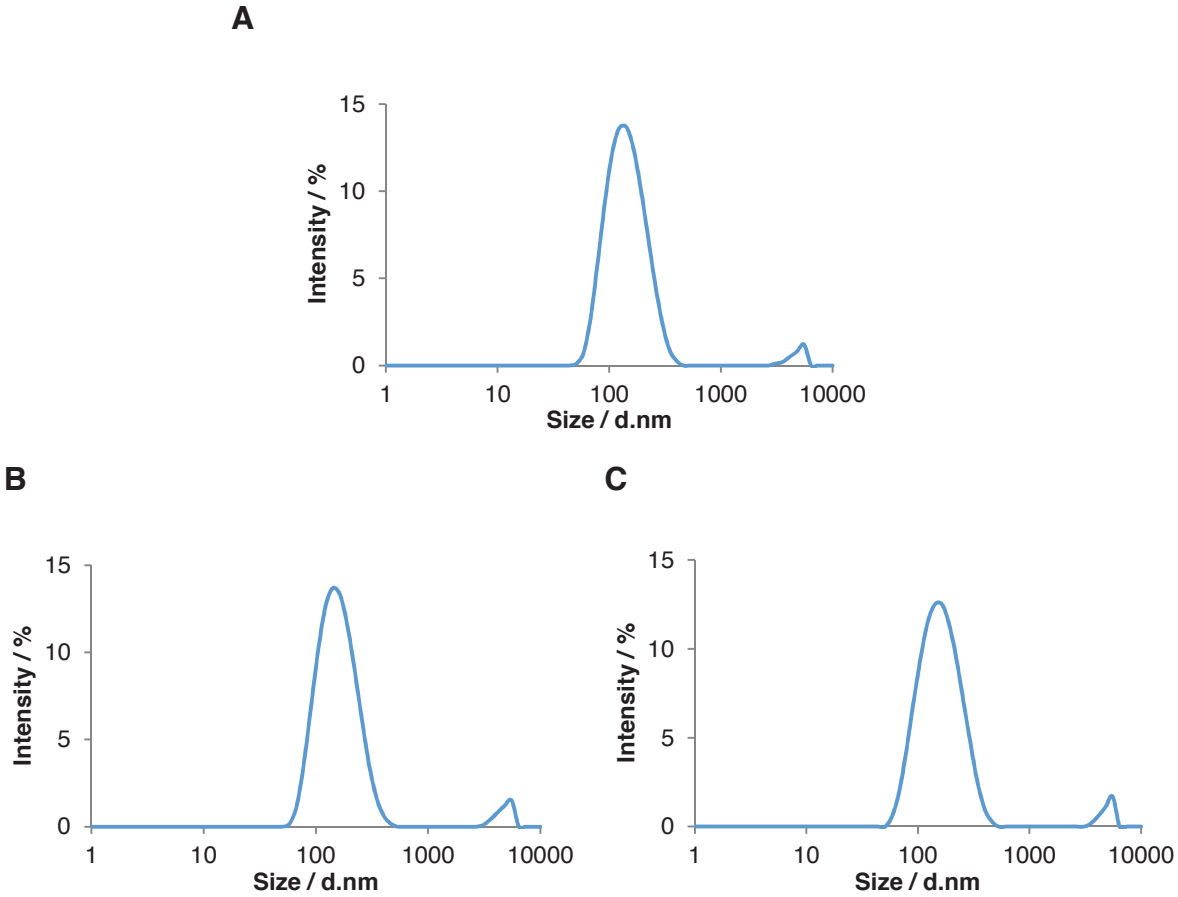

Figure 25: Size measurements (DLS) of lyophilized Sp-Ac-DEX particles after resuspension in PBS. Best results regarding the size distribution of the particles are shown for the addition of (A) 20% trehalose, (B) 10% sucrose, and (C) 20% sucrose (mass % cryoprotectant compared to total particle mass).

None of the cryoprotectants has a dramatic influence of the particle surface charge determined by zeta potential. The average potential was around 12.1 ± 1.89 mV for all particle samples. An overview of the zeta potential of all measured particle samples can be found in **Table 35** (section 6.5.1).

In summary, the time and energy needed for the resuspension of lyophilized Sp-Ac-DEX particles can be efficiently decreased by the addition of 10% sucrose as cryoprotectant. Two cycles of sonication and vortexing of the particle sample lead to particle sizes of about 100 nm with a narrow size distribution. The same resuspension procedure using for particles containing 3% of the standard cryoprotectant PVA leads to insufficient resuspension of the particles with huge amounts of big aggregates. These big aggregates can be reduced by intensive sonication and vortexing of the PVA containing particle sample for several minutes. But the high energy is not optimal for particles encapsulating nucleic acids which can be

degraded during the long and intensive sonication process. Therefore, the addition of 10% sucrose seems to be optimal to prevent particle aggregation during the freeze drying process. Before sucrose can be established as the new standard cryoprotectant, it should be analyzed in toxicity and uptake studies to ensure the unchanged behavior and characteristics of the particles. Further functionalization of the particles might be difficult after the addition of high amounts of sucrose so that the functionalization should be performed before the addition of cryoprotectant or the particles need to be purified first to remove the sucrose.

3.2 Surface Modification of Ac-Dextran Nanoparticles

As described in chapter 1.2, challenges of drug delivery are still omnipresent. Spermine-functionalized acetalated dextran particles are not very specific and can be taken up by several different cell types due to their cationic surface. First *in vitro* uptake experiments in HeLa cells confirmed this assumption (chapter 3.1.2). Therefore, further modification of the particle surface is needed to change their cationic character towards a neutral surface. Poly(ethylene glycol) (PEG) and dextran (DEX) are described as stealth compounds in the literature.[118, 126] These two agents shall be used to form a hydrophilic layer around the particles to decrease unspecific uptake. Afterwards, the addition of target structures is possible to guide the particles to specific cell types. The final goal should be the formation of a particle system with prolonged blood-circulation and target structures for specific cell uptake. First studies of attaching a hydrophilic layer, the change of the characteristics of the modified particles, and their *in vitro* and first *in vivo* behavior are described in this chapter.

3.2.1 PEGylation of Ac-Dextran Nanoparticles

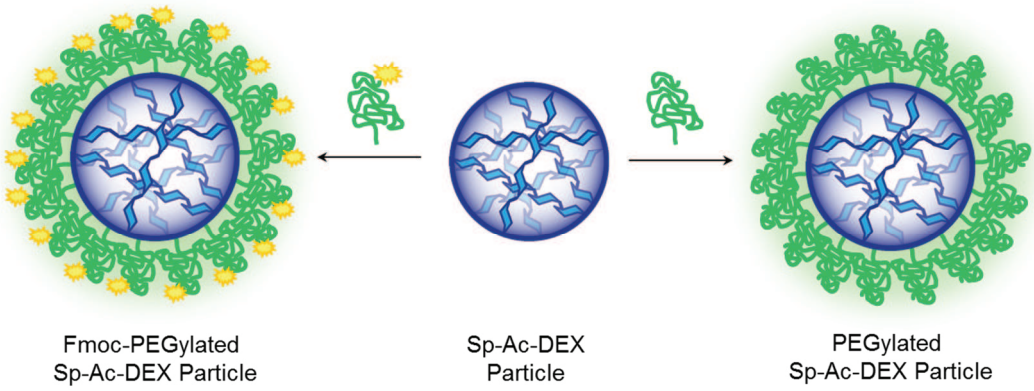

Figure 26: PEGylation of spermine-functionalized acetalated dextran particles with NHS-activated Fmoc-PEG (left) or methoxy-PEG (right).

Covering the surface of nanoparticles with PEG chains is called PEGylation and should enhance the hydrophilic character of the particles and reduce the positive surface charge. This modification might help to prevent aggregation of the particles in aqueous buffers and reduce the unspecific cell uptake. For the PEGylation of Sp-Ac-DEX particles, two commercially available succinimidyl succinate (*also: N*-hydroxysuccinimide, NHS) -activated PEGs (NHS-PEG) were used. NHS-PEG consists of an activated carbonic acid at one end of the chain that can easily react with the primary amines of the spermine on the particle surface leading to the formation of stable amide bonds. Secondary amines are less sensitive but can also react with NHS in minimal amounts leading to the formation of stable imide bonds. The reactivity of NHS esters increases with higher pH which is favorable for the Sp-Ac-DEX particle system since it undergoes hydrolysis in acidic environments. Unfortunately, the half-life of NHS esters decreases with higher pHs in aqueous buffers due to hydrolysis.[261] Therefore, higher

amounts of PEG-NHS esters are needed to obtain a sufficient PEGylation on the particle surface for the change of the surface character of the particles.

In general, Sp-Ac-DEX particles were suspended in PBS buffer with a pH of 8 and incubated with PEG-NHS dissolved in the same buffer for 2 hours. Afterwards, particles were purified by ultracentrifugation and rinsing with *dd*-H_2O pH 8 to remove unconjugated PEG. Finally, the PEGylated particles were lyophilized and obtained as a colorless, fluffy solid. The modified particles were stored then at -20 °C and resuspended in aqueous buffers before further use.

Figure 27 shows the PEGylation scheme of Sp-Ac-DEX particles. The electrophilic NHS reacts easily with the nucleophilic primary amines by formation of a stable amide bond. During this reaction the PEG-NHS hydrolyses and the water soluble by-product *N*-hydroxy-succinimide is formed.

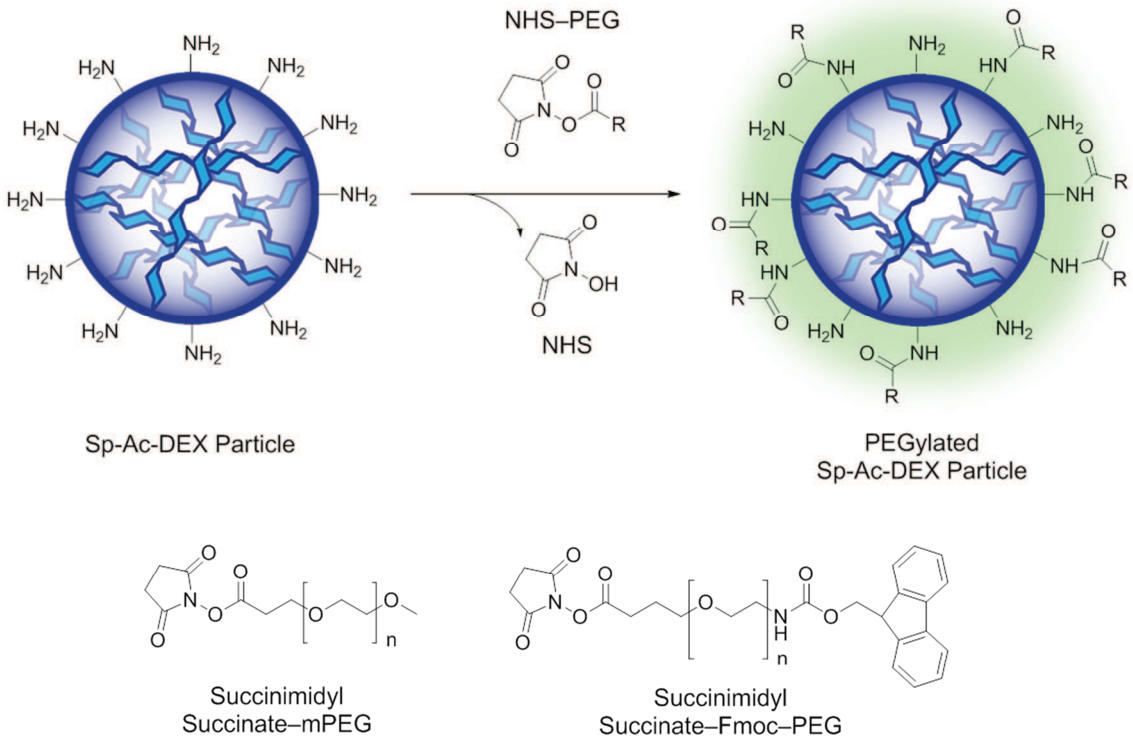

Figure 27: Scheme of PEGylation for Sp-Ac-DEX particles with NHS-activated PEGs.

The characterization of the PEGylated particles is shown in the next sections of this chapter in comparison to the DEXylated particles which are described in the following section.

3.2.2 DEXylation of Ac-Dextran Nanoparticles

An alternative to PEGylation is DEXylation. Here, the surface of the particles is modified with hydrophilic dextran chains to change the character of the particle surface (**Figure 28**). Dextran might have advantages compared to non-degradable PEG regarding the bio-compatibility since it is totally biodegradable by human dextranases into glucose units that can

be found in the human liver, spleen, kidney, and colon.[262] Glucose is ubiquitous present in the human body and needed as an energy source, for example in glycolysis.[263] Degradation products of dextran should be therefore not harmful when applied *in vivo*.

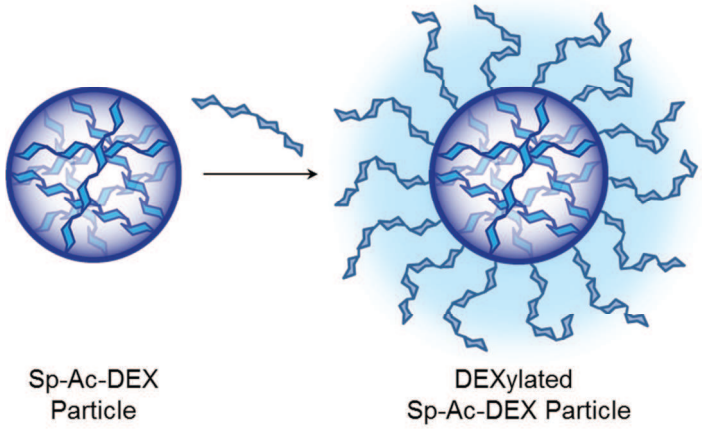

Figure 28: DEXylation of acetalated and spermine-functionalized dextran particles. Hydrophilic dextran, functionalized with thiol groups, was conjugated to the surface amines of Sp-Ac-DEX particles with a thiol- and amine-active crosslinker (SMCC).

Synthesis of a Thiol-Modified Dextran

Before dextran can be conjugated to Sp-Ac-DEX particles, the introduction of a new functional group is necessary. The introduction of a thiol-group at the reducing end of dextran results in an opportunity to conjugate the dextran specifically to the particle surface without crosslinking. This is possible since dextrans with low molecular weights are hardly crosslinked and contain ideally only one aldehyde at the reducing end.[58]

First, the linker 4-mercaptobutanehydrazide was synthesized by a protocol of von Delius *et al.* (2010)[264]. Therefore, γ-thiobutyrolactone was stirred with hydrazine monohydrate in methanol for 30 minutes followed by totally drying of the obtained product in high vacuum. The resulting colorless oil was analyzed by ^{1}H-NMR and used without further purification due to only minimal contamination.

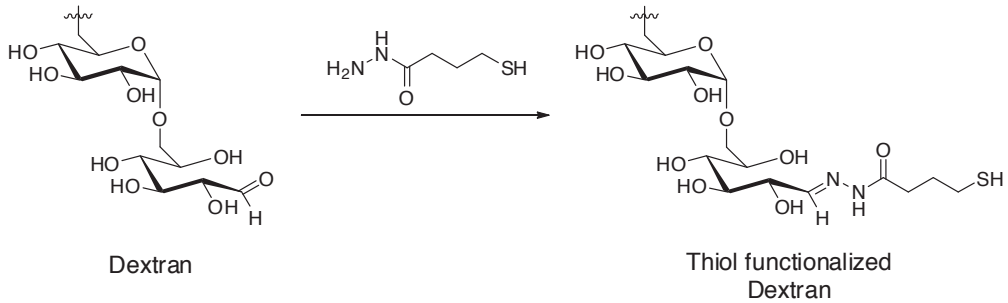

Figure 29: Conjugation of dextran with the bifunctional linker 4-mercaptobutanehydrazide for the introduction of thiol-groups.

For the thiol modification (**Figure 29**), dextran with a molecular weight of 3.5 kDa or 5 kDa was dissolved in phosphate buffer pH 7.4 and stirred overnight. The next day, the thiol-

modified dextran was purified by dialyzation and dried by lyophilization. The change of the molecular weight of unmodified and modified dextran is too low to separate the unmodified dextran from the thiol-modified dextran (DEX-SH) by dialyzation. Therefore, the amount of thiol-groups in the sample was determined by using Ellman's reagent. Ellman's reagent (5,5'-dithio-bis-(2-nitrobenzoic acid), DTNB) is a water-soluble compound that is known to react easily with free sulfhydryl groups at neutral pH (**Figure 30**). The by-product TNB^{2-} (2-nitro-5-thiobenzoic acid) is a yellow colored, water-soluble substance with an absorbance maximum at 412 nm. By measuring the absorbance of this by-product TNB^{2-}, the amount of thiol groups in an aqueous sample can be determined.

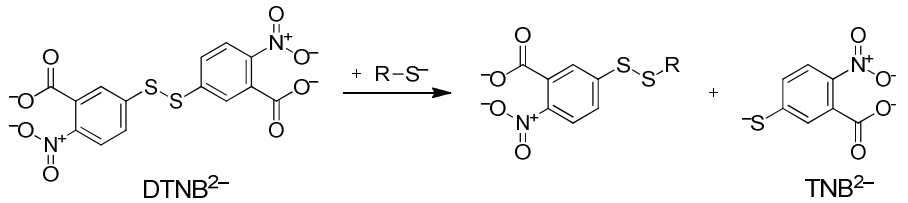

Figure 30: Reaction of Ellman's reagent ($DTNB^{2-}$) with a thiol-containing compound resulting in a yellow product TNB^{2-}.

The quantification of thiol-groups of DEX-SH by Ellman's assay results in 190 mmol thiol groups per 1 mol dextran 3.5 kDa (19% functionalization) and 110 mmol thiol groups per 1 mol dextran 5 kDa (11% functionalization). This means that only every 5th dextran chain 3.5 kDa and only every 10th dextran chain 5 kDa carries a thiol group at one end. This low degree of functionalization has to be taken in consideration when the thiol-modified dextrans are used for further functionalization with the Sp-Ac-DEX particles. The reaction of hydrazides with aldehydes leads to the formation of a stable Schiff base in slightly acidic or neutral buffers. Nonetheless, a hydrolysis of the formed hydrazone bond is possible. Low yields of the functionalized dextran during the reaction in aqueous buffers can be explained by this phenomenon.[265] Aniline is described as a nucleophilic catalyst to increase the formation of hydrazone bonds and may help to obtain higher yields in further studies.[266]

Activation of the Nanoparticle Surface with Sulfo-SMCC

Sp-Ac-DEX particles have to be activated for the conjugation of the primary surface amines with thiol-modified dextrans (see **Figure 31**). Therefore, a commercially available crosslinker 3-sulfo-*N*-succinimidyl 4-(*N*-maleimidomethyl)cyclohexane-1-carboxylate sodium salt (sulfo-SMCC) was used. Due to the acid-degradability of the particles and the hydrolysis of the maleimide group in alkaline buffers, particles were resuspended in PBS buffer containing 1 mM EDTA at pH 7.4 and were incubated with the water-soluble sulfo-SMCC for 2 hours.[267]

After ultracentrifugation the supernatant was removed and particles were resuspended in fresh buffer for the next conjugation step with the thiol-modified dextrans.

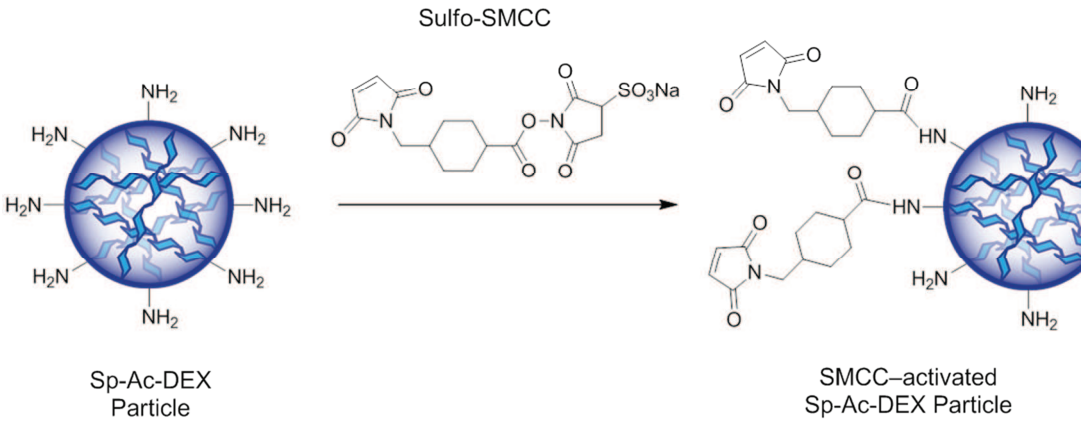

Figure 31: Activation of the surface amines of Sp-Ac-DEX nanoparticles with the bifunctional linker sulfo-SMCC leading to the introduction of maleimide groups.

DEXylation of SMCC-Activated Nanoparticles

The maleimide group of the sulfo-SMCC reacts specifically with thiol groups at pH 7.4 and lower pH. Higher pH might increase the reactivity of the maleimide groups with amines and could lead to crosslinking of the particles. Due to the acid-degradability of Sp-Ac-DEX particles buffers with pH 7.4 are favored.[268] The thiol-functionalized dextran was dissolved in PBS buffer (pH 7.4, 1 mM EDTA) and added to the SMCC-activated Sp-Ac-DEX particles in a five times excess. The EDTA addition in aqueous buffers helps to stabilize the thiol groups and therefore results in higher yields when used for crosslinking as it was described before elsewhere.[269] Particles were incubated for 4 hours with the thiol-modified dextrans before they were purified by ultracentrifugation. Afterwards particles were lyophilized and stored at -20 °C for further use.

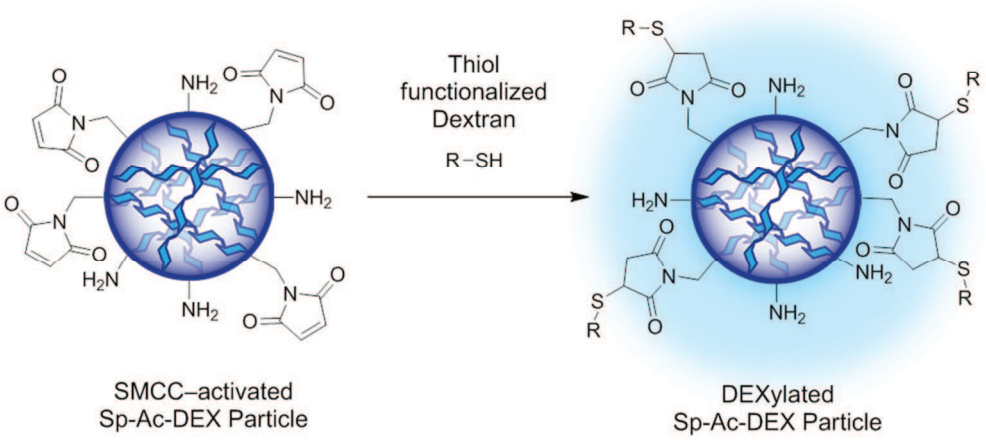

Figure 32: Conjugation of thiol-modified dextran to the surface of SMCC-activated Sp-Ac-DEX particles.

The thiol-modified dextran was added in a five times excess, taking the low thiol-functionalization in regard, compared to the conjugated sulfo-SMCC for activation of the particles. This should lead to a saturation of free maleimide groups on the particle surface.

Thiol groups can be found ubiquitous *in vivo*, *e.g.* at proteins, so that reactions with free maleimide groups of the particles are possible and should be prevented.

3.2.3 Quantification of the Attached Hydrophilic Layer

Quantification of the PEGylation and DEXylation via Fluorescamine Assay

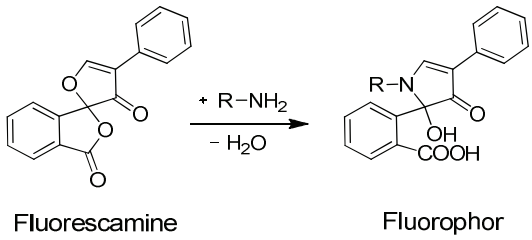

Figure 33: Reaction of fluorescamine with a primary amine-containing compound resulting in a fluorescent product.

Fluorescamine was originally used for the determination of the amount of primary amines on the surface of the spermine-modified Ac-DEX nanoparticles. Furthermore, the assay can be used to determine the quantity of conjugated PEG and dextran to the particles' surface. For this calculation, samples of unmodified and modified Sp-Ac-DEX nanoparticles were prepared. The decrease of primary amines on the particle surface corresponds to the amount of attached compounds. The spirolactone fluorescamine is not fluorescent but reacts rapidly with primary amines in a Michael addition. Thereby, a fluorescent product with an emission maximum at 460 nm is formed. The remained fluorescamine is hydrolyzed quickly so that the assay should be read out directly after the addition of the reactive compound.

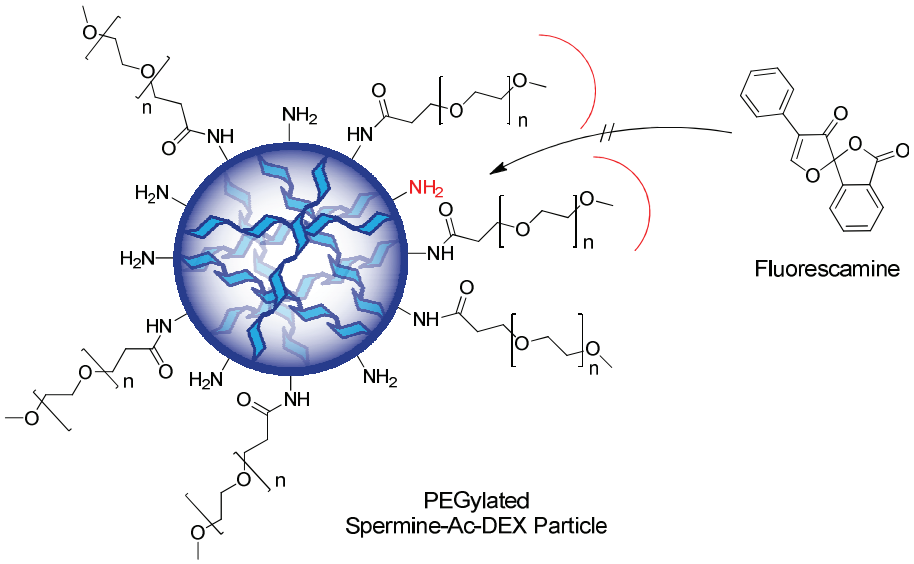

Figure 34: Attached PEG chains shield non-modified primary amines on the surface of PEGylated Sp-Ac-DEX nanoparticles. Fluorescamine cannot react with the primary amines, which in turn leads to a higher degree of modification.

The determination of the PEGylation and DEXylation with fluorescamine is an indirect detection method. The amounts of amines before and after the modification are measured and the difference corresponds then to the amount of PEG or DEX on the particle surface. Fluorescence measurements are very exact since the particles show no own emission signal compared to high absorbance signals. Furthermore, the reagent fluorescamine can only react with the primary amines on the particle surface.[270] Nevertheless, the fluorescamine assay has a few deficiencies. All fluorescence measurements can be quenched by high concentrated samples. Furthermore, it is possible that PEG or DEX chains shield primary amines so that they cannot react with fluorescamine which leads to the assumption of a higher degree of modification. A thorough resuspension of particles is also necessary, since aggregation of particles can lead to a decreased amount of reactive amines on the particle surface.

The amount of attached PEG and DEX was calculated by the reduced number of the surface amines determined by the fluorescamine assay. This calculation leads to the introduction of 11.7 nmol 2 kDa PEG-chains and 19.9 nmol 5 kDa PEG-chains per milligram PEGylated particles. The results for the DEXylation are comparable with the introduction of 15.7 nmol 3.5 kDa DEX-chains or 12.4 nmol 5 kDa DEX-chains per milligram DEXylated nanoparticles. It is remarkable, that the PEGylation with PEG 5 kDa is a little bit higher compared to the other modifications. This can be explained by possible shielding effects of the flexible PEG chains. Therefore, two other quantification methods for the PEGylation were performed to study this effect and its impact on the quantification by fluorescamine assay. First, PEGylation was determined by ^{1}H-NMR in a similar way like described before by Kang *et al.* (2015).[249] Second, the PEGylation was performed with an activated Fmoc-PEG-NHS and the fluorescence of the Fmoc group was directly measured afterwards.

Table 10: Shown are the amounts of the determined primary amines by the fluorescamine assay and the calculated degree of substitution of the modified Sp-Ac-DEX particles (NP). The DS describes the amount of amines which are substituted by PEG or DEX chains. The equations for the calculation can be found in section 5.3.8.

Modified NPs	nmol NH_2 per mg NP	Groups NH_2 per mg NP	mol NH_2 per NP	Groups NH_2 per NP	DS / %
Sp-Ac-DEX	81.1	4.88E+16	1.498E-19	90,137	–
PEGylated 2 kDa	69.4	4.18E+16	1.282E-19	77,207	14
PEGylated 5 kDa	61.2	3.68E+16	1.130E-19	67,972	25
DEXylated 3.5 kDa	65.4	3.94E+16	1.208E-19	72,774	19
DEXylated 5 kDa	68.7	4.13E+16	1.269E-19	76,284	15

For the calculation of the number of nanoparticles in a freeze-dried sample the density of polystyrene ($1.045 \cdot 10^3$ g·L^{-1}) is assumed.[271]

Quantification of the Nanoparticle PEGylation via ^{1}H-NMR

A second method to determine the degree of substitution of PEGylated Sp-Ac-DEX nanoparticles with mPEG-NHS can be performed by measuring a ^{1}H-NMR of PEGylated particles in deuterium oxide. Therefore, Sp-Ac-DEX particles were PEGylated with methoxy-PEG-

NHS (5 kDa), purified and lyophilized. For the quantification of the attached PEG, an exact amount of particles (5 mg) was dissolved in deuterium oxide followed by the addition of pyridine as an internal standard.

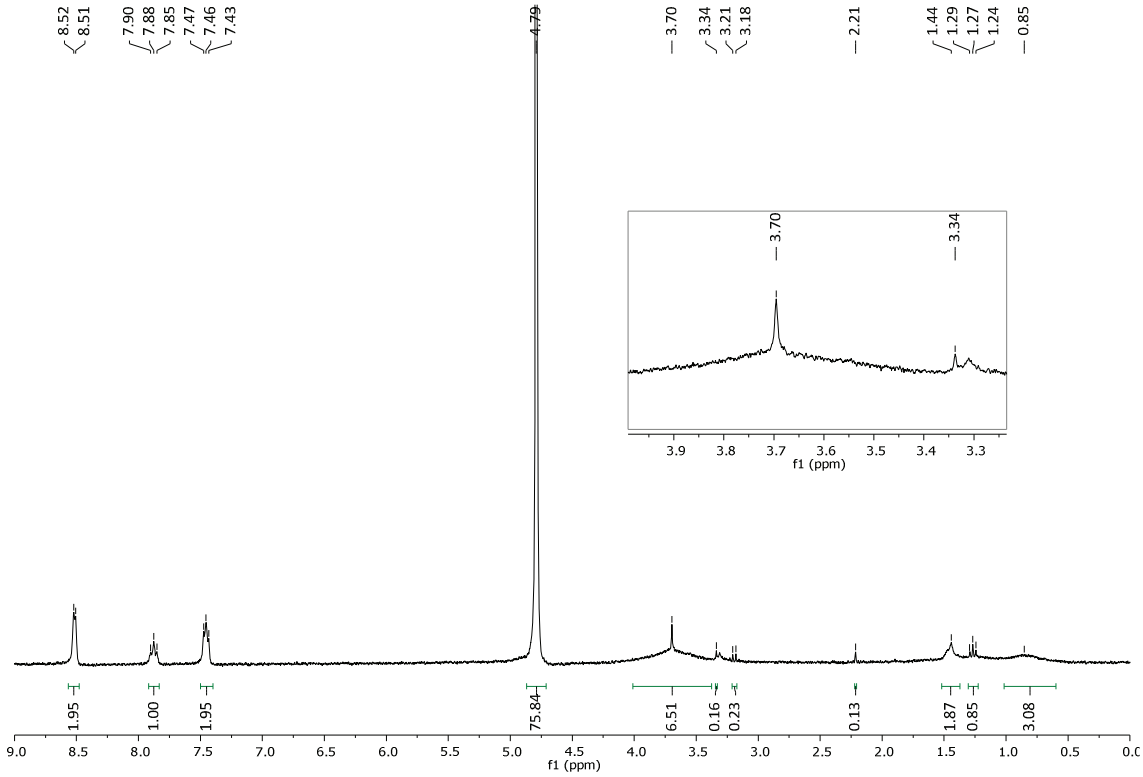

Figure 35: ^{1}H-NMR (300 MHz) spectrum of PEGylated Sp-Ac-DEX nanoparticles in deuterium oxide with pyridine as internal standard.

The integral of the methoxy group of the PEG (δ = 3.34 ppm) was compared to the signal of the protons of pyridine (δ = 7.85–7.90 ppm) and the following equation was used for the calculation of the molar mass of the attached PEG.

$$n(\text{PEG}) = \frac{1}{3} \cdot \frac{\int \text{-OCH}_3 \cdot n(\text{Pyridin})}{m(\text{NP})}$$

The quantification of PEG by a ^{1}H-NMR measurement results in 12.9 nmol PEG chains per milligram nanoparticles. The signal of the methoxy group can be increased in further experiments by using a NMR instrument with a higher frequency. The higher signal of the ethylene units of PEG (δ = 3.7 ppm) cannot be used for the quantification because the ethylene signal is covered by the signal of the dextran backbone. Therefore, an exact integration is not possible. The NMR-method is the most exact one but not practical for a daily quantitative analysis since a high amount of particles is needed for each measurement.

Quantification of the Fluorescence of Fmoc-PEGylated Nanoparticles

The advantage of quantifying PEGylated particles by the fluorescence emission of the Fmoc-group is a high sensitive measurement method. The fluorescence can be determined directly

without any further reaction in contrast to the fluorescamine assay. For the quantification with fluorescamine, particles have to react with the reagent to form a fluorescent product that was measured afterwards. Furthermore, dextran particles show no emission of their own. Absorbance measurements, for example, are hardly feasible due to the high absorbance of the particles.

Sp-Ac-DEX nanoparticles were PEGylated with Fmoc-PEG-NHS (5 kDa) as described before. After purification, the samples were lyophilized and dissolved in DMSO before the emission of the Fmoc-group was detected. A standard curve was measured by dissolving the pure Fmoc-PEG-NHS in DMSO and sample concentrations were analyzed in Microsoft Excel. This quantification method results in 12.3 nmol PEG chains per milligram nanoparticles.

Summary of the Quantification Methods for PEGylated Nanoparticles

Three different quantification methods were used to evaluate the degree of substitution for PEGylated Sp-Ac-DEX particles. These methods include the fluorescamine assay, ^{1}H-NMR spectroscopy, and fluorescence measurement of the Fmoc-group attached to the PEG chains. All particles were modified with a 10-times molar excess of a 5 kDa PEG-NHS for 2 hours so that the reaction conditions are comparable.

Table 11: Summary of the quantified amount of PEG (5 kDa) on the particle surface determined by three different quantification methods

Method	nmol PEG per mg NP
Fluorescamine	19.9
^{1}H-NMR	12.9
Fmoc	12.3

The results obtained by ^{1}H-NMR and the fluorescence measurement of the Fmoc-group show nearly the same degree of PEGylation of approx. 12–13 nmol PEG per milligram nanoparticles, whereas the degree of PEGylation determined by fluorescamine assay is slightly higher with approx. 20 nmol PEG per milligram nanoparticles. As described before the fluorescamine assay is an indirect quantification method compared to the ^{1}H-NMR and Fmoc method in which the amount of PEGylation is determined directly. Therefore, measurement errors have more impact on the results of the fluorescamine assay. A possible error can occur due to aggregation of the particles because fluorescamine cannot react then with the primary amines on the particle surface. A second error that was described before might be the shielding of the primary amines by the PEG chains. The fluorescamine reagent might not reach all primary amines so that less amines are detectable. This results then in a higher amount of modification when compared to the non-modified particles like it is shown in **Table 11**. An indication for a shielding effect of longer PEG chains is also the result from the

fluorescamine assay obtained for the PEGylation with PEG 2 kDa. This degree of substitution with a smaller PEG chain (11.7 nmol PEG 2 kDa per milligram nanoparticles) is comparable to the results obtained by ^{1}H-NMR and Fmoc quantification for the PEGylation with 5 kDa PEG-NHS.

3.2.4 Nanoparticle Size, Surface Charge and Morphology

After the attachment of a hydrophilic layer by PEGylation and DEXylation, the particles are first described by their size and the change of the net surface charge. Therefore, particles were suspended in PBS or HEPES buffer and sonicated and vortexed thoroughly to remove all aggregates. Especially, the lyophilized samples have to be treated in a sonication bath due to their dry and compact structure after lyophilization and the stronger tendency to form aggregates during the freeze drying process. Results of the particle size measurements and the zeta potentials are summarized in **Table 12**.

Determination of the Nanoparticle Size by NTA Measurement

Size measurements were performed by nanoparticle tracking analysis (NTA). Therefore, particles were suspended in PBS at concentrations of about 2 μg·mL^{-1}. Each measurement consisted of five runs and the average results of each particle type were compared. Spermine-functionalized, acetalated dextran particles have a size of about 150 nm in diameter after the preparation with a double emulsion method before they are purified. After the purification, particles were lyophilized and divided in five equal parts for the surface modification with PEG and DEX. The surface modified particles were stored lyophilized and suspended in PBS before the size was measured.

Lyophilized Sp-Ac-DEX particles increase in their size (190 nm, **Table 12**) due to observed aggregation behavior in PBS and due to the aggregation obtained after lyophilization that was described before in chapter 3.1.4. The aggregation behavior is displayed in the increasing number of the standard deviation (SD) that is an indicator of a more polydisperse sample (comparable to PDI in DLS). A second indicator for the aggregation of particles after lyophilization instead of the formation of bigger particles after the surface modification is the mode size. The average size of the entire particle sample is described by the mean value (comparable to Z-average in DLS), whereas the average size of the biggest population of particles in the sample is described by the mode value (comparable to number in DLS). The mode value of Sp-Ac-DEX particles before and after lyophilization changes not significantly so that the main population of particles is still present. Higher values of the particle sizes described by the mean are therefore an indicator for a particle aggregation due to lyophilization.

The sizes of the PEGylated and DEXylated particles were determined only after lyophilization since the original particle used for the modification was lyophilized before. It can be shown that the hydrophilic layer of PEG and DEX prevents aggregation of the particles when the lyophilized particles are resuspended in PBS. The mean sizes of the surface modified particles (PEG ~164 nm, DEX ~147 nm) hardly change in comparison to the lyophilized Sp-Ac-DEX

particles (190 nm). DEXylation seems to improve the hydrophilic behavior and the stability of the particles in PBS since the smallest sizes of all particles are displayed for the DEXylated particles. This can maybe be also an explanation for the decreased mode values of the DEXylated particles compared to the non-modified particles. Despite their smaller average sizes, DEXylated particles show a higher polydispersity compared to non-modified and PEGylated particles. First, this can be seen in the standard deviation of each size value and also in the SD of the entire particle sample. DEXylated particles show a size distribution around 100 nm whereas PEGylated particles show a distribution of only 71–75 nm. Since uniform particle suspensions are preferred due to different characteristics in particle size, regarding uptake mechanism or *in vivo* elimination, PEGylation seems the better method to enhance the hydrophilicity of the particles. A disadvantage of the particle size determination by NTA is that the sample is only measured in a defined window containing a few microliters of the sample, whereas the size measurement by DLS with a Zetasizer considers the entire particle sample. Few big aggregates can have more impact on the average size of the particles measured by NTA since their overall ratio seems to be higher. At the same time, big aggregates can also vanish in the particle sample if they do not arise in the analytical window. Therefore, NTA measurements should be evaluated carefully regarding the real distribution of particles in a sample.

Table 12: Overview of the particle sizes and surface potentials of Sp-Ac-DEX particles and their surface modified samples. Particle size was determined by nanoparticle tracking analysis (NTA) with five individual measurements per sample. Zeta potential was determined with a Malvern Zetasizer Nano ZS. The average sizes of five different particle batches and the zeta potential of four different particle batches are shown.

Particle Modification	Particle size measured by NTA			Zeta potential / mV
	Mean[a] / d.nm	Mode[b] / d.nm	SD[c] / d.nm	
*Sp-Ac-DEX NPs	150.1 ± 5.48	123.1 ± 6.05	56.0 ± 7.03	–
Sp-Ac-DEX NPs	190.8 ± 33.2	135.7 ± 24.1	88.4 ± 21.8	12.8 ± 1.25
NPs PEGylated 2 kDa	163.2 ± 24.8	126.3 ± 6.11	74.7 ± 20.9	9.7 ± 0.58
NPs PEGylated 5 kDa	165.0 ± 16.1	127.6 ± 3.32	70.7 ± 19.9	4.6 ± 0.82
NPs DEXylated 3.5 kDa	146.3 ± 39.5	106.3 ± 32.2	95.8 ± 6.36	3.7 ± 1.74
NPs DEXylated 5 kDa	147.6 ± 22.6	88.50 ± 33.0	111.8 ± 13.6	2.9 ± 1.87

*Particle size of Sp-Ac-DEX NPs measured before lyophilization; [a,c]mean size and SD (standard deviation) correspond to the arithmetic values based on the sizes of all particles detected in the NTA measurement; [b]mode values describe the average size of the main particle population.

Determination of the Nanoparticle Net Charge by Measuring Zeta Potential

Particles were suspended in HEPES buffer (25 mM, pH 7.4) before the measurement of the zeta potential to determine the net charge. As shown in **Table 12**, the non-modified Sp-Ac-DEX particles show a positive zeta potential about 12.8 mV due to the amines of the spermine on the particle surface. After PEGylation or DEXylation, the number of primary amines on the particle surface decreases, since PEG and DEX are conjugated to these amines.

This can be seen in a decreased zeta potential of the surface modified particles. PEGylation and DEXylation lead to a lower zeta potential of about 3 mV to 9 mV. Therefore, the first qualitative evidence of the successfully attached hydrophilic layer to the Sp-Ac-DEX nanoparticle surface was shown. It is described that particles with a neutral zeta potential tend to aggregate and are not stable in aqueous buffers anymore.[272] Here, the decrease of the zeta potential due to PEGylation shows no decreased stability and flocculation of the sample, whereas DEXylated particles form a pellet when stored suspended in PBS for a longer period (>1 hour).

SEM Images of Modified Nanoparticles

Particle morphologies were analyzed by scanning electron microscopy (SEM) in the group of [redacted] (Johannes Gutenberg-University, Mainz) by [redacted] Therefore, lyophilized particles were resuspended in water (pH 8), transferred to a wafer, and were totally dried before they were sputtered with a layer of gold.

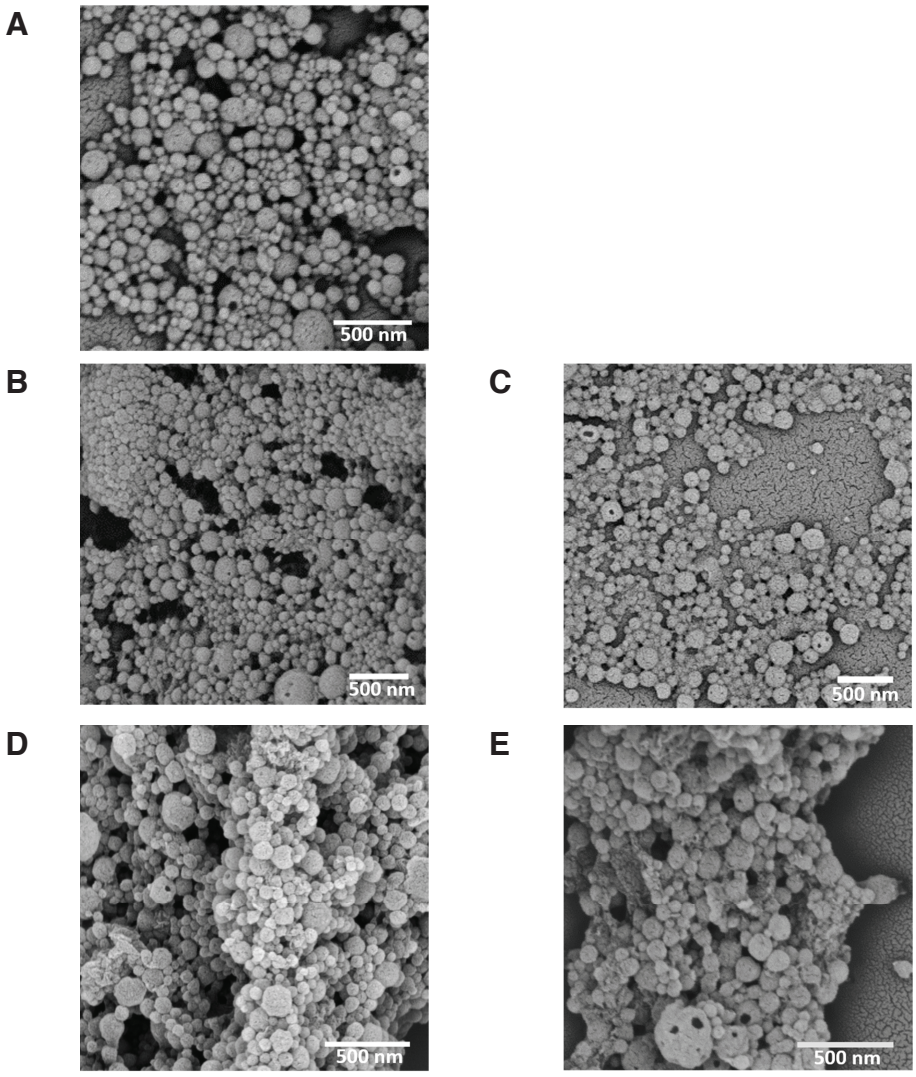

Figure 36: SEM images of non-modified NPs (A), PEGylated 2 kDa NPs (B), PEGylated 5 kDa NPs (C), DEXylated 3.5 kDa NPs (D), and DEXylated 5 kDa NPs (E) are shown.

Figure 36 displays the SEM images of the Sp-Ac-DEX particles and their modifications of a hydrophilic layer. The SEM images show no obvious change in the morphology of the surface modified particles as well as no significant growth of the particle size. Sporadic bigger hollow structures in the particle sample can occur due to the double emulsion method for the preparation of the particles.

3.2.5 Nanoparticle Aggregation Behavior

First NTA measurements in PBS, described in section 3.2.4, show an aggregation tendency of non-modified Sp-Ac-DEX nanoparticles after lyophilization. Furthermore, DEXylated nanoparticles show an elevated particle size distribution compared to the PEGylated particle formulations which is a second indicator for a potential aggregation behavior. The stability of particles in aqueous solutions is highly important. First, particles have to be prepared and packed in a form that can be stored and easily administered *in vivo*. Second, particles should be also stable in the blood since most particles are applied intravenously. After *in vivo* application, the particles will have at first contact with the proteins in the blood. This contact can lead to big aggregates of particles with the proteins, especially when the particles are not charge neutral so that they can interact electrostatically with the different proteins. Strong aggregation of the particles in the blood flow should be avoided since it can lead to accumulation of the particles in the lungs or small capillaries and cause decreased oxygen supply and thrombosis.[273-274] The most common buffer for *in vivo* applications of drugs is PBS. The salt content and buffer capacity with a neutral pH are very similar to the human blood and can be therefore used in humans without severe side reactions. In this experiment, particles were incubated in PBS or DMEM up to three days and the size of the particles was measured by NTA at certain time points. DMEM was mixed with 10% FCS to add proteins and to imitate the blood environment. It is also important to know how particles behave in cell culture medium to explain uptake or toxicity results obtained from *in vitro* experiments.

As described before, Sp-Ac-DEX particles were prepared using a double emulsion method, purified by ultracentrifugation and the batch was divided in five equal parts. Afterwards, the particles were PEGylated (2 kDa and 5 kDa) and DEXylated (3.5 kDa and 5 kDa) and labeled with the fluorescent dye TAMRA on their surface. Tetramethylrhodamine (TAMRA) is a fluorescent amine-reactive dye with high fluorescence stability. Particles were labeled on their surface since the NTA can also detect particles in the size range of proteins. A normal size measurement of particles is not possible in FCS containing DMEM due to the high concentration of proteins in the suspension. Therefore, the particles were labeled and the green laser (λ = 532 nm) and filter of the NTA were used to track the particles and shield the signal of the proteins. Since the proteins were not labeled with a fluorescent dye, the NTA can calculate the size of the particles by their Brownian motion in the cell culture medium.

Figure 37 shows the mean particle size (diameter) of non-modified, PEGylated, and DEXylated particles in PBS or DMEM. NTA measurements were performed directly after the suspension of the particles (0 h) as well as after 15 hours, 22 hours, 40 hours, and 3 days. It is

shown that particles of all five formulations have nearly the same size when measured in PBS up to three days. The smallest particles at first were the non-modified particles but their size increased from about 160–225 nm. PEGylated particles had the smallest distribution over time in PBS and their size increased from 180–210 nm. The only exception was the size of the 2 kDa PEGylated particles measured after three days that increased up to 250 nm. DEXylated particles had nearly the same size than PEGylated particles around 200 nm. Particles in DMEM however showed a different size distribution. Whereas non-modified and PEGylated particles increased only a little bit in the size in ranges from 200–250 nm, DEXylated particles showed a much higher rise in the particle size from 350–400 nm. The exact data of all particles can be found in the appendix (**Table 36**). The increase in the particle size indicates a strong interaction of proteins with the particle surface, especially for DEXylated particles. After three days, the size of the PEGylated and DEXylated particles decreased again a little bit. Maybe some of the proteins were removed again or particle aggregates were split due to the different surface charge of the attached proteins.

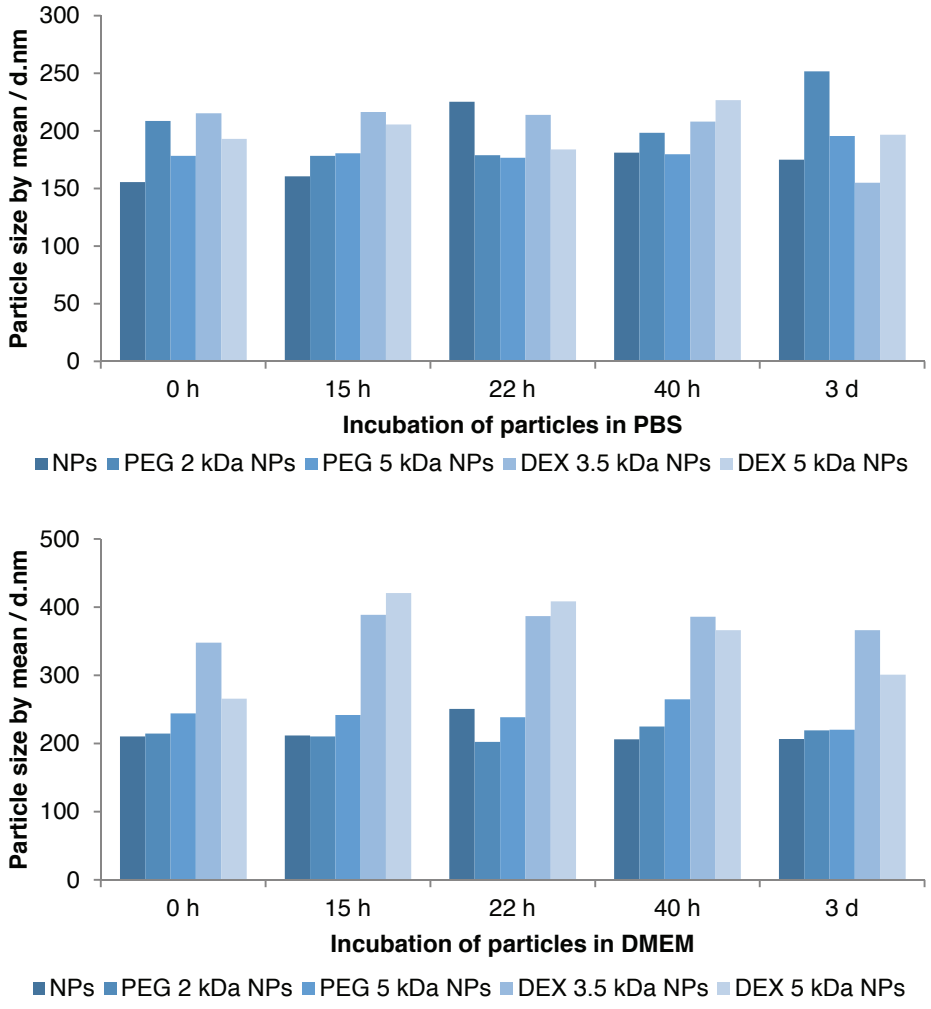

Figure 37: Shown are the mean sizes of Sp-Ac-DEX particles and surface modified particles after incubation in PBS and DMEM determined by NTA. The size measurements in FCS-enriched DMEM were performed using the fluorescence emission of the dye TAMRA attached on the particle surface to fade out the proteins from the size determination.

Figure 38 shows the standard deviation (SD) of the particles in nanometer. The SD is a quality parameter of the particle suspension. It describes the polydispersity of the sample and aggregation behavior can be detected. Non-modified Sp-Ac-DEX particles first have a small SD when suspended in PBS but it increases after a few hours of incubation. PEGylated and DEXylated particles show no big change in their SD that is overall higher from the first measurement (time point 0 h) compared to the non-modified particles. These data confirm the determination of the particle size in which non-modified particles form the population with the smallest size.

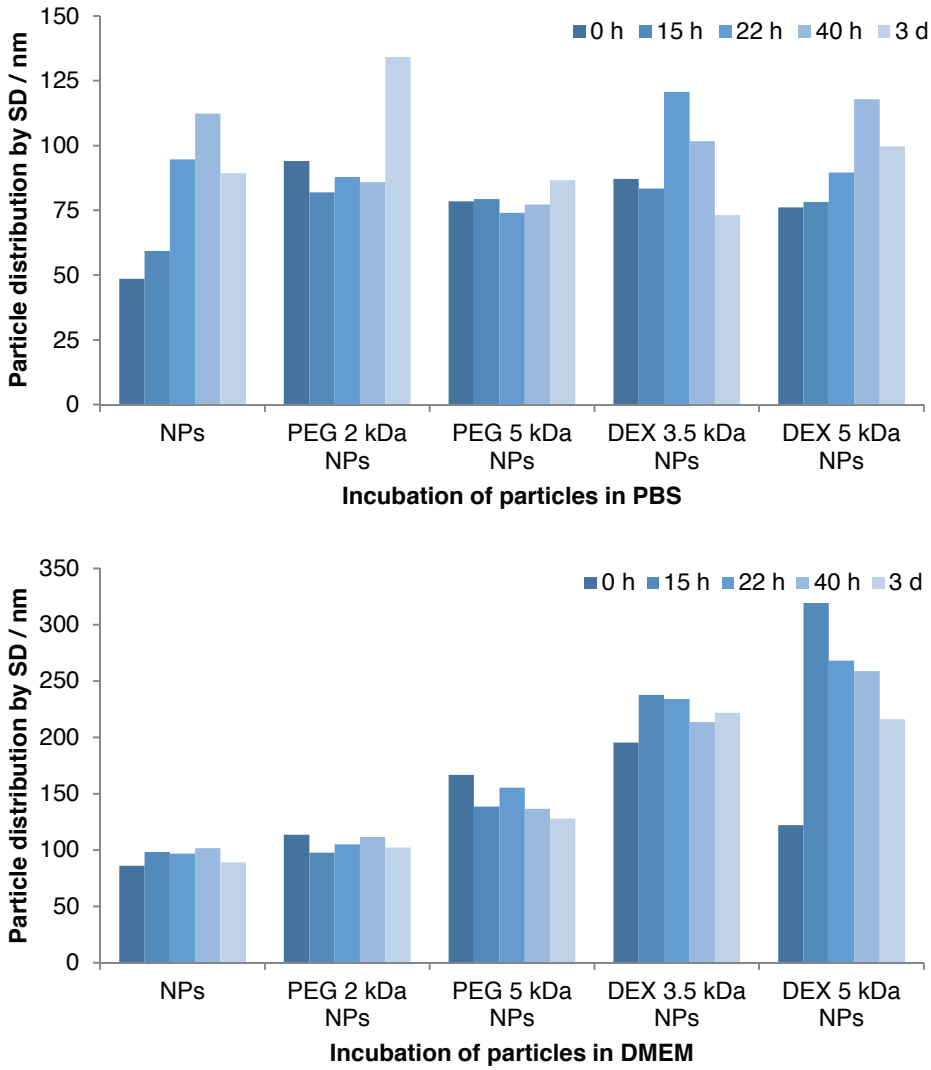

Figure 38: Shown are the size distributions described by the standard deviation (SD) of Sp-Ac-DEX particles without and with modified surfaces after incubation in PBS and DMEM. Particle sizes were measured using NTA.

In contrast to the NTA measurements of the particles in PBS, the particle SD of particles measured in DMEM varies between the different modified particles. Non-modified and the 2 kDa PEGylated particles show a low SD. The SD increases with the 5 kDa PEGylated particles and rises with the DEXylated particles. As it was described before in this section,

adsorbed proteins on the particle surface lead to a high aggregation of DEXylated particles and therefore a high polydispersity.

In summary, non-modified and PEGylated Sp-Ac-DEX particles show only a low increase in the particle size when stored in PBS but a high increase when suspended in protein containing cell culture medium (DMEM with 10% FCS). Especially, the size of DEXylated particles increases significantly in DMEM over time. The increased size may be a disadvantage regarding the particle uptake by cells *in vitro* or their behavior *in vivo*. In particular, big particles are recognized more easily by the MPS (mononuclear phagocytic system) in the blood. The binding of the particles by the immune cells of the blood leads to a fast excretion of the particles before they can arrive at their target sites. A second effect of the protein adsorption on the particle surface is a change in their surface character. The adsorbed proteins are then responsible for the recognition of specific cell receptors and the uptake or elimination of the particles. To get a more exact picture of the new particle surface the protein corona was analyzed and the results are described in the next section (3.2.6).

3.2.6 Evaluation of the Protein Corona of Ac-Dextran Nanoparticles

The protein corona experiments were performed by [redacted] (SDS-PAGE) and [redacted] (LC-MS) PhD students in the group of [redacted] (MPI Mainz).

Non-modified, PEGylated (5 kDa), and DEXylated (5 kDa) Sp-Ac-DEX particles were incubated with human plasma for one hour at 37 °C. The particles with the adsorbed proteins were purified and degraded before they were analyzed by SDS-PAGE. Due to the purification and preparation process of the particles, only the hard protein corona is detectable by SDS-PAGE, whereas the soft protein corona is removed before. The hard corona is formed by particles which are bound firmly and permanently to the particle surface, whereas the soft protein corona is formed by particles which are only adsorbed loosely to the particle surface and are in a permanently diffusion and exchange with the free plasma proteins. For the comparability, only the bigger PEG and DEX (5 kDa) are used for the particle modification, since they have the same molecular weights. There should not be a huge difference between the small and big PEG and DEX because they consist of the same structure with a difference in the chain length.

Figure 39 shows the results of the protein corona of the Sp-Ac-DEX particles displayed by SDS-PAGE. Non-modified (A) and PEGylated (B) particles show nearly the same protein cluster. They contain two significant protein bands with molecular weights around 60–70 kDa and smaller vague ones around 70–100 kDa. In contrast to these two particle formulations, DEXylated (C) particles show a totally different protein cluster. Instead of the two bigger bands around 60–70 kDa, the DEXylated particles show three bright bands in the range from 50–70 kDa. It is remarkable that the DEXylated particles increase in size the most but seem to adsorb less proteins than non-modified and PEGylated particles. Furthermore, there is a huge difference between the cluster of non-modified and DEXylated Sp-Ac-DEX particles, but

nearly no difference between non-modified and PEGylated Sp-Ac-DEX particles. The cluster of DEXylated particles shows an additional protein band at ~50 kDa but the protein band at ~100 kDa, which is detectable in the cluster of non-modified and PEGylated particles, is missing.

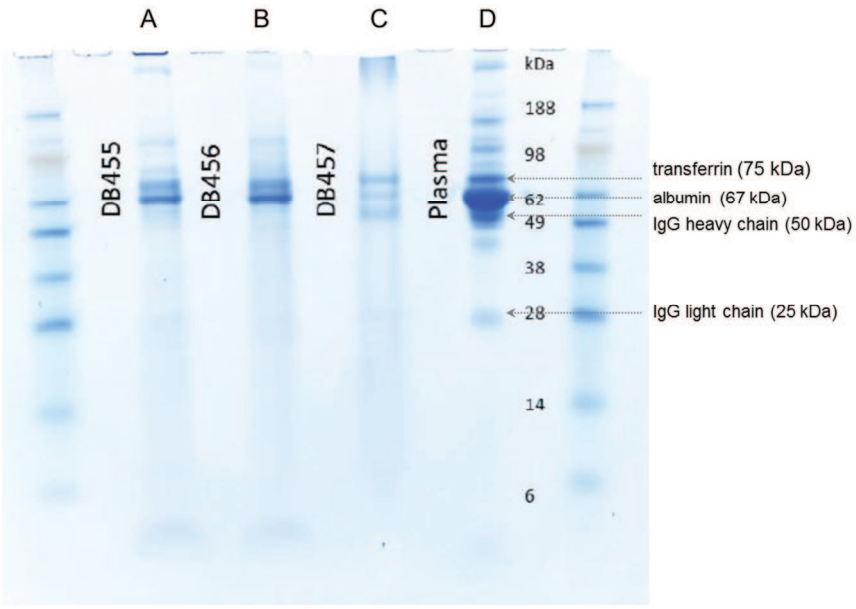

Figure 39: SDS-PAGE of the protein corona of non-modified (A), PEGylated (5 kDa) (B) or DEXylated (5 kDa) Sp-Ac-DEX particles (C), and human plasma (D); assignment of the protein bands was adapted from Winzen *et al.* (2015)[275].

To get a better understanding of the proteins on the particle surface, the proteins are analyzed qualitatively and quantitatively by liquid chromatography mass spectrometry (LC-MS). Therefore, the adsorbed proteins were removed from the particle surface and scanned afterwards. **Figure 40** shows the amount of adsorbed proteins on the particle surface determined by Pierce assay. As it is described in the literature, PEGylated and DEXylated particles adsorb less proteins than the non-modified cationic Sp-Ac-DEX particles.[102, 276] Furthermore, the data of the SDS-PAGE, which shows lower protein adsorption for DEXylated particles, is confirmed by the exact determination of the protein amount on the particles. DEXylated particles show only 0.67 mg protein per m^2 particle compared to 2.78 mg protein on PEGylated and 5.14 mg on non-modified particles.

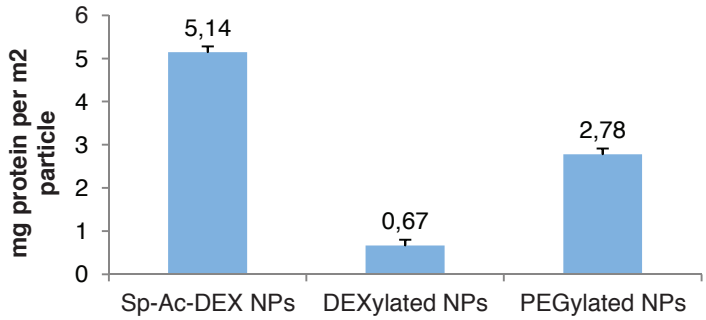

Figure 40: Shown are the amounts of adsorbed proteins on the surface of Sp-Ac-DEX particles after the incubation with human plasma. The adsorbed proteins were quantified by Pierce assay.

A more detailed composition of the protein corona of the particles can be found in **Figure 41**. The protein corona of the three different particle formulations is compared to the composition of the human plasma. Human plasma is dominated by albumin (~46%) followed by immunoglobulins (~31%). The smallest fraction of proteins in human plasma consists of tissue leakage (~1%), complement system proteins (~2%), and lipoproteins (~3%). The protein content of non-modified and PEGylated particles is comparable and confirms the data obtained from the SDS-PAGE. Both protein coronas are dominated by coagulation proteins (30%–41%) and lipoproteins (20%–24%). In contrast to these two formulations, the protein corona of DEXylated particles is dominated by lipoproteins (~60%) followed by smaller parts of immunoglobulins (> non-modified and PEGylated particles) and coagulation proteins.

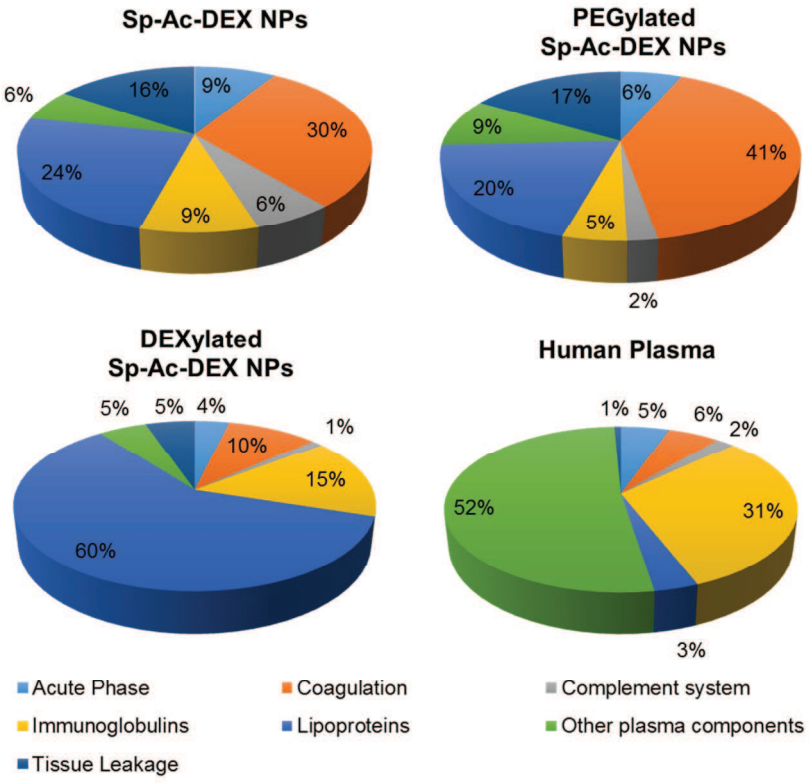

Figure 41: Protein composition of human plasma in comparison to the protein corona composition of the different Sp-Ac-DEX particle systems. The human plasma proteome is dominated by albumin which is placed in the section "other plasma components" (~46%). The protein corona analysis was performed with two biological replicates that were run each with two technical replicates on the LC-MS.

The exact composition of each protein corona of the different particles can be found in **Figure 42**. The protein corona of non-modified particles is dominated by the coagulation factor prothrombin followed by the lipoprotein clusterin, tissue leakage protein vitronectin, and acute phase protein ceruloplasmin. Nearly the same ratio of proteins can be found on the surface of PEGylated particles as well as an additional coagulation protein, the vitamin K-dependent protein S. DEXylated particles in contrast are dominated by apolipoprotein A-I and other lipoproteins. Coagulation proteins were hardly present. None of the particles shows

a significant affinity for the adsorption of albumin that is the main component of human plasma.

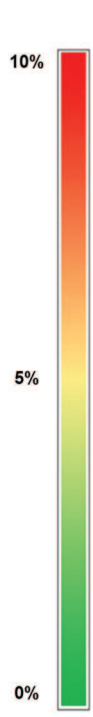

Annotation	Description	Sp-Ac-DEX NPs	DEXylated Sp-Ac-DEX NPs	PEGylated Sp-Ac-DEX NPs
Acute Phase	Ceruloplasmin	8,90	3,70	6,58
Coagulation	Coagulation factor IX	1,11	0,12	2,57
Coagulation	Fibrinogen beta chain	1,08	0,24	0,42
Coagulation	Fibrinogen gamma chain	0,57	0,09	0,15
Coagulation	Hyaluronan-binding protein 2	2,09	0,86	4,22
Coagulation	Prothrombin	18,33	1,94	20,36
Coagulation	Vitamin K-dependent protein S	4,85	6,02	10,75
Complement system	C4b-binding protein alpha chain	4,66	0,31	1,67
Immunoglobulins	Ig gamma-1 chain C region	1,24	1,94	0,33
Immunoglobulins	Ig gamma-2 chain C region	0,50	2,82	0,23
Immunoglobulins	Ig kappa chain C region	3,47	7,30	1,52
Immunoglobulins	Ig lambda-3 chain C regions	1,27	1,62	1,20
Immunoglobulins	Ig mu chain C region	1,96	0,50	0,99
Lipoproteins	Apolipoprotein A-I	2,30	29,59	2,04
Lipoproteins	Apolipoprotein A-IV	0,42	4,45	0,40
Lipoproteins	Apolipoprotein C-III	1,94	3,40	1,45
Lipoproteins	Apolipoprotein D	1,31	6,80	0,88
Lipoproteins	Apolipoprotein E	2,55	8,57	2,25
Lipoproteins	Clusterin	10,76	6,05	10,42
Lipoproteins	Serum paraoxonase/arylesterase 1	4,48	0,27	2,19
Other Plasma components	Insulin-like growth factor-binding protein 6	0,75	1,58	1,88
Other Plasma components	Probetacellulin	1,36	2,12	3,60
Other Plasma components	Protein AMBP	1,05	0,11	0,70
Other Plasma components	Serum albumin	0,86	0,81	1,76
Tissue Leakage	Cartilage oligomeric matrix protein	1,56	2,11	4,03
Tissue Leakage	Dermatopontin	2,19	-	0,49
Tissue Leakage	High mobility group nucleosome-binding domain-containing protein 5	1,43	2,09	3,62
Tissue Leakage	Vitronectin	10,33	1,06	8,47

Figure 42: Heat map of the protein corona of the different particles. Proteins with an amount >1% are listed calculated with the mol masses of the proteins.

The examination of the protein corona of Sp-Ac-DEX-based particles incubated in human plasma shows different protein patterns for DEXylated particles compared to non-modified and PEGylated particles. Therefore, non-modified dextran in comparison to acetalated and spermine-functionalized dextran seems to address different proteins in the human plasma and should behave different *in vivo*. The *in vivo* behavior of the protein-coated particles has to be analyzed in further studies regarding the biodistribution, blood circulation, and elimination. IgG, complement factors, and fibrinogen are known as opsonins. These proteins facilitate the recognition of the particles by the mononuclear phagocytic system (MPS) and their clearance from the blood circulation into the liver and spleen.[111, 277-278] In contrast to opsonins, dysopsonins are described as compounds which prolong particle circulation in blood, *e.g.* albumin.[279] The effect of the protein corona can help to understand the behavior of the particles *in vivo* and needs to be studied in further experiments.

3.2.7 Toxicity and Uptake of Ac-Dextran Nanoparticles in HeLa Cells

Determination of the Cell Viability of HeLa Cells by MTT Assay

First toxicity studies of surface-modified particles were performed by determination the cell viability of HeLa cells with a MTT assay (described before in section 3.1.2) after the incubation with the different particle samples.

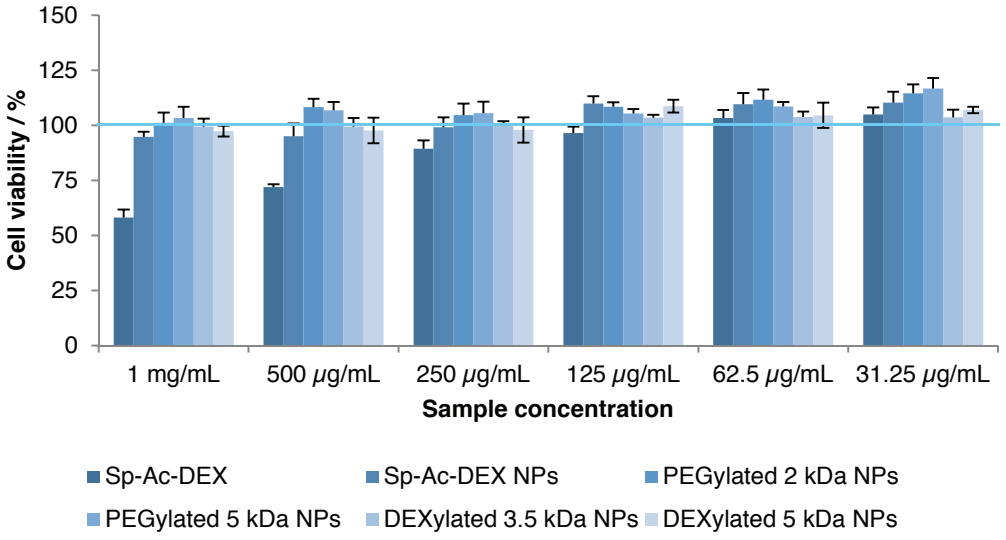

Figure 43: Cell viability of HeLa cells determined by MTT assay after the incubation with non-modified, PEGylated, and DEXylated Sp-Ac-DEX particles (NPs).

HeLa cells show no decreased cell viability when they are incubated with non-modified, PEGylated, and DEXylated Sp-A-DEX particles for 48 hours. Even with high particle concentrations of 1 mg·mL^{-1} HeLa cells show a viability of 100% compared to untreated cells. In contrast to these observations, the pure Sp-Ac-DEX material shows only a cell viability of about 50% in the highest concentration of 1 mg·mL^{-1}. This effect can be explained by the amount of available amines, since amines are known to induce toxic effects like described elsewhere for polyethylenimine (PEI).[280] The formation of particles leads to a decreased amount of amines in the sample since most of the material is incorporated inside the particles.

Uptake of Sp-Ac-DEX Nanoparticles in HeLa Cells

Schöttler *et al.* (2016)[102] described clusterin as the main protein responsible for the stealth effect and a reduced particle uptake by cells *in vitro*. Furthermore, they described the differences in the protein compositions of FCS, human plasma, and human serum displaying the proteins forming the biggest populations in the protein mixture.[281] *In vitro* uptake studies using FCS, here added to the cell culture medium of HeLa cells, have to be analyzed carefully, since the results of the uptake can be different due to the huge impact of the different protein corona *in vivo*.

First uptake studies of the surface-modified particles were performed analyzing the cell lysate of HeLas after incubation with the particle samples. The protocol was described before in chapter 3.1.2. **Figure 44** depicts the results of the particles taken up by HeLa cells after 4 hours or 24 hours. The upper image describes the total uptake of the particles, whereas the lower image describes the uptake of the particles related to the uptake of non-modified particles after 24 hours. After 4 hours of incubation, around 15%–26% of the particles were taken up by the HeLas. PEGylated particles and the DEXylated (3.5 kDa) particles were taken up less and DEXylated (5 kDa) particles were taken up more than non-modified particles. Same trends can be observed after incubation of the particles with HeLas for 24 hours. The

uptake of PEGylated particles was lower and the amount of DEXylated higher than the uptake of non-modified particles. In total, about 30% of the PEGylated particles are taken up by HeLas compared to 40% of the non-modified and 45%–50% of the DEXylated particles.

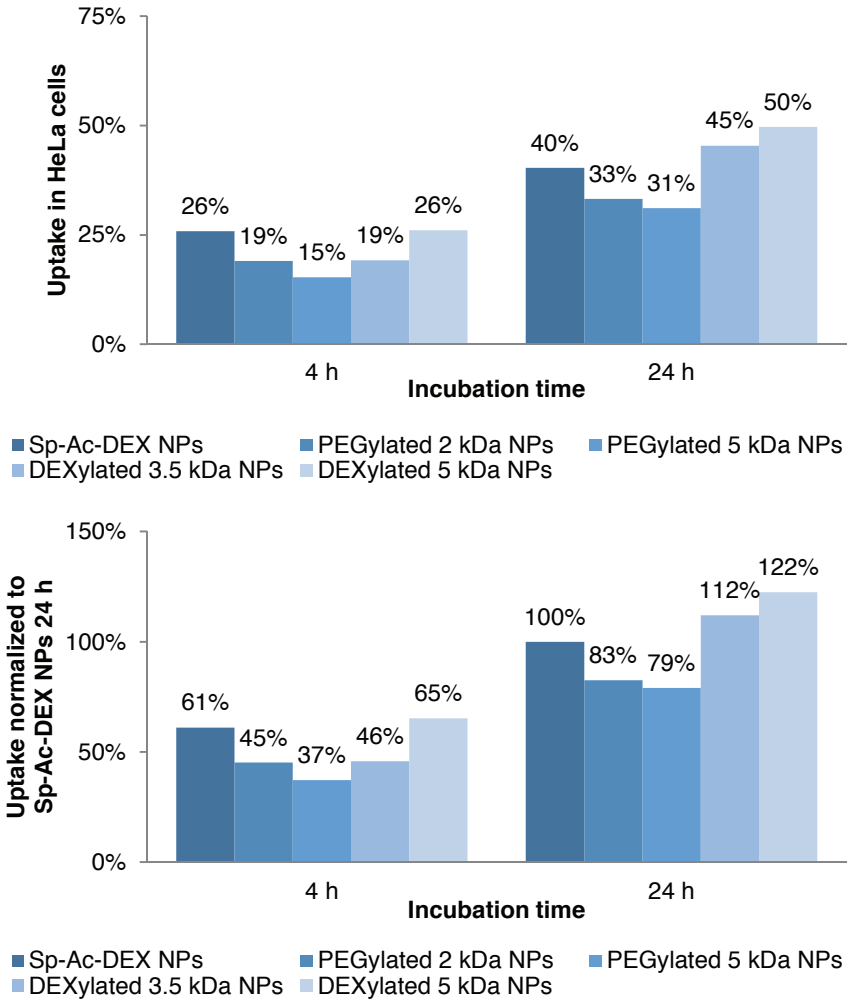

Figure 44: Uptake of modified Sp-Ac-DEX particles in HeLa cells by measuring the particle fluorescence in the cell lysate. Upper figure: total particle uptake compared to the initially applied particles; lower figure: same uptake of the particles normalized to the uptake of the non-modified Sp-Ac-DEX particles after 24 hours.

The amount of particles that are taken up by cells in relation to the non-modified particles illustrates the different behavior of the modified particles regarding their *in vitro* uptake. These results can be explained by the distinct surface of the particles due to different protein composition. Dextran is described as a stealth compound in the literature but here DEXylated particles are taken up better by HeLa cells than non-modified particles. Therefore, the influence of the modified particles is analyzed on further different cell lines and described in the following chapters.

3.2.8 *In Vitro* Studies of Ac-Dextran Nanoparticles in Murine Cells

The toxicity and uptake of modified Sp-Ac-DEX particles in murine cells obtained from the liver were tested in the group of [redacted] (Universitätsmedizin Mainz) by [redacted]

Toxicity of the Nanoparticles in Murine Cells

Cell viability of murine hepatocytes (AML12 cells), macrophages (RAW 264.7), and fibroblasts (NIH 3T3) incubated with non-modified and PEGylated (2 kDa) Sp-Ac-DEX particles was tested with the MTT assay using a protocol of Riss *et al.* (2004).[282]

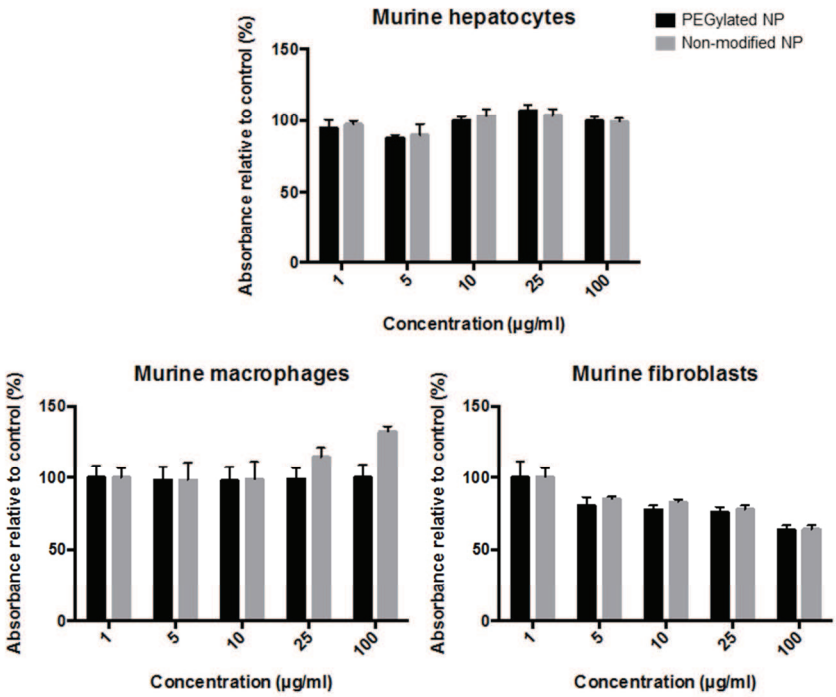

Figure 45: The cell viability of murine hepatocytes, macrophages, and fibroblasts was determined by MTT assay after the cell incubation with different concentrations of non-modified and PEGylated Sp-Ac-DEX particles.

Figure 45 displays the results of the cell viability of murine liver cells determined by the MTT assay. No change in the cell viability of murine hepatocytes and macrophages is detectable for particle concentrations up to 100 $\mu g \cdot mL^{-1}$. Only murine fibroblasts show reduced cell viability of about 80% for particle concentrations up to 5 $\mu g \cdot mL^{-1}$ and of about 70% for particle concentrations up to 100 $\mu g \cdot mL^{-1}$. In total, the cell toxicity is still in a tolerable level and the particles can be therefore stated as non-toxic in murine liver cells with concentrations up to 100 $\mu g \cdot mL^{-1}$.

Uptake of Ac-Dextran Nanoparticles in Murine Cells

The uptake of Oregon Green® 488-labeled non-modified and PEGylated Sp-Ac-DEX particles in murine liver cells was determined by flow cytometry (FACS). Particles were in-

cubated with the murine liver cells described in the section above and stained with 7-AAD (7-amino actinomycin D, eBioscience) before the read out. 7-AAD is a compound that forms stable bonds with DNA resulting in a fluorescence detectable product. Living cells excrete the dye so that no formation with the DNA is possible. This method can be used to separate live and dead cells in the FACS measurement.[283]

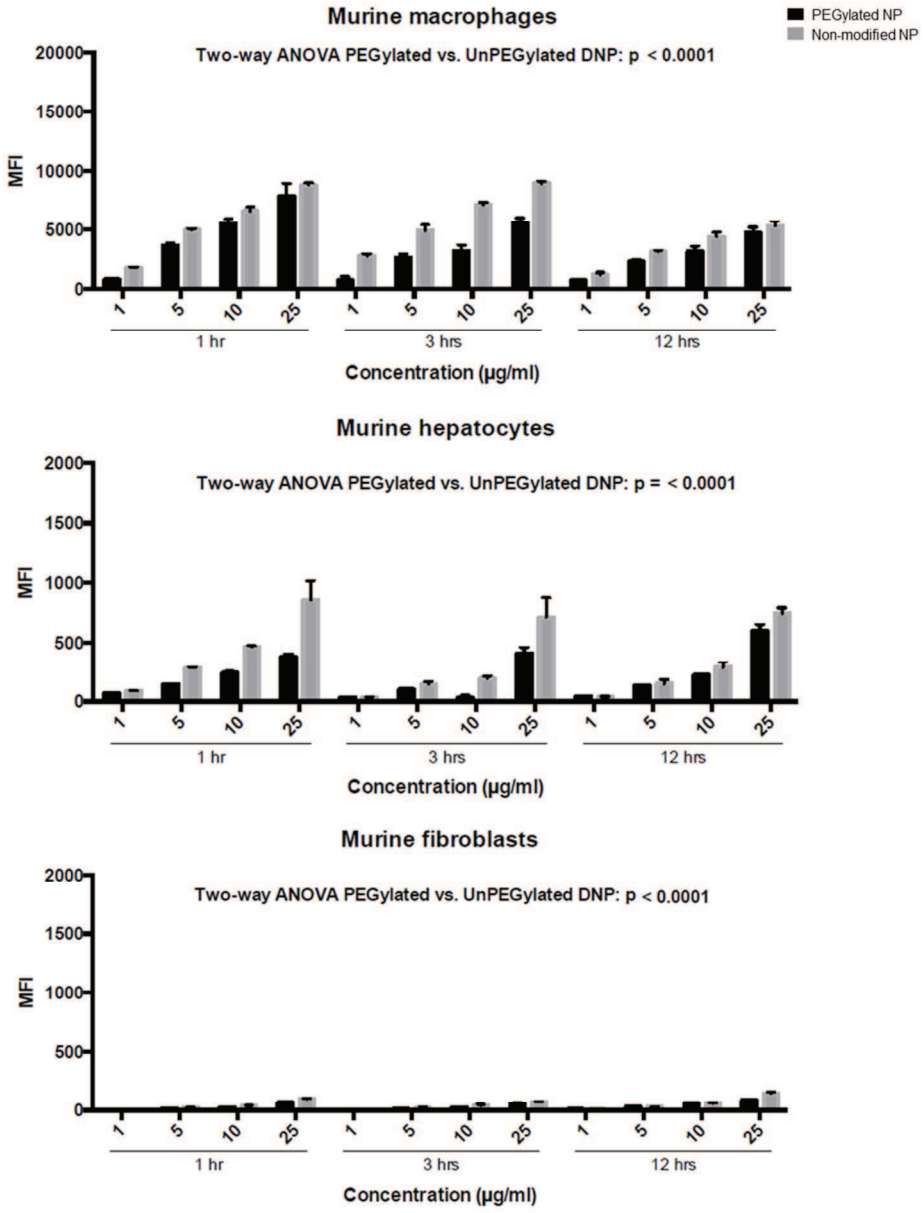

Figure 46: *In vitro* uptake of non-modified and PEGylated Sp-Ac-DEX particles by murine liver cells. The surface of the particles was labeled with Oregon Green® 488. The mean fluorescence intensity of the fluorescent dye in living cells is shown.

Both particle formulations, non-modified and PEGylated particles, are taken up time- and dose-dependent by murine macrophages and hepatocytes (shown in **Figure 46**). The uptake of non-modified particles is minimal favored, especially regarding the uptake in hepatocytes which is overall a little bit lower compared to the uptake in macrophages. After one hour of incubation the main particle uptake is completed, since no significant increase in the uptake of

particles was detected after 3 hours and 12 hours. The uptake of particles in hepatocytes is only about 10% compared to the uptake in macrophages. Fibroblasts show nearly no uptake of both particle formulations (only 1% compared to macrophages). In conclusion, the same trends that were observed with HeLa cells are detectable here for murine cells. PEGylated particles are taken up to a lower amount compared to non-modified particles.

3.2.9 *In Vitro* Studies of Ac-Dextran Nanoparticles in Murine Immune Cells

The toxicity and uptake / binding of surface-modified Sp-Ac-DEX particles in murine immune cells were analyzed in the group of [redacted] (Universitätsmedizin Mainz) by [redacted]

Determination of the Cell Viability of Murine Immune Cells

The spleen, as a part of the adaptive immune system, contains the majority of immune cells, namely macrophages, dendritic cells, B cells, and T cells.[284] Immune cells from the spleen can be therefore easily isolated and prepared for *in vitro* analysis. For the investigation of the particle toxicity, murine spleen cells and BMDCs were incubated with modified Sp-Ac-DEX particles (10 $\mu g \cdot mL^{-1}$) for 24 hours. Cells were stained with apoptosis (Annexin V, Biolegend, San Diego) and necrosis (7-AAD, Biolegend, San Diego) marker and cell viability was determined by flow cytometry.

Figure 47 shows the cell viability of the whole spleen cell population after the incubation with non-modified and surface-modified Sp-Ac-DEX nanoparticles. The different viability states of the cells in the apoptotic pathway are displayed in comparison to untreated cells (control). As it can be seen in **Figure 47**, untreated spleen cells consist of only 55% living cells. More than 40% of the untreated cells are in the late apoptotic or necrotic stage. Compared to the untreated cells (~19%), the fraction of necrotic cells is increased by the incubation with PEGylated particles (~34%) with a rising effect of non-modified (~41%) and DEXylated particles (~51%). Since the fraction of the apoptotic and necrotic cells represents a huge part of the untreated cells, only the living cells of the cells treated with particles are depicted compared to untreated cells (**Figure 47**, lower image). Changes in the cell viabilities can be described more clearly now regarding the decrease of living cells due to toxic effects of the particles. PEGylated particles show only a slightly decrease in the cell viability of living cells (PEG 2 kDa 86%, PEG 5 kDa 76%) compared to untreated cells (100%). Non-modified particles also lead to a slightly decreased cell viability (73%) compared to a stronger decrease in the fraction of living cells by DEXylated particles (DEX 3.5 kDa 69%, DEX 5 kDa 56%). Murine spleen cells are more sensitive regarding the cell viability compared to HeLa (3.2.7) or murine liver cells (3.2.8) which needs to be kept in mind for cell viability analysis, since cells start apoptotic cycles without any particle treatment.

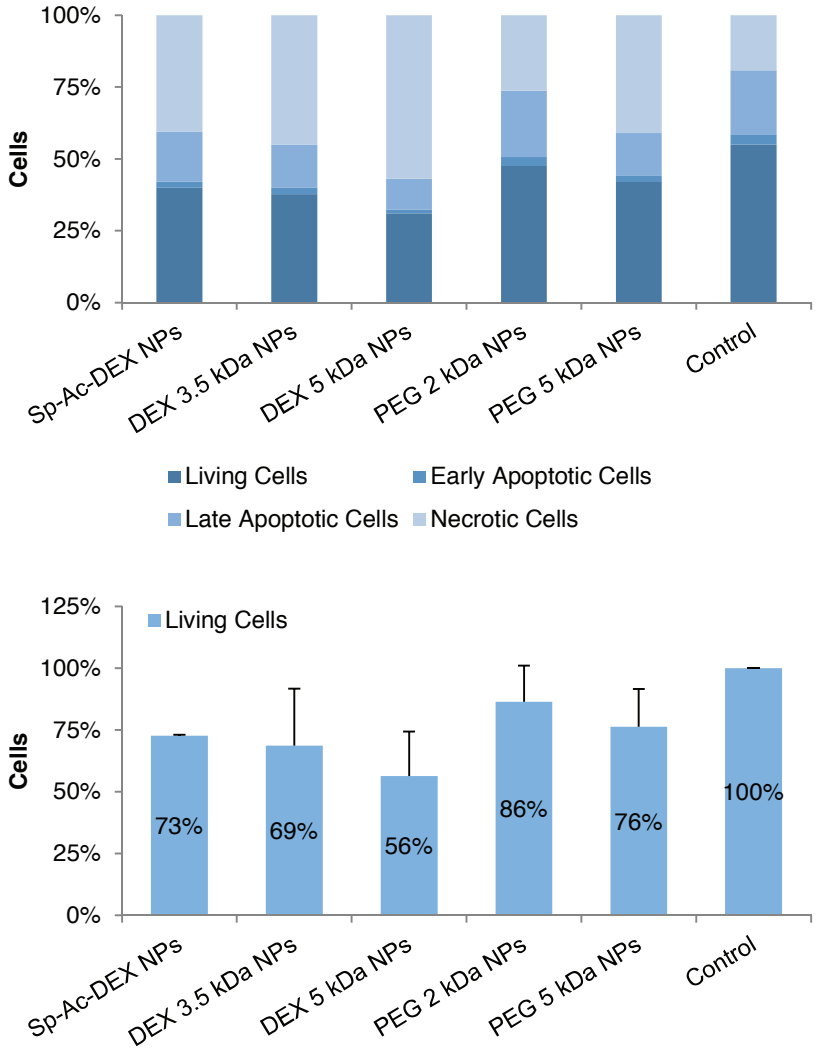

Figure 47: The cell viability of murine spleen cells was determined by flow cytometry. Shown are the mean cell viability data of two mice with untreated cells as the control. Cells were incubated with 10 μg/mL Sp-Ac-DEX particles for 24 hours. Upper image: All cells are normalized to untreated cells. Lower image: The population of the living cells is normalized to the living cells of the untreated cells (control).

Cell viabilities of BMDCs incubated with different formulations of Sp-Ac-DEX particles are shown in **Figure 48**. Compared to murine spleen cells, the untreated BMDCs consist primarily of living cells. Cell viability of BMDCs is nearly not altered after the incubation with non-modified and PEGylated particles for 24 hours. In contrast, the cell viability decreases to ~65% after the incubation of the cells with DEXylated particles. An increase in late apoptotic and necrotic cells can be detected when cells are treated with DEXylated particles, whereas the apoptotic and necrotic fractions hardly change after the treatment with non-modified and PEGylated Sp-Ac-DEX particles compared to the untreated cells.

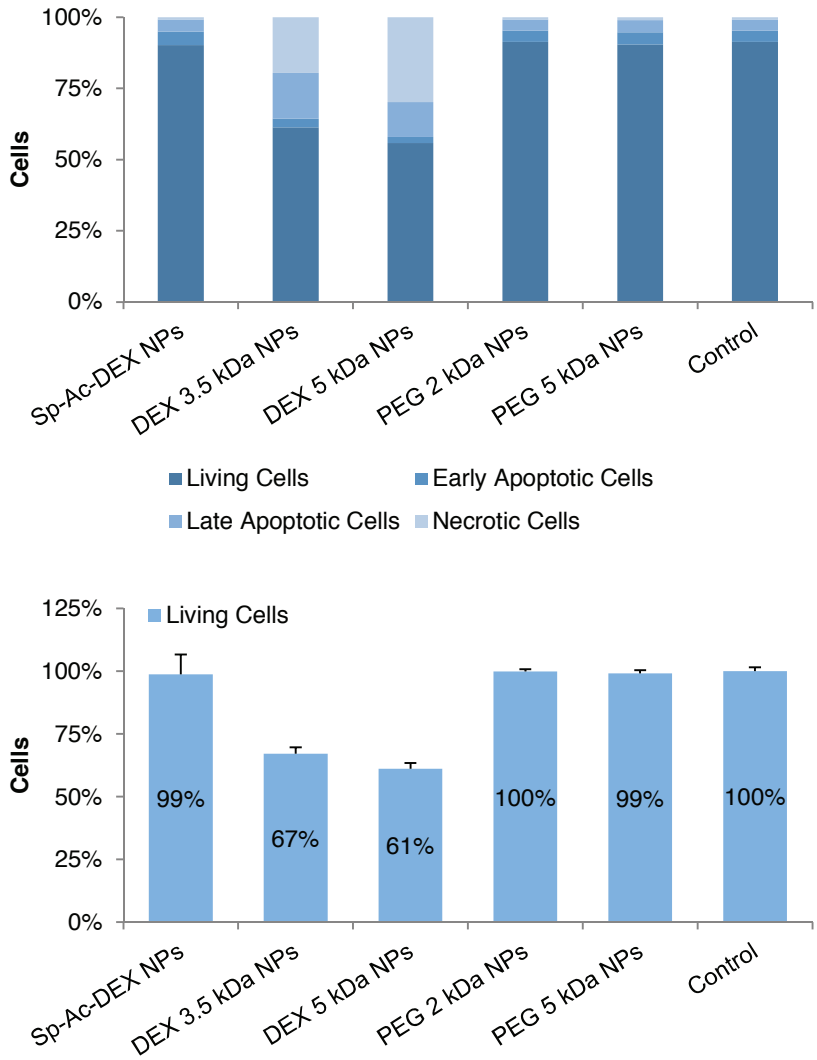

Figure 48: The cell viability of murine BMDCs was determined by flow cytometry. Shown are the mean cell viability data of two mice with untreated cells as the control. Cells were incubated with 10 μg/mL Sp-Ac-DEX particles for 24 hours. Upper image: All cells are normalized to untreated cells. Lower image: The population of the living cells is normalized to the living cells of the untreated cells (control).

In summary, PEGylation moderates toxic events of Sp-Ac-DEX particles compared to non-modified particles when incubated with spleen cells. Instead, DEXylated particles promote cytotoxic effects resulting in an increase of apoptotic and necrotic state of splenocytes and BMDCs in particle concentrations of 10 $\mu g \cdot mL^{-1}$. It should be noted that spleen cells represent a highly sensitive cell population with a great fraction of apoptotic and necrotic cells even before particle treatment.

Determination of the Endotoxin Content of the Ac-Dextran Nanoparticles

Endotoxins are lipopolysaccharides (LPS) from gram-negative bacteria and can lead to the stimulation of immune cells.[285] Therefore, a contamination of particle samples with LPS should be avoided to prevent unspecific activation of immune cells *in vitro* as well as *in vivo*.

Some particles can stimulate immune cells by themselves.[286] If a particle sample contains endotoxins the immunostimulatory capacity of the particle itself cannot be evaluated anymore. Furthermore, endotoxins can induce pyrogenic responses *in vivo* so that the FDA (Food and Drug Administration) has set a limit of the endotoxin content in drugs of 0.5 EU·mL^{-1}.[287]

The endotoxin levels of Sp-Ac-DEX-based particles were determined with a LAL (limulus amebocyte lysate) assay (Thermo Fisher Scientific) and the results are depicted in **Figure 49**. The highest endotoxin concentration can be found in the DEXylated (5 kDa) sample and resulted in 2.8 μg LPS per milligram particles. This led to an outcome of 70 ng·mL^{-1} LPS in the particle suspension of DEXylated (5 kDa) particles used for the following binding experiments (NP conc. 25 μg·mL^{-1}). PEGylated (5 kDa) particles contained 49 ng·mL^{-1} LPS and DEXylated (3.5 kDa) particles 37 ng·mL^{-1} LPS. All other particles, non-modified and PEGylated (2 kDa) particles, contained less endotoxins than the control PBS (3 ng·mL^{-1} LPS), in which the particles were resuspended. Typical concentrations of LPS to stimulate immune cells *in vitro* are around 1 μg·mL^{-1}.[288] Therefore, the minimal concentrations of LPS in all used particle samples should not lead to an activation of the immune cells. For *in vivo* application, all steps of the synthesis of the Sp-Ac-DEX particles and their modifications, started from the formulation of the particle material, have to be performed with commercially available endotoxin-free water. Contamination should be avoided since endotoxins can be hardly removed from the particle samples afterwards. Special cationic filter membranes (Charged Durapore, Merck Millipore, Germany) or endotoxin removal kits based on a polymyxin B membrane (ToxinEraser™ Endotoxin Removal System, GenScript, USA) are available to remove endotoxins from aqueous samples. It has to be proven if the systems can be also used for particles or if the particles will stick in the membranes of the purification devices. In summary, the shown endotoxin concentrations detected in the particle samples are still very low and the particles can be used for further *in vitro* and *in vivo* studies.

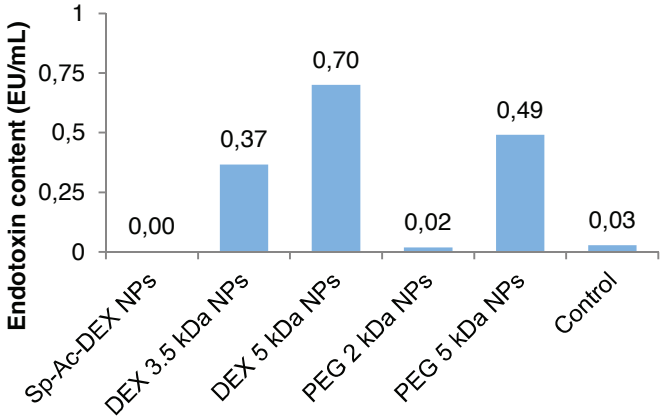

Figure 49: Determination of the endotoxin content of Sp-Ac-DEX particles using the LAL assay. 1 endotoxin unit (EU) is described by 0.1 ng LPS.[289]

Determination of Nanoparticle Binding by Flow Cytometry

For cell binding studies dextran-Oregon Green® 488 was encapsulated in Sp-Ac-DEX particles. The batch was divided into equal parts to modify the surface with PEG (2 kDa and 5 kDa) and DEX (3.5 kDa and 5 kDa). This guarantees that the fluorescence intensity of the different samples correlates with the same amount of particles. Non-modified and modified Sp-Ac-DEX particles (25 $\mu g \cdot mL^{-1}$) were incubated with murine spleen cells, BMDCs, and BMMCs. Cells were incubated with markers (cell-type specific antibodies) for dendritic cells (DC), macrophages, T cells, and B cells so that a separation of each single cell population was possible. Afterwards, the particle uptake in the different cell populations was quantified by flow cytometry.

The first experiment describes the uptake of non-modified and modified Sp-Ac-DEX particles in the different spleen cell fractions (see **Figure 50**). All particle formulations are hardly taken up by $CD3^+$ T cells which can be explained by the non-endocytotic nature of T cells in general.[290] In addition, PEGylated particles hardly bind to $CD19^+$ B cells, whereas non-modified and DEXylated particles show a minimal uptake of less than 20%. As it was seen before in murine liver cells, the main uptake occurs within the first hour of incubation (3.2.8). Dendritic cells ($CD11c^+$) and macrophages are known for high endocytic activity[291-292] and show the highest binding of particles in this experiment. Nevertheless, differences in the binding affinity for the different particle formulations are detectable. DCs bind PEGylated particles only to a small amount (~15%) with higher binding affinities for PEG 5 kDa than PEG 2 kDa particles in the first hours. Non-modified and DEXylated particles show much higher and faster binding affinities of about 50% to 60%. The results of the binding affinities for non-modified and DEXylated 5 kDa particles are comparable, whereas the particles modified with the smaller DEXylated 3.5 kDa show less binding and may be therefore suitable to prevent unspecific cell uptake.

In the first six hours, the binding affinity of $F4/80^+$ macrophages is comparable to the one shown for DCs. In the beginning, non-modified particles show a lower uptake in macrophages than described for DCs before (see **Figure 50**). After 6 hours, the binding of PEGylated particles by macrophages rises to 45%. Longer incubation times of the PEGylated particles (24 hours) lead to higher binding affinities compared to the other particle formulations. This effect can be explained by the endocytic character of macrophages and their different receptor cluster on the cell surface compared to DCs.[293-294] Summarized, DEXylated particles are significantly better bound to DCs and macrophages than PEGylated particles. Non-modified particles show a higher binding than PEGylated particles but less binding than DEXylated particles. These results lead to the assumption that DCs and macrophages have specific target receptors on their surface which enhance the binding of DEXylated Sp-Ac-DEX particles. Instead, PEGylated Sp-Ac-DEX particles show decreased uptake by the antigen-presenting cells due to stealth properties.

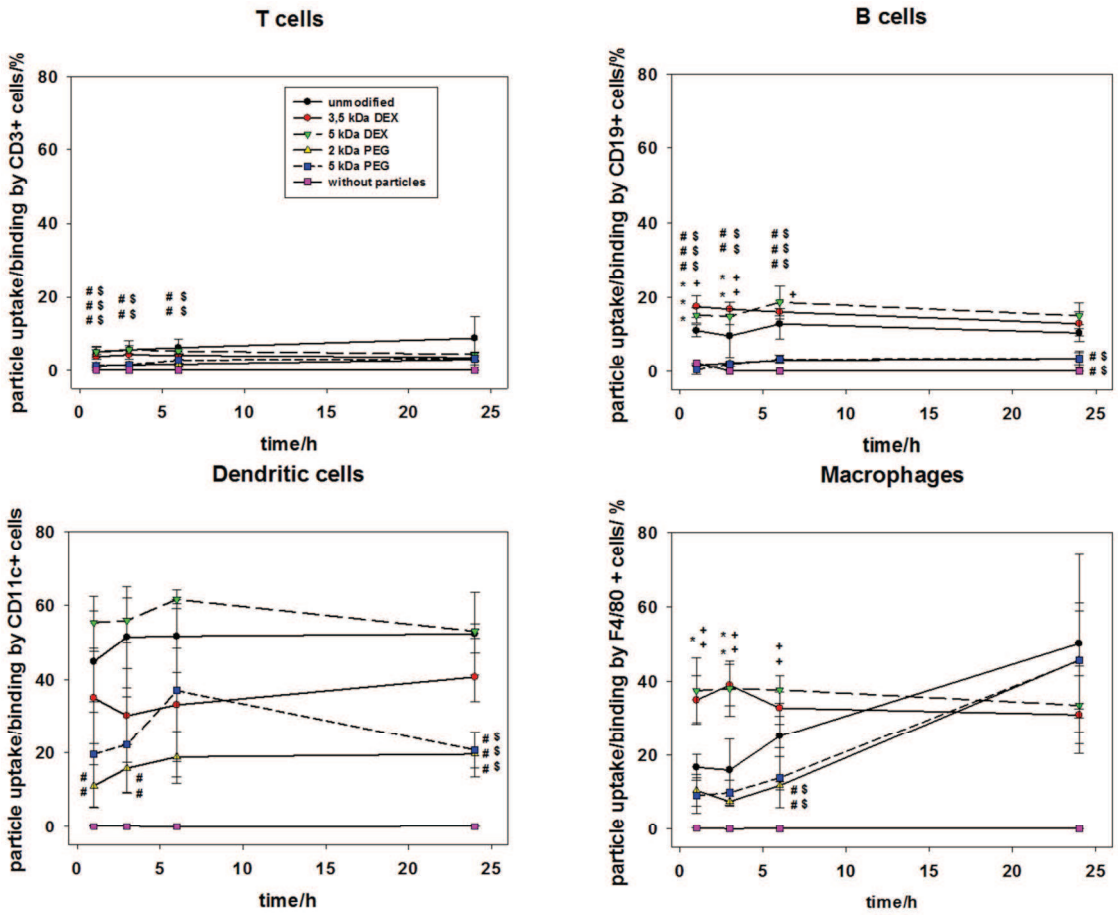

Figure 50: The binding of Sp-Ac-DEX particles by different spleen cell populations was analyzed by flow cytometry using untreated cells for the negative control. Four independent experiments were performed and the results are shown as the mean ± SD. The statistical analysis includes an ANOVA statistical test with ***p<0.001, **p<0.02, *p<0.05. Significant differences between the binding affinity of non-modified, PEGylated (# PEG 2 kDa, $ PEG 5 kDa), and DEXylated (* DEX 3.5 kDa, + DEX 5 kDa) particles can be shown.

For more information of the particle uptake by antigen-presenting cells, bone marrow-derived DCs (BMDC) and macrophages (BMMC) were analyzed in their binding affinities for Sp-Ac-DEX-based particles since the above describe spleen cell population consists only of less than 10% DCs and macrophages (see **Figure 51**).[295]

As described before in this section, PEGylated particles show only a low binding affinity to spleen cells which can be confirmed for the particle binding by BMDCs and BMMCs (**Figure 51**). Non-modified particles show only a slightly increased binding in the same experiment in contrast to DEXylated particles that show high binding affinities of about 40% to 60% within the first hour of incubation with BMDCs and BMMCs. The binding results for PEGylated and DEXylated particles by BMDCs and BMMCs are comparable to the binding affinities of splenic DCs and macrophages. Instead, non-modified particles show much lower binding by BMDCs and BMMCs compared to the previously shown binding by splenic antigen-presenting cells.

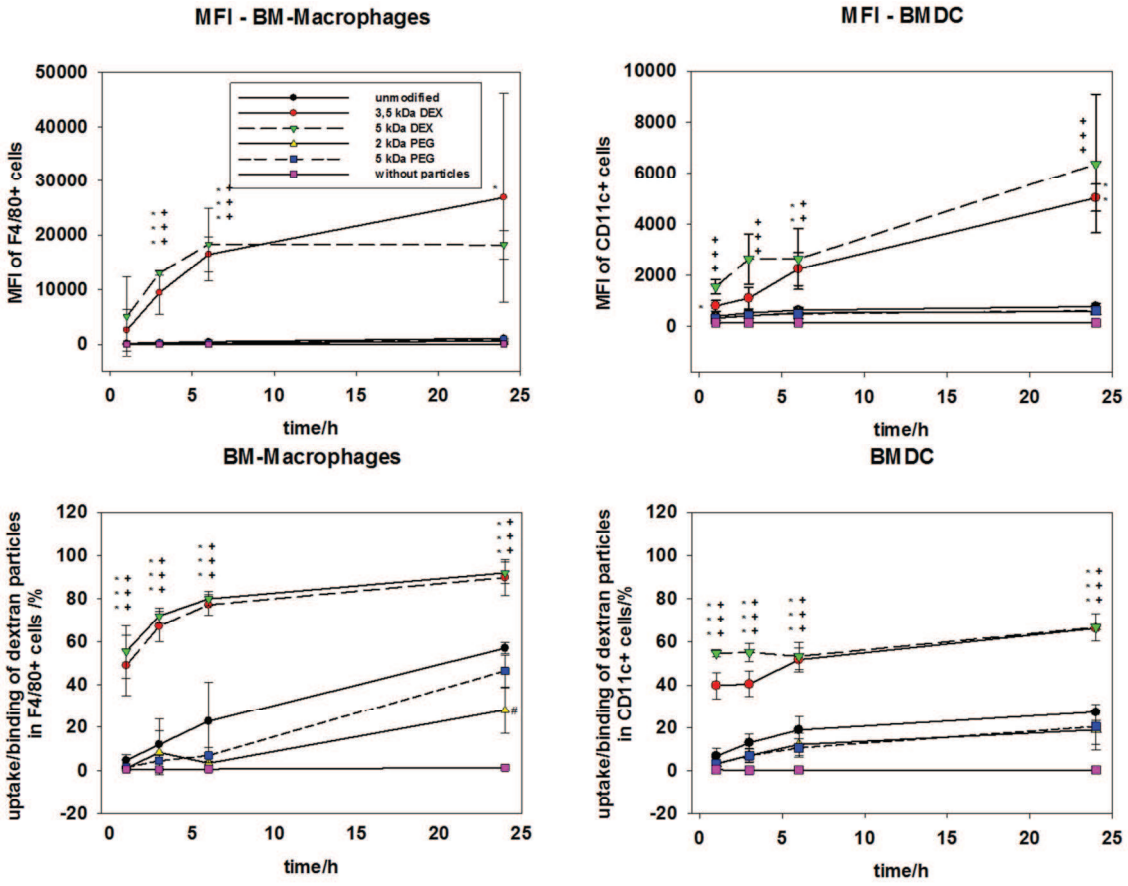

Figure 51: BMDCs and BMMCs were incubated with modified and non-modified Sp-Ac-DEX particles. The binding affinity of the particles was determined by flow cytometry consisting of three independent experiments. The upper row shows the MFI of the encapsulated fluorescent dex-OG488, whereas the lower row represents the mean ± SD uptake of the particles. The statistical analysis includes an ANOVA statistical test with ***p<0.001, **p<0.02, *p<0.05 and a significance of modified particles (# PEG 2 kDa, $ PEG 5 kDa, * DEX 3.5 kDa, and + DEX 5 kDa) compared to non-modified Sp-Ac-DEX particles.

In summary, PEGylation can prevent or at least reduce the binding of Sp-Ac-DEX particles by murine immune cells, spleen cells as well as bone-marrow derived APCs. In comparison, DEXylation of Sp-Ac-DEX particles enhances the binding by murine immune cells probably due to specific surface receptor interactions. Further experiments regarding the uptake mechanism of the particles by different cell populations show that Scavenger receptors have a huge impact in the uptake of the Sp-Ac-DEX particles (data of the manuscript "Surface Functionalization of Polysaccharide-Based Nanoparticles with PEG and Dextran Affects their Immune Cell Binding and Stimulatory Characteristics" listed in chapter 6.3).

Uptake of Ac-Dextran Nanoparticles in Murine Immune Cells Determined by Confocal Laser Scanning Microscopy

Since flow cytometry cannot distinguish between particles that stick on the cell surface and particles that are taken up by cells, confocal laser scanning microscopy was used to proof the cell uptake of the particles. Therefore, BMDCs and BMMCs were incubated with non-

modified, PEGylated (5 kDa) and DEXylated (5 kDa) Sp-Ac-DEX particles (10 $\mu g \cdot mL^{-1}$) for 4 hours. After staining the cell membrane and nucleus, particle uptake in the cells was pictured by confocal laser scanning microscopy (CLSM, **Figure 52**).

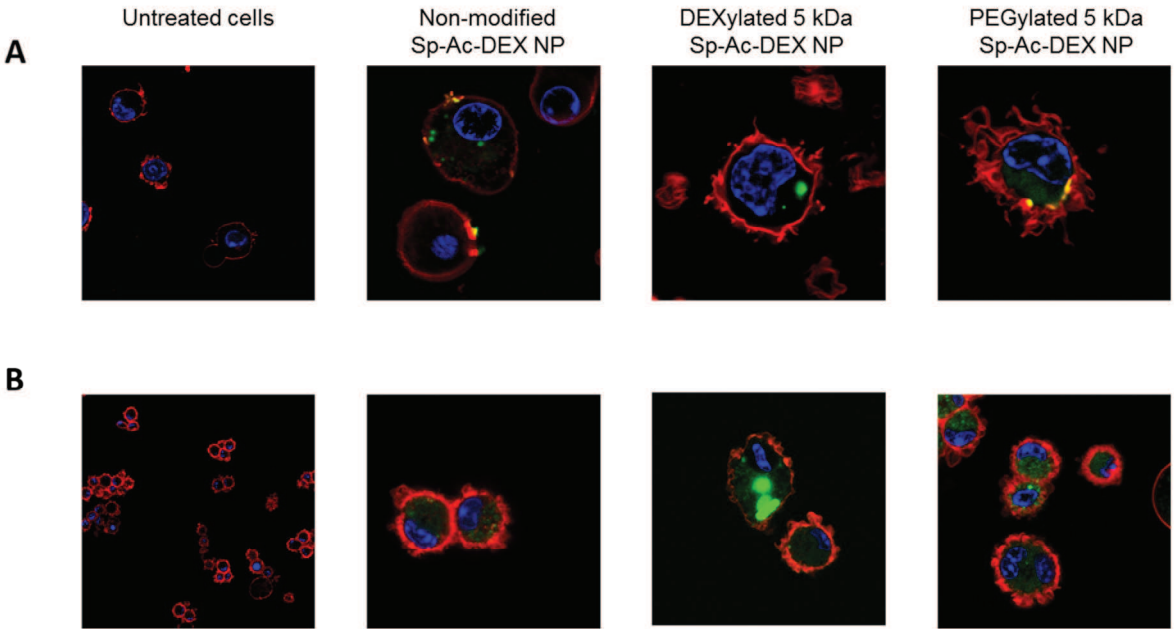

Figure 52: Confocal laser scanning microscopy images of BMDCs (A) and BMMCs (B) incubated with Sp-Ac-DEX-based particles (green) for 4 hours. The cell membrane (red) is stained with CellMask™ Orange and the nucleus (blue) with Hoechst 33342. The confocal images show that all detectable particles are taken up by cells and are not stuck on the cell surface. This proves the uptake results obtained by FACS measurements in the previous section that particles are taken up by the murine immune cells and are not only bound to the cell surface.

It can be shown that all three different particle formulations, mentioned above, are taken up by the cells after incubation for 4 hours. As described before in this section, DEXylated particles show higher fluorescence signals than PEGylated and non-modified particles which indicates that a higher number of particles are inside the cells. The fluorescence signals of PEGylated and non-modified particles are spread in the whole cytosol of the cells in contrast to distinct fluorescent areas in the cytosol of BMDCs incubated with DEXylated particles. This can be explained by a faster endosomal escape of PEGylated and non-modified particles compared to DEXylated particles that remain longer in intracellular vesicles. In summary, differences in cell binding, uptake, and localization of the modified Sp-Ac-DEX particles is shown.

3.2.10 *In Vitro* Transfection of DNA-Loaded Ac-Dextran Nanoparticles in HEK Cells

Since empty Sp-Ac-DEX-based particles show low toxicity and high uptake potential which is described in the above performed *in vitro* studies, further experiments include the encapsulation of a functional nucleic acid to analyze the transfection potential of the particles.

For first *in vitro* experiments, a plasmid DNA (pDNA) was encapsulated in Sp-Ac-DEX particles since siRNA encapsulation enhances the aggregation of Sp-Ac-DEX particles (described in section 3.1.2). Moreover, stable Ac-DEX microparticles encapsulating DNA were described by Beaudette *et al.* (2009)[78] before, so that the preparation of uniform DNA nanoparticles may be possible here using Sp-Ac-DEX as starting material. Therefore, a pDNA, encoding for luciferase, was encapsulated in Sp-Ac-DEX particles(8 μg DNA per mg NP) by a double emulsion evaporation method which was described in section 3.1.2. The particle batch was divided into two equal parts and one half of the particles was PEGylated (2 kDa) afterwards (described in section 3.2.1). The encapsulation efficiency of the encapsulated DNA was determined by Quant-iT™ PicoGreen® assay using the same DNA batch for the preparation of a standard curve. The quantification kit contains a compound which forms a fluorescent product after binding to the encapsulated DNA. The mechanism of the detection is similar to the Quant-iT™ RiboGreen® assay for the quantification of RNA which is described later in section 3.4.3. Although the dextran particles were degraded in acetate buffer pH 5 overnight and incubated with heparin for 1 hour before adding the PicoGreen® reagent, only 50.6% DNA (4 μg DNA per 1 mg NPs) was detected by the assay. The degradation of the particles in acetate buffer leads to the hydrolyzation of the acetals resulting in a water-soluble dextran modified with spermine which forms polyplexes with the pDNA. Therefore, heparin was added as a negatively charged agent which should compete with the bound DNA for the positively charged Sp-DEX material leading to the release of the DNA from the complex with spermine. Since Beaudette *et al.* (2009)[76] described an encapsulation efficiency of 99.8% for DNA in Ac-DEX microparticles, the here obtained low DNA encapsulation efficiency for Sp-Ac-DEX particles is surprising.

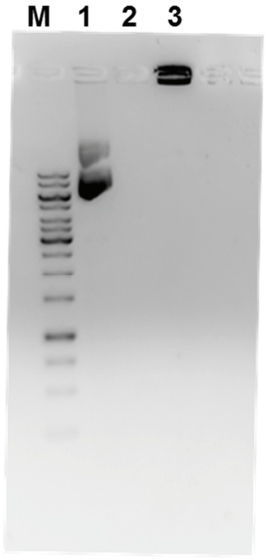

Figure 53: Agarose gel of the pDNA particle samples showing high amounts of DNA in the particle sample. The DNA was extracted by precipitation in ethanol after degradation of the Sp-Ac-DEX nanoparticles. The extraction of pDNA and the preparation of the agarose gel for the qualitative detection of the encapsulated pDNA were performed by [redacted] Line M: GeneRuler® 1 kB DNA ladder; line 1: 1699 plasmid DNA (200 ng/μL); line 2: Sp-Ac-DEX particles (-DNA); line 3: Sp-Ac-DEX particles (+DNA).

In cooperation with [redacted] the plasmid DNA was extracted with an ethanol precipitation from the degraded particle samples and analyzed on an agarose gel. **Figure 53** depicts the results of the agarose gel obtained after the run and staining with ethidium bromide. Line 1 shows the pure plasmid DNA sample and line 2 the negative control of the particle samples without DNA. Line 3 explains the low fluorescence yield after the quantification using the PicoGreen® assay. The spermine-modified dextran forms strong complexes with the pDNA so that a run of the pDNA in the gel is inhibited. The same complexes hinder the sufficient interaction of the pDNA with the PicoGreen® reagent leading to low encapsulation efficiencies.

In the following *in vitro* studies an encapsulation efficiency of 80% DNA was assumed due to the published results of Cohen *et al.* (2011).[86] Cohen showed an encapsulation efficiency of about 75% for siRNA in Sp-Ac-DEX nanoparticles. The mass of siRNA (8 μg siRNA per mg NP) is comparable to the here used mass of pDNA (8 μg pDNA per mg NP). Moreover, the here analyzed DNA particles consist of Sp-Ac-DEX-based nanoparticles, whereas Beaudette *et al.* (2009) used Ac-DEX microparticles for the encapsulation of DNA so that a different encapsulation potential between these two particle formulations is possible. Further quantification studies of encapsulated pDNA should be performed by measuring the free pDNA which is not encapsulated after the preparation of the particles. The same low encapsulation effect was observed for the quantification of encapsulated siRNA using the Quant-iT™ RiboGreen® assay leading to the method of detection of free siRNA in the particle supernatant (described in section 3.1.2).

Table 13: Sizes and zeta potentials of empty Sp-Ac-DEX nanoparticles (NP) and nanoparticles encapsulating a plasmid DNA (DNA-NP), both also in the PEGylated form (+ PEG), were measured by DLS using a Zetasizer Nano ZS.

Sp-Ac-DEX Particle Modification	Size before Purification			Size after Lyophilization			Zeta Potential (mV)
	Z-Av. (d.nm)	Number (d.nm)	PDI	Z-Av. (d.nm)	Number (d.nm)	PDI	
NP	192.4	113.4	0.221	241.7	233.7	0.283	14.4 ± 8.91
NP + PEG	137.0	99.3	0.088	229.3	209.0	0.213	10.5 ± 7.75
DNA-NP	204.9	129.8	0.187	288.0	225.0	0.357	6.20 ± 5.10
DNA-NP + PEG	257.0	218.7	0.253	305.3	242.3	0.347	3.71 ± 4.66

Table 13 shows the size and zeta potential of empty and DNA-loaded particles with the respective PEGylated particle samples. The obtained empty particles have an average size of about 140–190 nm before lyophilization, which increases after the lyophilization to 230–240 nm. As shown before in chapter 3.2.4, PEGylation prevents aggregation which leads to the formation of slightly smaller particle sizes. The encapsulation of DNA leads to an increase in the particle size. Particle sizes before purification are around 200–260 nm with a further increase in the size after lyophilization to 290–305 nm. Interestingly, PEGylation cannot prevent particle aggregation of DNA-loaded particles. The encapsulation of DNA leads to a decrease in the zeta potential from 14.4 mV to 6.2 mV for non-modified particles and from

10.5 mV to 3.7 mV for PEGylated particles. As mentioned before, particles with neutral zeta potential were described as not stable in aqueous buffers and start to flocculate. The decrease of the surface net charge of the particles that encapsulate DNA can be a reason for stronger aggregation effects.

First *in vitro* transfection experiments with pDNA-loaded Sp-Ac-DEX particles were performed using HEK 293T cells. HEK cells are human embryonic kidney cells, which are often used for transfection experiments due to their uncomplicated cell culture. The described DNA plasmid 1699 encodes for eGFP and luciferase but only the luciferase activities were detected. As it can be seen for the non-modified and PEGylated Sp-Ac-DEX particles (**Figure 54**), both particle formulations without DNA and the untreated cells show no luciferase signal so that false positive signals can be excluded. Therefore, the determined luciferase activity of the DNA-loaded particles can be related to an effective transfection of the pDNA.

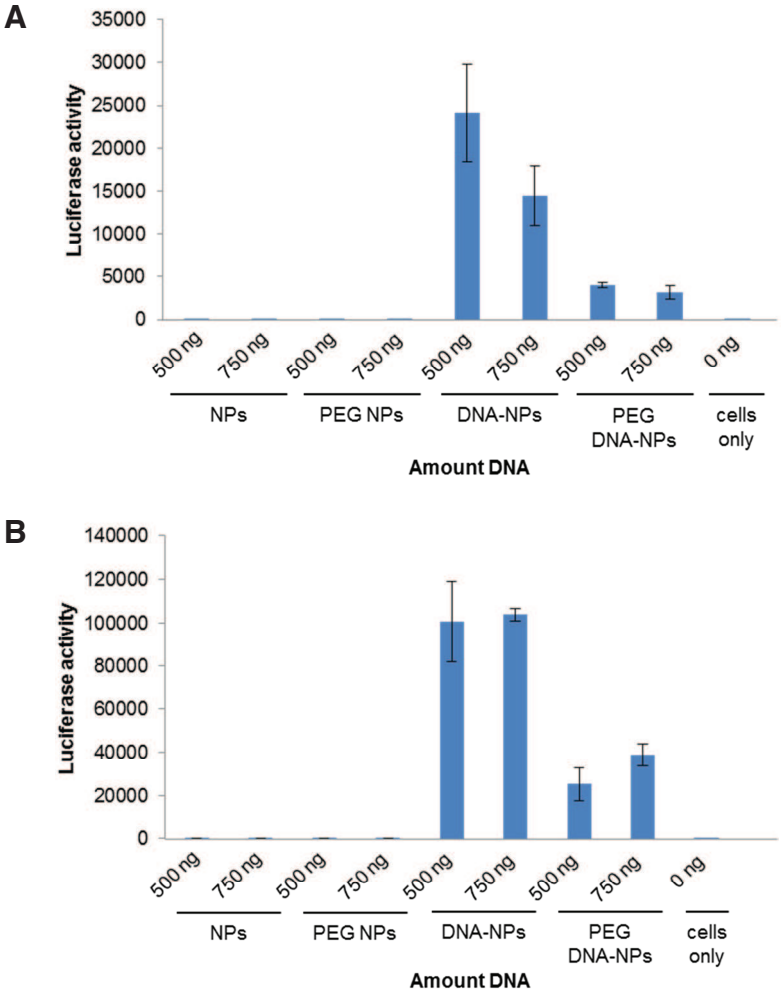

Figure 54: Shown is the transfection of the DNA plasmid 1699 with Sp-Ac-DEX-based nanoparticles in HEK 293T cells after the incubation for 24 hours (A) and 48 hours (B). **NPs:** empty Sp-Ac-DEX nanoparticles; **PEG NPs:** empty PEGylated (2 kDa) Sp-Ac-DEX nanoparticles; **DNA-NPs:** Sp-Ac-DEX nanoparticles encapsulating pDNA; **PEG DNA-NPs:** PEGylated (2 kDa) Sp-Ac-DEX nanoparticles encapsulating pDNA.

Since PEGylation reduces cell uptake of particles, as it was shown before (section 3.2.8 and 3.2.9), transfection efficiencies are also reduced compared to non-modified particles. Hence, the reduced uptake of PEGylated Sp-Ac-DEX particles leads to lower luciferase activities. The transfection efficiency can be enhanced by longer incubation times with the particles. In contrast, the application of more particles resulting in higher DNA amounts leads to controversial effects for non-modified particles. Maybe the cells are busy with particle uptake so that no difference in the transfection efficiency can be observed. Another reason can be enhanced toxicity of the non-modified particles in higher doses so that the cell number which can express the luciferase protein decreases. In further studies, the total protein content should be determined so that the outcome of the protein expression can be related directly to the amount of living cells. But a dose-dependent signal is detectable for PEGylated particles.

The uptake of the dextran-based particles was described as very fast before (section 3.2.9) and leads to hardly higher uptake effects after 3 hours of incubation. Increased luciferase activities can be explained by mechanisms inside the cell after the particle uptake. Particles with a size of 200 nm are known to be taken up by endocytic pathways (section 1.2.2). For an efficient transfection, the DNA has to reach the nucleus of the cells. Therefore, Sp-Ac-DEX particles have to escape from the endosomes and have to be degraded to release the encapsulated DNA. Particle fragments can cross the cell nucleus with the DNA or particles can be degraded before in acidic compartments and the DNA is delivered via different transport mechanism inside the nucleus. The mechanism of the DNA delivery to the nucleus has to be investigated in further experiments.

In summary, an efficient transfection of DNA was obtained in first experiments using Sp-Ac-DEX nanoparticles. Further studies should include transfection of DNA with PEGylated particles carrying targeting groups to specifically enhance the transfection efficiency again.

3.2.11 *In Vivo* Behavior of Ac-Dextran Nanoparticles

The *in vivo* biodistribution and toxicity experiments of modified Sp-Ac-DEX particles in mice were performed in the group of [redacted] (Universitätsmedizin Mainz) by [redacted]

Biodistribution of Sp-Ac-DEX Nanoparticles in Mice

Non-modified and PEGylated (2 kDa) Sp-Ac-DEX particles were suspended in PBS (1 mg·mL^{-1}) and injected retroorbital in anesthetized Balb/c wild type mice (500 μg NPs per mouse). The additional control group of mice was treated with PBS. Mice were imaged at certain time points using an IVIS series pre-clinical near infrared (NIR) *in vivo* imaging system with the Living Image® software to analyze the data (PerkinElmer, Waltham, MA, USA). After 24 hours, mice were sacrificed and organs were harvested for *ex vivo* imaging.

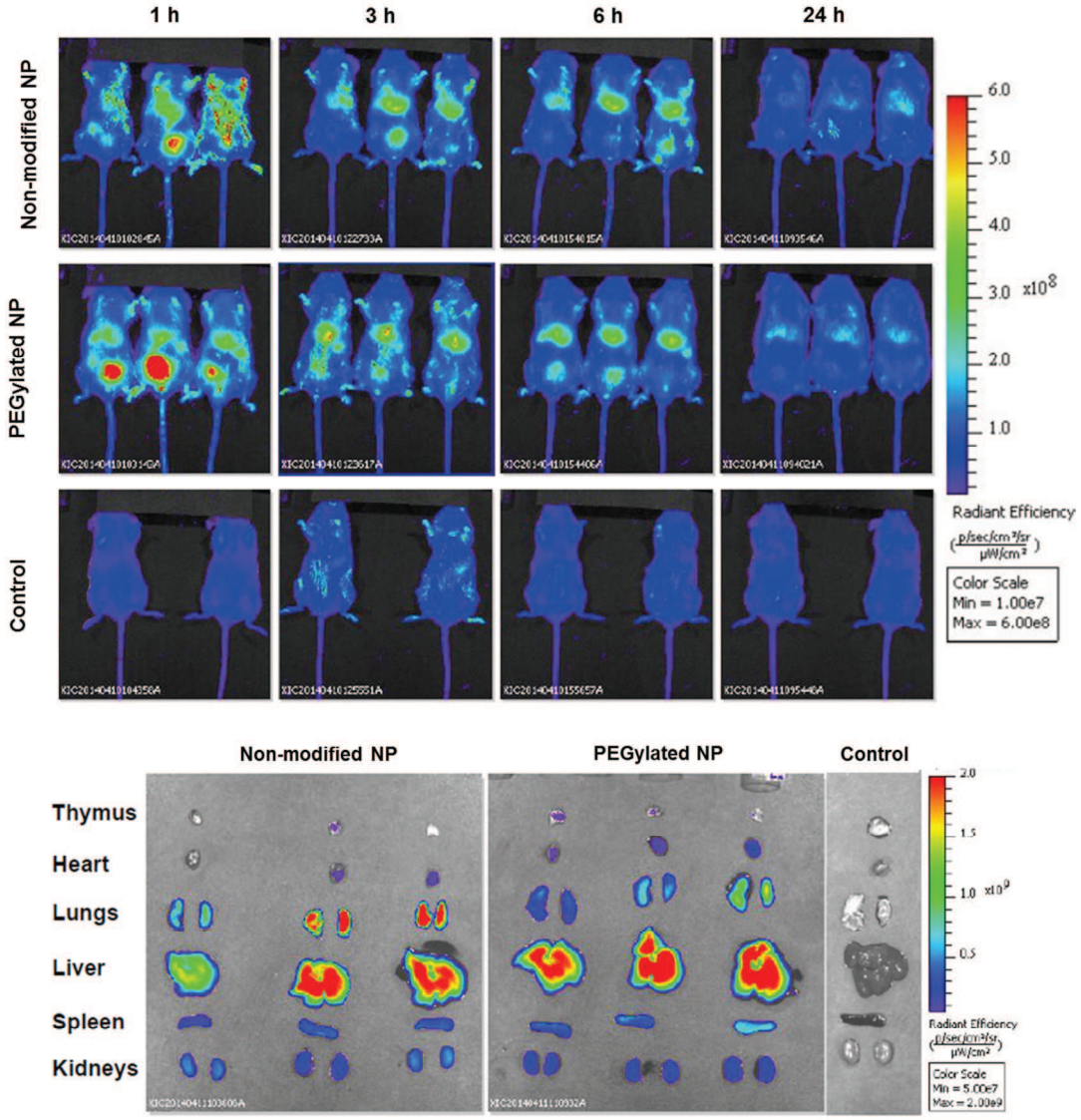

Figure 55: *In vivo* biodistribution of Cy5-labeled non-modified and PEGylated (2 kDa) Sp-Ac-DEX nanoparticles in Balb/c wild-type mice for up to 24 hours. Shown are the images of the living mice and the scan of the organs after 24 hours.

In vivo biodistribution of Sp-Ac-DEX particles shows that non-modified particles are spread in the whole mouse one hour after administration, whereas PEGylated particles are mainly located in the liver and bladder (see **Figure 55**). High bladder signals are signs for non-stable particles or very small particles that are cleared from the blood circulation by the kidneys. Particles less than 10 nm are known for a rapid renal clearance, whereas bigger particles stay in the blood circulation, are taken up by cells or recognized by the mononuclear phagocyte system (MPS).[115] After 24 hours, only a low particle signal in the living mice is detectable. Afterwards, the mice were sacrificed and the organs harvested to get more information about the particle distribution. The harvested organs show a high liver signal accompanied with a high signal of non-modified Sp-Ac-DEX particles in the lungs. The accumulation of the particles in the lungs can be explained by bigger aggregates of these non-modified particle types which are formed during the lyophilization process and hard to disaggregate. Another

explanation is the aggregation of the particles after *in vivo* administration due to strong interaction with plasma proteins. The interaction of adsorbed proteins on the nanoparticle surface or the high amount of adsorbed proteins can also lead to increased aggregation of Sp-Ac-DEX particles. Instead, PEGylated particles show only a strong liver signal due to smaller particle sizes and less aggregation behavior. It is remarkable that there is hardly any signal of both particle formulations in the kidneys after 24 hours. Sp-Ac-DEX particles can be classified therefore as highly stable and are probably taken up by liver cells, which needs to be analyzed in further experiments.

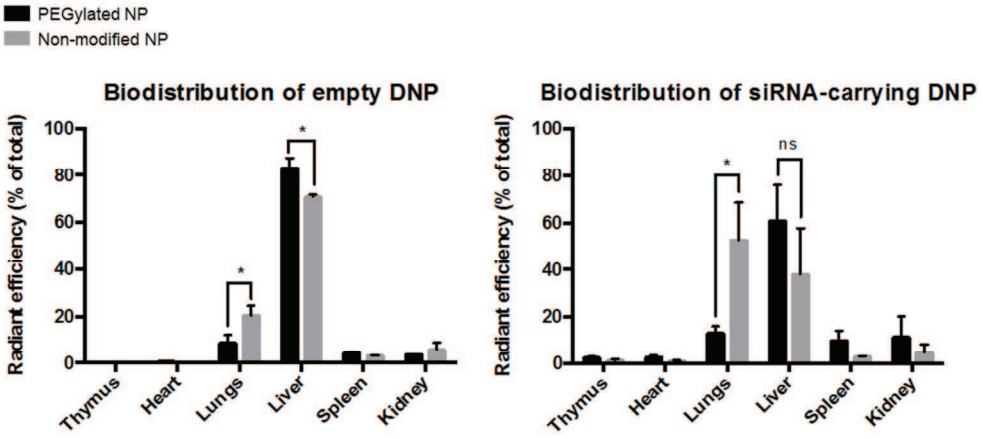

Figure 56: *In vivo* organ uptake of Sp-Ac-DEX nanoparticles (left: empty, right: siRNA-carrying) in the harvested organs is shown displayed as the fluorescence intensity (n = 3; *p<0.05). Empty nanoparticles are labeled with Cy5 on their surface, whereas Cy5-siRNA-carrying nanoparticles are labeled with Oregon Green® 488 on their surface.

Figure 56 displays the ratio of PEGylated vs. non-PEGylated particles in every organ. The harvested organs were prepared and the fluorescence of the particles scanned and quantified in relation to the total amount of particles taken up by cells. As it was described before in this section, most particles are taken up by the liver (more than 80% for PEGylated particles). Non-modified particles show a higher signal in the lungs (~25%) than PEGylated particles (~10%) due to stronger aggregation behavior and therefore accumulation in tiny lung capillaries. If siRNA is encapsulated in the nanoparticles this effect is even stronger due to enhanced aggregation behavior of the non-modified nanoparticles. Approx. 50% of the non-modified particles (+siRNA) accumulate in the lungs in contrast to PEGylated nanoparticles (<20%) after 24 hours. Liver signals are still high for both particle formulations with lower signals in the spleen and kidneys which are both organs for the clearance of particles from the blood. Smaller particles are cleared by the kidneys as mentioned before and larger particles are cleared by the mononuclear phagocyte system (MPS) located in the spleen and liver.[296]

PEGylation is described in the literature as a mechanism to prolong blood circulation of particles, which still needs to be analyzed. Maybe a denser PEG-layer or smaller particles can improve the particle behavior regarding blood circulation time. With the current particle formulations only targets in the liver can be addressed. However, the attachment of specific

targeting groups might lead to organ or cell specific uptake mechanisms. This has to be determined in future experiments.

Uptake of Sp-Ac-DEX Nanoparticles in Liver Cells

The main cell populations of the harvested liver were prepared to investigate the particle uptake in each cell type. Cells were scanned by flow cytometry using the fluorescence of the Oregon Green® 488-labeled particles to quantify their ratio in the different cell populations.

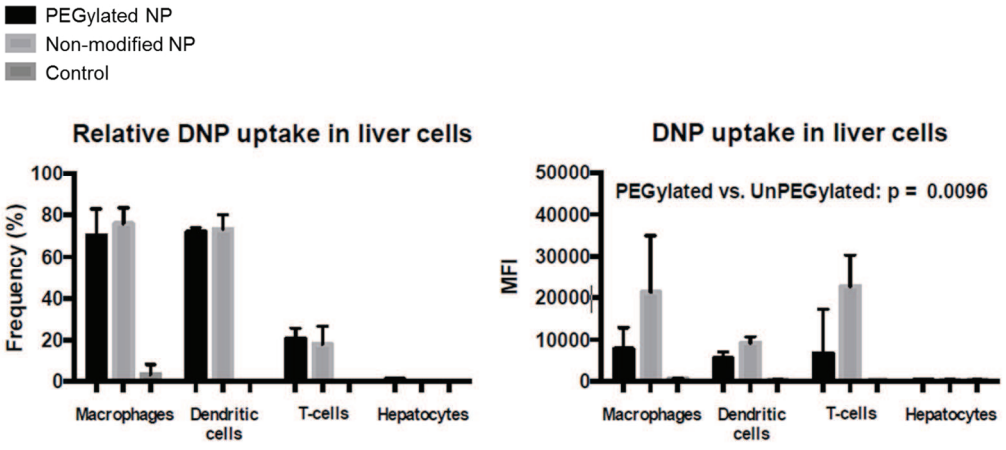

Figure 57: *In vivo* uptake of Sp-Ac-DEX particles in the liver. Liver cells of the harvested organs were isolated and stained to show the major cell populations (macrophages: CD45 and F4/80; dendritic cells: CD45 and CD11c; T-cells: CD3e; hepatocytes: albumin). Cells were analyzed by flow cytometry using the fluorescent dye Oregon Green® 488 on the nanoparticle surface for detection.

As it was shown before *in vitro* (chapter 3.2.8), most particles are taken up *in vivo* by liver macrophages and dendritic cells (~70%). It is remarkable that particles enter T cells *in vivo* in little concentrations (~20%) in contrast to the *in vitro* results for splenic T cells (chapter 3.2.9). Nearly none of the particles is taken up by hepatocytes (<1%). PEGylation has again a great impact on the particle uptake leading to decreased fluorescence signals compared to non-modified Sp-Ac-DEX particles. Therefore, PEGylation seems to reduce the uptake of particles in hepatic cells from 40% to 70% and the formerly described reduction of the cell uptake *in vitro* can be described here *in vivo*, too.

***In Vivo* Toxicity of Sp-Ac-DEX Nanoparticles**

To study the *in vivo* toxicity of non-modified and PEGylated Sp-Ac-DEX particles, particles (~20 mg NP·kg^{-1} body weight) were administered in Balb/c mice once a week. After three weeks, blood samples were taken and analyzed for the serum markers creatinine, alanine transaminase (ALT), aspartate transaminase (AST), and alkaline phosphatase (AP). These enzymes are related to inflammatory processes and are therefore indicators for organ damage (see **Figure 58**).[297-298]

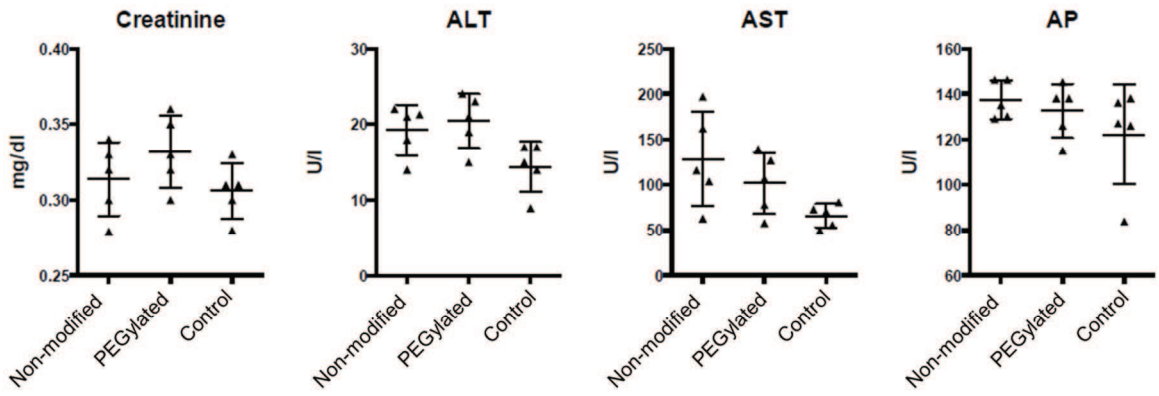

Figure 58: Serum markers extracted from the blood of Balb/c mice after 3 weeks. Increased concentrations are signs for toxic effects which cannot be detected here after the *in vivo* administration of Sp-Ac-DEX nanoparticles.

Regarding the serum markers, no liver (ALT, AST, and AP) or kidney (creatinine) damage was obtained although the mice were treated with high doses of nanoparticles for three weeks. The concentration of serum markers are not significantly changed compared to the samples of the control mice. Therefore, non-modified and PEGylated particles can be declared as biologically safe *in vivo*. Next studies should include an efficient siRNA transport and gene knockdown. Since most dextran-based particles are located in the liver macrophages, an appropriate model system can be evaluated for next applications, for example liver cancer.

3.3 Targeting Strategies

Chapter 3.1 describes the development of polysaccharide nanoparticles without further modification (first generation particles.) In the following chapter 3.2 these particles are modified on their surface with a hydrophilic layer that should prolong blood circulation and prevent aggregation of the particles (second generation particles). Now, this chapter will describe first strategies for the introduction of targeting groups (third generation particles). These particles are characterized by a hydrophilic PEG layer combined with the attachment of target structures. Therefore, Sp-Ac-DEX particles were surface-modified with a bifunctional PEG followed by first experiments for a later attachment of target structures.

Functionalization of Sp-Ac-DEX Nanoparticles with a Bifunctional PEG

For the PEGylation, Sp-Ac-DEX particles were resuspended in borate buffer (pH 8.5, 0.1 M) and incubated with a homo-bifunctional PEG-NHS for 2 hours (**Figure 59**). PEG was added in equimolar ratios to the surface amines of the particles to prevent cross-linking. The time for the bifunctional PEGylation was not changed compared to the monofunctional PEGylation described in chapter 3.2.1. But in this experiment for the bifunctional PEGylation the amount of used PEG was decreased from a 10-fold excess to equimolar ratios to the amines on the particle surface to prevent crosslinking of the PEGylated particles by the free NHS-group of the PEG. Furthermore, particles were resuspended more diluted in concentrations of 1 $mg \cdot mL^{-1}$ instead of 2 $mg \cdot mL^{-1}$ to reduce the risk of crosslinking.

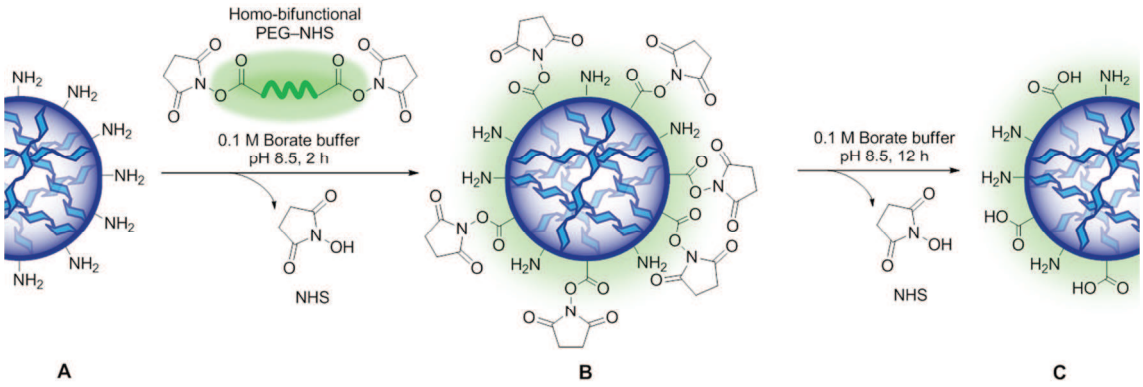

Figure 59: Scheme of the bifunctional PEGylation of Sp-Ac-DEX particles. Sp-Ac-DEX particles (A) are incubated with a homo-bifunctional PEG-NHS in borate buffer for 2 hours leading to PEGylated Sp-Ac-DEX particles with NHS-functions on the particle surface (B). Unreacted PEG-NHS is removed and particles are incubated for further 12 hours in borate buffer to hydrolyze the surface NHS-groups. Sp-Ac-DEX particles with surface carboxyl-functions are obtained (C).

After PEGylation, the particles were ultracentrifuged to remove unreacted PEG. Finally, the modified particles were resuspended in fresh borate buffer and stirred for 12 hours to hydrolyze the unconjugated NHS-groups of the PEG chains. More basic borate buffer was used here for the resuspension of the particles to prevent a hydrolysis of the Sp-Ac-DEX particles due to longer reaction times compared to the monofunctional PEGylation of the

particles. Finally, PEGylated Sp-Ac-DEX particles with free carboxyl groups were purified by ultracentrifugation and rinsing of the pellet. After lyophilization, purified PEGylated particles were obtained with a yield of 81% (compared to the initial particle mass).

Table 14: Reaction conditions for the PEGylation of Sp-Ac-DEX nanoparticles with a homo-bifunctional PEG-NHS

Medium	borate buffer (pH 8.5, 0.1 M)
PEG	1 eq.
M_W PEG	2 kDa
Conc. NPs	1 mg·mL^{-1}
Time (PEGylation)	2 h
Time (hydrolysis)	24 h
Temperature	rt

The particle size of the PEGylated dextran particles was measured by NTA leading to an average size of 240 nm (mean) with the biggest population around 154 nm (mode). Crosslinking of particles during the PEGylation cannot be observed due to small particle sizes and hardly an increase compared to the initial size (mean: 221 nm, mode: 148 nm). The zeta potential decreases from about +19 mV to +3 mV. This can be explained by the decrease of surface amines and the increase of carboxyl groups which can cause more negative surface net charges.[248]

Conjugation of Target Structures to a PEGylated Nanoparticle

For the first conjugation of a target structure, the amino acid lysine with a Fmoc-protection group was used as a model structure. The advantage of this compound is the detection possibility via the fluorescence of the Fmoc-group which can be used for the quantification of attached targeting moieties. Therefore, the PEGylated particles were resuspended in phosphate buffer (pH 7.4, 0.1 M) and incubated with *H*-Lys(Fmoc)-OMe · HCl (Lys) and the coupling agents EDC and NHS for 15 hours. As described before, particles were purified by ultracentrifugation and lyophilized afterwards.

Table 15: Reaction conditions for the attachment of targeting structures to PEGylated Sp-Ac-DEX nanoparticles

Medium	phosphate buffer (pH 7.4, 0.1 M)
Coupling agent	EDC·HCl (12 eq.)
Coupling additive	NHS (10 eq.)
Amino acid	*H*-Lys(Fmoc)-OMe · HCl (12 eq.)
Conc. NPs	2 mg·mL^{-1}
Time	15 h
Temperature	rt

Usually, EDC coupling is performed in acidic buffers. But Sp-Ac-DEX particles undergo hydrolyzation under acidic conditions so that a neutral reaction buffer compromise particle stability and EDC reactivity. The amine in the side chain of the amino acid lysine was protected by the Fmoc-group and the carboxyl group was protected by a methoxy group to prevent cross linking during the conjugation reaction. Only the primary amine of lysine can react with the carboxyl groups of the PEGylated particles. EDC activates the carboxyl groups on the PEG chains of the particles to enhance an activation reaction with NHS. As described before, NHS-activated carboxylic acids are highly reactive and easily form stable amide bonds with amines.

The obtained low particle yields (58%, compared to the initially used particle mass) can be explained by possible started hydrolysis of the particles during the conjugation reaction. It can be noted that Lys-modified particles hardly increased in their size (mean: 240 nm, mode: 170 nm). Higher mode values are in the range of the standard deviation but can be also explained by slightly aggregation of the particles. Slightly aggregation of the Lys-particles can occur due to the changed surface potential compared to non-modified particles which contain higher numbers of hydrophilic primary amines on their surface. The zeta potential increases again to 12 mV which is a qualitative proof for the reduction of carboxyl groups on the particle surface. The quantification of the attached lysine is described in the next section.

Quantification of the Attached Targeting Groups

First, the degree of PEGylation was determined by fluorescamine assay and compared to the amounts of primary amines on the particle surface before the modification with PEG. Since all NHS-esters should be hydrolyzed, the number of modified amines corresponds to the number of carboxyl groups on the particle surface. Afterwards, the attached amino acid was determined by measuring the fluorescence of the Fmoc-protection group using the pure amino acid for the preparation of a standard curve.

Approximately 23% of the primary amines on the Sp-Ac-DEX nanoparticle surface can be functionalized with the bifunctional PEG. The fluorescamine assay is very sensitive so that little changes in pipetting or particle preparation can have a high impact on the reactivity of fluorescamine with the primary amines. This can be seen in a relatively high standard deviation. Therefore, the degree of substitution for the attachment of the amino acid can be only described by an area. NHS-activated PEG can also react with secondary amines on the particle surface which can enhance the amount of carboxyl groups on the particle surface. But since secondary amines are less reactive and only a low amount of PEG was used for the functionalization most reaction should be occurred with the primary amines. The attachment of Fmoc-lysine quantified via the fluorescence of the Fmoc results in a high modification of around 88% to 100% of the introduced carboxyl functions (**Table 16**).

Table 16: Degree of substitution for PEGylated Sp-Ac-DEX particles with an attached target structure. The degree of substitution describes (A) the amount of reacted primary amines on the particle surface for the PEGylation and (B) the amount of reacted carboxyl-functions of the PEGylated particles with Fmoc-Lys.

Nanoparticle Modification	**Amount of groups / nmol·mg^{-1} NPs**	**Degree of Substitution / %**
PEG-COOH	26.2 ± 9.5	23 ± 4
Fmoc-Lys	29.4 ± 1.9	88–100

In summary, a successful targeting strategy of a PEGylated particle can be described. Next experiments should include the conjugation of a functional targeting group like mannose, folic acid or antibodies and the investigation of the particle uptake behavior *in vitro*. Consistent particle sizes during the surface modification promise a stable particle modification method for further studies.

3.4 Lipid-based Dextran Nanoparticles

Lipid-DEX nanoparticles were prepared, characterized and analyzed in the lab of [redacted] at the UT Southwestern Medical Center in Dallas (Texas, USA) during a research stay from October 2015 to April 2016. The intention included the development of a dextran-based particle system with high encapsulation of siRNA and small, uniform sizes of the particles. The encapsulation of high amounts of siRNA in Sp-Ac-DEX double emulsion particles leads to huge particle sizes and aggregation as described before in chapter 3.1.2. The lab of [redacted] has high expertise in the synthesis of lipid-based nanoparticles (LNPs) and the use of a special microfluidic mixing instrument for the preparation of small and uniform particles that are able to encapsulate high amounts of siRNA.[197] This NanoAssemblr™ mixing technology was used to prepare particles consisting of Sp-Ac-DEX (synthesis described in 5.4.1) and commercially available lipids (cholesterol, DSPC and PEG-lipid) with high amounts of siRNA.

3.4.1 Preparation of Lipid-DEX Nanoparticles

Lipid-DEX particles were prepared by dissolving Sp-Ac-DEX, cholesterol, 1,2-distearoyl-*sn*-glycero-3-phosphocholine (DSPC), and PEG-lipid (SUNBRIGHT® mPEG2000-DMG) or Pluronic® F-68, the main particle forming components, in ethanol. The siRNA, which should be encapsulated, was dissolved in PBS and the two solutions were rapidly mixed together using the NanoAssemblr™ technology. This instrument contained of a continuous flow system of two different streams (*here:* ethanol and PBS) that were mixed by a chaotic flow through a staggered herringbone micromixer resulting in small and uniform particles described before by Zhigaltsev *et al.* (2012).[299]

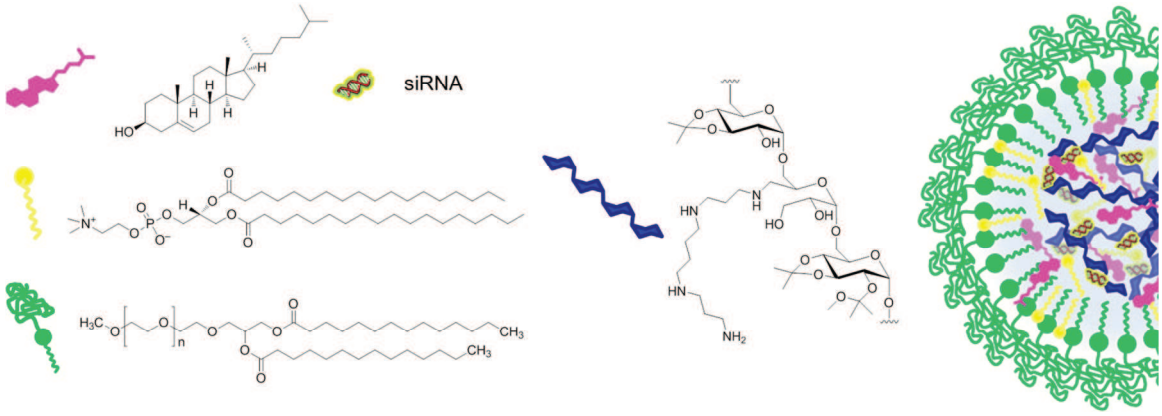

Figure 60: Scheme of a lipid-DEX nanoparticle. The negatively charged siRNA is bound to the cationic Sp-Ac-DEX (blue) and cationic head-groups of the DSPC (yellow) in the center of the nanoparticle. DSPC and cholesterol (pink) help to form a uniform particle. The outer layer is formed by a PEG-lipid (green).

The structure of these LNPs formed by a microfluidic mixing system was described before by Leung *et al.* (2012)[300]. During the mixing process, Sp-Ac-DEX as a cationic compound forms

complexes with the negatively charged siRNA. The helper lipids DSPC, containing a cationic end, and cholesterol form a layer around the Sp-Ac-DEX/siRNA complexes building the main particle. Finally, the PEG-lipid forms the outer layer between the hydrophilic and lipophilic interface. For the formulation of lipid-DEX nanoparticles an adapted protocol described by Hao *et al.* (2015)[197] was used combining different ratios of the lipid mixture and siRNA.

The prepared particles were obtained as an opaque, colorless suspension after formation with the NanoAssemblr™ and no change of the turbidity could be observed after purification by dialysis. Particles with a high siRNA concentration of 250 ng·μL^{-1}, which also contain high amounts of lipids and siRNA, are more opaque and tend to form aggregates after an hour when stored in an Eppendorf tube on the bench. Therefore, a more diluted particle mixture resulting in a siRNA concentration of 25 ng·μL^{-1} was the preferred method of choice for most particle preparations. In the following we discuss several ratios of the individual particle components and the influence on the resulting particle size and transfection efficiency.

3.4.2 Determination of the Nanoparticle Size and Zeta Potential

The hydrodynamic diameter and zeta potential of the particles was measured in aqueous buffers using a Malvern Zetasizer Nano ZS and dynamic light scattering (DLS) technology.

Influence of Different Amounts of PEG-lipid

Lipid-DEX particles with a relative high amount of PEG-lipid (10% PEG-lipid) lead to the formation of small particles with a uniform size of approx. 200 nm in diameter (**Figure 61**). The mixture of lipids containing only 5% PEG-lipid forms big particles in the micrometer scale, whereas the same mixture of lipids (5% PEG-lipid) without Sp-Ac-DEX leads to small and uniform particles again. The composition and ratio of PEG-lipid and Sp-Ac-DEX seem to be important for the formation of small and uniform nanoparticles. But it can be also shown that the cationic Sp-Ac-DEX is not necessarily needed for the preparation of small particles.

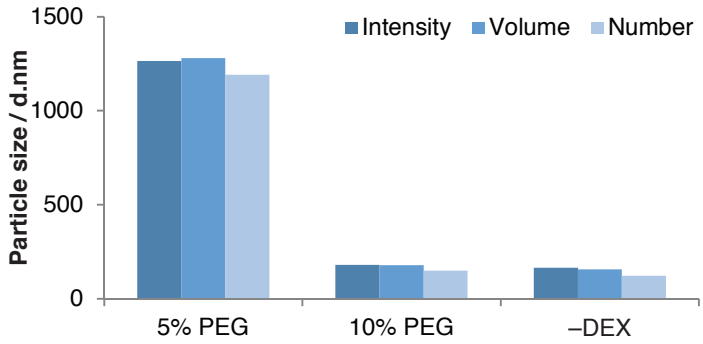

Figure 61: Size measurements of lipid-DEX particles with different ratios of PEG-lipid.

Influence of Different Amounts of siRNA

DLS measurements of particles with high siRNA concentrations (250 ng·μL^{-1}) show that the lipid-mixture with 10% PEG (see lipid-mixture A in **Figure 62**), which results in small particles for an siRNA concentration of 25 ng·μL^{-1}(see previous section), leads to increased particle sizes of about 1 μm. The increase of DSPC (B) or cholesterol (C) leads to the formation of even bigger particles compared to the initial mixture with 10% PEG-lipid (A) and cannot prevent aggregation or help to prepare monodisperse, small nanoparticles. But when the ratio of PEG-lipid is increased to 17%, the nanoparticle formulation is able to form smaller particles (see lipid-mixture D in **Figure 62**). The main population has a size of approx. 200 nm but bigger aggregates with a size of about 500 nm are still detectable. The same mixture of 10% PEG-lipid without Sp-Ac-DEX (E) leads to the smallest and more uniform particles. These results show that an increase of the siRNA concentration in the particle sample by concentrating the two mixing solutions of PBS and ethanol is not possible without an increase in the particle size. But it can be shown, as described before, that Sp-Ac-DEX is the critical component influencing the size. Particles without the cationic dextran are 3-times smaller than the same formulations containing Sp-Ac-DEX (D, 17% PEG-lipid). The increase of PEG-lipid in the formulation is able to reduce the size of the particles but aggregates are still detectable resulting in a bigger particle size shown by the size values of intensity and volume determined by DLS measurements.

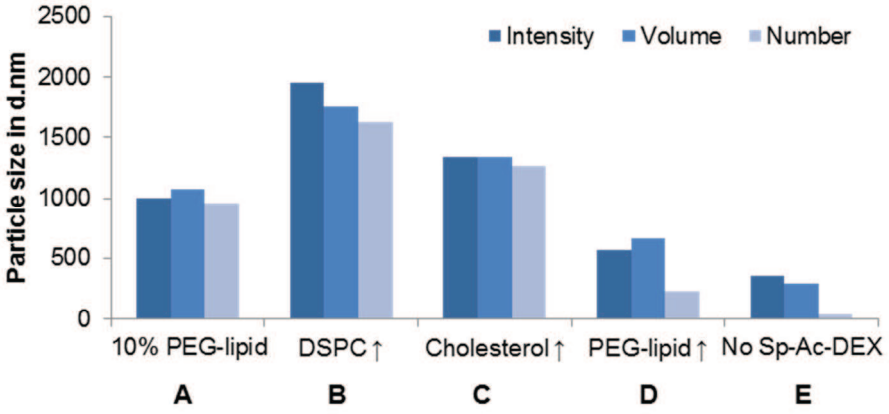

Figure 62: Size measurements of lipid-DEX particles with increased siRNA concentrations (250 ng·μL^{-1}) and increased ratios of the used lipids (B), (C), and (D). (A) Lipid formulation with 10% PEG-lipid which was described before as the best formulation for a siRNA concentration of 25 ng·μL^{-1}. (E) Same lipid formulation as mix D with increased PEG-lipid but without Sp-Ac-DEX.

Influence of Different Types of Surfactants

As described before in this chapter, a certain amount of PEG-lipid (10% for a siRNA concentration of 25 ng·μL^{-1}) is necessary to form uniform particles of Sp-Ac-DEX using the NanoAssemblr™ technology. Since the particle size of the optimized formulations is still around 200 nm, a different surfactant is analyzed to further reduce the particle size (**Figure 63**). Pluronic® F-68, a poloxamer, is known in the pharmaceutical industry as a surfactant with micelle-building opportunities.[301] PEG-lipid was substituted with Pluronic® F-68 and the size

of the particles in PBS was determined 2 hours after the particle preparation. It seems that Pluronic® F-68 cannot help to perform smaller particles but can slightly prevent aggregation when particles are stored in PBS over time. This might be useful since particles sometimes need to be stored for a few hours after preparation before they can be applied *in vitro* or *in vivo*.

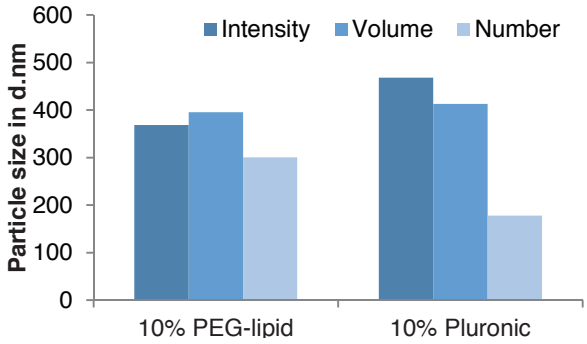

Figure 63: Size of lipid-DEX particles prepared with PEG-lipid or Pluronic® F-68 as surfactant.

The particle size by number describes the biggest population of particles in the sample and it is therefore expected that an increase of the size by intensity and volume can be explained by the formation of aggregates during storage. Summarized, particle diameters are still around 200 nm and the particle size cannot be further reduced by replacing PEG-lipid with Pluronic® F-68 (see **Figure 63**). The increase of the particle size after storage in PBS for 2 hours demonstrates the aggregation behavior of the particles so that a subsequent use of the particle suspension should follow directly after the particle synthesis.

Both particle formulations, using 10% PEG-lipid or Pluronic® F-68, show a negative zeta potential although they consist of a high amount of cationic Sp-Ac-DEX. Pluronic® F-68 particles (-5 mV to -7 mV) are less negative than the 10% PEG-lipid particles (-10 mV to -16 mV). Buffers with increased HEPES concentrations lead to an increased zeta potential which can be explained by an enhanced interaction of the buffer with the charged particle surface. The surface charge can be a critical point regarding the cell uptake of particles. Cell membranes are known to be negatively charged because of their protein and lipid composition.[302] For a high uptake, cationic charged particles are preferred since they can interact with the negative charges of the cell membrane. The uptake behavior of the particles is described later in chapter 3.4.5.

Table 17: Zeta potential measurements of lipid-DEX particles with the final lipid-DEX formulation (10% PEG-lipid) compared to Pluronic® F-68 particles as PEG-lipid alternative.

HEPES buffer	PEG-lipid	Pluronic® F-68
5 mM	-15.5 mV	-6.9 mV
25 mM	-10.2 mV	-4.9 mV

In conclusion, the best particle formulation can be obtained with the use of 10% PEG-lipid regarding the determined particle sizes. Small particles can be only obtained with a final siRNA concentration in the particle suspension of 25 ng·μL^{-1} in PBS. The trials to concentrate the lipid and siRNA mixture with a final siRNA concentration of 250 ng·μL^{-1} in PBS led to disappointing results with particles of micrometer sizes. With the mixture of 10% PEG-lipid and siRNA of 25 ng·μL^{-1}, uniform particle sizes of around 200 nm can be achieved. If significantly smaller particles can be formed with Pluronic® F-68 needs to be proven in further mixture experiments.

3.4.3 siRNA Binding and Encapsulation Efficiency by Lipid-DEX Nanoparticles

The encapsulation efficiency of the prepared particle samples was determined by using Quant-iT™ RiboGreen® RNA reagent (Invitrogen). Samples of the particle suspensions were taken directly after the preparation with the NanoAssemblr™. Only unbound siRNA that is not encapsulated in a particle is able to react with the RiboGreen® reagent and can form a fluorescent compound. Low signals of the fluorescent dye result therefore in a high binding or encapsulation of siRNA on or in the particles.

Both particle formulations with 5% and 10% PEG-lipid show a high encapsulation of siRNA-*luc* over 94% (intended siRNA conc. 25 ng·μL^{-1}, **Figure 64**). Particles without the cationic Sp-Ac-DEX instead show only an encapsulation of 48.7% siRNA-*luc*. Therefore, Sp-Ac-DEX is important for the formation of uniform particles with a high encapsulation of siRNA.

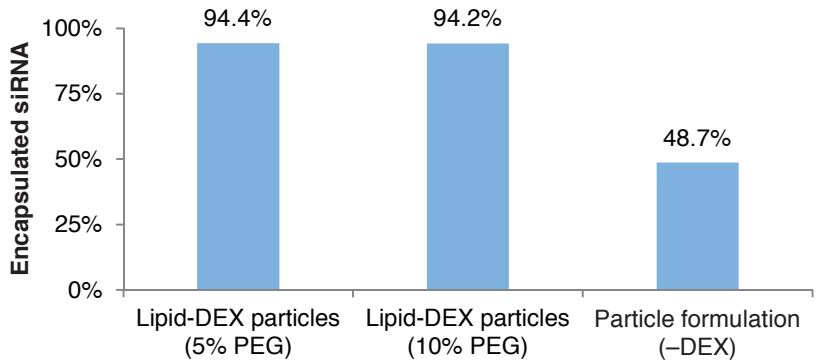

Figure 64: Quantification of the encapsulated siRNA-*luc* in lipid-DEX particles with different amounts of PEG-lipid in the formulation.

PEG-lipid particles compared to particles with Pluronic® F-68 show no advantage in the encapsulation efficiency of siRNA-*luc* (**Figure 65**). Both systems encapsulate high amounts of siRNA with efficacies of about 93%. This can be explained by the assumption that the cationic Sp-Ac-DEX and minimally also the cationic DSPC are mainly responsible for high loading efficiencies of siRNA in the particles. Low encapsulation of siRNA without Sp-Ac-DEX proves this theory as it is shown in **Figure 64** and **Figure 66**.

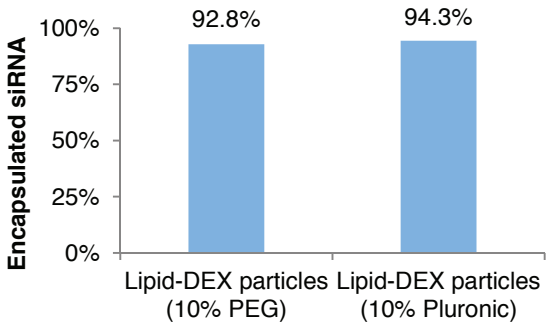

Figure 65: Encapsulation efficiency of siRNA-*luc* by lipid-DEX particles containing either PEG-lipid or Pluronic® F-68 as surfactant.

A variation in the lipid ratios, using different concentrations of DSPC (B), cholesterol (C) and PEG-lipid (D) for the particle preparation, shows no drawbacks regarding the siRNA encapsulation efficiency. Since the ratio of Sp-Ac-DEX is nearly the same in all particle formulations, this component seems to be principally responsible for the siRNA binding. All prepared particles show high encapsulation efficiencies of siRNA over 98% (shown in **Figure 66**). Particles without the cationic Sp-Ac-DEX (E) show only an encapsulation of 31.9% siRNA-*luc*. As described before, the amount of Sp-Ac-DEX seems to be the most important factor to form particles with a high encapsulation efficiency of siRNA.

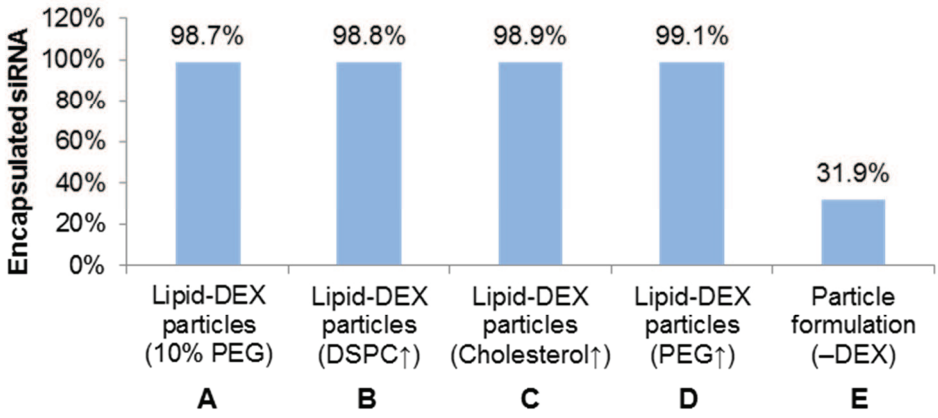

Figure 66: Encapsulation efficiencies of siRNA-*luc* in lipid-DEX particles with increased amounts of DSPC (B), cholesterol (C) or PEG-lipid (D) in the particle formulations compared to the previously described 10% PEG-lipid formulation (A). Particle formulation (E) is based on formulation D without the addition of Sp-Ac-DEX. The exact protocol can be found in chapter 5.4.1.

In summary, lipid-DEX particles are able to encapsulate siRNA efficiently. Since there is hardly a loss of siRNA material detectable during the preparation process, lipid-DEX particles are highly potent for the binding of these nucleic acids. This can be very important regarding the *in vivo* use of siRNA and limiting the costs for these applications since the preparation of specific nucleic acids is still very expensive.

3.4.4 Determination of the pK_a of Lipid-DEX Particles by the TNS Assay

Particle size and surface charge can affect the uptake of particles into cells as described in the previous chapters. Therefore, the titration of the pK_a can give additional information about the particle surface at different pHs. Alabi *et al.* (2013) report a pK_a of 6–7 for an efficient knockdown with lipid-based particles. Regarding the *Henderson-Hasselbalch* equation, the pK_a is equal with the pH when 50% of the particles are charged.[303] This value can be determined by incubation the particles with a fluorescent dye TNS that binds to the particle surface due to electrostatic interactions. The fluorescence of TNS (6-(*p*-toluidino)-2-naphthalenesulfonic acid sodium salt) is quenched by the presence of water. When the particles are ionized the negatively charged TNS can interact with the cationic parts of the particles. This interaction leads to the removal of water and the fluorescence intensity of TNS increases. Minimum fluorescence of the dye TNS represents zero charge, and maximum fluorescence represents 100% charge of the particle samples resulting in the pK_a that corresponds to the pH of the half equivalence point of the titration curve.[304]

The titration was performed using an adjusted protocol that was described before elsewhere.[305] Shortly, particles were incubated with the fluorescent dye TNS in HEPES/MES buffers with different pHs from 2.5–11 for five minutes before the fluorescence was read using a Tecan microplate reader.

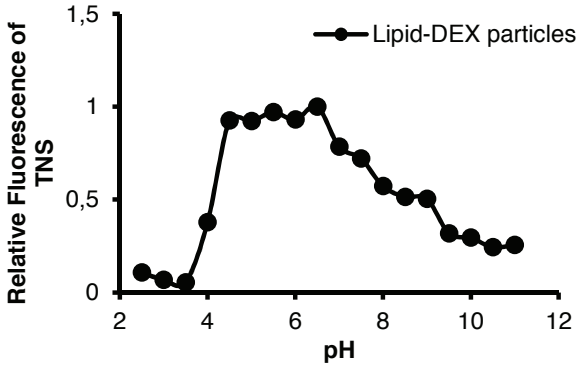

Figure 67: Incubation of the lipid-DEX particles with TNS in buffers with a pH range from 2.5 to 11 for the determination of the pK_a of the lipid-DEX particle formulation.

The maximal cationic charge of the particles is in the pH area from 4.5–6.5 which correlates to the highest fluorescence intensity of TNS in this range. In buffers with pHs higher than 7 the fluorescence intensity of TNS decreases. This can be explained by a deprotonation of the amines of Sp-Ac-DEX and therefore a less cationic surface of the particles. In a more acidic environment (pH<4), the acetals of the Sp-Ac-DEX can be hydrolyzed more rapidly so that the particle structure changes. Then TNS forms complexes with the single cationic dextran chains but the displacement of water is not high enough to remove the quenching effects of the TNS fluorescence. A clear statement of the particle pK_a cannot be made with this titration so that a further titration of the particles using acids and bases by measuring the pH change can be helpful.

3.4.5 *In Vitro* Knockdown of Luciferase with Lipid-DEX Nanoparticles

For *in vitro* knockdown experiments with the prepared particle formulations in chapter 3.4.1, HeLa-*luc* cells (stably expressing luciferase) were incubated with the lipid-DEX particles for 24 hours or 48 hours, respectively. Cell viability and luciferase activity were determined in the same experiment using ONE-Glo™ + Tox Luciferase Reporter and Cell Viability Assay (Promega). The advantage of this assay is a control of the living cells in the same experiment so that a second assay, for example a BCA assay, for quantification of the cell proteins is not necessary. The quantification of the proteins can be related to the number of cells per well and is often used to calculate the real knockdown of a special protein. Cell death can lead to a false positive knockdown signal due to the fact that a lower number of cells can express the luciferase enzyme and therefore less luciferase signal is detectable.

***In Vitro* Knockdown of Lipid-DEX Nanoparticles with Various PEG-lipid Ratios**

Smaller particles containing 10% PEG-lipid show a higher knockdown effect in HeLa-*luc* cells than bigger particles containing 5% PEG-lipid. The highest knockdown of approx. 80% is achieved with 500 ng siRNA per well (equivalent to 20 μL particle suspension with a siRNA concentration of 25 ng·μL^{-1}) and 10% PEG-lipid (see **Figure 68**). Longer incubation times for 48 hours show no tremendous effect regarding the knockdown efficiency. But increased concentrations of particles lead to more efficient knockdown since more siRNA is available to be delivered into the cells. Best knockdown results can be obtained with the commercial transfection agent RNAiMax which is used as a positive control during the knockdown experiments. This commercially available reagent is highly potent *in vitro* but cannot be used for *in vivo* experiments due to its assumed low *in vivo* stability compared to the results for other polyplexes[306]. Particles without Sp-Ac-DEX form small and uniform particles but can encapsulate only a little amount of siRNA as shown in the previous chapters. Although the particles are loaded with siRNA, no knockdown effect was detectable. Furthermore, no toxic effects can be observed with any of the particle formulations. In conclusion, Sp-Ac-DEX is not only necessary for the sufficient encapsulation of siRNA but also for the efficient delivery of siRNA into cells and knockdown of the specific enzyme luciferase.

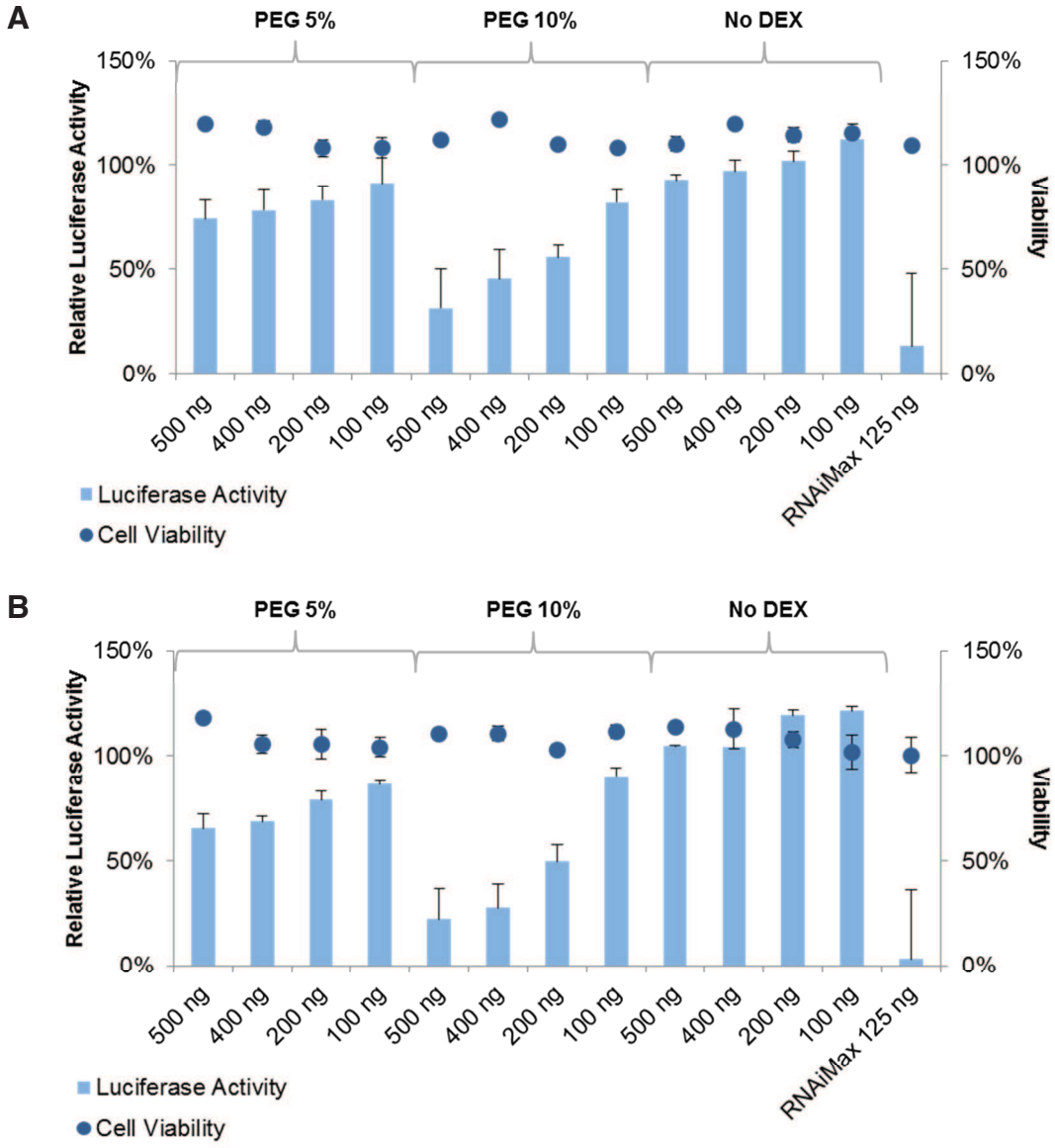

Figure 68: Cell viability and knockdown of luciferase in HeLa-*luc* cells with lipid-DEX particles consisting of different ratios of PEG-lipid. Cells are incubated with lipid-DEX particles for (A) 24 hours and (B) 48 hours. Shown is the knockdown for different ratios of siRNA (ng) per well.

Comparison of the *In Vitro* Knockdown in HeLa-*luc* Cells and A549-*luc* Cells

Since good knockdown results were obtained in HeLa-*luc* cells, the knockdown should be transferred to a second cell line to show the universal application of the lipid-DEX particles. Particle formulations containing 10% PEG-lipid and siRNA-*luc* were prepared with (+DEX) and without (-DEX) Sp-Ac-DEX and incubated in different concentrations with HeLa-*luc* or A549-*luc* cells for 24 hours. Afterwards, toxicity and luciferase knockdown was determined by using ONE-Glo + Tox as described in the previous section (see **Figure 69**).

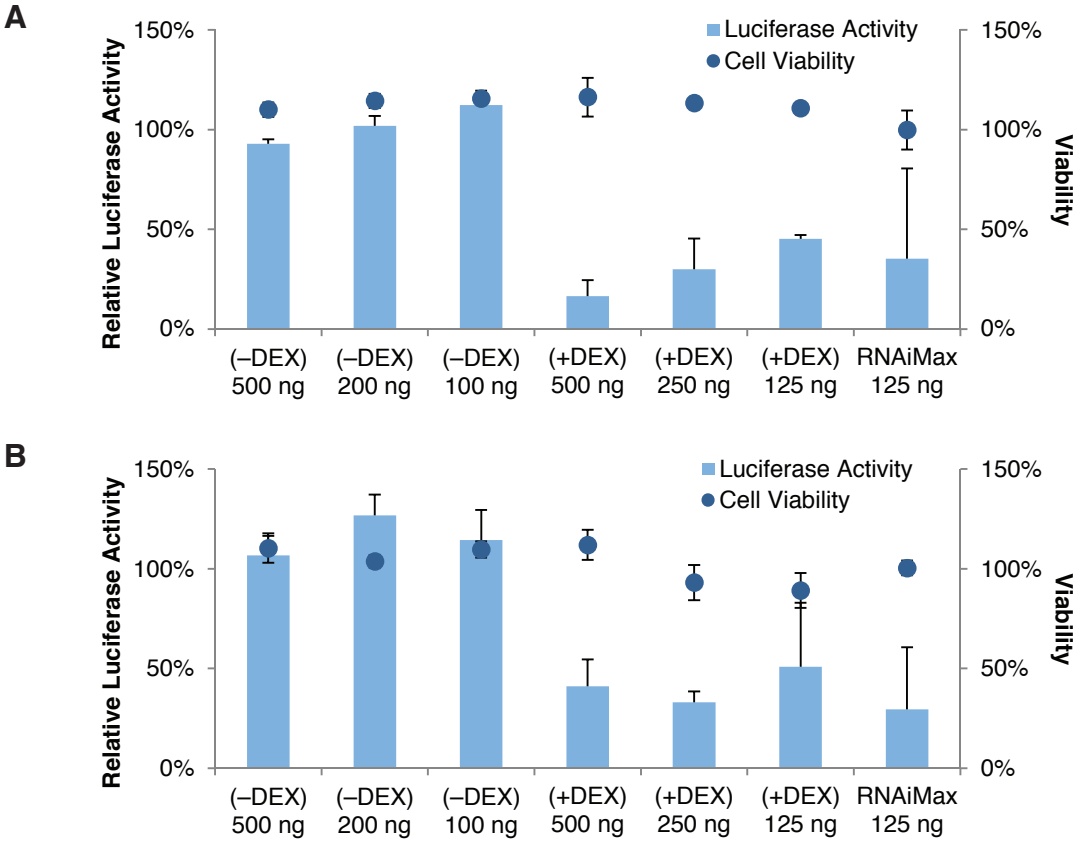

Figure 69: Cell viability and knockdown of luciferase in (A) HeLa-*luc* cells or (B) A549-*luc* cells. Particles are prepared using 10% PEG-lipid (+DEX) and are compared to particles containing no Sp-Ac-DEX (-DEX). RNAiMax is used as a positive control. All particle formulations are incubated with the cells for 24 hours using different amounts of siRNA (ng per well).

As described before, Sp-Ac-DEX is obligatory in the particle formulation for the efficient delivery of siRNA to the cytosol to obtain a knockdown effect. Best effects of approx. 80% luciferase knockdown were achieved in HeLa-*luc* cells with 500 ng siRNA per well. These results are comparable to the RNAiMax formulation, a commercially available optimized transfection agent for siRNA that is based on lipofectamine. In A549-*luc* cells, a luciferase knockdown of approx. 60% was achieved with the same amount of siRNA. Overall, none of the particles shows toxic effects in any of the cell lines. It can be shown that lipid-DEX particles are not only able to knockdown a specific gene in commonly used HeLa cells which are known to be transfected more easily. But the knockdown system can be also transferred to a lung cancer cell line A549 that is more complex than the universal used comparison model HeLa cell.

In Vitro Knockdown of Particles with PEG-lipid compared to Pluronic® F-68

The in chapter 3.4.1 prepared particles with 10% PEG-lipid or Pluronic® F-68 were incubated with HeLa-*luc* or A549-*luc* cells for 12 hours and the cell viability and luciferase activity was determined afterwards as described before.

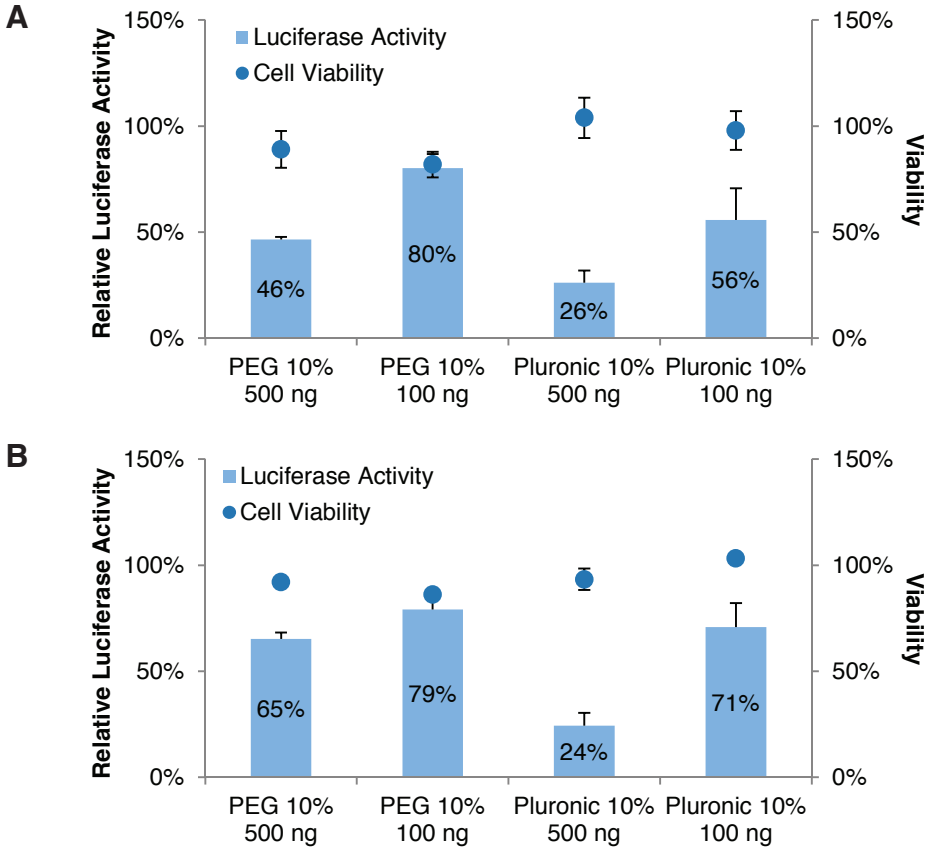

Figure 70: Cell viability and knockdown efficiency of luciferase with PEG-lipid or Pluronic® F-68 particles in (A) HeLa-*luc* cells (B) A549-*luc* cells. Cells are incubated with the particles for 12 hours.

Pluronic® F-68 particles show minimal less toxicity than PEG-lipid particles. But overall, none of the particle formulations shows high toxic effects. Furthermore, Pluronic® F-68 particles seem to be more effective than PEG-lipid particles regarding the knockdown efficiency. In HeLa-*luc* as well as A549-*luc* cells, Pluronic® F-68 particle formulations containing 500 ng of siRNA-*luc* show a luciferase knockdown of about 75% while PEG-lipid particles show only 55% or 35% knockdown. In conclusion, Pluronic® F-68 can be used as a PEG-lipid substitute in future experiments to enhance the knockdown efficiency.

3.4.6 *In Vivo* Biodistribution of Lipid-DEX Nanoparticles

Particles containing 10% PEG-lipid were prepared using a protocol described in 3.4.1 with a final siRNA concentration of 25 ng·μL^{-1}. The siRNA mixture consisted of siRNA-*luc* and Cy5.5-siRNA-*luc* in equal parts (V/V) so that a tracking of the particles by following the fluorescence of the Cy5.5-siRNA is possible. Particles were injected intravenously into the tail vein of each female, black C57BL/6 mouse resulting in a siRNA dose of 0.25 mg·kg^{-1}. Mice were sacrificed 3 hours or 24 hours after particle injection and organs were harvested followed by scanning their fluorescence using an IVIS Lumina System (Caliper Life Sciences).

After 3 hours, high Cy5.5-signals in the liver and spleen are detectable (see **Figure 71**). A lower signal of the particles in the kidneys can be a sign for the beginning degradation of the

particles, whereas the very low signal in the lung can be explained by some bigger, single particle aggregates. After 24 hours, only the signal in the liver and a lower signal in the kidneys are detectable. In summary, the lipid-DEX particles are highly stable *in vivo* compared to other cationic lipid particles previously described by Hao *et al.* (2015)[197]. The cationic particles used by Hao show good knockdown results after intratumoral application of the particles. But biodistribution studies after i.v. application of the particles show a high signal of the particles in the kidneys after 2.5 hours which can be explained by rapid degradation of the particles. Here, a high fluorescence signal in the liver is still detectable 24 hours after the application of lipid-DEX particles. No signals of the particles in the lung and spleen are detectable after 24 hours which can be explained by disaggregation of the particles (lung) or degradation of the particles by the immune system (spleen) over time.

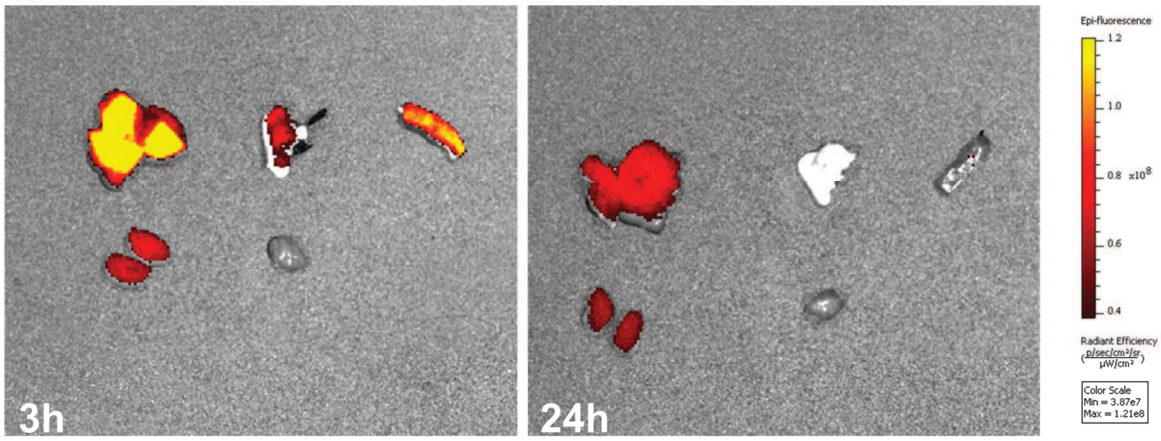

Figure 71: Biodistribution of Cy5.5-labeled siRNA-*luc* lipid-DEX particles in female, black C57BL/6 mice. Time points are taken after 3 hours and 24 hours by sacrificing the mouse and harvesting the organs. From left to right and upper to lower row: Lung, liver, spleen, kidneys, and heart.

In conclusion, the optimal lipid-DEX particle formulation consists of 46.3% Sp-Ac-DEX, 35.2% cholesterol, 9.25% DSPC, and 9.25% PEG-lipid (regarding molar ratios) with a final siRNA concentration of 25 ng·μL^{-1}. These new lipid-DEX particles can efficiently encapsulate large amounts of siRNA and show high *in vitro* knockdown of luciferase in HeLa-*luc* and A549-*luc* cells after 24 hours. None of the prepared particle batches show toxic effects. First *in vivo* biodistribution studies show a strong signal of the particles in the liver with low degradation of the particles. Compared to similar lipid particles described by Hao *et al.* (2015), lipid-DEX particles stand out with high stability. Furthermore, a 100-fold lower siRNA concentration for a high *in vivo* biodistribution signal is needed using lipid-DEX particles (0.25 mg·kg^{-1}) compared to the lipid particles by Hao *et al.* (25 mg·kg^{-1}). Moreover, the encapsulation of siRNA in uniform Sp-Ac-DEX nanoparticles can be increased by the mixture of Sp-Ac-DEX with the lipids cholesterol, DSPC, and PEG-lipid. A pure Sp-Ac-DEX nanoparticle suspension, prepared by double emulsion, can contain only a maximal siRNA concentration of 8 μg·mL^{-1} to prevent strong aggregation of the particles (shown by Cohen *et al.* (2011)[86] and in chapter 3.1.2). Instead, the here described lipid-DEX particles can

contain a siRNA concentration of 25 $\mu g \cdot mL^{-1}$, which can be probably increased by concentration of the lipid-DEX particle suspension using centrifugal filter units. This needs to be evaluated in next experiments as well as *in vivo* knockdown studies in an appropriate tumor or liver model. Further development of the particle system might lead to a liver specific siRNA delivery system to cure severe diseases like liver fibrosis or liver cancer.

4 CONCLUSION AND OUTLOOK

The focus of this work was the development of an improved biodegradable nanoparticle system for the delivery of genetic material. Therefore, different biocompatible polysaccharides were acetalated using a method described by Bachelder *et al.* (2008)[31]. The subsequent particle preparation led to new biodegradable and biocompatible nanoparticle carriers with innovative characteristics. In parallel, the first generation of spermine-modified Ac-DEX particles was further developed regarding the surface properties towards a targeted nanocarrier with improved *in vivo* behavior. Furthermore, a combination of cationic lipids and Sp-Ac-DEX using a microfluidic mixing strategy led to a second nanoparticle formulation with enhanced encapsulation of siRNA and improved *in vitro* knockdown results. In the end, two highly multifunctional and tunable acetalated dextran-based particle systems were created for the delivery of nucleic acids.

Successful Acetalation of Various Polysaccharides

In the first part of the thesis work, it was shown that the method of acetalation, previously described by Bachelder *et al.* (2008)[31], was transferrable to the polysaccharides amylopectin, dextrin, and HES. The following particle preparation using a double emulsion method led to nanoparticles which were slightly bigger than Ac-DEX particles with sizes of 200–300 nm in diameter. The main emphasis of these new polysaccharide-based particles was the increase in drug encapsulation and reduced unspecific uptake which was shown for HES particles but need to be shown in further experiments for amylopectin and dextrin particles. With regard to the delivery of nucleic acids, HES was modified with the polyamine spermine and showed reduced uptake in HeLa cells in first *in vitro* experiments. Ac-HES particles seem to encapsulate hydrophilic compounds more efficiently than Ac-DEX particles which was shown with a 10 kDa Oregon Green-labeled dextran, so that HES particles should be further characterized *in vitro* regarding their transfection efficiency and uptake behavior before *in vivo* biodistribution studies can start. Next steps for the further development of amylopectin, dextrin, and HES particles as drug carriers should include the encapsulation of an active compound and *in vitro* experiments to investigate the transfection behavior of the particles. Ideally, the new polysaccharide particles will show improved or additional characteristics compared to Ac-DEX-based nanoparticles in *in vitro* and *in vivo* studies.

Shielding of the Nanoparticle Surface by PEGylation and DEXylation

The main focus of the PhD work was the surface modification of spermine-modified Ac-DEX nanoparticles to prevent unspecific cell uptake and prolong blood circulation *in vivo*. Poly(ethylene glycol) (PEG) and hydrophilic dextran (DEX) were successfully attached to the particle surface without changing the nanoparticle size of around 150–200 nm. First qualitative proof of the attached layer showed the decreased zeta potential. Quantitative evidence was obtained after the determination of the reduced amounts of amine groups on the particle surface using the fluorescamine assay. The fluorescamine assay was overall a reliable indirect

detection method if the attached compounds were not too big to shield the non-modified amines from the fluorescamine reagent. Therefore, further quantification methods were used to proof the fluorescamine results for PEGylated particles. The Fmoc-PEGylation and quantification of PEG-groups via ^{1}H-NMR confirmed the results which were obtained with the fluorescamine assay.

The attachment of a hydrophilic layer should prevent recognition of the particles by the MPS, which encourages premature elimination of the particles *in vivo*. Therefore, the aggregation behavior of the PEGylated and DEXylated particles was examined in PBS and DMEM containing FCS to get more information about the particle interaction in protein-enriched medium. It was shown that non-modified particles aggregate in PBS and slightly more in DMEM over time. DEXylated particles gain extremely in size after incubation in DMEM for 3 days due to aggregation of the particles, whereas PEGylation prevents aggregation and stabilizes Sp-Ac-DEX particles in PBS and DMEM. Particles should be therefore stored lyophilized to prevent self-aggregation of the particles and resuspended freshly before each application.

These observations led to further examination of the hard protein corona formed on the particle surface after incubation in human plasma. LC-MS data showed similar protein patterns for non-modified and PEGylated particles. The most numerous proteins were prothrombin, clusterin, and vitronectin. Whereas coagulation proteins formed the biggest population on non-modified and PEGylated particles, lipoproteins, especially Apo A-I, formed the biggest population on DEXylated particles. Although DEXylated particles showed the strongest aggregation behavior in protein-enriched media, the particles adsorbed much less proteins than PEGylated and especially non-modified particles. Since the FCS used for *in vitro* experiments and human plasma differ a lot in the protein composition, further *in vitro* uptake studies should include the previous incubation of particles in human plasma to imitate *in vivo* behavior and improve the reaction conditions for *in vitro* experiments.

First *in vitro* toxicity studies in HeLa cells using the MTT assay showed no change in the cell viability in high concentrations of the surface modified Sp-Ac-DEX particles. In further trials the cell viability of murine liver macrophages and hepatocytes was analyzed and confirmed the low toxicity of the particles shown in HeLa cells before. However, a decrease of the cell viability to 60% was observed in fibroblasts for high particle concentrations. In murine BMDCs nearly no change in the cell viability was detectable after the incubation with non-modified and PEGylated particles, but the cell viability decreased to approx. 65% after the incubation with DEXylated particles. Murine spleen cells showed higher sensitivities and the cell viability decreased to 60%–80% after the incubation with dextran-based particles. In summary, surface-modified Sp-Ac-DEX particles are still biocompatible and can be called non-toxic. This was confirmed by first *in vivo* experiments in mice showing no change in the serum markers regarding toxic effects in the liver or kidneys.

Surface Modification Changes *In Vitro* and *In Vivo* Behavior of the Particles

All uptake experiments showed the same tendency for the modified particles in different cell types. DEXylated particles were taken up in higher amounts than non-modified particles, whereas the uptake of PEGylated particles was lower compared to non-modified particles. High uptake of the DEXylated particles was detected *in vitro* in HeLa cells, murine macrophages, murine spleen macrophages, and DCs as well as murine BMMCs and BMDCs. Less uptake of all particles in general was observed in murine hepatocytes and B cells and nearly no uptake of all particle types was detectable in murine fibroblasts and T cells. Further experiments should include the encapsulation of active compounds or nucleic acids to examine the transfection effectivity in macrophages and DCs. Especially DEXylated particles were taken up rapidly in high amounts in these antigen-presenting cells so that great transfection potency can be expected of this particle system. *In vivo* biodistribution in mice showed high particle signals in the liver so that without the introduction of targeting groups the particles can be used to deliver siRNA efficiently to liver macrophages.

First *in vitro* transfection experiments were performed in HEK cells using non-modified and PEGylated Sp-Ac-DEX particles encapsulating pDNA. High luciferase signals were obtained for non-modified Sp-Ac-DEX particles and low signals for PEGylated particles. Next experiments should include the attachment of specific targeting groups to PEGylated particles to enhance their uptake efficiency and improve the targeted delivery of the particles and encapsulated pDNA. Besides DNA delivery, the transfection efficiency of siRNA carrying particles should be also specified by the introduction of targeting moieties on the particle surface. DEXylation might be a first targeting strategy to enhance the transfection efficiency in DCs and macrophages which has to be proven in further studies.

Initial strategies to introduce a targeting moiety were performed with a bifunctional PEGylation and the attachment of a model targeting group which can be determined by fluorescence measurements. Future projects should include the attachment of functional targeting groups like mannose or folic acid to the PEGylated surface and *in vitro* experiments to proof the functionality of the targeting groups regarding enhanced accumulation of the particles at the target site and increased transfection of the encapsulated drug.

Enhanced siRNA Encapsulation with New Lipid-DEX Nanoparticles

Since high amounts of encapsulated siRNA led to increased aggregation behavior of the Sp-Ac-DEX particles, a new particle composition and preparation method was used to encapsulate high amounts of siRNA. The development of this new particle system was performed in cooperation with the group of [redacted] during a research stay at the UT Southwestern Medical Center in Dallas (Texas, USA). The composition of lipid compounds, consisting of DSPC, cholesterol, and a PEG-lipid, and the cationic Sp-Ac-DEX combines the advantages of both building blocks including great transfection potential and high siRNA binding. The perfect ratio of the single components was developed by the formation of small particles using a microfluidic mixing system. The obtained lipid-DEX nanoparticles showed promising knockdown results *in vitro* in HeLa cells and also A549 cells

which are more challenging regarding siRNA transfection. *In vivo* biodistribution studies of these lipid-DEX particles showed a strong accumulation of the particles inside the spleen and liver. Further experiments should focus on the examination of the particle destination inside the liver cell populations followed by the delivery of functional siRNA *in vivo* to target disorders in the liver.

In summary, it was possible to show that different dextran-based nanoparticle systems are promising delivery vehicles for nucleic acids with high biocompatibility. A hydrophilic PEG-layer prevents aggregation of the particles and excessive uptake in several cell types, whereas DEXylation enhances the uptake of Sp-Ac-DEX particles in most cell types, especially antigen-presenting cells. With this on hand next generation particle system the *in vivo* delivery of nucleic acids can be controlled precisely due to reduced unspecific cell uptake and targeted delivery of the particles. Future particle generations potentially can be used to target different tissues and cell types *in vivo* due to the tunable surface of the dextran-based particles. The simple conjugation technique of targeting moieties to the particle surface opens a versatile tool box and wide range of potential structures, like small synthetic compounds, monosaccharides, peptides, and antibodies.

Therapeutic applications in humans require safe and highly efficient delivery forms to prevent cytotoxic events of the active compound and reduce unwanted side effects. The dextran-based particle systems comprise delivery vehicles with high reproducibility in particle size and drug encapsulation as well as the potential for sterile production which is required for intravenous administration forms. In particular, organs like the liver and spleen are easily accessible with dextran-based particles due to their size and surface character. Therefore, severe diseases like liver cancer or fibrosis represent possible therapeutic approaches. Moreover, great particle uptake was observed in dendritic cells and macrophages which are both cells of the immune system. Therefore, dextran-based particles can potentially be used to treat different serious diseases which are connected to the immune system, like cancer, leukemia, asthma, diabetes, and rheumatic or autoimmune disorders.

5 EXPERIMENTAL SECTION

5.1 Materials

5.1.1 Reagents and Solvents

Chemicals, reagents and commercial buffers were obtained from the German suppliers unless otherwise mentioned.

Chemical	Supplier	CAS
Acetic acid	Sigma-Aldrich	64-19-7
N-Acetyl-*L*-cysteine	Sigma-Aldrich	616-91-1
Ammonium acetate	Sigma-Aldrich	631-61-8
Amylopectin from maize starch	Sigma-Aldrich	9037-22-3
Bovine albumin fraction V (BSA)	Carl Roth	90604-29-8
tert-Butanol	Carl Roth	75-65-0
Chloroform-*d*	Deutero	865-49-6
Cholesterol	Sigma-Aldrich	57-88-5
Deuterium chloride 38% in deuterium oxide	Carl Roth	7698-05-7
Deuterium oxide	Deutero	7789-20-0
Dextran, from Leuconostoc mesenteroides	Sigma-Aldrich	9004-54-0
Dextran T3.5	Pharmacosmos, Denmark	
Dextran T5	Pharmacosmos, Denmark	
Dextran, Oregon Green® 488; 10,000 MW	Life Technologies	
Dextrin from potato starch	Sigma-Aldrich	9004-53-9
Dichloromethane anhydrous, ≥99.8%, contains 40–150 ppm amylene as stabilizer	Sigma-Aldrich	75-09-2
Dimethyl sulfoxide anhydrous, ≥99.9%	Sigma-Aldrich	67-68-5
5,5'-Dithiobis(2-nitrobenzoic acid) (DTNB, Ellman's reagent)	Sigma-Aldrich	69-78-3
N-(3-Dimethylaminopropyl)-*N*'-ethylcarbodiimide hydrochloride (EDC hydrochloride)	Sigma-Aldrich	25952-53-8
DMEM GlutaMAX™ (Dulbecco's Modified Eagle's Medium high glucose)	Sigma-Aldrich, USA	

Chemical	Supplier	CAS
DMEM HyClone™	Fisher Scientific, USA	
DSPC (1,2-distearoyl-*sn*-glycero-3-phosphocholine)	Avanti Lipids, USA	816-94-4
Ethanol	Fisher Scientific, USA	64-17-5
Ethylenediaminetetraacetic acid (EDTA)	Sigma-Aldrich	60-00-4
Fetal Calf Serum (FCS)	Life Technologies	
Fluorescamine	TCI, Belgium	38183-12-9
Glycerol	Sigma-Aldrich	56-81-5
Glycine	Sigma-Aldrich	56-40-6
D-(+)-Glucose	Sigma-Aldrich	50-99-7
Heparin sodium salt	AppliChem	9041-08-1
Hydroxyethyl starch 70/0.5	Serumwerk Bernburg AG	
Hydroxyethyl starch 130/0.42	Serumwerk Bernburg AG	
Hydroxyethyl starch 200/0.5	Serumwerk Bernburg AG	
n-Hexylamine	Sigma-Aldrich	111-26-2
Hydrazine monohydrate	Sigma-Aldrich	7803-57-8
Hydrochloric acid 37%	Carl Roth	7647-01-0
Hydrochloric acid 1 M	Carl Roth	7647-01-0
Lipofectamine® RNAiMAX Transfection Reagent	Invitrogen, USA	
H-Lys(Fmoc)-OMe · HCl (Novabiochem®)	VWR	252049-10-8
D-(+)-Mannose	Sigma-Aldrich	3458-28-4
MES (2-(*N*-Morpholino)ethanesulfonic acid)	Sigma-Aldrich	4432-31-9
Methanol	Sigma-Aldrich	67-56-1
2-Methoxypropene	Sigma-Aldrich	116-11-0
N-Hydroxysuccinimide (NHS)	Sigma-Aldrich	6066-82-6
Ninhydrin	VWR	485-47-2
ONE-Glo™ + Tox Luciferase Reporter and Cell Viability Assay	Promega, USA	

Chemical	Supplier	CAS
OptiMEM®	Thermo Scientific, USA	
Oregon Green® 488-X, Succinimidyl Ester, 6-isomer	Life Technologies	
Phosphate buffered saline (10x concentrate, BioPerformance Certified)	Sigma-Aldrich	
PEG (CH_3O-PEG-NHCO-C_2H_4-CONHS 2 kDa)	Rapp Polymere	
PEG (CH_3O-PEG-NHCO-C_2H_4-CONHS 5 kDa)	Rapp Polymere	
PEG (Fmoc-NH-PEG-O-C_3H_6-CONHS 5 kDa)	Rapp Polymere	
PEG (PEG-(NHCO-C_2H_4-CONHS)$_2$ 2 kDa)	Rapp Polymere	
Penicillin-streptomycin (5,000 U/mL) Gibco™	Thermo Scientific	
Pluronic® F-68	Sigma-Aldrich, USA	9003-11-6
Poly(vinyl alcohol)	Sigma-Aldrich	9002-89-5
Pyridine	Carl Roth	110-86-1
Pyridinium *p*-toluenesulfonate	Sigma-Aldrich	24057-28-1
Quant-iT™ PicoGreen® Assay	Life Technologies	
Quant-iT™ RiboGreen® RNA Assay	Life Technologies	
Roti®-Quant universal	Carl Roth	
Sodium acetate	Sigma-Aldrich	127-09-3
Sodium borohydride	Sigma-Aldrich	16940-66-2
Sodium chloride	Carl Roth	7647-14-5
Sodium hydroxide	Carl Roth	1310-73-2
Sodium hydroxide solution 1 M	Carl Roth	
Sodium (*meta*)periodate	Sigma-Aldrich	7790-28-5
Sodium phosphate monobasic monohydrate	Amresco, USA	7558-80-7
Sodium pyruvate (100 mM) Gibco™	Thermo Scientific	
Spermine	Iris Biotech	71-44-3
Sucrose	Sigma-Aldrich	57-50-1
Sulfo-Cyanine 5 NHS-Ester (Cy5-NHS)	Lumiprobe	
3-Sulfo-*N*-succinimidyl 4-(*N*-Maleimidomethyl)cyclohexane-1-carboxylate Sodium Salt (sulfo-SMCC)	TCI, Belgium	92921-24-9
SUNBRIGHT® mPEG2000-DMG	Avanti Lipids, USA	

Chemical	Supplier	CAS
TE Buffer, 1x, Molecular Biology Grade	Promega, USA	
5/6-TAMRA-SE (5/6-Carboxytetramethylrhodamine NHS ester, mixed isomers)	emp Biotech	246256-50-8
Thiazolyl blue tetrazolium bromide (MTT)	Sigma-Aldrich	298-93-1
γ-Thiobutyrolactone	Sigma-Aldrich	1003-10-7
TNS (6-(*p*-toluidino)-2-naphthalenesulfonic acid sodium salt)	Sigma-Aldrich	53313-85-2
D-(+)-Trehalose dihydrate	Sigma-Aldrich	6138-23-4
Triethylamine > 99,5%	Carl Roth	121-44-8
Triton™ X-100	Sigma-Aldrich	9002-93-1
Water, sterile-filtered, BioReagent, suitable for cell culture	Sigma-Aldrich	7732-18-5

5.1.2 siRNA and Plasmids

Cy5-labeled siRNA targeting CD68
(sense strand: 5'-GAAAUGCAAGCAUAGUUCU-3', anti-sense strand: 5'-AGAACUAUGCUUGCAUUUC-3', purchased from Biospring, Frankfurt am Main, Germany) was a gentle gift from the group of [redacted] University Medical Center Mainz, Germany.

siRNA against luciferase
(sense strand: 50-GAUUAUGUCCGGUUAUGUA[dT][dT]-30; anti-sense strand: 30-UACAUAACCGGACAUAAUC[dT][dT]-50) was purchased from Sigma-Aldrich by [redacted] UTSW Medical Center Dallas, Texas, USA. Cy5.5-siRNA-*luc* had the same sequence, but was labeled with Cy5.5 dye at one end.

DNA plasmid 1699
The pCMV_GFP-2A-click_beetle luciferase (green) polyA DNA plasmid encoding for luciferase and eGFP (DKFZ) was a gentle gift from the group of [redacted] University Medical Center Mainz, Germany.

5.1.3 Buffers and Media

All buffers were prepared in a volume of 1 liter and filtered through a sterile syringe filter with a pore size of 0.22 μm (CME membrane, Rotilabo®). Aqueous buffers were stored at 4 °C to prevent bacterial contamination unless otherwise noticed.

Acetate buffer (0.3 M, pH 5)
40.8 g sodium acetate trihydrate (Sigma-Aldrich, M_W 136.08 g·mol^{-1}) were dissolved in *dd*-H_2O and adjusted to pH 5 with acetic acid.

Borate buffer (0.1 M, pH 8.5)
6.2 g boric acid (Sigma-Aldrich, M_W 61.83 g·mol^{-1}) were dissolved in *dd*-H_2O and adjusted to pH 8.5 with NaOH.

***dd*-H_2O (pH 8)**
dd-H_2O was adjusted to pH 8 with TEA (approx. 10 μL TEA per 1 L *dd*-H_2O).

DMEM for HeLa cells
DMEM GlutaMAX™ (high glucose) with phenol red was mixed with 10% FCS, 1% pyruvate and 1% penicillin-streptomycin.

DMEM for HeLa-*luc* cells
DMEM HyClone™ (high glucose) without phenol red was mixed with 5% FCS and 1% penicillin-streptomycin.

Glycine buffer (0.1 M, pH 10.5)
7.5 g glycine (Sigma-Aldrich, M_W 75.07 g·mol^{-1}) and 5.8 g sodium chloride (Carl Roth, M_W 58.44 g·mol^{-1}) were dissolved in *dd*-H_2O and adjusted to pH 10.5 with NaOH.

HEPES buffer (25 mM, pH 7.4)
6.0 g 4-(2-hydroxyethyl)-1-piperazineethanesulfonic acid (Amresco, M_W 238.30 g·mol^{-1}) were dissolved in *dd*-H_2O and the pH was adjusted to pH 7.4 with NaOH.

Ninhydrin solution (acidic)
0.2 g ninhydrin were dissolved 0.5 mL acetic acid, 100 mL *n*-butanol and 4.5 mL *d*-H_2O. The solution was stored at room temperature protected from light.

PBS buffer (pH 7.4)
PBS 10x concentrate (Sigma-Aldrich, 100 mL) was diluted with *dd*-H_2O (900 mL); containing 154 mM NaCl, 8 mM $NaHPO_4$ and 2 mM KH_2PO_4 with a final pH of 7.4.

PBS buffer (pH 8)
PBS buffer (1x) was adjusted to pH 8 with NaOH.

PBS buffer (1 mM EDTA, pH 7.4)
PBS buffer (1x) was mixed with 133 mg ethylenediaminetetraacetic acid dihydrochloride (Alfa, M_W 133.02 g·mol^{-1}).

PBS buffer (1% Triton™ X-100, pH 7.4)
PBS buffer (1x) was mixed with 10 mL Triton™ X-100 (Sigma-Aldrich).

Phosphate buffer (0.1 M, pH 7.4)
12 g sodium dihydrogen phosphate (Amresco, M_W 119.98 g·mol^{-1}) were dissolved in *dd*-H_2O and adjusted to pH 7.4 with NaOH.

Phosphate buffer (0.1 M, 1 mM EDTA, pH 8)
12 g sodium dihydrogen phosphate (Amresco, M_W 119.98 g·mol^{-1}) and 133 mg ethylenediaminetetraacetic acid dihydrochloride (Alfa, M_W 133.02 g·mol^{-1}) were dissolved in *dd*-H_2O and the pH was adjusted to pH 8 with NaOH.

Phosphate buffer (4%, pH 7.4)
40 g sodium dihydrogen phosphate (Amresco, M_W 119.98 g·mol^{-1}) were dissolved in *dd*-H_2O and the pH was adjusted to pH 7.4 with NaOH.

3% PVA in PBS pH 7.4
30 g poly(vinyl alcohol) (Sigma-Aldrich, M_W 13,000–23,000 g·mol^{-1}) were dissolved in 970 mL 1x PBS under gentle heating (40 °C).

0.3% PVA as cryoprotectant
3 g poly(vinyl alcohol) (Sigma-Aldrich, M_W 13,000–23,000 g·mol^{-1}) were dissolved in 997 mL *dd*-H_2O under gentle heating (40 °C).

5.1.4 Disposables

Consumables	Manufacturer
BRAND® UV cuvettes micro (c = 8.5 mm)	VWR
CELLSTAR® cell culture flasks 25 cm², 75 cm²	Greiner Bio-One
Coverslips, precision (diameter 1.8 cm, thickness of 0.17 ±0.005 mm, borosilicate glass)	Carl Roth GmbH
Disposable hypodermic needles (size: 21 G)	B.Braun
Disposable pipettes 2 mL, 5 mL, 10 mL, 20 mL	Sarstedt
Disposable syringes 1 mL, 2 mL, 5 mL, 10 mL, 20 mL	B.Braun
Eppendorf Tubes 1.5 mL, 2 mL, 5 mL	Eppendorf
Filtropur S 0.2 (sterile, non-pyrogenic)	Sarstedt
Glass pipettes	Carl Roth GmbH
Locking clips for dialysis	Carl Roth GmbH
Micro-centrifuge tubes for high G-force 1.5 mL	VWR
Microplate 12-well, flat bottom, clear, sterile	Greiner Bio-One
Microplate 24-well, flat bottom, clear, sterile	Greiner Bio-One
Microplate 96-well, flat bottom, clear	Sarstedt
Microplate 96-well, flat bottom, clear, sterile	Greiner Bio-One
Microplate 96-well, flat bottom, black	Greiner Bio-One
Microplate 96-well, flat bottom, white	Corning-Costar, USA
Microscope slides, standard (soda-lime glass, 76 x 26 mm, 1 mm thick)	Carl Roth GmbH
NMR tubes	Sigma-Aldrich
Parafilm	Pechiney Plastic Packing
Pipette tips 2 µL, 250 µL, 1000 µL	Sarstedt
SuperSpin™ Microcentrifuge Tubes, polypropylene (1.5 mL, max. rcf 35 k)	VWR
Tubes 13 mL, 100x16 mm, PP	Sarstedt
Tubes 15 mL, 120x17 mm, PP	Sarstedt
Tubes 50 mL, 114x28 mm, PP	Sarstedt

5.1.5 Cell Lines and Animal Studies

HeLa Cells

An epitheloid cervix carcinoma cell line, established from a cervical cancer tissue sample of Henrietta Lacks in 1951. Cells were a kind gift from the group of [redacted] (Institute of Pharmacy and Biochemistry, Johannes Gutenberg-University, Mainz).

HeLa-*luc* and A549-*luc* Cells

HeLa (or A549) cells stably expressing firefly luciferase (HeLa-l*uc* or A549-*luc*) were derived from HeLa (or A549) cells (ATCC, American Type Culture Collection) by stable transfection of the luciferase gene using lentiviral infection followed by clonal selection. Cells were used in the lab of [redacted] (UT Southwestern Medical Center, Cancer Center, Dallas, USA).

Animal Studies

Animal studies were performed with [redacted] in the lab of [redacted] All experiments were approved by the Institutional Animal Care and Use Committees (IACUC) of the University of Texas Southwestern Medical Center and were consistent with local, state and federal regulations as applicable. Female C57BL/6 mice were purchased from UTSW Mouse Breeding Core (Dallas, TX).

5.2 Equipment

Absorption and Fluorescence Measurements

Equipment: Victor RX5 Multilabel Plate Reader, Waltham, Massachusetts, United States, Perkin Elmer. Analysis was carried out using WorkOut 2.5 software and Microsoft Excel.
Infinite® M200 Pro Plate Reader, Tecan Group Ltd., Switzerland. Analysis was carried out using i-control 1.7 software and Microsoft Excel.

Absorption measurements were performed with clear 96-well microplates (flat bottom). Fluorescence measurements were performed with black 96-well microplates (flat bottom).

Bath-Sonicator

Equipment: Sonorex Super RK 102 H, Bandelin electronic.

Samples were sonicated until complete dissolving could be observed. Nanoparticles were suspended until no aggregates were detectable.

Centrifuges

Equipment: Heraeus™ Multifuge™ X3R, Thermo Scientific.
Heraeus™ Megafuge™ 8 R, Thermo Scientific*[a]
BECKMAN Type AvantiTM J-25*[b]

Centrifugation for particle purification was performed at 45,000 x *g**[a] or 30,000 x *g**[b] for 20 minutes if not otherwise stated.

Dialysis

Equipment: Spectra/Por® 6, regenerated cellulose, MWCO 1,000 $g \cdot mol^{-1}$, Carl Roth GmbH.
ZelluTrans Roth, regenerated cellulose, MWCO 3,500 $g \cdot mol^{-1}$, Carl Roth GmbH.
ZelluTrans Roth V-Serien, regenerated cellulose, MWCO 25,000 $g \cdot mol^{-1}$, Carl Roth GmbH.
Pur-A-Lyzer™ Midi Dialysis Kit, MWCO 3.5 kDa, Sigma-Aldrich, USA.

Dialysis membranes were inserted in *d*-H_2O for 30 minutes and rinsed with water before loading with the samples. Dialysis was performed against *d*-H_2O or PBS in a beaker glass under constant stirring. Water was changed 5-times in 24 hours.

FT-IR

Equipment: Nicolet Avatar 330-IR ATR-Einheit, Thermo Electron Corporation.

The compounds were measured without further preparation on the diamond crystal surface of the device.

Incubator

Equipment: Heraeus® BB15 FUNCTION Line, Thermo Scientific.

Cell incubations were performed in a humidified incubator at 37 °C with 5% CO_2 atmosphere.

Inert Gas

Equipment: Argon gas bomb in 99.998% purity N46, Air Liquide Deutschland GmbH.

Argon was used as inert gas to flood flasks and reaction containers. Balloons were attached to the reaction flasks to prevent the contact of reagents with air.

Lyophilizer

Equipment: ALPHA 1-4 LSC, Martin Christ Gefriertrocknungsanlagen GmbH.

Samples were dissolved or suspended in water, frozen in liquid nitrogen and then stored in the lyophilizer for freeze-drying for at least one day. Before lyophilization of nanoparticles, 100 μL 0.3% PVA in *dd*-H_2O were added as a standard cryoprotectant.

Mass Spectrometry (ESI-MS)

Equipment: ESI MAT95, ionization energy 5 KV; Finnigan FD QTof Ultima3, micromass / waters; Institute of Organic Chemistry, Johannes Gutenberg-University Mainz.

Samples were prepared in MeOH at concentrations of max. 0.1 mg·mL^{-1}.

Microscopy

Equipment: TCS SP5 Confocal Microscope, Leica Microsystems, Wetzlar, Germany.

TCS SP5 is a confocal microscope with an inverse microscope stand provided by the Microscopy Core Facility, IMB, Mainz, Germany. With 4 PMTs, 4 laser lines (405 / 458, 476, 488, 496, 514 / 561 / 633 nm lines), 6 objectives (10x/0.3 dry; 20x/0.7 dry; 20x/0.7 imm; 40x/1.3 oil; 63x/1.4 oil; 63x/1.2 water) and a fast resonance scanner. Microscopy pictures were analyzed by the software ImageJ 1.48 (Java) and LAS AF Lite (Leica).

Nuclear Magnetic Resonance (NMR)

Equipment: Bruker Topspin Fourier 300 MHz.

For standard analytical purpose ^{1}H-NMR spectra were recorded at 300 MHz. The experiments were performed at room temperature using the indicated solvents, mostly $CDCl_3$ and D_2O. The chemical shifts were reported in ppm against the solvent signal of TMS. For the description of the signals the following abbreviations were used: s = singlet, d = doublet, t = triplet, q = quartet, m = multiplet, br = broad signal. Integrals were calculated by using MestReNova Software. Assignments were carried out according to literature. Peaks resulting from solvent residues were determined by literature[307].

Particle Sonicator

Equipment: Bandelin Ultrasonic Homogenisator Sonoplus UW 70 (v220-240w), microtip MS 73 SH70G Stufenhorn 20 kHz, BANDELIN electronic GmbH & CO. KG, Berlin, Germany.

Sonication of all nanoparticle samples was carried out while cooling the samples on an ice bath (Settings: power 75%, cycle 70% MS 72/D).

pH measurement

Equipment: SevenCompact™ pH/Ion S220 with a InLab® Micro special electrode, Mettler Toledo, Mettler-Toledo Ltd., Beaumont Leys, Leicester, United Kingdom.

The pH-meter was calibrated with commercial available buffer standards (pH 4.00, pH 7.00, and pH 11.00).

Rotary Evaporation

Equipment: IKA RV06-ML Janke-Kunkel rotavapor; IKA HB4 basic water bath; Vacuubrand CVC24 vacuum controller; Vacuubrand 1715550193 Membrane pump.

Sample concentration under reduced pressure was performed by rotary evaporation in a water bath at 40–50 °C and the adjusted pressure for the used solvent.

Safety Cabinet

Equipment: HERA Safe®, Kendro Laboratory Products, Langenselbold, Germany.

All cell culture experiments were performed in a sterile environment using a safety cabinet.

Scales

Equipment: Mettler Toledo Excellence Plus.
Sartorius™ M-Prove™ Scales AY303, Sartorius, Göttingen, Germany.

Samples below 500 mg were weighed on the fine balance from Mettler. For samples above 500 mg, the standard laboratory balance from Sartorius was used.

Particle size measurements

Equipment: Malvern Zetasizer Nano ZS, Malvern Instruments GmbH, Herrenberg, Germany.
NanoSight LM 10 microscope, Malvern Instruments GmbH, Herrenberg, Germany.

Dynamic Light Scattering (DLS) was performed with nanoparticle samples suspended in PBS (filtered 0.22 μm) with a concentration of about 20 $\mu g \cdot mL^{-1}$ and sonicated for 20 seconds before measurements. Samples were prepared in polystyrene micro cuvettes (Brand) using 110 μL of freshly prepared particle solution. Generally, after equilibration to 20 °C, three

measurements each consisting of 12 runs were performed. The refractive index (RI) of the dispersant (preset: water) was set to 1.330 and the viscosity to 1.0031 cP, respectively. The RI of the particle was set to 1.590. Both attenuator and measurement position were controlled by the instrument and Mark-Houwink parameters and all measurements were performed at a scattering angle of 173° (backscatter, NIBS default).

Nanoparticle Tracking Analysis (NTA) was performed with a NanoSight LM 10 microscope (Malvern Instruments) equipped with a green laser (532 nm) and a sCMOS camera. All samples were prepared in PBS (filtered 0.22 μm) with a concentration of about 2 $\mu g \cdot mL^{-1}$ and sonicated for 20 seconds before measurement. Movements of the particles were recorded as videos for 30 seconds at 25 °C. The size calculation was performed with NTA software version 3.0 build 0068.

Solvents

All solvents were either bought dry or dried before use. Methanol (Sigma-Aldrich) was purified before use by distillation with a rotary evaporator.

TLC

Equipment: Universal UV-Lampe CAMAG TL-900, West-Berlin, Germany
Pre-coated TLC sheets Alugram Xtra SIC G/UV254, Layer 0.2 mm with fluorescent indicator UV254, Macherey-Nagel GmbH & Co. KG, Düren, Germany.

The synthesis of the bifunctional linker 4-mercaptobutanehydrazide was monitored by TLC on silica gel pre-coated normal phase plates. Visualization of the spots was carried out by fluorescence detection with 254 nm UV light and staining with an acidic ninhydrin solution in *t*-butanol (for detection of amines). The ninhydrin treated plate needed to be activated by using a heat gun.

Water

Equipment: Direct-Q® 5 UV Remote Water Purification System, Merck Millipore, Germany.

Water (*dd*-H_2O) for buffers and particle washing steps was purified by a Direct-Q® 5 UV Remote Water Purification System. Water (*dd*-H_2O) used for the particle treatment was adjusted to pH 8 with triethylamine (TEA, Carl Roth, Germany, approx. 0.001% (V/V)).

Zeta potential

Equipment: Malvern Zetasizer Nano ZS, Malvern Instruments GmbH, Herrenberg, Germany.

Zeta potential (particle charge) was measured by a Malvern Zetasizer Nano ZS instrument using a clear disposable zeta cell (Malvern). Three measurements with 12 individual runs were performed at 25 °C. Particle samples were prepared at concentrations of 0.1 $mg \cdot mL^{-1}$ in

HEPES buffer (5 or 25 mM, pH 7.4). The refractive index (RI) of the dispersant (preset: water) was adjusted to 1.330 and the viscosity to 0.8872 cP with a dielectric constant of 78.5. The RI of the particle material dextran was set to 1.590. The data was analyzed by the model of Smoluchowski[308] with the Malvern Zetasizer software 6.20.

5.3 Preparation Methods for Acetalated Polysaccharide Nanoparticles

5.3.1 Modification of Polysaccharides

Synthesis of Acetalated Polysaccharides

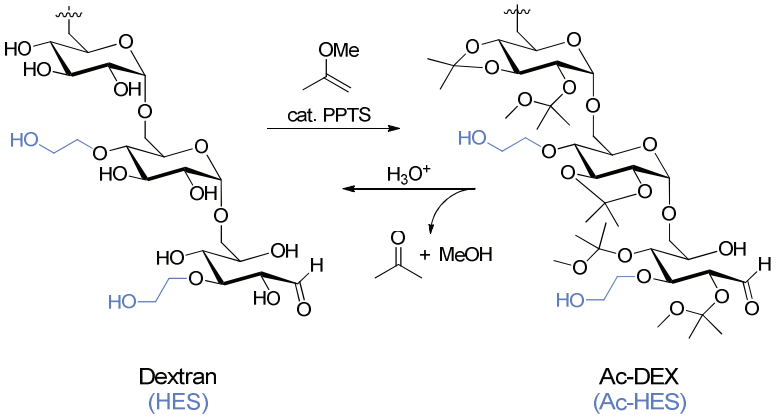

Figure 72: Acetalation of dextran or hydroxyethyl starch (HES). The acetalation of amylopectin and dextrin was performed in the same manner.

The synthesis was performed after a protocol of Bachelder *et al.* (2008)[31] For the acetalation, a flame-dried flask was charged with the according polysaccharide (2.0 g, 12.3 mmol AGU) dissolved in anhydrous DMSO (20 mL) and purged with argon. After total dissolution of the polysaccharide, pyridinium *p*-toluenesulfonate (33.0 mg, 0.131 mmol) was added, followed by the dropwise addition of 2-methoxypropene (6.8 mL, 71.2 mmol). The reaction was stirred for 10 minutes if not otherwise noticed and kept in an argon atmosphere at all times. Finally, the reaction was quenched with TEA (2 mL) and stirred for another 5 minutes before precipitation of the product in *dd*-H_2O (pH 8, 200 mL). The modified polysaccharide was isolated by centrifugation (12,000 x *g*, 15 min.) and rinsed 5-times with 50 mL *dd*-H_2O (pH 8). The pellet needed to be vortexed and sonicated thoroughly to remove all DMSO. In the end, the purified polysaccharide was resuspended in *dd*-H_2O pH 8 and dried by lyophilization, yielding in acetalated polysaccharide as a fine, colorless powder. Amylopectin had to be dissolved in 40 mL DMSO regarding the enhanced viscosity of the polysaccharide until a clear solution was obtained. The acetalation of dextrin followed the same protocol than the synthesis of Ac-DEX besides it had to be stirred overnight for total dissolution.

^{1}H-NMR Ac-DEX (300 MHz, $CDCl_3$): δ 1.40 (s, br, CH_3 acetal), 1.80 (s), 3.25 (br, OCH_3 acetal), 3.47, 3.54–4.33 (m, AGU-H dextran), 4.85 (br, AGU-H dextran), 5.15 (br, anomeric H dextran)

^{1}H-NMR Ac-HES 70 kDa (300 MHz, $CDCl_3$): δ 1.33 (s, br, CH_3 acetal), 1.70 (s), 2.61 (s), 3.18 (s, br, OCH_3 acetal), 3.32 (s, br), 3.53 (s), 3.4–4.2 (m, AGU-H HES), 4.60 (s, br, AGU-H HES), 5.06 (s, br, anomeric H HES)

^{1}H-NMR Ac-HES 130 kDa (300 MHz, $CDCl_3$): δ 1.27 (s, br, CH_3 acetal), 1.65 (s), 2.55 (s), 3.11 (s, br, OCH_3 acetal), 3.26 (s, br), 3.46 (s), 3.4–4.3 (m, AGU-H HES), 4.56 (s, br, AGU-H HES), 5.01 (s, br, anomeric H HES)

^{1}H-NMR Ac-HES 200 kDa (300 MHz, $CDCl_3$): δ 1.27 (s, br, CH_3 acetal), 1.62 (s), 2.55 (s), 3.11 (s, br, OCH_3 acetal), 3.25 (s, br), 3.4–4.3 (m, AGU-H HES), 4.55 (s, br, AGU-H HES), 5.02 (s, br, anomeric H HES)

^{1}H-NMR Ac-AMY 10 min. (300 MHz, $CDCl_3$): δ 0.83–0.85 (d, br), 1.33 (s, br, CH_3 acetal), 1.61 (s), 2.17 (s), 2.62 (s), 3.19 (s, br, OCH_3 acetal), 3.32 (s, br), 3.41–4.38 (m, AGU-H AMY), 5.06 (s, br, anomeric H AMY)

^{1}H-NMR Ac-AMY 60 min. (300 MHz, $CDCl_3$): δ 1.19 (s), 1.33 (s, br, CH_3 acetal), 1.62 (s), 1.82, 2.28 (s), 2.61 (s), 3.19 (s, br, OCH_3 acetal), 3.22 (s), 3.43–4.31 (m, AGU-H AMY), 3.51 (s), 5.10 (s, br, anomeric H AMY)

^{1}H-NMR Ac-DIX 10 min. (300 MHz, $CDCl_3$): δ 1.33 (s, br, CH_3 acetal), 1.63 (s), 3.18 (s, br, OCH_3 acetal), 3.33 (s, br), 3.43–4.33 (m, AGU-H DIX), 5.04 (s, br, anomeric H DIX)

^{1}H-NMR Ac-DIX 60 min. (300 MHz, $CDCl_3$): δ 1.34 (s, br, CH_3 acetal), 1.67 (s), 1.83 (s), 2.61 (s), 3.19 (s, br, OCH_3 acetal), 3.28 (s, br), 3.39–4.37 (m, AGU-H DIX), 5.09 (s, br, anomeric H DIX), 5.56 (s, br)

Degree of Acetalation by ^{1}H-NMR

The degree of acetalation of the polysaccharides was determined by ^{1}H-NMR. Therefore, approx. 10 mg of modified polysaccharide was dissolved under vortexing in 700 μL D_2O by adding one drop of DCl.

Partial Oxidation of the Polysaccharides

The synthesis of spermine-functionalized dextran, described before by Cohen *et al.* (2011)[86], started with the partial oxidation of the polysaccharides, followed by their acetalation and functionalization with spermine. The protocol had to be adjusted for the different polysaccharides.

All polysaccharides (5.0 g, 30 mmol AGU) were dissolved in *dd*-H_2O (20 mL). After total dissolution, sodium periodate was added and the solution was stirred for 5 hours at room temperature. The partial oxidation of HES was quenched by adding glycerol before purification. The oxidized polysaccharides were purified by dialyzation of the yellowish solution against *d*-H_2O using a regenerated cellulose membrane with a MWCO of 3,500 g·mol^{-1} or 12,000–14,000 g·mol^{-1} (Zellu Trans Roth®). The water was changed 5-times in 24 hours and the sample was lyophilized to obtain a colorless powder.

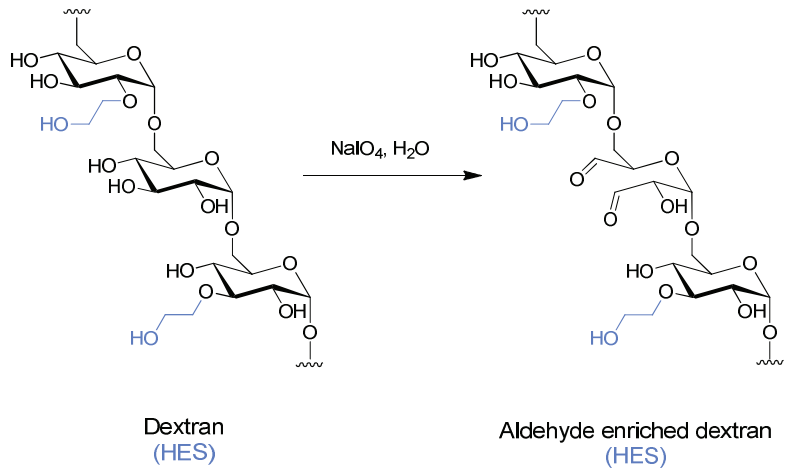

Figure 73: Partial oxidation of dextran or hydroxyethyl starch with sodium periodate.

Amylopectin and dextrin were oxidized under the same conditions than dextran resulting in a yield of 3.5 g partially oxidized amylopectin (70%) and 2.9 g partially oxidized dextrin (59%). For the total dissolution of the polysaccharides in water, both polysaccharide solutions had to be heated up to 50 °C under constant stirring. The clear solutions were cooled down to room temperature before adding the oxidizing agents.

Table 18: Composition of the reagents for the partial oxidation of dextran and HES

Reagent	Dextran 10 kDa	HES 70 kDa	HES 130 kDa	HES 200 kDa
Sodium periodate	1.1 g, 5.14 mmol	556 mg, 2.6 mmol	321 mg, 1.5 mmol	321 mg, 1.5 mmol
Molar ratio (AGU : $NaIO_4$)	6:1	12:1	20:1	20:1
Glycerol	–	1 mL	2 mL	2 mL
Yield	4.2 g / 84%	4.7 g / 94%	4.5 g / 90%	4.1 g / 82%

PCA Assay for the Quantification of Aldehydes

The degree of oxidation was determined colorimetrically using a reductometric bicinchoninic acid assay (Roti®-Quant universal, Carl Roth) according to the manufacturer's protocol and dextran (M_W 9,000–11,000 g·mol^{-1}, from Leuconostoc mesenteroides, Sigma-Aldrich) for calibration.

In short, 50 μL of each sample (ox-DEX, ox-AMY, ox-DIX: 0.5 mg·mL^{-1}; ox-HES: 0.25 mg·mL^{-1}) or standard was added to a clear, flat bottom 96-well microplate (Sarstedt). Standards were prepared from dextran 10 kDa at concentrations of 0.31 mg·mL^{-1} up to 10 mg·mL^{-1} in *dd*-H_2O. Afterwards, 100 μL working solution of the PCA assay Roti®-Quant universal was added to each sample and standard. The samples were incubated at room temperature for 2 hours and the absorbance was measured with a Victor microplate reader at 492 nm. The degree of oxidation was calculated using Microsoft Excel.

Acetalation of Partially Oxidized Polysaccharides

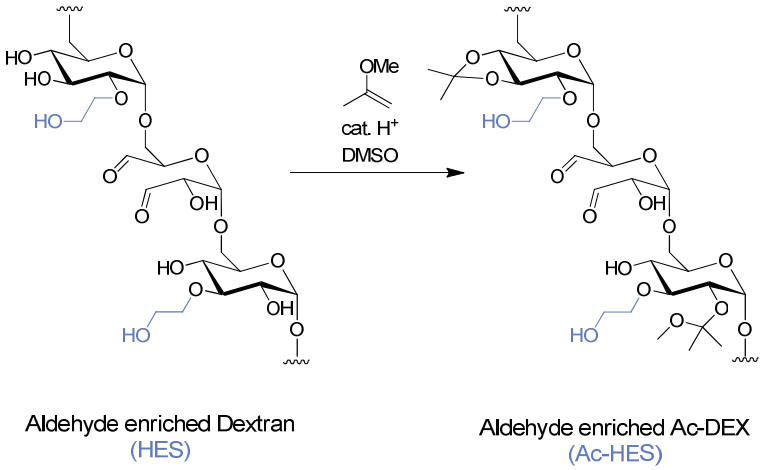

Figure 74: Acetalation of partially oxidized dextran or hydroxyethyl starch with methoxypropene and PPTS as catalyzator.

The acetalation of the partially oxidized dextran, hydroxyethyl starches, amylopectin, and dextrin was performed as described in the beginning of the chapter.

Table 19: Composition of the reagents for the acetalation of partially oxidized dextran and HES

Reagent	ox-DEX 10 kDa	ox-HES 70 kDa	ox-HES 130 kDa	ox-HES 200 kDa
Polysaccharide	1.5 g, 9.3 mmol AGU	2.3 g, 14.3 mmol AGU	2.2 g, 13.8 mmol AGU	1.8 g, 11.4 mmol AGU
DMSO	20 mL	55 mL	50 mL	50 mL
PPTS	23.4 mg, 0.093 mmol	36.2 mg, 0.144 mmol	34.5 mg, 0.137 mmol	28.9 mg, 0.115 mmol
2-methoxypropene	5.3 mL, 55.5 mmol	7.9 mL, 85.8 mmol	7.6 mL, 82.8 mmol	6.3 mL, 68.4 mmol
Reaction time	10 min.	120 min.	120 min.	120 min.
TEA	1.5 mL, 10.5 mmol	2.3 mL, 16 mmol	2.2 mL, 15.7 mmol	1.8 mL, 12.9 mmol
dd-H_2O pH 8	200 mL	500 mL	500 mL	500 mL
Yield	2.2 g	2.1 g	3.1 g	2.3 g

For the total dissolution of partially oxidized amylopectin and dextrin in DMSO, the amount of solvent had to be enhanced to 55 mL. Reaction times for the acetalation of ox-AMY and ox-DIX were 10 minutes or 60 minutes, respectively. The degree of functionalization was determined by ^{1}H-NMR spectroscopy in DCl/D_2O according to the method described by Broaders *et al.* (2009).[75]

Reductive Amination of Acetalated and Oxidized Polysaccharides with Spermine

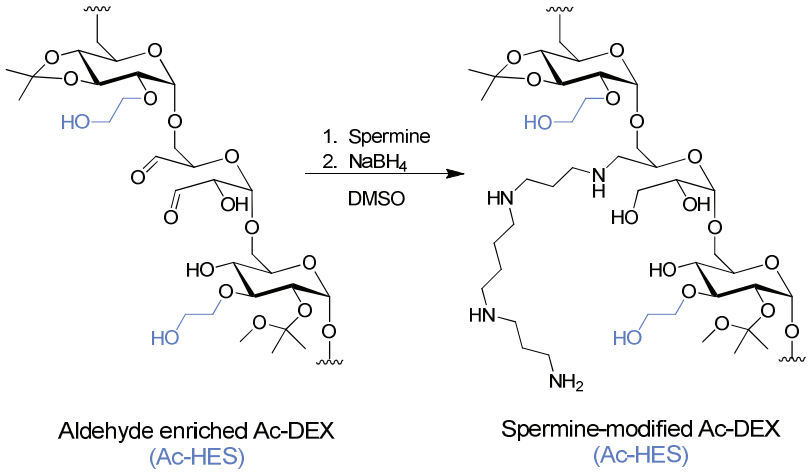

Figure 75: Reductive amination of partially oxidized and acetalated dextran (or HES) with spermine and sodium borohydride in DMSO.

Partially oxidized Ac-DEX or Ac-HES and spermine (Iris Biotech) were stirred under the protection of argon gas in anhydrous DMSO for 22 hours. Afterwards, $NaBH_4$ was added to the solution and stirred for further 18 hours. The spermine-modified polysaccharides were precipitated in *dd*-H_2O (pH 8) and the product was isolated by centrifugation at 12,000 x *g* for 15 minutes. The resulting pellet was purified with *dd*-H_2O (7 x 40 mL, pH 8) by resuspension in *dd*-H_2O (pH 8) followed by centrifugation and removal of the supernatant. The purified pellet was resuspended in *dd*-H_2O (pH 8) and dried by lyophilization, yielding in spermine-functionalized acetalated polysaccharides as a colorless powder.

Table 20: Composition of the reagents for the reductive amination of partially oxidized and acetalated dextran and HES

Reagent	Ac-ox-DEX 10 kDa	Ac-ox-HES 70 kDa	Ac-ox-HES 130 kDa	Ac-ox-HES 200 kDa
Polysaccharide	5.6 g, 34.6 mmol AGU	1.5 g, 9.3 mmol AGU	2.0 g, 12.3 mmol AGU	2.0 g, 12.3 mmol AGU
Spermine	10.1 g, 49.9 mmol	3.0 g, 15.0 mmol	4.0 g, 19.9 mmol	4.0 g, 19.9 mmol
DMSO	25 mL	15 mL	15 mL	15 mL
Reaction time / temperature	22 hours, 50 °C	22 hours, 50 °C	22 hours, 55 °C	22 hours, 55 °C
Sodium borohydride	5.1 g, 133.6 mmol	1.5 g, 39.7 mmol	2.0 g, 53.2 mmol	2.0 g, 53.2 mmol
Reaction time / temperature	18 hours, 40 °C	18 hours, 40 °C	18 hours, 40 °C	18 hours, 40 °C
dd-H_2O pH 8	150 mL	60 mL	60 mL	60 mL
Yield	5.2 g	1.1 g	1.9 g	1.8 g

The degree of functionalization was determined by elemental analysis using the nitrogen content for the calculation.

^{1}H-NMR Sp-Ac-DEX (300 MHz, $CDCl_3$): δ 0.83 (s), 1.25 (s), 1.40 (s, br, CH_3 acetal), 1.80 (s), 2.04 (s, br), 2.17 (s), 2.61 (s), 2.75 (br, spermine), 3.25 (s), 3.30 (br, OCH_3 acetal), 3.40–4.40 (m, AGU-H dextran), 4.82 (s, br, AGU-H dextran), 5.14 (s, br, anomeric H dextran)

^{1}H-NMR Sp-Ac-HES 70 kDa (300 MHz, $CDCl_3$): δ 0.83 (s), 1.25 (s), 1.33 (s, br, CH_3 acetal), 1.82 (s, br), 2.61 (s), 2.61 (s), 2.77 (br, spermine), 3.18 (s), 3.31 (br, OCH_3 acetal), 3.40–4.40 (m, AGU-H HES), 5.07 (s, br, AGU-H HES), 5.55 (s, br, anomeric H HES)

^{1}H-NMR Sp-Ac-HES 130 kDa (300 MHz, $CDCl_3$): δ 0.82 (s), 1.25 (s), 1.33 (s, br, CH_3 acetal), 1.82 (s), 2.61 (s), 2.76 (br, spermine), 3.18 (s), 3.32 (br, OCH_3 acetal), 3.40–4.40 (m, AGU-H HES), 5.08 (s, br, AGU-H HES), 5.55 (s, br, anomeric H HES)

^{1}H-NMR Sp-Ac-HES 200 kDa (300 MHz, $CDCl_3$): δ 0.83 (s), 1.19 (s), 1.25 (s), 1.33 (s, br, CH_3 acetal), 1.69 (s, br), 2.61 (s), 2.76 (br, spermine), 3.17, 3.22 (br, OCH_3 acetal), 3.40–4.40 (m, AGU-H HES), 5.09 (s, br, AGU-H HES), 5.54 (s, br, anomeric H HES)

5.3.2 Preparation of Nanoparticles

Preparation of Empty Nanoparticles by Double Emulsion

The preparation of particles made out of acetalated dextran was published before by Bachelder *et al.* (2008)[31] and was adjusted for the following experiments. In short, 10 mg of acetalated polysaccharide was dissolved in 800 μL of ice-cold dichloromethane (DCM) in a round bottom cell culture tube and stored on ice for the whole preparation. A primary emulsion was prepared by adding 100 μL PBS to the dextran solution and sonication of the sample for 10 seconds with a probe sonicator (Bandelin Ultrasonic Homogenisator Sonoplus UW 70, power MS 72/D, cycle 70%). Afterwards, 4 mL of a PVA solution (3% in PBS) were added to the first dextran emulsion and sonicated again for 30 seconds to get a secondary water-in-oil-in-water double emulsion. The emulsion was stirred vigorously overnight to remove all DCM. Purification was done by ultracentrifugation (45,000 x *g*, 20 min) and the pellet was rinsed 2-times with 3 mL *dd*-H_2O (pH 8). Finally, 100 μL PVA solution (0.3% in *dd*-H_2O, pH 8) were added as a cryoprotectant before lyophilization resulting in a colorless fluffy powder (approx. 4–5 mg).

Encapsulation of Dextran-Oregon Green® 488 in Nanoparticles

Nanoparticles were prepared with a double emulsion method like described before. Instead of PBS, 50 μL dextran-Oregon Green® 488 in PBS (100 ng·μL^{-1}, M_W 10,000 g·mol^{-1}, anionic, Life Technologies) was added to prepare a primary emulsion. The following preparation steps were described before. The dextran-Oregon Green® 488-loaded particles were obtained as a bright yellow, fluffy product (approx. 4–5 mg compared to the initial weight) and were stored protected from light at all times.

Encapsulation of siRNA in Sp-Ac-DEX Nanoparticles

For the encapsulation of siRNA, nanoparticles based on Sp-Ac-DEX were prepared with a double emulsion method like described before. Instead of PBS, 50–100 μL siRNA (diluted in PBS) were added to the dissolved acetalated polymer to prepare a primary emulsion. The following synthesis steps were performed as described above.

Table 21: Composition of siRNA-loaded nanoparticles

Target siRNA	Conc. siRNA stock / μM	Added volume of siRNA / μL	siRNA per polymer / nmol·mg^{-1}	/ μg·mg^{-1}
Cy5-siRNA targeting CD68	100	60	0.6	8
siRNA-*luc*	740	60	4.4	60
		80	5.9	80
		100	7.4	100

Encapsulation of pDNA in Sp-Ac-DEX Nanoparticles

Nanoparticles based on Sp-Ac-DEX were prepared with a double emulsion method like described before. Instead of 100 μL PBS, ~10 μL pDNA 1699 coding for eGFP and firefly luciferase per 1 mg Sp-Ac-DEX was added to prepare a primary water-in-oil emulsion. Concentrations of the DNA solution in PBS, provided by the group of [redacted] (Universitätsmedizin Mainz, Germany), varied between 2.1 and 3.0 μg·μL^{-1}.

Labeling of Nanoparticles with Fluorescent Dyes

Spermine-functionalized particles were labeled with fluorescent dyes on their surface so that a tracking during flow cytometry, microscopy and *in vivo* imaging was possible. Therefore, the particles were suspended in PBS buffer (pH 8.0, NaOH) at concentrations of 2 mg·mL^{-1}. For 1 mg particle material, 200 pmol to 2 nmol of amine reactive NHS-fluorescent-dye in a stock solution of anhydrous DMSO (10 mM) was added. Particles were incubated protected from light for 2 hours and purified with Amicon® Ultra 4 centrifugal filter membranes (regenerated cellulose, MWCO 30 kDa, 7,500 x *g*, 10 min., Merck Millipore). Particles were rinsed with *dd*-H_2O (pH 8, 2 mL, 5-times centrifugation) and 0.3% PVA in *dd*-H_2O (pH 8.0, 10 μL·mg^{-1} particles) was added as a cryoprotectant before lyophilization overnight. The product was obtained as a colored, fluffy powder and stored protected from light at all times.

Table 22: Commercial available fluorescent, NHS-activated dyes used for the surface labeling of amine-bearing particles

Additional Information	Structure of Dye
Oregon Green® 488-X, N-hydroxy-succinimide ester (NHS), 6-isomer (Life Technologies, M_W 622.53 g·mol^{-1}, $\lambda_{ex.}$ 494 nm, $\lambda_{em.}$ 519 nm)	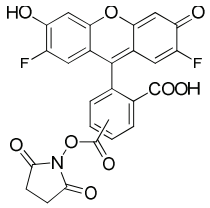
5/6-Carboxytetramethylrhodamine NHS ester, mixed isomers (5/6-TAMRA-SE) (emp Biotech, M_W 527.5 g·mol^{-1}, $\lambda_{ex.}$ 546 nm, $\lambda_{em.}$ 575 nm)	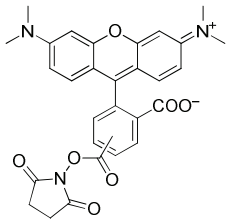
Sulfo-Cy5 NHS-Ester (Lumiprobe, M_W 761.84 g·mol^{-1}, $\lambda_{ex.}$ 646 nm, $\lambda_{em.}$ 662 nm)	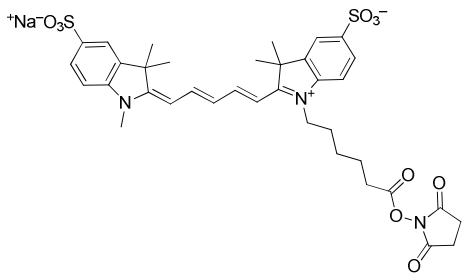

5.3.3 Purification of Nanoparticles with Centrifugal Units

Preparation of Test Particles (Conjugation of Fluorescent Dyes)

For the comparison of different centrifugal units, test particles were prepared by labeling the surface of empty Sp-Ac-DEX particles with fluorescent dyes and separation of the free dye by centrifugation with the filter units listed in **Table 23**.

Table 23: Characterized centrifugal filter units for the purification of fluorescent dye-labeled Sp-Ac-DEX nanoparticles

Centrifugal unit	Membrane	MWCO
Centrisart®I	Polyethersulfone	100,000
Vivaspin 2 PES	Polyethersulfone	30,000
Vivaspin 2 CTA	Cellulose triacetate	20,000
Vivaspin 2 Hydrosart®	Hydrosart® regenerated cellulose	30,000

Sp-Ac-DEX particles (2 mg·mL^{-1} in PBS pH 8.0) were incubated with a) sulfo-Cy5-NHS (2 mg·mL^{-1} in PBS pH 8.0, 200 pmol dye per mg particles) or b) Oregon Green® 488-NHS (10 mM in DMSO, 2 nmol dye per mg particles) for 2 hours protected from light. Afterwards,

1.8 mL (3.6 mg) Cy5- and 1.7 mL (3.4 mg) Oregon Green-labeled particles were transferred to each centrifugal unit and particles were purified by centrifugation for 5-times at 2,500 x *g* for 15 minutes (RT) and rinsing the particles with *dd*-H_2O (pH 8.0, 2 mL). Particles were lyophilized afterwards to determine the yield by mass.

Determination of Conjugated Sulfo-Cy5

The lyophilized Cy5-particles were resuspended in PBS (pH 7.4, 3.9 mg·mL^{-1}) and 75 μL of each suspension was transferred in triplets to a black 96-well microplate (flat bottom). The pure sulfo-Cy5 dye (stock: 20 nmol·mL^{-1} in DMSO) was diluted in PBS and used for the preparation of a standard curve with concentrations from 12.2 to 780 pmol·mL^{-1}. Each standard was transferred in triplets (75 μL) to the black microplate and the emission of the sulfo-Cy5 was read with a Tecan microplate reader ($\lambda_{ex.}$ 642 nm, $\lambda_{em.}$ 667 nm).

Determination of Conjugated Oregon Green® 488

The lyophilized Oregon Green® 488-particles were resuspended in PBS (pH 7.4, 1 mg·mL^{-1}) and 75 μL of each suspension was transferred in triplets to a black 96-well microplate (flat bottom). The pure Oregon Green® 488 dye (stock: 20 nmol·mL^{-1} in DMSO) was diluted in PBS and used for the preparation of a standard curve with concentrations from 31.25 to 2000 pmol·mL^{-1}. Each standard was transferred in triplets (75 μL) to the black microplate and the emission of the Oregon Green® 488 was read with a Tecan microplate reader ($\lambda_{ex.}$ 488 nm, $\lambda_{em.}$ 514 nm).

5.3.4 Addition of Cryoprotectants

After the nanoparticle preparation by a double emulsion evaporation method described in 5.3.2, different cryoprotectants were added to the particle suspension before lyophilization overnight. Cryoprotectants were dissolved in *dd*-H_2O at concentrations of 10 g·L^{-1} (PVA 30 g·L^{-1}) and filtered (Ø 0.22 μm) before further use. In first studies, cryoprotectants were added to obtain a final concentration of 1%, 5%, 10%, 20%, and 40% (PVA 3%) in the particle suspension compared to the mass of the particles. After lyophilization, particles were resuspended in PBS buffer at a concentration of 0.5 mg·mL^{-1} by sonicating for 5 minutes and vortexing for 10 seconds, repeating the procedure twice. 100 μL of this nanoparticle suspension were mixed with 900 μL PBS and poured into a DLS cuvette, vortexed slightly and size was measured with a Zetasizer Nano ZS. Zeta potential was measured in 25 mM HEPES buffer by mixing 100 μL particle suspension with 800 μL HEPES buffer.

5.3.5 PEGylation of Nanoparticles

Surface Modification of Sp-Ac-DEX Nanoparticles with Methoxy-PEG-NHS

For the PEGylation with monofunctional NHS-activated methoxy-PEG, particles were suspended in PBS buffer (pH 8.0, NaOH) at a concentration of 2 mg·mL^{-1}. Methoxy-PEG-*N*-hydroxysuccinimide ester (2 kDa or 5 kDa, 10x molar excess; 50 mg·mL^{-1}, Rapp Polymere)

was dissolved in the above mentioned buffer and added dropwise to the nanoparticle suspension. It was shown in first studies using the fluorescamine assay that 100–150 nmol primary amines per milligram nanoparticles are available on the nanoparticle surface. The modified particles were stirred for 2 hours and purified by ultracentrifugation (45,000 x *g*, 20 min.) and rinsing the pellet with *dd*-H_2O (pH 8, 2-times). Before lyophilization, 0.3% PVA in *dd*-H_2O (pH 8.0, 10 $\mu L \cdot mg^{-1}$ particles) was added as a cryoprotectant and a colorless, fluffy powder was obtained.

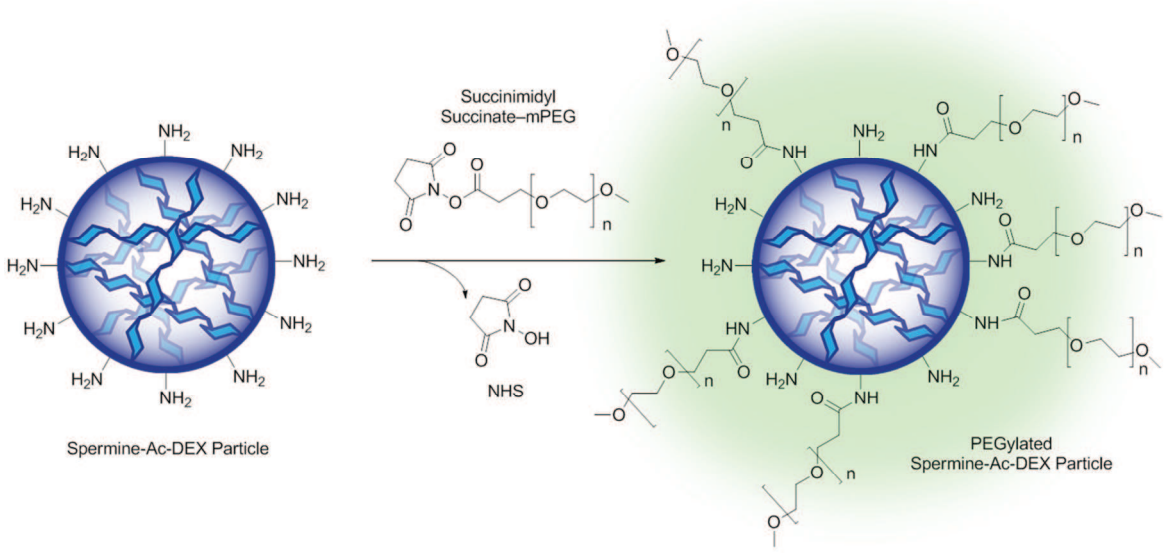

Figure 76: Surface modification of spermine-modified Ac-DEX particles with NHS-activated poly(ethylene glycol) (PEG-NHS).

Surface Modification of Sp-Ac-DEX Nanoparticles with Fmoc-PEG-NHS

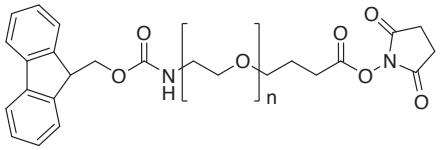

Figure 77: Fmoc-functionalized and NHS-activated poly(ethylene glycol) for the surface modification of spermine-modified Ac-DEX particles.

PEGylation with Fmoc-NH-PEG-NHS (5 kDa, Rapp Polymere) was performed under the same reaction conditions described in the previous section. Due to the fluorescence-active fluorenylmethyloxycarbonyl (Fmoc) group, the particles were stored protected from light at all times.

5.3.6 DEXylation of Nanoparticles

Synthesis of a Bifunctional Thiol-Linker (4-Mercaptobutanehydrazide)

The synthesis of the bifunctional linker 4-mercaptobutanehydrazide (M_W 134.05 $g \cdot mol^{-1}$) was described before by von Delius *et al.* (2010)[264]. γ-Thiobutyrolactone (1.0 g, 9.79 mmol, 1.0 eq., M_W 102.16 $g \cdot mol^{-1}$) was added dropwise to a solution of hydrazine monohydrate (0.74 g,

14.69 mmol, 1.5 eq., M_W 50.06 g·mol^{-1}) in MeOH (2 mL). The reaction was performed under the protection of argon gas and was stirred at room temperature for 30 minutes before removing the solvent under reduced pressure. The product was totally dried under high vacuum and obtained as a colorless oil (TLC: MeOH/Et_2O 1:5 (V/V); 0.97 g, 74%).

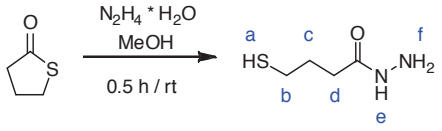

Figure 78: Reaction of γ-thiobutyrolactone and hydrazine monohydrate resulting in 4-mercapto-butanehydrazide.

^{1}H-NMR (300 MHz, $CDCl_3$): δ 1.34 (t, J = 8.0 Hz, 1H, H_a), 1.94 (m, J = 7.0 Hz, 2H, H_c), 2.35–2.24 (m, 2H, H_d), 2.56 (q, J = 7.1 Hz, 2H, H_b), 3.93 (s, br, 2H, H_f), 7.16 (s, br, 1H, H_e)

(ESI$^+$): m/z = 134.2188 [M] (calc. 134.2010 for $C_4H_{10}ON_2S$)

Conjugation of the Thiol-Linker with Dextran

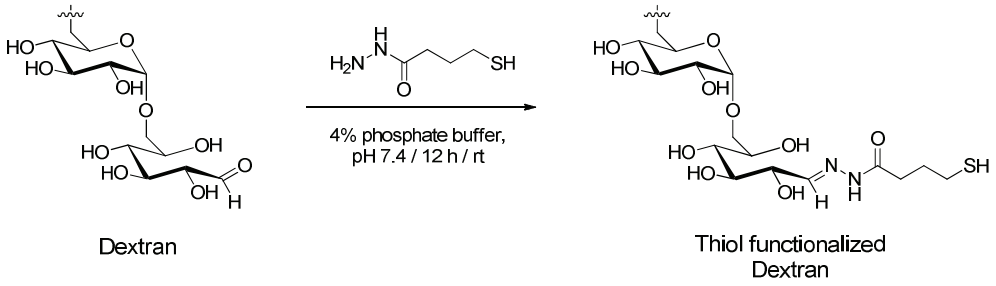

Figure 79: Conjugation of 4-mercaptobutanehydrazide with dextran in 4% phosphate buffer.

For the conjugation of dextran with the bifunctional linker 4-mercaptobutanehydrazide, 1.0 g dextran was dissolved in 2 mL 4% sodium phosphate buffer pH 7.4. After total dissolution of the dextran, the unpurified crosslinker was dissolved in buffer (0.2 g·mL^{-1}) with 5-times molar excess to the aldehyde content of the dextran. The linker was added dropwise to the dextran solution and was stirred overnight. Finally, the thiol-modified dextran (DEX-SH) was purified by dialysis using a regenerated cellulose membrane (Spectra/Por® 6 dialysis membrane, regenerated cellulose, MWCO 1 kDa, Carl Roth) against *dd*-H_2O pH 8 and the water was changed 5-times in 24 hours. After lyophilization, a colorless, Styrofoam-like product was obtained. The amount of thiol groups per dextran was determined by Ellman's assay.

Table 24: Aldehyde content of dextran used for the introduction of thiol groups. It is assumed that each dextran chain has one aldehyde group at the reducing end of the molecule.

Molecular weight of dextran	Aldehyde per 1 g of dextran
3.5 kDa	285.7 μmol
5 kDa	200.0 μmol

Ellman's Assay for the Quantification of Thiol Groups

For the Ellman's assay, thiol-modified dextran (50 mg·mL^{-1}) was dissolved in sodium phosphate buffer (0.1 M, pH 8) containing 1 mM EDTA. Ellman's reagent was dissolved in the reaction buffer (4 mg·mL^{-1}) and 4 μL of this solution were added to 200 μL reaction buffer and 20 μL sample in a clear, flat bottom 96-well microplate (Sarstedt). The reaction was incubated for 15 minutes under gentle agitation and the absorbance was measured with a Victor microplate reader at 405 nm. All samples were prepared and measured in triplets and the mean absorbance was used for the determination of the contained thiol groups. *N*-acetyl-*L*-cysteine at concentrations of 31.25 μM to 1 mM was used to prepare a standard curve.

Table 25: Calculated thiol groups per dextran chain determined by Ellman's assay. The degree of substitution describes the amount of aldehydes which have reacted with the thiol-linker.

Molecular weight of dextran	Thiol groups per 1 mol dextran	Degree of Substitution
3.5 kDa	190 mmol	19%
5 kDa	110 mmol	11%

Conjugation of DEX-SH to Sp-Ac-DEX Nanoparticles

For the DEXylation of Sp-Ac-DEX nanoparticles, surface amine containing Sp-Ac-DEX particles were suspended in PBS buffer (pH 7.4, 1 mM EDTA) at a concentration of 2 mg·mL^{-1}. For the calculation of the needed amount of conjugation reagent, the amount of 150 nmol primary amines per 1 mg nanoparticles, determined by fluorescamine assay, was assumed. First, the bifunctional crosslinker 3-sulfo-*N*-succinimidyl 4-(*N*-Maleimido-methyl)cyclohexane-1-carboxylate sodium salt (sulfo-SMCC, TCI chemicals) was conjugated via NHS chemistry to the primary amines of the Sp-Ac-DEX particles to introduce maleimide groups on the particle surface. Sulfo-SMCC (M_W 436.37 g·mol^{-1}, 10x molar excess, 2 mg·mL^{-1}) was dissolved in the above mentioned buffer and added dropwise to the nanoparticle suspension. The reaction was incubated under gentle stirring for 2 hours and the unconjugated crosslinker was eliminated by ultracentrifugation (45,000 x *g*, 20 min.) or in VWR® SuperSpin™ microcentrifuge tubes (30,000 x *g*, 20 min.) followed by removal of the super-natant. The particles were suspended in buffer (2 mg·mL^{-1}) and finally a solution of thiol-modified dextran in buffer (5x molar excess, 15 mg·mL^{-1}) was added to the maleimide-functionalized nanoparticles. The reaction was incubated for further 4 hours and purified by ultracentrifugation (45,000 x *g*, 20 min.) or in VWR® SuperSpin™ microcentrifuge tubes (30,000 x *g*, 20 min.). The resulting pellet was rinsed with *dd*-H_2O (pH 8, 3 mL, 2-times). Before lyophilization, 0.3% PVA in *dd*-H_2O (pH 8.0, 10 μL·mg^{-1} particles) was added as cryoprotectant and a colorless, fluffy powder was obtained. The DEXylated particles were characterized by size, zeta potential, SEM, and fluorescamine assay to determine the amount of conjugated DEX.

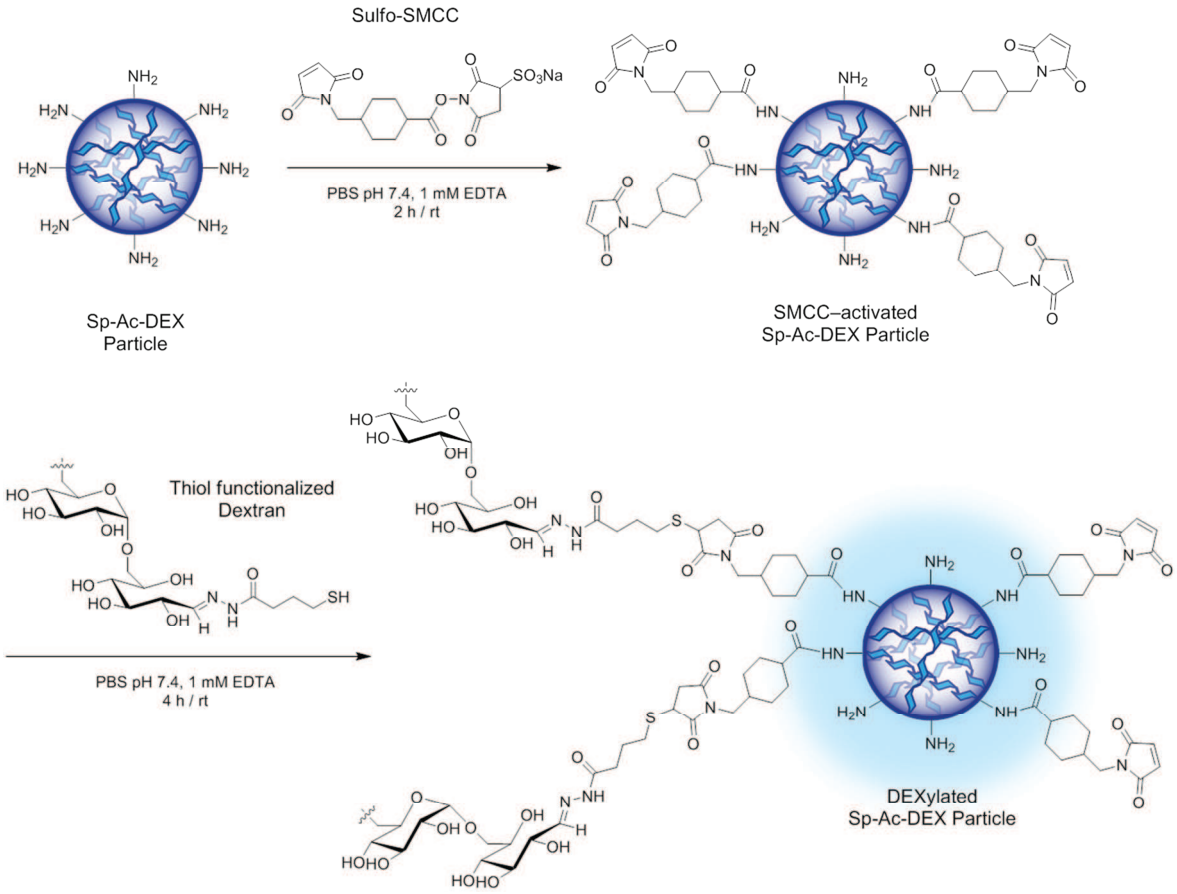

Figure 80: Scheme of DEXylation; amine-bearing Sp-Ac-DEX particles are activated on their surface with the bifunctional linker sulfo-SMCC. The introduction of SMCC leads to maleimide groups on the particle surface which can react with the thiol-modified dextran resulting in a hydrophilic dextran-coated Sp-Ac-DEX particle.

5.3.7 Introduction of Targeting Groups via Bifunctional PEGylation

PEGylation of Nanoparticles with PEG-$(NHS)_2$

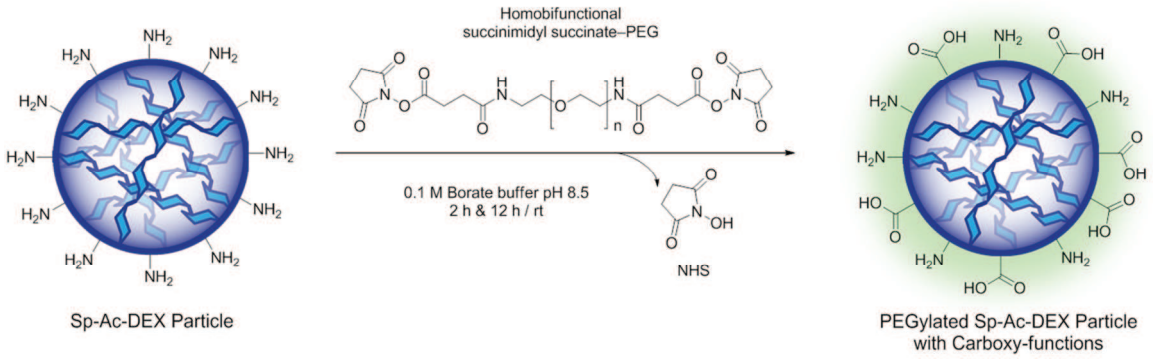

Figure 81: PEGylation of Sp-Ac-DEX particles with homobifunctional PEG-$(NHS)_2$ and following hydrolysis to introduce carboxyl groups on the particle surface.

Sp-Ac-DEX particles were suspended in borate buffer (0.1 M, pH 8.5, 1 mg·mL^{-1}, 1 eq.) and incubated with the homobifunctional PEG-(NHCO-C_2H_4-CONHS)$_2$ (2 kDa) dissolved in

borate buffer (3 mg·mL^{-1}, 1 eq.) for 2 hours. Particles were centrifuged (45,000 x *g*, 20 min.), the supernatant removed, and particles suspended in fresh borate buffer (1 mg·mL^{-1}). Afterwards, the particle suspension was stirred overnight in buffer to hydrolyze the containing NHS groups. Purification was performed by ultracentrifugation (45,000 x *g*, 20 min.) and rinsing the pellet with *dd*-H_2O (pH 8, 2 mL, 2-times). Particles were lyophilized with 0.3% PVA (10 μL·mg^{-1} particles) as a cryoprotectant (yield 81%) and characterized by size, zeta potential and fluorescamine assay.

EDC Coupling of Fmoc-Lys

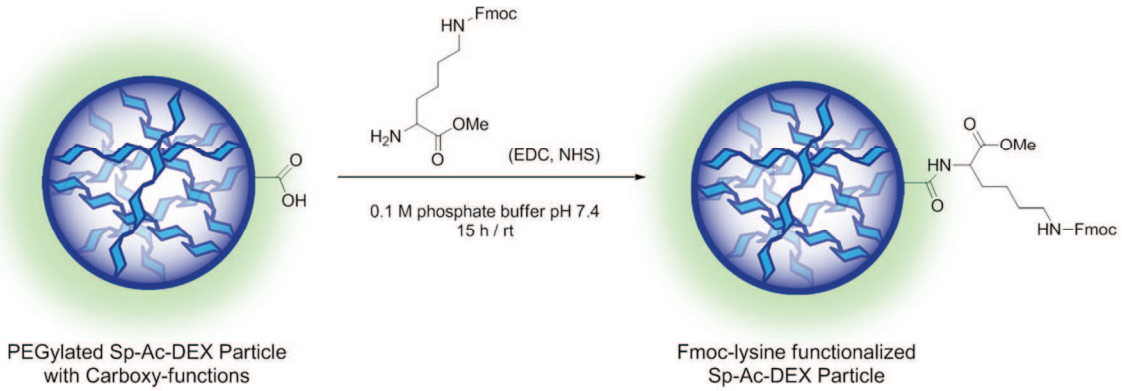

Figure 82: EDC-coupling of Fmoc-lysine with carboxy-functionalized Sp-Ac-DEX particles.

EDC coupling of an amine containing compound to PEGylated particles containing carboxyl groups on their surface, was performed in a similar reaction described before by Carrillo-Conde *et al.* (2011)[309]. Sp-Ac-DEX nanoparticles containing carboxyl groups on their surface were suspended in phosphate buffer (0.1 M, pH 7.4) and incubated with solutions of EDC · HCl, NHS, and *H*-Lys(Fmoc)-OMe · HCl in phosphate buffer for 15 hours. Particles were purified by centrifugation (30,000 x *g*, 20 min.) and rinsed with *dd*-H_2O (pH 8, 2-times). After lyophilization with 0.3% PVA as a cryoprotectant (10 μL·mg^{-1} particles), particles were obtained as a colorless, fluffy powder (yield 58%).

Table 26: Composition of reagents used for the surface functionalization of Sp-Ac-DEX particles containing carboxyl groups with Fmoc-lysine

Compound	Amount*			Conc. in buffer
Sp-Ac-DEX-NP-COOH	20 nmol	2.6 mg	1 eq.	3.25 mg·mL^{-1}
EDC · HCl	614.5 nmol	117.8 μg	12 eq.	1 mg·mL^{-1}
NHS	512.6 nmol	59.0 μg	10 eq.	1 mg·mL^{-1}
H-Lys(Fmoc)-OMe · HCl	614.5 nmol	257.4 μg	12 eq.	0.5 mg·mL^{-1}

(* amount of COOH-groups in mol per 1 mg nanoparticles)

5.3.8 Particle Characterization

Determination of Particle Size by Nanoparticle Tracking Analysis

Particle size and aggregation was determined by Nanoparticle Tracking Analysis (NTA). NTA was performed with a NanoSight LM 10 microscope (Malvern Instruments) equipped with a green laser (532 nm) and a sCMOS camera. Unless otherwise mentioned, samples were prepared in PBS (filtered 0.22 μm) at concentrations of approx. 2 $\mu g \cdot mL^{-1}$ and sonicated (Bandelin Sonorex RK 102 H) as well as vortexed thoroughly before each measurement. Movements of the particles were recorded as videos for 30 seconds at 25 °C in triplets. The size calculation was performed with NTA software version 3.1 build 3.1.54.

Table 27: Software settings for NTA measurements of nanoparticles

Capture:	Screen Gain 1.0
	Camera level 10
Process:	Screen Gain 1.0
	Detection Threshold 5

Determination of Particle Size by Dynamic Light Scattering (DLS)

Size, aggregation, and polydispersity of the surface modified Sp-Ac-DEX particles were determined with a second method using DLS with a Malvern Zetasizer Nano ZS instrument. Evaluation of the data was performed with the Zetasizer software 6.20 and Mark-Houwink parameters. Settings are displayed in the following **Table 28**. Particles were suspended in PBS (filtered 0.22 μm) at concentrations of approx. 0.25 $\mu g \cdot mL^{-1}$ and suspensions were sonicated as well as vortexed thoroughly before each measurement.

Table 28: Software settings for the DLS measurements of nanoparticles with the Zetasizer Nano ZS from Malvern

Sample:	Material dextran
	RI 1.590
Dispersant:	Water
	Temperature 20 °C
	Viscosity 1.0031 cP
	RI 1.330
Cell:	ZEN0117-Disposable Low Volume Cuvette 100 μL
	173° Backscatter (NIBS default)
Runs:	3x12

Determination of Particle Surface Charge by Measuring Zeta Potential

Zeta potential (particle charge) was measured by a Malvern Zetasizer Nano ZS instrument using a clear disposable zeta cell. Three measurements with 12 individual runs were performed at 25 °C. Particle samples were prepared at concentrations of 0.1 mg·mL^{-1} in HEPES buffer (25 mM, pH 7.4). The refractive index (RI) of the dispersant (preset: water) was adjusted to 1.330 and the viscosity to 0.8872 cP with a dielectric constant of 78.5. The RI of the particle material dextran was set to 1.590. The data was analyzed by the model of Smoluchowski with the Malvern Zetasizer software 6.20.

Scanning Electron Microscopy (SEM)

The surface morphology of the particles was visualized by scanning electron microscopy (SEM) using a Nova NanoSEM 630 (FEI) at an acceleration voltage of 5 kV and a working distance from 4 nm. A low voltage high contrast detector (vCD) was used as secondary electron detector. All samples were prepared on a silicon-wafer (Si) and sputter-coated with 7.5 nm of gold (Au) to reduced charging of the sample. Measurements were performed by [redacted] in the group of [redacted] Johannes Gutenberg-University, Mainz.

Quantification of the PEGylation of Sp-Ac-DEX Particles by Fluorescamine Assay

Particles were suspended in PBS at concentrations of 2 and 4 mg·mL^{-1}. Hexylamine was used as a standard diluted in PBS at concentrations of 19 up to 40 μg·mL^{-1}. The assay was prepared in triplets in a black, flat bottom 96-well microplate (Greiner Bio-One). Into each well, 125 μL buffer (PBS) and 25 μL sample, standard or PBS (blank) was added in triplets. Directly before the read out, 50 μL of an ice-cold fluorescamine solution in acetone (0.3 mg·mL^{-1}, TCI, Belgium) was added and the emission measured with a Tecan microplate reader ($\lambda_{ex.}$ 380 nm, $\lambda_{em.}$ 460 nm). The amount of amines per particle sample was calculated with Microsoft Excel with a standard curve.

Quantification of the PEGylation of Sp-Ac-DEX Particles by ^{1}H-NMR

5.11 mg PEGylated (5 kDa) particles were suspended in deuterium oxide (700 μL) and pyridine (1.239 μmol) was added as an internal standard. ^{1}H-NMR was measured and analyzed by MestReNova software.

Quantification of the PEGylation of Sp-Ac-DEX Particles by Measuring Fmoc-Fluorescence

For the determination of the amount of Fmoc-PEG chains on the nanoparticle surface, nanoparticles were dissolved in DMSO at concentrations of 0.5 mg·mL^{-1}. Pure Fmoc-PEG (5 kDa) dissolved in DMSO was used as a standard at concentrations of 3.125 to 200 nmol·mL^{-1}. Each standard and sample (100 μL) was added in triplets to a black, flat bottom 96-well microplate and the fluorescence was read with a Tecan microplate reader ($\lambda_{ex.}$ 265 nm, $\lambda_{em.}$ 306 nm). The amount of Fmoc-PEG on the particle surface was calculated with Microsoft Excel.

Calculation of the Number of Amines per Particle Sample

The average size of the particles (NP) determined by DLS and NTA measurements is around 150 nm in diameter (≙ $75 \cdot 10^{-9}$ m radius) with a density of $1.045 \cdot 10^{3}$ g · L^{-1}. The equations for the calculation of the amine groups per mass particles and per particle are shown below (used in **Table 10**).

Groups NH_2 per mg NP	= mol NH_2 per mg NP × Avogadro constant (Avogadro constant: $6.022 \cdot 10^{23}$ mol^{-1})
Volume NP	= $^{4}/_{3}\ \pi \times (\text{NP radius})^3$ = $1.767 \cdot 10^{-18}$ L ($1\ m^3$ ≙ 1000 L)
Mass NP	= NP density × NP volume = $1.847 \cdot 10^{-15}$ g
Number NP per 1 mg sample	= mass sample / mass 1 NP = $5.41 \cdot 10^{11}$ NP
mol NH_2 per NP	= mol NH_2 / $5.41 \cdot 10^{11}$ NP
Groups NHs per NP	= mol NH_2 per NP × Avogadro constant

5.3.9 Determination of the Encapsulation Efficiencies

Quantification of Encapsulated Dextran-Oregon Green® 488

The encapsulation efficiency of the encapsulated dextran-Oregon Green® 488 (dex-OG488) was determined by measuring the emission of the fluorescent dye Oregon Green® 488. Sp-Ac-DEX nanoparticles were dissolved in acetate buffer (0.3 M, pH 5, 5 mg·mL^{-1}) overnight. 10 μL of the dissolved nanoparticle solution and 90 μL PBS were added to a black, flat bottom 96-well microplate (Greiner Bio-One). The pure dex-OG488 was used to prepare a standard curve at concentrations of 31 ng·mL^{-1} up to 2 μg·mL^{-1}. Standard solutions were prepared in PBS containing 10% (V/V) acetate buffer (0.3 M, pH 5). Samples and standards (100 μL per well) were added in triplets to the microplate and the emission was read with a Victor microplate reader ($\lambda_{ex.}$ 496 nm, $\lambda_{em.}$ 524 nm).

PicoGreen Assay for the Determination of DNA

The encapsulation efficiency of the encapsulated DNA was determined by Quant-iT™ PicoGreen® dsDNA Assay Kit (Invitrogen™) regarding the manufacturer's protocol. Nanoparticles were dissolved in acetate buffer (0.3 M, pH 5, 10 mg·mL^{-1}) overnight. In preparation of the assay, 1 μL of the dissolved nanoparticle solution, 49 μL TE buffer (1x) and

50 μL heparin solution (40 mg·mL^{-1} in TE buffer) were incubated for 1 hour. The pure DNA was used to prepare a standard curve. PicoGreen® reagent solution (100 μL) was added to the samples, incubated for 5 minutes and the emission was read with a Victor microplate reader ($\lambda_{ex.}$ 496 nm, $\lambda_{em.}$ 524 nm).

RiboGreen Assay for the Determination of RNA

The Quant-iT™ RiboGreen® Assay was used to determine the encapsulated siRNA in double emulsion particles. The amount of free siRNA before the particle purification was measured and compared to the initial used concentration of siRNA. Only the non-encapsulated siRNA was able to react with the RiboGreen® reagent resulting in a fluorescent compound with an emission maximum at 535 nm ($\lambda_{ex.}$ 485 nm). Therefore, particles were ultracentrifuged and 10 μL of the particle supernatant were mixed with 90 μL PBS in a 96-well microplate (black, flat bottom). The pure siRNA-*luc* was diluted in PBS at a concentration that fit 100% encapsulation. The RiboGreen® reagent was diluted 1:200 in PBS and 100 μL were added to each well. The reagent was incubated with the particles for 5 minutes protected from light before reading the fluorescence of the reacted dye with a Tecan microplate reader. Particle results were compared to the fluorescence of the theoretical amount of encapsulated siRNA using Microsoft Excel.

Fluorescence Measurement of Labeled siRNA

In case of fluorescence-labeled RNA or DNA, the encapsulation efficiency was directly determined by reading the emission of the fluorescence dye. Therefore, an exact amount of particles (10 mg·mL^{-1}) was dissolved in acetate buffer (0.3 M, pH 5) overnight. Dissolved particles (10 μL) were mixed with 90 μL PBS in a 96-well microplate (black, flat bottom) and fluorescence was read. The pure siRNA was used to prepare a standard curve.

5.3.10 Cell Culture

HeLa cells were grown in Dulbecco's Modified Eagle Medium (DMEM GlutaMAX™) supplemented with 10% (V/V) fetal calf serum (FCS), 1% pyruvate, and 1% penicillin-streptomycin (Life Technologies). Cell incubations were performed in a humidified incubator at 37 °C with 5% CO_2 atmosphere. All used buffers were either autoclaved, sterile filtered or already sterile when supplied and were preheated to 37 °C before usage. Cells were grown in 25 cm^2 or 75 cm^2 standard cell culture flasks (Greiner Bio-One).

Determination of the Cell Viability by MTT Assay

For the MTT assay, HeLa cells were precultured in DMEM containing 10% FCS and 1% P/S. Cells were seeded in a sterile clear, flat bottom 96-well cell culture microplate (Greiner Bio-One) at a concentration of 15,000 cells per well and a volume of 100 μL. Cells were allowed to attach overnight and incubated with particle samples the next day. Therefore, the nanoparticles were suspended in DMEM at concentrations of 31.25 μg·mL^{-1} up to 1 mg·mL^{-1}. DMEM was removed from HeLa cells and replaced by 100 μL sample suspension or DMEM

as blank in triplets followed by incubation for 48 hours at 37 °C in 5% CO_2. After 48 hours, 40 μL MTT solution (3 mg·mL^{-1} in DMEM) was added to each well and incubated at 37 °C for 20 minutes. After total removal of the medium, a mixture of 200 μL DMSO and 25 μL glycine buffer (0.1 M glycine, NaCl, pH 10.5) was added to each well and softly shaken for 15 minutes to dissolve the purple formazan salt. 50 μL of this concentrated, purple DMSO solution was added to a second clear, flat bottom 96-well microplate containing a mixture of 17 μL glycine buffer and 133 μL DMSO per well. Finally, the absorbance of the formazan was read using a Victor microplate reader at 595 nm. Furthermore, the background was measured at 670 nm and subtracted from the data obtained from the first read out.[310] Cell viability was calculated with Microsoft Excel. HeLa cells containing no particle samples were set as 100% and were compared to the absorbance of the cells treated with the nanoparticle samples.

Uptake of Nanoparticles in Cell Lysate of HeLa Cells

The uptake of the modified polysaccharide nanoparticles in HeLa cells was measured from the emission of encapsulated dextran-Oregon Green® 488 (dex-OG488) identified in the cell lysate. HeLa cells were cultured in DMEM like described before and seeded in a clear, flat bottom 24-well cell culture microplate (80,000 cells per well in 500 μL DMEM, Greiner Bio-One). Cells were allowed to attach overnight and incubated with particles (10 μg·mL^{-1}) the following day. For the incubation with the nanoparticle samples, all DMEM was removed and replaced by particles suspended in DMEM (10 μg·mL^{-1}, 500 μL). Cells were incubated with particles for 4 hours or 24 hours before removing the medium. Afterwards, cells were washed 2-times with 500 μL PBS and lysed with 150 μL PBS containing 1% Triton™ X-100 incubated on ice for 30 minutes and centrifuged (10,000 x *g*) to remove all cell fragments. To determine the containing particles in the HeLa suspension, the emission of the dex-OG488 was measured and correlated with the amount of cells determined by the PCA assay to avoid discrepancy in the cell growth.

50 μL of each lysate sample was mixed with 50 μL PBS and added to a black, flat bottom 96-well microplate, using pure dex-OG488 as a standard. 50 μL of standard and 50 μL cell lysate containing no particles were also added to the microplate at concentrations of 3.9 up to 250 ng·mL^{-1}. For the relative quantification of the nanoparticles, the stock solution of nanoparticles in PBS was measured at concentrations that corresponded to the nanoparticle concentration put on cells. DMSO (100 μL) was added to each well to dissolve all nanoparticles and the plate was incubated protected from light for two hours. The emission was measured with a Victor microplate reader ($\lambda_{ex.}$ 496 nm, $\lambda_{em.}$ 524 nm).

For the determination of the containing proteins, 50 μL of each cell lysate sample was added to a clear, flat bottom 96-well microplate as well as 50 μL BSA standard at concentrations of 125 μg·mL^{-1} up to 2 mg·mL^{-1} in PBS containing 1% Triton™ X-100. Afterwards, 100 μL working solution of the PCA assay Roti®-Quant universal using the manufacturer's protocol was added to each sample and standard. The samples were incubated for 2 hours and the absorbance was measured with a Victor microplate reader at 492 nm. For the determination of

the real particle amount per cell the calculated fluorescence was referred to the identified protein content.

5.4 Preparation Methods for Lipid-based Dextran Nanoparticles

5.4.1 Preparation of Lipid-DEX Nanoparticles with NanoAssemblr™ Technology

In general, lipid-DEX particles were prepared by dissolving Sp-Ac-DEX and all lipids in ethanol and diluting the siRNA, which should be encapsulated, in PBS. The two different solutions were rapidly mixed together using the NanoAssemblr™ technology. The standard settings used with the NanoAssemblr™ are described in **Table 29**.

Table 29: Settings for the formulation of lipid-DEX particles with the NanoAssemblr™ technology

Flow Rate (PBS/EtOH)	3:1
Total Flow Rate	12 mL·min.$^{-1}$
Switching volume (start)	100 μL
Switching volume (end)	50 μL

Sp-Ac-DEX, cholesterol, DSPC, and PEG-lipid or Pluronic® F-68 formed the main particle that encapsulated siRNA. Stock solutions of these compounds were prepared in the concentrations described in **Table 30**.

Table 30: Stock solutions in ethanol of the basic particle forming lipid compounds

Component	M_W / g·mol^{-1}	Stock in EtOH / mM	Stock in EtOH / g·L^{-1}
Sp-Ac-DEX	10,000	6	60.0
Cholesterol	386.65	50	19.3
DSPC	790	10	7.9
PEG-lipid	2526	7.5	18.9
Pluronic® F-68	8350	2	16.7

Variation of PEG-lipid

Sp-Ac-DEX, cholesterol, DSPC and PEG-lipid stock solutions in ethanol were mixed together in the following ratios (**Table 31**) yielding in a final volume of 150 μL lipid mix that was injected into the NanoAssemblr™. An extra volume of about 100 μL was prepared due to the rapid evaporation of the solvent ethanol.

Table 31: Composition and needed volumes of the used polymer and lipids dissolved in ethanol for the preparation of lipid-DEX particles with different PEG ratios

Component	5% PEG		10% PEG		No DEX	
	Mol ratio	µL stock	Mol ratio	µL stock	Mol ratio	µL stock
Sp-Ac-DEX	48.5	11.2	46.3	10.9	–	–
Cholesterol	36.9	0.7	35.2	0.7	71.7	0.7
DSPC	9.7	0.9	9.25	0.9	18.9	0.9
PEG-lipid	4.9	1.4	9.25	2.7	9.4	1.4
EtOH	–	235.7	–	234.8	–	246.9

1.5 µL siRNA-luc (stock 10 $g \cdot L^{-1}$) was diluted in 448.5 µL PBS resulting in a final siRNA concentration of 25 $ng \cdot \mu L^{-1}$ in the particle suspension. Particles were purified by dialyzation against PBS using the Pur-A-Lyzer™ Midi Dialysis Kit (MWCO 3.5 kDa, Sigma-Aldrich). Total change of a volume of 100 µL needed 30 minutes. The duration of the dialyzation was adjusted to the prepared volumes of particles for each batch. Size was measured directly after the purification and particles were used for *in vitro* experiments.

Pluronic® F-68 as PEG Alternative

Polymer and lipids were mixed together using the stock solutions described in **Table 30** with the following ratios (**Table 32**). The total volume of lipid mix was 100 µL injected together with 300 µL siRNA solution containing 10 µg siRNA-*luc* into the NanoAssemblr™. The particles were purified by dialysis like described before and the mixture yielded in a final siRNA concentration of 25 $ng \cdot \mu L^{-1}$.

Table 32: Composition and volumes of the used polymers and lipids dissolved in ethanol for the preparation of lipid-based particles with PEG-lipid or Pluronic® F-68

Component	10% PEG		10% Pluronic® F-68	
	Mol ratio	µL stock	Mol ratio	µL stock
Sp-Ac-DEX	46.3	6.1	46.3	5.5
Cholesterol	35.2	0.6	35.2	0.5
DSPC	9.25	0.7	9.25	0.7
PEG-lipid	9.25	1.0	–	–
Pluronic® F-68	–	–	9.25	3.3
EtOH	–	191.7	–	190.0

Enhanced siRNA Concentration

Polymers with enhanced ratios of the lipids were mixed together using the following protocol (**Table 33**) and resulted in a final lipid in ethanol volume of 150 µL. This ethanol solution was injected into the NanoAssemblr™ with 450 µL siRNA-*luc* solution (containing 150 µg siRNA-

luc) in PBS to form particles with a final concentration of 250 ng·μL^{-1} siRNA. Particles were purified by dialysis like described before.

Table 33: Composition and volumes of the used polymers and lipids dissolved in ethanol for the preparation of lipid-based particles with a high siRNA concentration

Component	10% PEG		DSPC↑		Cholesterol↑		PEG↑		No DEX	
	Mol ratio	μL stock	Mol ratio	μL stock	Mol ratio	μL stock	Mol ratio	μL stock	Mol ratio	μL stock
Sp-Ac-DEX	46.3	108.6	42.4	107.0	34.2	105.8	42.4	103.1	–	–
Cholesterol	35.2	6.9	32.2	6.8	52.1	13.4	32.2	6.5	65.5	6.9
DSPC	9.25	9.1	16.9	17.8	6.85	8.8	8.5	8.6	17.25	9.1
PEG-lipid	9.25	27.2	8.5	26.7	6.85	26.4	16.9	51.6	17.25	27.2
EtOH	–	98.3	–	91.6	–	95.6	–	80.2	–	206.9

5.4.2 Measurement of the Particle Size by DLS

Particle size of lipid-DEX particles with different amounts of PEG was measured by Dynamic Light Scattering (DLS) with a Malvern Zetasizer Nano ZS (He-Ne laser, $\lambda = 632$ nm). Therefore, 10 μL of the dialyzed particle suspension was diluted with 100 μL PBS and transferred to a disposable cuvette (BRAND® UV cuvettes micro, VWR) before the measurement. Particle samples were measured 5-times while each measurement consisted of 5 runs at 20 °C.

5.4.3 Measurement of the Surface Charge with a Zetasizer Nano ZS

Particles (20 μL) were suspended in two different HEPES buffers (700 μL, pH 7.4) for zeta potential measurements with a Malvern Zetasizer Nano ZS. Five measurements with five individual runs were performed at 25 °C.

5.4.4 Quant-iT™ RiboGreen® Assay for the Quantification of Encapsulated siRNA

The Quant-iT™ RiboGreen® Assay was described before in section 5.3.9. For the lipid-DEX particles, the amount of free siRNA was measured and compared to the initial used concentration of siRNA. Only the non-encapsulated siRNA was able to react with the RiboGreen® reagent resulting in a fluorescent compound with an emission maximum at 535 nm ($\lambda_{ex.}$ 485 nm). Therefore, 10 μL of the particle sample was mixed with 90 μL PBS in a 96-well microplate (black, flat bottom). The pure siRNA-*luc* was diluted in PBS at a concentration that fit 100% encapsulation. The RiboGreen® reagent was diluted 1:200 in PBS and 100 μL were added to each well. The reagent was incubated with the particles for 5 minutes protected from light before reading the fluorescence of the dye with a Tecan

microplate reader. Particle results were compared to the fluorescence of the theoretical amount of encapsulated siRNA using Microsoft Excel.

5.4.5 Protocol for TNS Assay

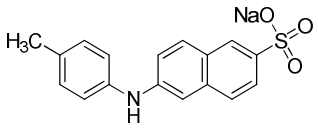

Figure 83: Structure of TNS (6-(*p*-toluidino)-2-naphthalenesulfonic acid sodium salt).

The titration of the particles with the fluorescent dye TNS (6-(*p*-toluidino)-2-naphthalene-sulfonic acid sodium salt) was performed using an adjusted protocol that was described before elsewhere.[305] Reaction buffers consisted of 10 mM HEPES, 10 mM MES, 10 mM ammonium acetate, and 130 mM NaCl with pHs from 2.5 to 11. Buffers were prepared in 0.5 pH steps using hydrochloric acid and sodium hydroxide solutions for the adjustment of the pH. Briefly, 5 μL of the lipid-DEX particles (siRNA conc.: 25 ng·μL^{-1} in PBS) were mixed with 100 μL of the reaction buffer and 5 μL of TNS in *dd*-H_2O (20 μM, M_W 335.35 g·mol^{-1}) in each well of a 96-well microplate (black, flat bottom). Samples were incubated for 5 minutes protected from light and fluorescence was read with a Tecan microplate reader ($\lambda_{ex.}$ 321 nm, $\lambda_{em.}$ 445 nm).

5.4.6 Quantification of *In Vitro* Luciferase Knockdown with ONE-Glo™ + Tox Assay

HeLa-*luc* and A549-*luc* cells were grown in high glucose DMEM without phenol red supplemented with 5% (V/V) FCS and 1% penicillin-streptomycin. More detailed information for the cell culture of HeLa cells was described in chapter 5.3.10.

For *in vitro* knockdown experiments, 10,000 HeLa-*luc* cells (stably expressing luciferase) were seeded in a volume of 100 μL phenol red-free DMEM (5% FCS, 1% P/S) into each well of an opaque white, flat bottom 96-well microplate (Corning-Costar, USA) and cells were incubated at 37 °C with 5% CO_2 overnight. The next day, medium was replaced by fresh DMEM (200 μL/well). One hour after the change of the medium, particles in PBS were added to the cells and incubated for 24 hours or 48 hours. Cell viability and luciferase activity was determined by using ONE-Glo™ + Tox Luciferase Reporter and Cell Viability Assay (Promega). Therefore, all medium was removed and cells were incubated with 150 μL CellTiter-Fluor™ in medium (1.2 mL CTF reagent mixed with 15 mL medium) for 1 hour at 37 °C with 5% CO_2. Fluorescence was read with a Tecan microplate reader ($\lambda_{ex.}$ 390 nm, $\lambda_{em.}$ 505 nm). Afterwards, luciferase knockdown was determined by adding 20 μL ONE-Glo™ Reagent per well and incubated for 5 minutes before luminescence was read with a Tecan microplate reader. Transfections were always performed in triplicates. RNAiMax control samples were diluted in OptiMEM® before adding to the cells which were cultured in DMEM using the manufacturer's protocol. All results were normalized to untreated cells.

5.4.7 *In Vivo* Biodistribution

Particles containing 10% PEG-lipid were prepared by a protocol described in 5.4.1 with a final siRNA concentration of 25 ng·μL^{-1}. The siRNA mixture consisted of siRNA-*luc* and Cy5.5-siRNA-*luc* in equal parts (V/V). 200 μL particles were injected intravenously into the tail vein of each female, black C57BL/6 mouse resulting in a siRNA dose of 0.25 mg·kg^{-1}. Mice were sacrificed and organs harvested followed by scanning their fluorescence with an IVIS machine using the setup for Cy5.5 detection. The whole *in vivo* experiment was performed in collaboration with [redacted] Cancer Center, UTSW Medical Center Dallas, USA).

6 APPENDIX

6.1 List of Abbreviations

Abbreviation	Meaning
Ø	diameter
Abs.	absorbance
Ac	acetalated
AGU	anhydrous glucose unit
ALT	alanine transaminase
AMY	amylopectin
AP	alkaline phosphatase
APC	antigen-presenting cell
Apo	apolipoprotein
Approx.	approximately
AST	aspartate transaminase
BMDC	bone-marrow derived dendritic cell
BMMC	bone-marrow derived mast cell
c	centi-
C	carbon
CD	cluster of differentiation
$CDCl_3$	deuterated chloroform
CME	cellulose mixed ester
conc.	concentration
COOH	carboxyl group
cP	centipoise
CPP	cell penetrating peptide
CTA	cellulose triacetate
CTF	cell titer fluor
dd-	double distilled
D_2O	deuterium oxide
d_6	deuterated (6-times)
Da	Dalton
DAPI	4',6-diamidino-2-phenylindole
DBCO	dibenzocyclooctyne
DC	dendritic cell
DCl	deuterium chloride
DCM	dichloromethane
DEX	dextran

Abbreviation	Meaning
DIX	dextrin
DLS	Dynamic Light Scattering
DMEM	Dulbecco's modified Eagle's medium
DMSO	dimethyl sulfoxide
DNA	deoxyribonucleic acid
d.nm	particle size in diameter (nm scale)
DS	Degree of Substitution
DSPC	1,2-distearoyl-*sn*-glycero-3-phosphocholine
dsRNA	double-stranded RNA
DTNB	5,5'-dithio-bis-(2-nitrobenzoic acid)
EDC	*N*-(3-dimethylaminopropyl)-*N*'-ethylcarbodiimide
EDTA	ethylenediaminetetraacetic acid
e.g.	*exempli gratia*, means: for example
eGFP	green fluorescent protein
em.	emission
eq.	equivalent
ER	endoplasmic reticulum
esiRNA	endoribonuclease-prepared short interfering RNA
et al.	*et alii*, means: and others
Et_2O	diethylether
EtOH	ethanol
EU	endotoxin unit
ex.	excitation
FACS	flow cytometry
FCS	fetal calf serum
FDA	Food and Drug Administration
Fmoc	fluorenylmethyloxycarbonyl
FTIR	Fourier transform infrared spectroscopy
g	gram
g	gravity of Earth
h	hour
H	hydrogen
H_2O	water
HeLa	tumor cells from the patient Henrietta Lacks
HEPES	4-(2-hydroxyethyl)-1-piperazineethanesulfonic acid
HES	hydroxyethyl starch
IgG	immunoglobulin G
IL	interleukin

Abbreviation	Meaning
IR	infrared spectroscopy
k	kilo-
KBr	potassium bromide
λ	wavelength
L	liter
LC-MS	liquid chromatography-mass spectrometry
LPS	lipopolysaccharide
luc	luciferase
Lys	lysine
μ	micro-
m	mass
m	meter
m	milli-
M	molar
max.	maximum
MeOH	methanol
MES	2-(*N*-morpholino)ethanesulfonic acid
MHC	major histocompatibility complex
MHz	mega hertz
min.	minute
miRNA	micro-RNA
MPI	Max Planck Institute
MPS	mononuclear phagocytic system
mRNA	messenger RNA
MTT	3,(4,5-dimethylthiazol-2-yl)-2,5-diphenyl-tetrazoliumbromide
M_W	molecular weight
MWCO	molecular weight cut-off
n	nano-
N	nitrogen
N_3	azide
n.a.	not available
$NaBH_4$	sodium borohydride
NHS	*N*-hydroxysuccinimide
NK cell	natural killer cell
NMR	nuclear magnetic resonance
NP	nanoparticle
NTA	nanoparticle tracking analysis
OVA	ovalbumin

Abbreviation	Meaning
ox	oxidized
p	pico-
P	phosphorous
PBS	phosphate buffered saline
PCA	poly(cinchonic acid)
PDI	polydispersity index
pDNA	plasmid DNA
PEG	poly(ethylene glycol)
PEG-lipid	mPEG2000-DMG
PEI	polyethylenimine
PES	polyethersulfone
piRNA	P-element induced wimpy testis interacting-RNA
PLGA	poly(lactic *co*-glycolic acid)
P/S	penicillin-streptomycin
PVA	poly(vinyl alcohol)
RI	refractive index
RISC	RNA induced silencing complex
RNA	ribonucleic acid
RNAi	RNA interference
RT	room temperature
SD	standard deviation
SDS-PAGE	sodium dodecyl sulfate polyacrylamide gel electrophoresis
SEM	scanning electron microscopy
shRNA	short hairpin RNA
siLuc	RNA encoding for luciferase mRNA
siRNA	short interfering RNA
SMCC	succinimidyl 4-(*N*-maleimidomethyl)cyclohexane-1-carboxylate
Sp	spermine
ssRNA	single-stranded RNA
TAMRA	carboxytetramethylrhodamine NHS ester
TEA	triethylamine
TLC	thin layer chromatography
TLR	Toll-like receptor
TMS	tetramethylsilane
TNS	6-(*p*-toluidino)-2-naphthalenesulfonic acid sodium salt
USA	United States of America
UTSW	University of Texas Southwestern
UV	ultraviolet

Abbreviation	Meaning
V	Volt
V	volume

6.2 Collaboration partners

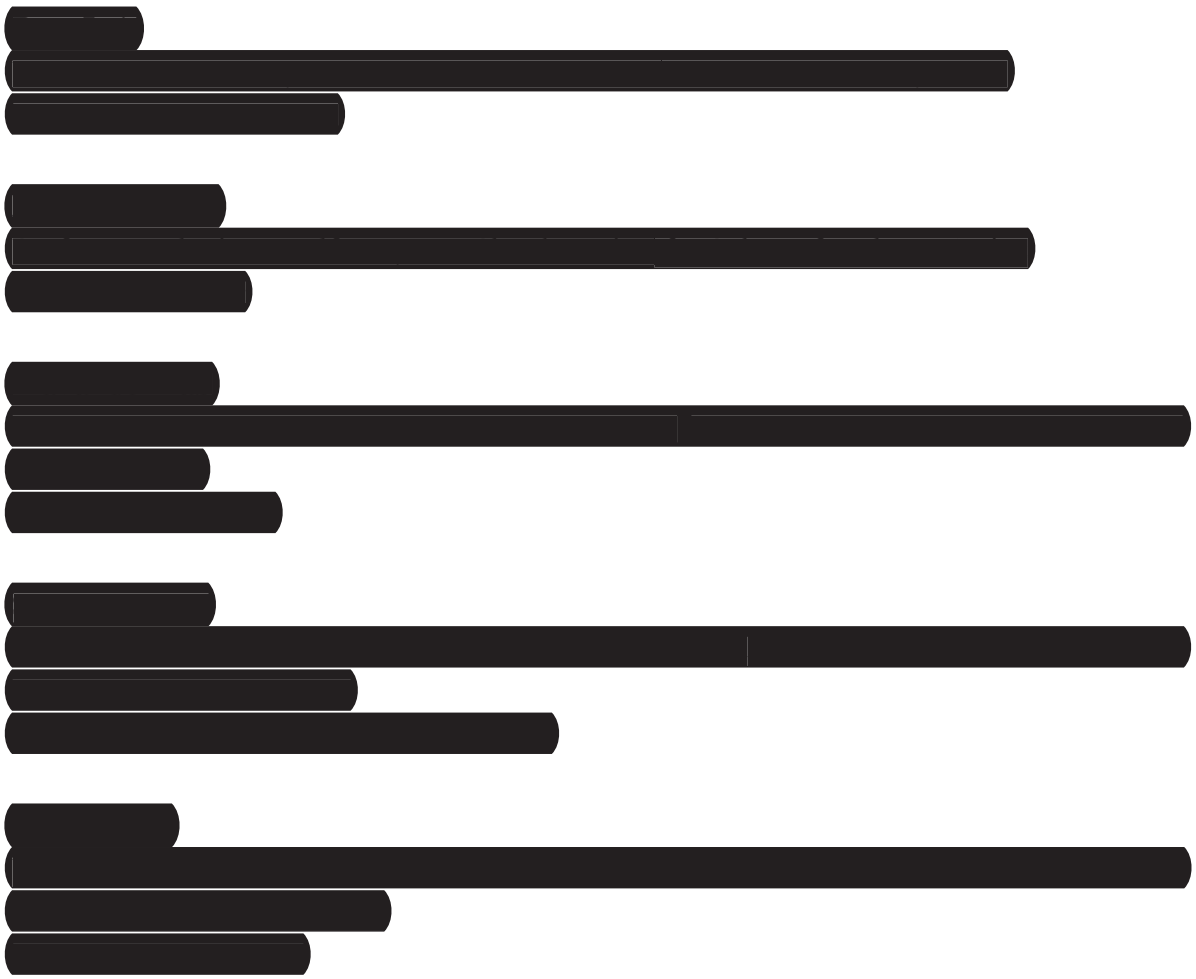

6.3 Publications

[1] T. Schirmeister, J. Kesselring, S. Jung, T. H. Schneider, A. Weickert, J. Becker, W. Lee, D. Bamberger, P. R. Wich, U. Distler, S. Tenzer, P. Johé, U. A. Hellmich, B. Engels, Quantum Chemical-Based Protocol for the Rational Design of Covalent Inhibitors, *J. Am. Chem. Soc.*, accepted June 2016.

[2] F. Foerster, D. Bamberger, J. Schupp, M. Weilbächer, L. Kaps, S. Strobl, L. Radi, M. Diken, D. Strand, A. Tüttenberg, P. R. Wich, D. Schuppan, Dextran-based Therapeutic Nanoparticles for Hepatic Drug Delivery, *Nanomedicine*, accepted June 2016.

[3] D. Bamberger, D. Hobernik, R. Schröder, W. Tremel, M. Bros, P. R. Wich, Surface Functionalization of Polysaccharide-Based Nanoparticles with PEG and Dextran Affects their Immune Cell Binding and Stimulatory Characteristics, manuscript in preparation.

[4] D. Bamberger, P. Kos, D. J. Siegwart, P. R. Wich, Lipid Dextran Nanoparticles for Highly Efficient siRNA Delivery, manuscript in preparation.

6.4 Bibliography

[1] E. Merisko-Liversidge, G. G. Liversidge, E. R. Cooper, Nanosizing: a formulation approach for poorly-water-soluble compounds, *Eur. J. Pharm. Sci.* **2003**, *18*, 113-120.

[2] K. R. Vega-Villa, J. K. Takemoto, J. A. Yanez, C. M. Remsberg, M. L. Forrest, N. M. Davies, Clinical toxicities of nanocarrier systems, *Adv. Drug Del. Rev.* **2008**, *60*, 929-938.

[3] J. B. Swarbrick, J.C. (Eds.), Nanoparticles, *Encycl. Pharm. Techn.* **1994**, *10*, 165-190.

[4] J. Kreuter, Nanoparticles--a historical perspective, *Int. J. Pharm.* **2007**, *331*, 1-10.

[5] J. Nicolas, S. Mura, D. Brambilla, N. Mackiewicz, P. Couvreur, Design, functionalization strategies and biomedical applications of targeted biodegradable/biocompatible polymer-based nanocarriers for drug delivery, *Chem. Soc. Rev.* **2013**, *42*, 1147-1235.

[6] H. R. Kim, I. K. Kim, K. H. Bae, S. H. Lee, Y. Lee, T. G. Park, Cationic solid lipid nanoparticles reconstituted from low density lipoprotein components for delivery of siRNA, *Mol. Pharm.* **2008**, *5*, 622-631.

[7] B. S. Pattni, V. V. Chupin, V. P. Torchilin, New Developments in Liposomal Drug Delivery, *Chem. Rev.* **2015**, *115*, 10938-10966.

[8] R. Kedmi, N. Ben-Arie, D. Peer, The systemic toxicity of positively charged lipid nanoparticles and the role of Toll-like receptor 4 in immune activation, *Biomaterials* **2010**, *31*, 6867-6875.

[9] C. Chen, D. Han, C. Cai, X. Tang, An overview of liposome lyophilization and its future potential, *J. Controlled Release* **2010**, *142*, 299-311.

[10] P. Mastorakos, S. P. Kambhampati, M. K. Mishra, T. Wu, E. Song, J. Hanes, R. M. Kannan, Hydroxyl PAMAM dendrimer-based gene vectors for transgene delivery to human retinal pigment epithelial cells, *Nanoscale* **2015**, *7*, 3845-3856.

[11] H. Chen, Y. Zhao, S. Cui, D. Zhi, S. Zhang, X. Peng, 6-O-dodecyl-chitosan carbamate–based pH-responsive polymeric micelles for gene delivery, *J. Appl. Polym. Sci.* **2015**, *132*, 42469.

[12] C. Hörtz, A. Birke, L. Kaps, S. Decker, E. Wächtersbach, K. Fischer, D. Schuppan, M. Barz, M. Schmidt, Cylindrical Brush Polymers with Polysarcosine Side Chains: A Novel Biocompatible Carrier for Biomedical Applications, *Macromolecules* **2015**, *48*, 2074-2086.

[13] B. M. Discher, Y. Y. Won, D. S. Ege, J. C. Lee, F. S. Bates, D. E. Discher, D. A. Hammer, Polymersomes: tough vesicles made from diblock copolymers, *Science (New York, N.Y.)* **1999**, *284*, 1143-1146.

[14] A. V. Kabanov, S. V. Vinogradov, Nanogels as pharmaceutical carriers: finite networks of infinite capabilities, *Angew. Chem. Int. Ed.* **2009**, *48*, 5418-5429.

[15] K. Letchford, H. Burt, A review of the formation and classification of amphiphilic block copolymer nanoparticulate structures: micelles, nanospheres, nanocapsules and polymersomes, *European Journal of Pharmaceutics and Biopharmaceutics* **2007**, *65*, 259-269.

[16] R. G. Crystal, Transfer of genes to humans: early lessons and obstacles to success, *Science (New York, N.Y.)* **1995**, *270*, 404-410.

[17] V. P. Shastri, Non-degradable biocompatible polymers in medicine: past, present and future, *Curr. Pharm. Biotechnol.* **2003**, *4*, 331-337.

[18] Y. Zhou, B. Yang, X. Ren, Z. Liu, Z. Deng, L. Chen, Y. Deng, L. M. Zhang, L. Yang, Hyperbranched cationic amylopectin derivatives for gene delivery, *Biomaterials* **2012**, *33*, 4731-4740.

[19] K. S. Soppimath, T. M. Aminabhavi, A. R. Kulkarni, W. E. Rudzinski, Biodegradable polymeric nanoparticles as drug delivery devices, *J. Controlled Release* **2001**, *70*, 1-20.

[20] B. Kang, T. Opatz, K. Landfester, F. R. Wurm, Carbohydrate nanocarriers in biomedical applications: functionalization and construction, *Chem. Soc. Rev.* **2015**, *44*, 8301-8325.

[21] K. Raemdonck, T. F. Martens, K. Braeckmans, J. Demeester, S. C. De Smedt, Polysaccharide-based nucleic acid nanoformulations, *Adv. Drug Del. Rev.* **2013**, *65*, 1123-1147.

[22] L. L. H. Huang-Lee, D. T. Cheung, M. E. Nimni, Biochemical changes and cytotoxicity associated with the degradation of polymeric glutaraldehyde derived crosslinks, *J. Biomed. Mater. Res.* **1990**, *24*, 1185-1201.

[23] H. Brøndsted, C. Andersen, L. Hovgaard, Crosslinked dextran – a new capsule material for colon targeting of drugs, *J. Controlled Release* **1998**, *53*, 7-13.

[24] Q. Gan, T. Wang, C. Cochrane, P. McCarron, Modulation of surface charge, particle size and morphological properties of chitosan–TPP nanoparticles intended for gene delivery, *Colloids Surf. B. Biointerfaces* **2005**, *44*, 65-73.

[25] L. W. Chan, Y. Jin, P. W. S. Heng, Cross-linking mechanisms of calcium and zinc in production of alginate microspheres, *Int. J. Pharm.* **2002**, *242*, 255-258.

[26] Y.-H. Lin, K. Sonaje, K. M. Lin, J.-H. Juang, F.-L. Mi, H.-W. Yang, H.-W. Sung, Multi-ion-crosslinked nanoparticles with pH-responsive characteristics for oral delivery of protein drugs, *J. Controlled Release* **2008**, *132*, 141-149.

[27] H. V. Sæther, H. K. Holme, G. Maurstad, O. Smidsrød, B. T. Stokke, Polyelectrolyte complex formation using alginate and chitosan, *Carbohydr. Polym.* **2008**, *74*, 813-821.

[28] A. Drogoz, L. David, C. Rochas, A. Domard, T. Delair, Polyelectrolyte Complexes from Polysaccharides: Formation and Stoichiometry Monitoring, *Langmuir.* **2007**, *23*, 10950-10958.

[29] H.-W. Lu, L.-M. Zhang, J.-Y. Liu, R.-F. Chen, Synthesis of an Amphiphilic Polysaccharide Derivative and Its Micellization for Drug Release, *J. Bioact. Compatible Polym.* **2008**, *23*, 154-170.

[30] N. Goodarzi, R. Varshochian, G. Kamalinia, F. Atyabi, R. Dinarvand, A review of polysaccharide cytotoxic drug conjugates for cancer therapy, *Carbohydr. Polym.* **2013**, *92*, 1280-1293.

[31] E. M. Bachelder, T. T. Beaudette, K. E. Broaders, J. Dashe, J. M. Frechet, Acetal-derivatized dextran: an acid-responsive biodegradable material for therapeutic applications, *J. Am. Chem. Soc.* **2008**, *130*, 10494-10495.

[32] R. Karnik, F. Gu, P. Basto, C. Cannizzaro, L. Dean, W. Kyei-Manu, R. Langer, O. C. Farokhzad, Microfluidic Platform for Controlled Synthesis of Polymeric Nanoparticles, *Nano Lett.* **2008**, *8*, 2906-2912.

[33] R. K. Shah, H. C. Shum, A. C. Rowat, D. Lee, J. J. Agresti, A. S. Utada, L.-Y. Chu, J.-W. Kim, A. Fernandez-Nieves, C. J. Martinez, D. A. Weitz, Designer emulsions using microfluidics, *Mater. Today* **2008**, *11*, 18-27.

[34] P. Vangeyte, S. Gautier, R. Jérôme, About the methods of preparation of poly(ethylene oxide)-b-poly(ε-caprolactone) nanoparticles in water: Analysis by dynamic light scattering, *Colloids Surf. Physicochem. Eng. Aspects* **2004**, *242*, 203-211.

[35] O. Felt, P. Buri, R. Gurny, Chitosan: A Unique Polysaccharide for Drug Delivery, *Drug Dev. Ind. Pharm.* **1998**, *24*, 979-993.

[36] R. Ravindra, K. R. Krovvidi, A. A. Khan, Solubility parameter of chitin and chitosan, *Carbohydr. Polym.* **1998**, *36*, 121-127.

[37] H. Katas, H. O. Alpar, Development and characterisation of chitosan nanoparticles for siRNA delivery, *J. Controlled Release* **2006**, *115*, 216-225.

[38] I. M. van der Lubben, J. C. Verhoef, G. Borchard, H. E. Junginger, Chitosan and its derivatives in mucosal drug and vaccine delivery, *Eur. J. Pharm. Sci.* **2001**, *14*, 201-207.

[39] C. Corbet, H. Ragelle, V. Pourcelle, K. Vanvarenberg, J. Marchand-Brynaert, V. Préat, O. Feron, Delivery of siRNA targeting tumor metabolism using non-covalent PEGylated chitosan nanoparticles: Identification of an optimal combination of ligand structure, linker and grafting method, *J. Controlled Release* **2016**, *223*, 53-63.

[40] S. Mizrahy, D. Peer, Polysaccharides as building blocks for nanotherapeutics, *Chem. Soc. Rev.* **2012**, *41*, 2623-2640.

[41] K. Y. Lee, D. J. Mooney, Alginate: properties and biomedical applications, *Prog. Polym. Sci.* **2012**, *37*, 106-126.

[42] S. Jain, T.-H. Tran, M. Amiji, Macrophage repolarization with targeted alginate nanoparticles containing IL-10 plasmid DNA for the treatment of experimental arthritis, *Biomaterials* **2015**, *61*, 162-177.

[43] J. Carvalho, C. Gonçalves, A. M. Gil, F. M. Gama, Production and characterization of a new dextrin based hydrogel, *Eur. Polym. J.* **2007**, *43*, 3050-3059.

[44] S. Manchun, C. R. Dass, K. Cheewatanakornkool, P. Sriamornsak, Enhanced anti-tumor effect of pH-responsive dextrin nanogels delivering doxorubicin on colorectal cancer, *Carbohydr. Polym.* **2015**, *126*, 222-230.

[45] R. F. Tester, J. Karkalas, X. Qi, Starch—composition, fine structure and architecture, *Journal of Cereal Science* **2004**, *39*, 151-165.

[46] S. Jobling, Improving starch for food and industrial applications, *Curr. Opin. Plant Biol.* **2004**, *7*, 210-218.

[47] R. Zarychanski, A. M. Abou-Setta, A. F. Turgeon, et al., Association of hydroxyethyl starch administration with mortality and acute kidney injury in critically ill patients requiring volume resuscitation: A systematic review and meta-analysis, *J. Am. Med. Assoc.* **2013**, *309*, 678-688.

[48] A. J. Bircher, T. Harr, L. Hohenstein, D. A. Tsakiris, Hypersensitivity reactions to anticoagulant drugs: diagnosis and management options, *Allergy* **2006**, *61*, 1432-1440.

[49] M. E. Brecher, H. G. Owen, N. Bandarenko, Alternatives to albumin: starch replacement for plasma exchange, *J. Clin. Apher.* **1997**, *12*, 146-153.

[50] C. M. Paleos, Z. Sideratou, T. A. Theodossiou, D. Tsiourvas, Carboxylated Hydroxyethyl Starch: A novel Polysaccharide for the Delivery of Doxorubicin, *Chem. Biol. Drug Des.* **2015**, *85*, 653-658.

[51] M. Fichter, G. Baier, M. Dedters, L. Pretsch, A. Pietrzak-Nguyen, K. Landfester, S. Gehring, Nanocapsules generated out of a polymeric dexamethasone shell suppress the inflammatory response of liver macrophages, *Nanomed. Nanotechnol. Biol. Med.* **2013**, *9*, 1223-1234.

[52] M. Noga, D. Edinger, E. Wagner, G. Winter, A. Besheer, Characterization and compatibility of hydroxyethyl starch–polyethylenimine copolymers for DNA delivery, *Journal of Biomaterials Science, Polymer Edition* **2014**, *25*, 855-871.

[53] J. S. Roberts, S. L. Bratton, Colloid volume expanders. Problems, pitfalls and possibilities, *Drugs* **1998**, *55*, 621-630.

[54] M. Lombardo, N. Micali, V. Villari, S. Serrao, G. Pucci, R. Barberi, G. Lombardo, Ultraviolet A: Visible spectral absorbance of the human cornea after transepithelial soaking with dextran-enriched and dextran-free riboflavin 0.1% ophthalmic solutions, *J. Cataract Refract. Surg.* **2015**, *41*, 2283-2290.

[55] J. D. Paull, Dextrans, *Dev. Biol. Stand.* **1987**, *67*, 133-138.

[56] D. Arora, N. Sharma, V. Sharma, V. Abrol, R. Shankar, S. Jaglan, An update on polysaccharide-based nanomaterials for antimicrobial applications, *Appl. Microbiol. Biotechnol.* **2016**, 2603-2615.

[57] L. Yi, Y. Ouyang, X. Sun, N. Xu, R. J. Linhardt, Z. Zhang, Qualitative and quantitative analysis of branches in dextran using high-performance anion exchange chromatography coupled to quadrupole time-of-flight mass spectrometry, *J. Chromatogr. A* **2015**, *1423*, 79-85.

[58] R. Mehvar, Dextrans for targeted and sustained delivery of therapeutic and imaging agents, *J. Controlled Release* **2000**, *69*, 1-25.

[59] L. O. Lamke, S. O. Liljedahl, Plasma volume changes after infusion of various plasma expanders, *Resuscitation.* **1976**, *5*, 93-101.

[60] H. Hedin, W. Richter, J. Ring, Dextran-induced anaphylactoid reactions in man: role of dextran reactive antibodies, *Int. Arch. Allergy Appl. Immunol.* **1976**, *52*, 145-159.

[61] E. Michelson, Anaphylactic reaction to dextrans, *N. Engl. J. Med.* **1968**, *278*, 552.

[62] K. G. Ljungstrom, H. Renck, K. Strandberg, H. Hedin, W. Richter, E. Widerlov, Adverse reactions to dextran in Sweden 1970-1979, *Acta Chirurgica Scandinavica* **1983**, *149*, 253-262.

[63] S. W. Neiser, M.; Schwarz, K.; Funk, F.; Geisser, P.; Burckhardt, S., Assessment of dextran antigenicity of intravenous iron products by an immunodiffusion assay, *Port. J. Nephrol. Hypert.* **2011**, *25*, 219-222.

[64] C. E. Zinderman, L. Landow, R. P. Wise, Anaphylactoid reactions to Dextran 40 and 70: reports to the United States Food and Drug Administration, 1969 to 2004, *J. Vasc. Surg.* **2006**, *43*, 1004-1009.

[65] G. Arturson, G. Wallenius, The Renal Clearance of Dextran of Different Molecular Sizes in Normal Humans, *Scand. J. Clin. Lab. Invest.* **1964**, *16*, 81-86.

[66] G. Arturson, G. Wallenius, The Intravascular Persistence of Dextran of Different Molecular Sizes in Normal Humans, *Scand. J. Clin. Lab. Invest.* **1964**, *16*, 76-80.

[67] J. Porath, P. Flodin, Gel filtration: a method for desalting and group separation, *Nature* **1959**, *183*, 1657-1659.

[68] I. Wasiak, A. Kulikowska, M. Janczewska, M. Michalak, I. A. Cymerman, A. Nagalski, P. Kallinger, W. W. Szymanski, T. Ciach, Dextran Nanoparticle Synthesis and Properties, *PLoS One* **2016**, *11*, 1-17.

[69] H. Jiang, D. Fang, B. S. Hsiao, B. Chu, W. Chen, Optimization and characterization of dextran membranes prepared by electrospinning, *Biomacromolecules* **2004**, *5*, 326-333.

[70] W. N. E. van Dijk-Wolthuls, S. K. Y. Tsang, J. J. Kettenes-van den BoschW.E. Hennink, A new class of polymerizable dextrans with hydrolyzable groups: hydroxyethyl methacrylated dextran with and without oligolactate spacer, *Polymer* **1997**, *38*, 6235-6242.

[71] L. De Backer, T. Naessens, S. De Koker, E. Zagato, J. Demeester, J. Grooten, S. C. De Smedt, K. Raemdonck, Hybrid pulmonary surfactant-coated nanogels mediate efficient in vivo delivery of siRNA to murine alveolar macrophages, *J. Controlled Release* **2015**, *217*, 53-63.

[72] W. Tiyaboonchai, N. Limpeanchob, Formulation and characterization of amphotericin B–chitosan–dextran sulfate nanoparticles, *Int. J. Pharm.* **2007**, *329*, 142-149.

[73] J. A. Cadee, M. J. van Luyn, L. A. Brouwer, J. A. Plantinga, P. B. van Wachem, C. J. de Groot, W. den Otter, W. E. Hennink, In vivo biocompatibility of dextran-based hydrogels, *J. Biomed. Mater. Res.* **2000**, *50*, 397-404.

[74] C. J. De Groot, M. J. Van Luyn, W. N. Van Dijk-Wolthuis, J. A. Cadee, J. A. Plantinga, W. Den Otter, W. E. Hennink, In vitro biocompatibility of biodegradable dextran-based hydrogels tested with human fibroblasts, *Biomaterials* **2001**, *22*, 1197-1203.

[75] K. E. Broaders, J. A. Cohen, T. T. Beaudette, E. M. Bachelder, J. M. Frechet, Acetalated dextran is a chemically and biologically tunable material for particulate immunotherapy, *Proc. Natl. Acad. Sci. USA* **2009**, *106*, 5497-5502.

[76] T. T. Beaudette, J. A. Cohen, E. M. Bachelder, K. E. Broaders, J. L. Cohen, E. G. Engleman, J. M. Frechet, Chemoselective ligation in the functionalization of polysaccharide-based particles, *J. Am. Chem. Soc.* **2009**, *131*, 10360-10361.

[77] J. A. Cohen, T. T. Beaudette, J. L. Cohen, K. E. Brooders, E. M. Bachelder, J. M. J. Frechet, Acetal-Modified Dextran Microparticles with Controlled Degradation Kinetics and Surface Functionality for Gene Delivery in Phagocytic and Non-Phagocytic Cells, *Adv. Mater.* **2010**, *22*, 3593-3597.

[78] T. T. Beaudette, E. M. Bachelder, J. A. Cohen, A. C. Obermeyer, K. E. Broaders, J. M. Frechet, E. S. Kang, I. Mende, W. W. Tseng, M. G. Davidson, E. G. Engleman, In vivo studies on the effect of co-encapsulation of CpG DNA and antigen in acid-degradable microparticle vaccines, *Mol. Pharm.* **2009**, *6*, 1160-1169.

[79] L. Cui, J. A. Cohen, K. E. Broaders, T. T. Beaudette, J. M. Frechet, Mannosylated dextran nanoparticles: a pH-sensitive system engineered for immunomodulation through mannose targeting, *Bioconjugate Chem.* **2011**, *22*, 949-957.

[80] E. M. Bachelder, T. T. Beaudette, K. E. Broaders, J. M. Frechet, M. T. Albrecht, A. J. Mateczun, K. M. Ainslie, J. T. Pesce, A. M. Keane-Myers, In vitro analysis of acetalated dextran microparticles as a potent delivery platform for vaccine adjuvants, *Mol. Pharm.* **2010**, *7*, 826-835.

[81] K. J. Kauffman, N. Kanthamneni, S. A. Meenach, B. C. Pierson, E. M. Bachelder, K. M. Ainslie, Optimization of rapamycin-loaded acetalated dextran microparticles for immunosuppression, *Int. J. Pharm.* **2012**, *422*, 356-363.

[82] K. J. Peine, E. M. Bachelder, Z. Vangundy, T. Papenfuss, D. J. Brackman, M. D. Gallovic, K. Schully, J. Pesce, A. Keane-Myers, K. M. Ainslie, Efficient delivery of the toll-like receptor agonists polyinosinic:polycytidylic acid and CpG to macrophages by acetalated dextran microparticles, *Mol. Pharm.* **2013**, *10*, 2849-2857.

[83] K. L. Schully, M. G. Bell, A. M. Prouty, M. D. Gallovic, S. Gautam, K. J. Peine, S. Sharma, E. M. Bachelder, J. T. Pesce, M. A. Elberson, K. M. Ainslie, A. Keane-Myers, Evaluation of a biodegradable microparticulate polymer as a carrier for Burkholderia pseudomallei subunit vaccines in a mouse model of melioidosis, *Int. J. Pharm.* **2015**, *495*, 849-861.

[84] M. A. Collier, K. J. Peine, S. Gautam, S. Oghumu, S. Varikuti, H. Borteh, T. L. Papenfuss, A. R. Sataoskar, E. M. Bachelder, K. M. Ainslie, Host-mediated Leishmania donovani treatment using AR-12 encapsulated in acetalated dextran microparticles, *Int. J. Pharm.* **2016**, *499*, 186-194.

[85] C. Ornelas-Megiatto, P. N. Shah, P. R. Wich, J. L. Cohen, J. A. Tagaev, J. A. Smolen, B. D. Wright, M. J. Panzner, W. J. Youngs, J. M. Frechet, C. L. Cannon, Aerosolized antimicrobial agents based on degradable dextran nanoparticles loaded with silver carbene complexes, *Mol. Pharm.* **2012**, *9*, 3012-3022.

[86] J. L. Cohen, S. Schubert, P. R. Wich, L. Cui, J. A. Cohen, J. L. Mynar, J. M. Frechet, Acid-degradable cationic dextran particles for the delivery of siRNA therapeutics, *Bioconjugate Chem.* **2011**, *22*, 1056-1065.

[87] E. Larraneta, M. T. McCrudden, A. J. Courtenay, R. F. Donnelly, Microneedles: A New Frontier in Nanomedicine Delivery, *Pharm. Res.* **2016**, *33*, 1055-1073.

[88] H. Yu, T.-T. Tran, J. Teo, K. Hadinoto, Dry powder aerosols of curcumin-chitosan nanoparticle complex prepared by spray freeze drying and their antimicrobial efficacy against common respiratory bacterial pathogens, *Colloids Surf. Physicochem. Eng. Aspects* **2016**, *504*, 34-42.

[89] J. D. Bos, M. M. H. M. Meinardi, The 500 Dalton rule for the skin penetration of chemical compounds and drugs, *Experimental Dermatology* **2000**, *9*, 165-169.

[90] M. R. Prausnitz, R. Langer, Transdermal drug delivery, *Nat. Biotechnol.* **2008**, *26*, 1261-1268.

[91] M. Prabaharan, J. F. Mano, Stimuli-responsive hydrogels based on polysaccharides incorporated with thermo-responsive polymers as novel biomaterials, *Macromol. Biosci.* **2006**, *6*, 991-1008.

[92] S. K. Lai, Y.-Y. Wang, J. Hanes, Mucus-penetrating nanoparticles for drug and gene delivery to mucosal tissues, *Adv. Drug Del. Rev.* **2009**, *61*, 158-171.

[93] A. L. Sheffner, E. M. Medler, L. W. Jacobs, H. P. Sarett, The in vitro reduction in viscosity of human tracheobronchial secretions by acetylcysteine, *Am. Rev. Respir. Dis.* **1964**, *90*, 721-729.

[94] D. F. Evans, G. Pye, R. Bramley, A. G. Clark, T. J. Dyson, J. D. Hardcastle, Measurement of gastrointestinal pH profiles in normal ambulant human subjects, *Gut* **1988**, *29*, 1035-1041.

[95] L. M. Ensign, R. Cone, J. Hanes, Oral drug delivery with polymeric nanoparticles: The gastrointestinal mucus barriers, *Adv. Drug Del. Rev.* **2012**, *64*, 557-570.

[96] H. Yamamoto, Y. Kuno, S. Sugimoto, H. Takeuchi, Y. Kawashima, Surface-modified PLGA nanosphere with chitosan improved pulmonary delivery of calcitonin by mucoadhesion and opening of the intercellular tight junctions, *J. Controlled Release* **2005**, *102*, 373-381.

[97] A. Gabizon, D. Papahadjopoulos, Liposome formulations with prolonged circulation time in blood and enhanced uptake by tumors, *Proc. Natl. Acad. Sci. USA* **1988**, *85*, 6949-6953.

[98] N. Bertrand, J. C. Leroux, The journey of a drug-carrier in the body: an anatomo-physiological perspective, *J. Controlled Release* **2012**, *161*, 152-163.

[99] M. Lundqvist, J. Stigler, G. Elia, I. Lynch, T. Cedervall, K. A. Dawson, Nanoparticle size and surface properties determine the protein corona with possible implications for biological impacts, *Proc. Natl. Acad. Sci. USA* **2008**, *105*, 14265-14270.

[100] D. E. Owens, 3rd, N. A. Peppas, Opsonization, biodistribution, and pharmacokinetics of polymeric nanoparticles, *Int. J. Pharm.* **2006**, *307*, 93-102.

[101] S. Ritz, S. Schottler, N. Kotman, G. Baier, A. Musyanovych, J. Kuharev, K. Landfester, H. Schild, O. Jahn, S. Tenzer, V. Mailander, Protein corona of nanoparticles: distinct proteins regulate the cellular uptake, *Biomacromolecules* **2015**, *16*, 1311-1321.

[102] S. Schottler, G. Becker, S. Winzen, T. Steinbach, K. Mohr, K. Landfester, V. Mailander, F. R. Wurm, Protein adsorption is required for stealth effect of poly(ethylene glycol)- and poly(phosphoester)-coated nanocarriers, *Nat. Nanotechnol.* **2016**, *11*, 372-377.

[103] J. T. Andersen, I. Sandlie, The versatile MHC class I-related FcRn protects IgG and albumin from degradation: implications for development of new diagnostics and therapeutics, *Drug. Metab. Pharmacokinet.* **2009**, *24*, 318-332.

[104] M. R. Green, G. M. Manikhas, S. Orlov, B. Afanasyev, A. M. Makhson, P. Bhar, M. J. Hawkins, Abraxane, a novel Cremophor-free, albumin-bound particle form of paclitaxel for the treatment of advanced non-small-cell lung cancer, *Ann. Oncol.* **2006**, *17*, 1263-1268.

[105] K. M. Wasan, D. R. Brocks, S. D. Lee, K. Sachs-Barrable, S. J. Thornton, Impact of lipoproteins on the biological activity and disposition of hydrophobic drugs: implications for drug discovery, *Nat. Rev. Drug Discov.* **2008**, *7*, 84-99.

[106] S. Tenzer, D. Docter, S. Rosfa, A. Wlodarski, J. Kuharev, A. Rekik, S. K. Knauer, C. Bantz, T. Nawroth, C. Bier, J. Sirirattanapan, W. Mann, L. Treuel, R. Zellner, M. Maskos, H. Schild, R. H. Stauber, Nanoparticle Size Is a Critical Physicochemical Determinant of the Human Blood Plasma Corona: A Comprehensive Quantitative Proteomic Analysis, *ACS Nano* **2011**, *5*, 7155-7167.

[107] T. Cedervall, I. Lynch, M. Foy, T. Berggard, S. C. Donnelly, G. Cagney, S. Linse, K. A. Dawson, Detailed identification of plasma proteins adsorbed on copolymer nanoparticles, *Angew. Chem. Int. Ed.* **2007**, *46*, 5754-5756.

[108] A. Akinc, W. Querbes, S. De, J. Qin, M. Frank-Kamenetsky, K. N. Jayaprakash, M. Jayaraman, K. G. Rajeev, W. L. Cantley, J. R. Dorkin, J. S. Butler, L. Qin, T. Racie, A. Sprague, E. Fava, A. Zeigerer, M. J. Hope, M. Zerial, D. W. Sah, K. Fitzgerald, M. A. Tracy, M. Manoharan, V. Koteliansky, A. Fougerolles, M. A. Maier, Targeted delivery of RNAi therapeutics with endogenous and exogenous ligand-based mechanisms, *Mol. Ther.* **2010**, *18*, 1357-1364.

[109] P. C. Rensen, N. Herijgers, M. H. Netscher, S. C. Meskers, M. van Eck, T. J. van Berkel, Particle size determines the specificity of apolipoprotein E-containing triglyceride-rich emulsions for the LDL receptor versus hepatic remnant receptor in vivo, *J. Lipid Res.* **1997**, *38*, 1070-1084.

[110] J. Kreuter, T. Hekmatara, S. Dreis, T. Vogel, S. Gelperina, K. Langer, Covalent attachment of apolipoprotein A-I and apolipoprotein B-100 to albumin nanoparticles enables drug transport into the brain, *J. Controlled Release* **2007**, *118*, 54-58.

[111] M. M. Frank, L. F. Fries, The role of complement in inflammation and phagocytosis, *Immunol. Today* **1991**, *12*, 322-326.

[112] M. R. Ehrenstein, C. A. Notley, The importance of natural IgM: scavenger, protector and regulator, *Nat. Rev. Immunol.* **2010**, *10*, 778-786.

[113] H. L. Kutscher, P. Chao, M. Deshmukh, Y. Singh, P. Hu, L. B. Joseph, D. C. Reimer, S. Stein, D. L. Laskin, P. J. Sinko, Threshold size for optimal passive pulmonary targeting and retention of rigid microparticles in rats, *J. Controlled Release* **2010**, *143*, 31-37.

[114] E. Wisse, F. Jacobs, B. Topal, P. Frederik, B. De Geest, The size of endothelial fenestrae in human liver sinusoids: implications for hepatocyte-directed gene transfer, *Gene Ther.* **2008**, *15*, 1193-1199.

[115] M. Elsabahy, K. L. Wooley, Design of polymeric nanoparticles for biomedical delivery applications, *Chem. Soc. Rev.* **2012**, *41*, 2545-2561.

[116] Z. J. Deng, M. Liang, M. Monteiro, I. Toth, R. F. Minchin, Nanoparticle-induced unfolding of fibrinogen promotes Mac-1 receptor activation and inflammation, *Nat. Nanotechnol.* **2011**, *6*, 39-44.

[117] H. Carrstensen, R. H. Müller, B. W. Müller, Particle size, surface hydrophobicity and interaction with serum of parenteral fat emulsions and model drug carriers as parameters related to RES uptake, *Clin. Nutr.* **1992**, *11*, 289-297.

[118] R. Gref, M. Luck, P. Quellec, M. Marchand, E. Dellacherie, S. Harnisch, T. Blunk, R. H. Muller, 'Stealth' corona-core nanoparticles surface modified by polyethylene glycol (PEG): influences of the corona (PEG chain length and surface density) and of the core composition on phagocytic uptake and plasma protein adsorption, *Colloids Surf. B. Biointerfaces* **2000**, *18*, 301-313.

[119] A. Chanan-Khan, J. Szebeni, S. Savay, L. Liebes, N. M. Rafique, C. R. Alving, F. M. Muggia, Complement activation following first exposure to pegylated liposomal doxorubicin (Doxil): possible role in hypersensitivity reactions, *Ann. Oncol.* **2003**, *14*, 1430-1437.

[120] G. Pasut, F. M. Veronese, Polymer–drug conjugation, recent achievements and general strategies, *Prog. Polym. Sci.* **2007**, *32*, 933-961.

[121] A. Nel, T. Xia, L. Madler, N. Li, Toxic potential of materials at the nanolevel, *Science (New York, N.Y.)* **2006**, *311*, 622-627.
[122] A. Verma, O. Uzun, Y. Hu, Y. Hu, H.-S. Han, N. Watson, S. Chen, D. J. Irvine, F. Stellacci, Surface-structure-regulated cell-membrane penetration by monolayer-protected nanoparticles, *Nat. Mater.* **2008**, *7*, 588-595.
[123] K. Knop, R. Hoogenboom, D. Fischer, U. S. Schubert, Poly(ethylene glycol) in drug delivery: pros and cons as well as potential alternatives, *Angew. Chem. Int. Ed.* **2010**, *49*, 6288-6308.
[124] S. A. Abouelmagd, Y. J. Ku, Y. Yeo, Low molecular weight chitosan-coated polymeric nanoparticles for sustained and pH-sensitive delivery of paclitaxel, *J. Drug Targeting* **2015**, *23*, 725-735.
[125] C. Duehrkop, G. Leneweit, C. Heyder, K. Fromell, K. Edwards, K. N. Ekdahl, B. Nilsson, Development and characterization of an innovative heparin coating to stabilize and protect liposomes against adverse immune reactions, *Colloids Surf. B. Biointerfaces* **2016**, *141*, 576-583.
[126] C. Passirani, G. Barratt, J. P. Devissaguet, D. Labarre, Long-circulating nanoparticles bearing heparin or dextran covalently bound to poly(methyl methacrylate), *Pharm. Res.* **1998**, *15*, 1046-1050.
[127] C. Lemarchand, R. Gref, C. Passirani, E. Garcion, B. Petri, R. Muller, D. Costantini, P. Couvreur, Influence of polysaccharide coating on the interactions of nanoparticles with biological systems, *Biomaterials* **2006**, *27*, 108-118.
[128] C. Lemarchand, R. Gref, P. Couvreur, Polysaccharide-decorated nanoparticles, *European Journal of Pharmaceutics and Biopharmaceutics* **2004**, *58*, 327-341.
[129] M. Zorko, Ü. Langel, Cell-penetrating peptides: mechanism and kinetics of cargo delivery, *Adv. Drug Del. Rev.* **2005**, *57*, 529-545.
[130] A. Aderem, D. M. Underhill, Mechanisms of phagocytosis in macrophages, *Annu. Rev. Immunol.* **1999**, *17*, 593-623.
[131] H. H. Gustafson, D. Holt-Casper, D. W. Grainger, H. Ghandehari, Nanoparticle uptake: The phagocyte problem, *Nano Today* **2015**, *10*, 487-510.
[132] M. C. Kerr, R. D. Teasdale, Defining Macropinocytosis, *Traffic* **2009**, *10*, 364-371.
[133] M. Amyere, M. Mettlen, P. Van Der Smissen, A. Platek, B. Payrastre, A. Veithen, P. J. Courtoy, Origin, originality, functions, subversions and molecular signalling of macropinocytosis, *Int. J. Med. Microbiol.* **2001**, *291*, 487-494.
[134] O. Harush-Frenkel, N. Debotton, S. Benita, Y. Altschuler, Targeting of nanoparticles to the clathrin-mediated endocytic pathway, *Biochem. Biophys. Res. Commun.* **2007**, *353*, 26-32.
[135] S. Mukherjee, R. N. Ghosh, F. R. Maxfield, Endocytosis, *Physiol. Rev.* **1997**, *77*, 759-803.
[136] S. Mayor, R. E. Pagano, Pathways of clathrin-independent endocytosis, *Nat. Rev. Mol. Cell Biol.* **2007**, *8*, 603-612.
[137] I. A. Khalil, K. Kogure, H. Akita, H. Harashima, Uptake Pathways and Subsequent Intracellular Trafficking in Nonviral Gene Delivery, *Pharmacol. Rev.* **2006**, *58*, 32-45.
[138] B. Yameen, W. I. Choi, C. Vilos, A. Swami, J. Shi, O. C. Farokhzad, Insight into nanoparticle cellular uptake and intracellular targeting, *J. Controlled Release* **2014**, *190*, 485-499.
[139] M. Dominska, D. M. Dykxhoorn, Breaking down the barriers: siRNA delivery and endosome escape, *J. Cell Sci.* **2010**, *123*, 1183-1189.
[140] M. A. Zanta, P. Belguise-Valladier, J.-P. Behr, Gene delivery: A single nuclear localization signal peptide is sufficient to carry DNA to the cell nucleus, *Proceedings of the National Academy of Sciences* **1999**, *96*, 91-96.
[141] B. Fahrenkrog, U. Aebi, The nuclear pore complex: nucleocytoplasmic transport and beyond, *Nat. Rev. Mol. Cell Biol.* **2003**, *4*, 757-766.
[142] M. J. Reilly, J. D. Larsen, M. O. Sullivan, Polyplexes Traffic through Caveolae to the Golgi and Endoplasmic Reticulum en Route to the Nucleus, *Mol. Pharm.* **2012**, *9*, 1280-1290.
[143] A. K. Iyer, G. Khaled, J. Fang, H. Maeda, Exploiting the enhanced permeability and retention effect for tumor targeting, *Drug Discovery Today* **2006**, *11*, 812-818.
[144] R. Haag, F. Kratz, Polymer Therapeutics: Concepts and Applications, *Angew. Chem. Int. Ed.* **2006**, *45*, 1198-1215.
[145] S. D. Perrault, C. Walkey, T. Jennings, H. C. Fischer, W. C. Chan, Mediating tumor targeting efficiency of nanoparticles through design, *Nano Lett.* **2009**, *9*, 1909-1915.
[146] E. Markovsky, H. Baabur-Cohen, A. Eldar-Boock, L. Omer, G. Tiram, S. Ferber, P. Ofek, D. Polyak, A. Scomparin, R. Satchi-Fainaro, Administration, distribution, metabolism and elimination of polymer therapeutics, *J. Controlled Release* **2012**, *161*, 446-460.
[147] M. E. Davis, J. E. Zuckerman, C. H. Choi, D. Seligson, A. Tolcher, C. A. Alabi, Y. Yen, J. D. Heidel, A. Ribas, Evidence of RNAi in humans from systemically administered siRNA via targeted nanoparticles, *Nature* **2010**, *464*, 1067-1070.
[148] C. Yewale, D. Baradia, I. Vhora, S. Patil, A. Misra, Epidermal growth factor receptor targeting in cancer: A review of trends and strategies, *Biomaterials* **2013**, *34*, 8690-8707.

[149] E. M. Pridgen, F. Alexis, T. T. Kuo, E. Levy-Nissenbaum, R. Karnik, R. S. Blumberg, R. Langer, O. C. Farokhzad, Transepithelial Transport of Fc-Targeted Nanoparticles by the Neonatal Fc Receptor for Oral Delivery, *Sci. Transl. Med.* **2013**, *5*, 213ra167.

[150] R. Bazak, M. Houri, S. El Achy, S. Kamel, T. Refaat, Cancer active targeting by nanoparticles: a comprehensive review of literature, *J. Cancer Res. Clin. Oncol.* **2015**, *141*, 769-784.

[151] S. D. Steichen, M. Caldorera-Moore, N. A. Peppas, A review of current nanoparticle and targeting moieties for the delivery of cancer therapeutics, *Eur. J. Pharm. Sci.* **2013**, *48*, 416-427.

[152] S. Xu, B. Z. Olenyuk, C. T. Okamoto, S. F. Hamm-Alvarez, Targeting receptor-mediated endocytotic pathways with nanoparticles: Rationale and advances, *Adv. Drug Del. Rev.* **2013**, *65*, 121-138.

[153] A. A. D'Souza, P. V. Devarajan, Asialoglycoprotein receptor mediated hepatocyte targeting — Strategies and applications, *J. Controlled Release* **2015**, *203*, 126-139.

[154] M. Hashida, M. Nishikawa, Y. Takakura, Proceedings of the Third European Symposium on Controlled Drug DeliveryHepatic targeting of drugs and proteins by chemical modification, *J. Controlled Release* **1995**, *36*, 99-107.

[155] L. East, C. M. Isacke, The mannose receptor family, *Biochim. Biophys. Acta* **2002**, *1572*, 364-386.

[156] H.-T. Schon, M. Bartneck, E. Borkham-Kamphorst, J. Nattermann, T. Lammers, F. Tacke, R. Weiskirchen, Pharmacological Intervention in Hepatic Stellate Cell Activation and Hepatic Fibrosis, *Frontiers in Pharmacology* **2016**, *7*, 33.

[157] M. J. Ernsting, M. Murakami, A. Roy, S.-D. Li, Factors controlling the pharmacokinetics, biodistribution and intratumoral penetration of nanoparticles, *J. Controlled Release* **2013**, *172*, 782-794.

[158] R. P. Bagwe, L. R. Hilliard, W. Tan, Surface Modification of Silica Nanoparticles to Reduce Aggregation and Nonspecific Binding, *Langmuir.* **2006**, *22*, 4357-4362.

[159] S. Barua, J. W. Yoo, P. Kolhar, A. Wakankar, Y. R. Gokarn, S. Mitragotri, Particle shape enhances specificity of antibody-displaying nanoparticles, *Proc. Natl. Acad. Sci. USA* **2013**, *110*, 3270-3275.

[160] K. Michaelis, M. M. Hoffmann, S. Dreis, E. Herbert, R. N. Alyautdin, M. Michaelis, J. Kreuter, K. Langer, Covalent Linkage of Apolipoprotein E to Albumin Nanoparticles Strongly Enhances Drug Transport into the Brain, *J. Pharmacol. Exp. Ther.* **2006**, *317*, 1246-1253.

[161] I. Mellman, Endocytosis and molecular sorting, *Annu. Rev. Cell Dev. Biol.* **1996**, *12*, 575-625.

[162] J.-P. Behr, The Proton Sponge: a Trick to Enter Cells the Viruses Did Not Exploit, *CHIMIA Int. J. Chem.* **1997**, *51*, 34-36.

[163] S. Binauld, M. H. Stenzel, Acid-degradable polymers for drug delivery: a decade of innovation, *Chem. Commun.* **2013**, *49*, 2082-2102.

[164] D. Schmaljohann, Thermo- and pH-responsive polymers in drug delivery, *Adv. Drug Del. Rev.* **2006**, *58*, 1655-1670.

[165] H. Lv, S. Zhang, B. Wang, S. Cui, J. Yan, Toxicity of cationic lipids and cationic polymers in gene delivery, *J. Controlled Release* **2006**, *114*, 100-109.

[166] L. Wasungu, D. Hoekstra, Cationic lipids, lipoplexes and intracellular delivery of genes, *J. Controlled Release* **2006**, *116*, 255-264.

[167] A. K. Varkouhi, M. Scholte, G. Storm, H. J. Haisma, Endosomal escape pathways for delivery of biologicals, *J. Controlled Release* **2011**, *151*, 220-228.

[168] D. Terrone, S. L. Sang, L. Roudaia, J. R. Silvius, Penetratin and related cell-penetrating cationic peptides can translocate across lipid bilayers in the presence of a transbilayer potential, *Biochemistry* **2003**, *42*, 13787-13799.

[169] A. N. Koo, H. J. Lee, S. E. Kim, J. H. Chang, C. Park, C. Kim, J. H. Park, S. C. Lee, Disulfide-cross-linked PEG-poly(amino acid)s copolymer micelles for glutathione-mediated intracellular drug delivery, *Chem. Commun.* **2008**, 6570-6572.

[170] M. F. Rahman, J. Wang, T. A. Patterson, U. T. Saini, B. L. Robinson, G. D. Newport, R. C. Murdock, J. J. Schlager, S. M. Hussain, S. F. Ali, Expression of genes related to oxidative stress in the mouse brain after exposure to silver-25 nanoparticles, *Toxicol. Lett.* **2009**, *187*, 15-21.

[171] L. S. Nair, C. T. Laurencin, Biodegradable polymers as biomaterials, *Prog. Polym. Sci.* **2007**, *32*, 762-798.

[172] M. A. Swartz, J. A. Hubbell, S. T. Reddy, Lymphatic drainage function and its immunological implications: From dendritic cell homing to vaccine design, *Semin. Immunol.* **2008**, *20*, 147-156.

[173] T. Yamaoka, Y. Tabata, Y. Ikada, Distribution and Tissue Uptake of Poly(ethylene glycol) with Different Molecular Weights after Intravenous Administration to Mice, *J. Pharm. Sci.* **1994**, *83*, 601-606.

[174] B. Romberg, W. E. Hennink, G. Storm, Sheddable Coatings for Long-Circulating Nanoparticles, *Pharm. Res.* **2008**, *25*, 55-71.

[175] T. P. Szatrowski, C. F. Nathan, Production of large amounts of hydrogen peroxide by human tumor cells, *Cancer Res.* **1991**, *51*, 794-798.

[176] J. P. Bottcher, P. A. Knolle, D. Stabenow, Mechanisms balancing tolerance and immunity in the liver, *Dig. Dis. Sci.* **2011**, *29*, 384-390.

[177] R. E. Mebius, G. Kraal, Structure and function of the spleen, *Nat. Rev. Immunol.* **2005**, *5*, 606-616.
[178] M. A. Dobrovolskaia, S. E. McNeil, Immunological properties of engineered nanomaterials, *Nat. Nanotechnol.* **2007**, *2*, 469-478.
[179] T. Ishihara, M. Takeda, H. Sakamoto, A. Kimoto, C. Kobayashi, N. Takasaki, K. Yuki, K. Tanaka, M. Takenaga, R. Igarashi, T. Maeda, N. Yamakawa, Y. Okamoto, M. Otsuka, T. Ishida, H. Kiwada, Y. Mizushima, T. Mizushima, Accelerated blood clearance phenomenon upon repeated injection of PEG-modified PLA-nanoparticles, *Pharm. Res.* **2009**, *26*, 2270-2279.
[180] A. Fire, S. Xu, M. K. Montgomery, S. A. Kostas, S. E. Driver, C. C. Mello, Potent and specific genetic interference by double-stranded RNA in Caenorhabditis elegans, *Nature* **1998**, *391*, 806-811.
[181] A. P. McCaffrey, L. Meuse, T. T. Pham, D. S. Conklin, G. J. Hannon, M. A. Kay, RNA interference in adult mice, *Nature* **2002**, *418*, 38-39.
[182] D. Grimm, Small silencing RNAs: state-of-the-art, *Adv. Drug Del. Rev.* **2009**, *61*, 672-703.
[183] D. P. Bartel, MicroRNAs: target recognition and regulatory functions, *Cell* **2009**, *136*, 215-233.
[184] Y. Lee, C. Ahn, J. Han, H. Choi, J. Kim, J. Yim, J. Lee, P. Provost, O. Radmark, S. Kim, V. N. Kim, The nuclear RNase III Drosha initiates microRNA processing, *Nature* **2003**, *425*, 415-419.
[185] S. M. Hammond, E. Bernstein, D. Beach, G. J. Hannon, An RNA-directed nuclease mediates post-transcriptional gene silencing in Drosophila cells, *Nature* **2000**, *404*, 293-296.
[186] J. B. Preall, E. J. Sontheimer, RNAi: RISC gets loaded, *Cell* **2005**, *123*, 543-545.
[187] V. Ambros, The functions of animal microRNAs, *Nature* **2004**, *431*, 350-355.
[188] P. J. Paddison, A. A. Caudy, E. Bernstein, G. J. Hannon, D. S. Conklin, Short hairpin RNAs (shRNAs) induce sequence-specific silencing in mammalian cells, *Genes Dev.* **2002**, *16*, 948-958.
[189] S. Rother, G. Meister, Small RNAs derived from longer non-coding RNAs, *Biochimie* **2011**, *93*, 1905-1915.
[190] G. Tang, siRNA and miRNA: an insight into RISCs, *Trends Biochem. Sci* **2005**, *30*, 106-114.
[191] S. Saxena, Z. O. Jonsson, A. Dutta, Small RNAs with imperfect match to endogenous mRNA repress translation. Implications for off-target activity of small inhibitory RNA in mammalian cells, *J. Biol. Chem.* **2003**, *278*, 44312-44319.
[192] D. W. Bartlett, M. E. Davis, Insights into the kinetics of siRNA-mediated gene silencing from live-cell and live-animal bioluminescent imaging, *Nucleic Acids Res.* **2006**, *34*, 322-333.
[193] M. Stevenson, Dissecting HIV-1 through RNA interference, *Nat. Rev. Immunol.* **2003**, *3*, 851-858.
[194] J. A. Doudna, E. Charpentier, Genome editing. The new frontier of genome engineering with CRISPR-Cas9, *Science (New York, N.Y.)* **2014**, *346*, 1077.
[195] H. Yin, C.-Q. Song, J. R. Dorkin, L. J. Zhu, Y. Li, Q. Wu, A. Park, J. Yang, S. Suresh, A. Bizhanova, A. Gupta, M. F. Bolukbasi, S. Walsh, R. L. Bogorad, G. Gao, Z. Weng, Y. Dong, V. Koteliansky, S. A. Wolfe, R. Langer, W. Xue, D. G. Anderson, Therapeutic genome editing by combined viral and non-viral delivery of CRISPR system components in vivo, *Nat. Biotechnol.* **2016**, *34*, 328-333.
[196] M. J. R. Ruigrok, H. W. Frijlink, W. L. J. Hinrichs, Pulmonary administration of small interfering RNA: The route to go?, *J. Controlled Release* **2016**, *235*, 14-23.
[197] J. Hao, P. Kos, K. Zhou, J. B. Miller, L. Xue, Y. Yan, H. Xiong, S. Elkassih, D. J. Siegwart, Rapid Synthesis of a Lipocationic Polyester Library via Ring-Opening Polymerization of Functional Valerolactones for Efficacious siRNA Delivery, *J. Am. Chem. Soc.* **2015**, *137*, 9206-9209.
[198] S. Gao, F. Dagnaes-Hansen, E. J. Nielsen, J. Wengel, F. Besenbacher, K. A. Howard, J. Kjems, The effect of chemical modification and nanoparticle formulation on stability and biodistribution of siRNA in mice, *Mol. Ther.* **2009**, *17*, 1225-1233.
[199] A. D. Judge, V. Sood, J. R. Shaw, D. Fang, K. McClintock, I. MacLachlan, Sequence-dependent stimulation of the mammalian innate immune response by synthetic siRNA, *Nat. Biotechnol.* **2005**, *23*, 457-462.
[200] D. M. Dykxhoorn, D. Palliser, J. Lieberman, The silent treatment: siRNAs as small molecule drugs, *Gene Ther.* **2006**, *13*, 541-552.
[201] J. Harborth, S. M. Elbashir, K. Vandenburgh, H. Manninga, S. A. Scaringe, K. Weber, T. Tuschl, Sequence, chemical, and structural variation of small interfering RNAs and short hairpin RNAs and the effect on mammalian gene silencing, *Antisense Nucleic Acid Drug Dev.* **2003**, *13*, 83-105.
[202] Y. L. Chiu, T. M. Rana, siRNA function in RNAi: a chemical modification analysis, *RNA.* **2003**, *9*, 1034-1048.
[203] C. Lorenz, P. Hadwiger, M. John, H. P. Vornlocher, C. Unverzagt, Steroid and lipid conjugates of siRNAs to enhance cellular uptake and gene silencing in liver cells, *Bioorg. Med. Chem. Lett.* **2004**, *14*, 4975-4977.
[204] Y. C. Tseng, S. Mozumdar, L. Huang, Lipid-based systemic delivery of siRNA, *Adv. Drug Del. Rev.* **2009**, *61*, 721-731.

[205] S. Warashina, T. Nakamura, Y. Sato, Y. Fujiwara, M. Hyodo, H. Hatakeyama, H. Harashima, A lipid nanoparticle for the efficient delivery of siRNA to dendritic cells, *J. Controlled Release* **2016**, *225*, 183-191.
[206] K. A. Howard, S. R. Paludan, M. A. Behlke, F. Besenbacher, B. Deleuran, J. Kjems, Chitosan/siRNA nanoparticle-mediated TNF-alpha knockdown in peritoneal macrophages for anti-inflammatory treatment in a murine arthritis model, *Mol. Ther.* **2009**, *17*, 162-168.
[207] J. D. Heidel, Z. Yu, J. Y. Liu, S. M. Rele, Y. Liang, R. K. Zeidan, D. J. Kornbrust, M. E. Davis, Administration in non-human primates of escalating intravenous doses of targeted nanoparticles containing ribonucleotide reductase subunit M2 siRNA, *Proc. Natl. Acad. Sci. USA* **2007**, *104*, 5715-5721.
[208] J. T. Marques, B. R. G. Williams, Activation of the mammalian immune system by siRNAs, *Nat. Biotechnol.* **2005**, *23*, 1399-1405.
[209] W. J. Kleischmidt, L. F. Ellis, R. M. Van Frank, E. B. Murphy, Interferon stimulation by a double stranded RNA of a mycophage in statolon preparations, *Nature* **1968**, *220*, 167-168.
[210] S. Agrawal, E. R. Kandimalla, Role of Toll-like receptors in antisense and siRNA [corrected], *Nat. Biotechnol.* **2004**, *22*, 1533-1537.
[211] T. Kawai, S. Akira, The role of pattern-recognition receptors in innate immunity: update on Toll-like receptors, *Nat. Immunol.* **2010**, *11*, 373-384.
[212] E. Check, News Feature: A crucial test, *Nat. Med.* **2005**, *11*, 243-244.
[213] K. Fitzgerald, M. Frank-Kamenetsky, S. Shulga-Morskaya, A. Liebow, B. R. Bettencourt, J. E. Sutherland, R. M. Hutabarat, V. A. Clausen, V. Karsten, J. Cehelsky, S. V. Nochur, V. Kotelianski, J. Horton, T. Mant, J. Chiesa, J. Ritter, M. Munisamy, A. K. Vaishnaw, J. A. Gollob, A. Simon, Effect of an RNA interference drug on the synthesis of proprotein convertase subtilisin/kexin type 9 (PCSK9) and the concentration of serum LDL cholesterol in healthy volunteers: a randomised, single-blind, placebo-controlled, phase 1 trial, *Lancet.* **2014**, *383*, 60-68.
[214] M. Frank-Kamenetsky, A. Grefhorst, N. N. Anderson, T. S. Racie, B. Bramlage, A. Akinc, D. Butler, K. Charisse, R. Dorkin, Y. Fan, C. Gamba-Vitalo, P. Hadwiger, M. Jayaraman, M. John, K. N. Jayaprakash, M. Maier, L. Nechev, K. G. Rajeev, T. Read, I. Rohl, J. Soutschek, P. Tan, J. Wong, G. Wang, T. Zimmermann, A. de Fougerolles, H. P. Vornlocher, R. Langer, D. G. Anderson, M. Manoharan, V. Koteliansky, J. D. Horton, K. Fitzgerald, Therapeutic RNAi targeting PCSK9 acutely lowers plasma cholesterol in rodents and LDL cholesterol in nonhuman primates, *Proc. Natl. Acad. Sci. USA* **2008**, *105*, 11915-11920.
[215] A. P. Inc., Alnylam Pharmaceuticals Inc., **2015**.
[216] A. Borodovsky, K. Yucius, A. Sprague, N. K. Banda, V. M. Holers, A. Vaishnaw, M. Maier, R. Kallanthottathil, K. Charisse, S. Kuchimanchi, M. Manoharan, D. J. Salant, K. Fitzgerald, R. Meyers, B. Sorensen, ALN-CC5, an Investigational RNAi Therapeutic Targeting C5 for Complement Inhibition, *access June 15 2016*, http://www.alnylam.com/web/assets/ALN-CC5_ASH_Dec2014_panel-by-panel.pdf, **2014**
[217] P. N. Hawkins, Y. Ando, A. Dispenzeri, A. Gonzalez-Duarte, D. Adams, O. B. Suhr, Evolving landscape in the management of transthyretin amyloidosis, *Ann. Med.* **2015**, *47*, 625-638.
[218] K. Garber, Alnylam's RNAi therapy targets amyloid disease, *Nat. Biotechnol.* **2015**, *33*, 577-577.
[219] I. Alnylam Pharmaceuticals, Alnylam Development Pipeline, *access June 24 2016*, http://www.alnylam.com/product-pipeline/, **2016**
[220] A. Biologics, APN401 (Cbl-b), *access June 15 2016*, http://www.apeiron-biologics.com/index.php/projects/apn401-cbl-b.html, **2014**
[221] Arbutus, Tekmira provides update on TKM-PLK1 Phase I/II clinical study in patients with advanced gastrointestinal neuroendocrine tumors and adrenocortical carcinoma. News Release, Dec. 31., *access June 15 2016*, http://globenewswire.com/news-release/2014/12/31/694562/10113745/en/Tekmira-Provides-Update-on-TKM-PLK1-Phase-I-II-Clinical-Study-in-Patients-With-Advanced-Gastrointestinal-Neuroendocrine-Tumors-and-Adrenocortical-Carcinoma.html, **2014**
[222] R. S. Geary, B. F. Baker, S. T. Crooke, Clinical and Preclinical Pharmacokinetics and Pharmacodynamics of Mipomersen (Kynamro®): A Second-Generation Antisense Oligonucleotide Inhibitor of Apolipoprotein B, *Clinical Pharmacokinetics* **2015**, *54*, 133-146.
[223] A. Mullard, 2013 FDA drug approvals, *Nat. Rev. Drug Discov.* **2014**, *13*, 85-89.
[224] L. M. Kranz, M. Diken, H. Haas, S. Kreiter, C. Loquai, K. C. Reuter, M. Meng, D. Fritz, F. Vascotto, H. Hefesha, C. Grunwitz, M. Vormehr, Y. Husemann, A. Selmi, A. N. Kuhn, J. Buck, E. Derhovanessian, R. Rae, S. Attig, J. Diekmann, R. A. Jabulowsky, S. Heesch, J. Hassel, P. Langguth, S. Grabbe, C. Huber, O. Tureci, U. Sahin, Systemic RNA delivery to dendritic cells exploits antiviral defence for cancer immunotherapy, *Nature* **2016**.
[225] P. Sharma, J. P. Allison, Immune checkpoint targeting in cancer therapy: toward combination strategies with curative potential, *Cell* **2015**, *161*, 205-214.

[226] A. Iwasaki, R. Medzhitov, Control of adaptive immunity by the innate immune system, *Nat. Immunol.* **2015**, *16*, 343-353.
[227] E. Vivier, S. Ugolini, D. Blaise, C. Chabannon, L. Brossay, Targeting natural killer cells and natural killer T cells in cancer, *Nat. Rev. Immunol.* **2012**, *12*, 239-252.
[228] C. Hagerling, A. J. Casbon, Z. Werb, Balancing the innate immune system in tumor development, *Trends Cell Biol.* **2015**, *25*, 214-220.
[229] M. Vanneman, G. Dranoff, Combining immunotherapy and targeted therapies in cancer treatment, *Nat. Rev. Cancer* **2012**, *12*, 237-251.
[230] M. H. Kershaw, J. A. Westwood, P. K. Darcy, Gene-engineered T cells for cancer therapy, *Nat. Rev. Cancer* **2013**, *13*, 525-541.
[231] M. Kortylewski, P. Swiderski, A. Herrmann, L. Wang, C. Kowolik, M. Kujawski, H. Lee, A. Scuto, Y. Liu, C. Yang, J. Deng, H. S. Soifer, A. Raubitschek, S. Forman, J. J. Rossi, D. M. Pardoll, R. Jove, H. Yu, In vivo delivery of siRNA to immune cells by conjugation to a TLR9 agonist enhances antitumor immune responses, *Nat. Biotechnol.* **2009**, *27*, 925-932.
[232] H. Yu, M. Kortylewski, D. Pardoll, Crosstalk between cancer and immune cells: role of STAT3 in the tumour microenvironment, *Nat. Rev. Immunol.* **2007**, *7*, 41-51.
[233] W. L. Byrne, K. H. G. Mills, J. A. Lederer, G. C. O'Sullivan, Targeting Regulatory T Cells in Cancer, *Cancer Res.* **2011**, *71*, 6915-6920.
[234] I. M. Verma, N. Somia, Gene therapy - promises, problems and prospects, *Nature* **1997**, *389*, 239-242.
[235] J. M. Stribley, K. S. Rehman, H. Niu, G. M. Christman, Gene therapy and reproductive medicine, *Fertil. Steril.* **2002**, *77*, 645-657.
[236] S. Han, R. I. Mahato, Y. K. Sung, S. W. Kim, Development of biomaterials for gene therapy, *Mol. Ther.* **2000**, *2*, 302-317.
[237] C. Scholz, E. Wagner, Therapeutic plasmid DNA versus siRNA delivery: Common and different tasks for synthetic carriers, *J. Controlled Release* **2012**, *161*, 554-565.
[238] D. Bouard, D. Alazard-Dany, F. L. Cosset, Viral vectors: from virology to transgene expression, *Br. J. Pharmacol.* **2009**, *157*, 153-165.
[239] J. Villemejane, L. M. Mir, Physical methods of nucleic acid transfer: general concepts and applications, *Br. J. Pharmacol.* **2009**, *157*, 207-219.
[240] X. Gao, K. S. Kim, D. Liu, Nonviral gene delivery: what we know and what is next, *The AAPS journal* **2007**, *9*, E92-104.
[241] O. N. Gofrit, S. Benjamin, S. Halachmi, I. Leibovitch, Z. Dotan, D. L. Lamm, N. Ehrlich, V. Yutkin, M. Ben-Am, A. Hochberg, DNA based therapy with diphtheria toxin-A BC-819: a phase 2b marker lesion trial in patients with intermediate risk nonmuscle invasive bladder cancer, *J. Urol.* **2014**, *191*, 1697-1702.
[242] BioCancell, Biocancell receives FDA fast track designation for BC-819 for treatment of bladder cancer patients, *access June 24 2016*, http://www.biocancell.com/biocancell-receives-fda-fast-track-designation-for-bc-819-for-treatment-of-bladder-cancer-patients/, **2015**
[243] M. A. Kharfan-Dabaja, T. Nishihori, Vaccine therapy for cytomegalovirus in the setting of allogeneic hematopoietic cell transplantation, *Expert Rev. Vaccines* **2015**, *14*, 341-350.
[244] M. K. Wloch, L. R. Smith, S. Boutsaboualoy, L. Reyes, C. Han, J. Kehler, H. D. Smith, L. Selk, R. Nakamura, J. M. Brown, T. Marbury, A. Wald, A. Rolland, D. Kaslow, T. Evans, M. Boeckh, Safety and immunogenicity of a bivalent cytomegalovirus DNA vaccine in healthy adult subjects, *J. Infect. Dis.* **2008**, *197*, 1634-1642.
[245] I. Astellas Pharma Global Development, A Study to Evaluate a Therapeutic Vaccine, ASP0113, in Cytomegalovirus (CMV)-Seropositive Recipients Undergoing Allogeneic, Hematopoietic Cell Transplant (HCT) (HELIOS), *access June 24 2016*, https://clinicaltrials.gov/ct2/show/NCT01877655, **2016**
[246] J. Lisziewicz, N. Bakare, S. A. Calarota, D. Banhegyi, J. Szlavik, E. Ujhelyi, E. R. Toke, L. Molnar, Z. Lisziewicz, B. Autran, F. Lori, Single DermaVir immunization: dose-dependent expansion of precursor/memory T cells against all HIV antigens in HIV-1 infected individuals, *PLoS One* **2012**, *7*, e35416.
[247] G. Immunity, Repeated DermaVir Immunizations in HIV-1 Infected Treatment-naïve Patients (GIEU006), *access June 24 2016*, https://clinicaltrials.gov/ct2/show/NCT00711230?term=NCT00711230&rank=1, **2013**
[248] G. Baier, D. Baumann, J. M. Siebert, A. Musyanovych, V. Mailander, K. Landfester, Suppressing unspecific cell uptake for targeted delivery using hydroxyethyl starch nanocapsules, *Biomacromolecules* **2012**, *13*, 2704-2715.

[249] B. Kang, P. Okwieka, S. Schottler, O. Seifert, R. E. Kontermann, K. Pfizenmaier, A. Musyanovych, R. Meyer, M. Diken, U. Sahin, V. Mailander, F. R. Wurm, K. Landfester, Tailoring the stealth properties of biocompatible polysaccharide nanocontainers, *Biomaterials* **2015**, *49*, 125-134.
[250] J. R. Masters, HeLa cells 50 years on: the good, the bad and the ugly, *Nat. Rev. Cancer* **2002**, *2*, 315-319.
[251] D. Fischer, Y. Li, B. Ahlemeyer, J. Krieglstein, T. Kissel, In vitro cytotoxicity testing of polycations: influence of polymer structure on cell viability and hemolysis, *Biomaterials* **2003**, *24*, 1121-1131.
[252] R. N. Dsouza, U. Pischel, W. M. Nau, Fluorescent Dyes and Their Supramolecular Host/Guest Complexes with Macrocycles in Aqueous Solution, *Chem. Rev.* **2011**, *111*, 7941-7980.
[253] B. S. Krieg, Johannes Gutenberg-Universität (Mainz), **2014**.
[254] T. S. Zimmermann, A. C. Lee, A. Akinc, B. Bramlage, D. Bumcrot, M. N. Fedoruk, J. Harborth, J. A. Heyes, L. B. Jeffs, M. John, A. D. Judge, K. Lam, K. McClintock, L. V. Nechev, L. R. Palmer, T. Racie, I. Rohl, S. Seiffert, S. Shanmugam, V. Sood, J. Soutschek, I. Toudjarska, A. J. Wheat, E. Yaworski, W. Zedalis, V. Koteliansky, M. Manoharan, H. P. Vornlocher, I. MacLachlan, RNAi-mediated gene silencing in non-human primates, *Nature* **2006**, *441*, 111-114.
[255] P. V. Turner, T. Brabb, C. Pekow, M. A. Vasbinder, Administration of Substances to Laboratory Animals: Routes of Administration and Factors to Consider, *Journal of the American Association for Laboratory Animal Science : JAALAS* **2011**, *50*, 600-613.
[256] M. Chacon, J. Molpeceres, L. Berges, M. Guzman, M. R. Aberturas, Stability and freeze-drying of cyclosporine loaded poly(D,L lactide-glycolide) carriers, *Eur. J. Pharm. Sci.* **1999**, *8*, 99-107.
[257] D. Quintanar-Guerrero, A. Ganem-Quintanar, E. Allemann, H. Fessi, E. Doelker, Influence of the stabilizer coating layer on the purification and freeze-drying of poly(D,L-lactic acid) nanoparticles prepared by an emulsion-diffusion technique, *J. Microencapsulation* **1998**, *15*, 107-119.
[258] E. Zimmermann, R. H. Muller, K. Mader, Influence of different parameters on reconstitution of lyophilized SLN, *Int. J. Pharm.* **2000**, *196*, 211-213.
[259] Y. N. Konan, R. Gurny, E. Allemann, Preparation and characterization of sterile and freeze-dried sub-200 nm nanoparticles, *Int. J. Pharm.* **2002**, *233*, 239-252.
[260] W. Abdelwahed, G. Degobert, S. Stainmesse, H. Fessi, Freeze-drying of nanoparticles: formulation, process and storage considerations, *Adv. Drug Del. Rev.* **2006**, *58*, 1688-1713.
[261] P. Cuatrecasas, I. Parikh, Adsorbents for affinity chromatography. Use of N-hydroxysuccinimide esters of agarose, *Biochemistry* **1972**, *11*, 2291-2299.
[262] R. Widenbring, G. Frenning, M. Malmsten, Chain and pore-blocking effects on matrix degradation in protein-loaded microgels, *Biomacromolecules* **2014**, *15*, 3671-3678.
[263] D. E. Kelley, J. P. Reilly, T. Veneman, L. J. Mandarino, Effects of insulin on skeletal muscle glucose storage, oxidation, and glycolysis in humans, *Am. J. Physiol. Endocrinol. Metab.* **1990**, *258*, E923-929.
[264] M. von Delius, E. M. Geertsema, D. A. Leigh, D. T. Tang, Design, synthesis, and operation of small molecules that walk along tracks, *J. Am. Chem. Soc.* **2010**, *132*, 16134-16145.
[265] S. Raddatz, J. Mueller-Ibeler, J. Kluge, L. Wass, G. Burdinski, J. R. Havens, T. J. Onofrey, D. Wang, M. Schweitzer, Hydrazide oligonucleotides: new chemical modification for chip array attachment and conjugation, *Nucleic Acids Res.* **2002**, *30*, 4793-4802.
[266] A. Dirksen, S. Dirksen, T. M. Hackeng, P. E. Dawson, Nucleophilic catalysis of hydrazone formation and transimination: implications for dynamic covalent chemistry, *J. Am. Chem. Soc.* **2006**, *128*, 15602-15603.
[267] R. G. Barradas, S. Fletcher, J. D. Porter, The hydrolysis of maleimide in alkaline solution, *Can. J. Chem.* **1976**, *54*, 1400-1404.
[268] D. G. Smyth, O. O. Blumenfeld, W. Konigsberg, Reactions of N-ethylmaleimide with peptides and amino acids, *Biochem. J* **1964**, *91*, 589-595.
[269] S. Yoshitake, Y. Yamada, E. Ishikawa, R. Masseyeff, Conjugation of glucose oxidase from Aspergillus niger and rabbit antibodies using N-hydroxysuccinimide ester of N-(4-carboxycyclohexylmethyl)-maleimide, *Eur. J. Biochem.* **1979**, *101*, 395-399.
[270] N. Nakai, C. Y. Lai, B. L. Horecker, Use of fluorescamine in the chromatographic analysis of peptides from proteins, *Anal. Biochem.* **1974**, *58*, 563-570.
[271] A. Musyanovych, R. Rossmanith, C. Tontsch, K. Landfester, Effect of hydrophilic comonomer and surfactant type on the colloidal stability and size distribution of carboxyl- and amino-functionalized polystyrene particles prepared by miniemulsion polymerization, *Langmuir.* **2007**, *23*, 5367-5376.
[272] J. Jiang, G. Oberdörster, P. Biswas, Characterization of size, surface charge, and agglomeration state of nanoparticle dispersions for toxicological studies, *J. Nanopart. Res.* **2009**, *11*, 77-89.
[273] A. Radomski, P. Jurasz, D. Alonso-Escolano, M. Drews, M. Morandi, T. Malinski, M. W. Radomski, Nanoparticle-induced platelet aggregation and vascular thrombosis, *Br. J. Pharmacol.* **2005**, *146*, 882-893.
[274] J. C. Sung, B. L. Pulliam, D. A. Edwards, Nanoparticles for drug delivery to the lungs, *Trends Biotechnol.* **2007**, *25*, 563-570.

[275] S. Winzen, S. Schoettler, G. Baier, C. Rosenauer, V. Mailaender, K. Landfester, K. Mohr, Complementary analysis of the hard and soft protein corona: sample preparation critically effects corona composition, *Nanoscale* **2015**, *7*, 2992-3001.
[276] C. Perrino, S. Lee, S. W. Choi, A. Maruyama, N. D. Spencer, A Biomimetic Alternative to Poly(ethylene glycol) as an Antifouling Coating: Resistance to Nonspecific Protein Adsorption of Poly(l-lysine)-graft-dextran, *Langmuir.* **2008**, *24*, 8850-8856.
[277] J. C. Leroux, F. De Jaeghere, B. Anner, E. Doelker, R. Gurny, An investigation on the role of plasma and serum opsonins on the internalization of biodegradable poly(D,L-lactic acid) nanoparticles by human monocytes, *Life Sci.* **1995**, *57*, 695-703.
[278] L. Illum, S. S. Davis, R. H. Muller, E. Mak, P. West, The organ distribution and circulation time of intravenously injected colloidal carriers sterically stabilized with a block copolymer--poloxamine 908, *Life Sci.* **1987**, *40*, 367-374.
[279] S. M. Moghimi, I. S. Muir, L. Illum, S. S. Davis, V. Kolb-Bachofen, Coating particles with a block co-polymer (poloxamine-908) suppresses opsonization but permits the activity of dysopsonins in the serum, *Biochim. Biophys. Acta* **1993**, *1179*, 157-165.
[280] W. T. Godbey, K. K. Wu, A. G. Mikos, Poly(ethylenimine)-mediated gene delivery affects endothelial cell function and viability, *Biomaterials* **2001**, *22*, 471-480.
[281] S. Schottler, K. Klein, K. Landfester, V. Mailander, Protein source and choice of anticoagulant decisively affect nanoparticle protein corona and cellular uptake, *Nanoscale* **2016**, *8*, 5526-5536.
[282] T. L. Riss, R. A. Moravec, A. L. Niles, H. A. Benink, T. J. Worzella, L. Minor, in *Assay Guidance Manual* (Eds.: G. S. Sittampalam, N. P. Coussens, H. Nelson, M. Arkin, D. Auld, C. Austin, B. Bejcek, M. Glicksman, J. Inglese, P. W. Iversen, Z. Li, J. McGee, O. McManus, L. Minor, A. Napper, J. M. Peltier, T. Riss, O. J. Trask, Jr., J. Weidner), Eli Lilly & Company and the National Center for Advancing Translational Sciences, Bethesda (MD), **2004**.
[283] I. Schmid, W. J. Krall, C. H. Uittenbogaart, J. Braun, J. V. Giorgi, Dead cell discrimination with 7-amino-actinomcin D in combination with dual color immunofluorescence in single laser flow cytometry, *Cytometry* **1992**, *13*, 204-208.
[284] M. Langeveld, L. E. Gamadia, I. J. ten Berge, T-lymphocyte subset distribution in human spleen, *Eur. J. Clin. Invest.* **2006**, *36*, 250-256.
[285] R. J. Ulevitch, P. S. Tobias, Receptor-dependent mechanisms of cell stimulation by bacterial endotoxin, *Annu. Rev. Immunol.* **1995**, *13*, 437-457.
[286] T. Fifis, A. Gamvrellis, B. Crimeen-Irwin, G. A. Pietersz, J. Li, P. L. Mottram, I. F. McKenzie, M. Plebanski, Size-dependent immunogenicity: therapeutic and protective properties of nano-vaccines against tumors, *J. Immunol.* **2004**, *173*, 3148-3154.
[287] M. B. Gorbet, M. V. Sefton, Endotoxin: The uninvited guest, *Biomaterials* **2005**, *26*, 6811-6817.
[288] P. Ziegler, S. Boettcher, H. Takizawa, M. G. Manz, T. H. Brummendorf, LPS-stimulated human bone marrow stroma cells support myeloid cell development and progenitor cell maintenance, *Ann. Hematol.* **2016**, *95*, 173-178.
[289] B. D. Gitter, L. M. Cox, R. E. Rydel, P. C. May, Amyloid beta peptide potentiates cytokine secretion by interleukin-1 beta-activated human astrocytoma cells, *Proc. Natl. Acad. Sci. USA* **1995**, *92*, 10738-10741.
[290] J. W. Bulte, P. G. Laughlin, E. K. Jordan, V. A. Tran, J. Vymazal, J. A. Frank, Tagging of T cells with superparamagnetic iron oxide: uptake kinetics and relaxometry, *Acad. Radiol.* **1996**, *3 Suppl 2*, S301-303.
[291] M. Moghaddami, G. Mayrhofer, L. G. Cleland, MHC class II compartment, endocytosis and phagocytic activity of macrophages and putative dendritic cells isolated from normal tissues rich in synovium, *Int. Immunol.* **2005**, *17*, 1117-1130.
[292] R. M. Steinman, J. Swanson, The endocytic activity of dendritic cells, *J. Exp. Med.* **1995**, *182*, 283-288.
[293] M. Prabhudas, D. Bowdish, K. Drickamer, M. Febbraio, J. Herz, L. Kobzik, M. Krieger, J. Loike, T. K. Means, S. K. Moestrup, S. Post, T. Sawamura, S. Silverstein, X. Y. Wang, J. El Khoury, Standardizing scavenger receptor nomenclature, *J. Immunol.* **2014**, *192*, 1997-2006.
[294] K. Drickamer, M. E. Taylor, Recent insights into structures and functions of C-type lectins in the immune system, *Curr. Opin. Struct. Biol.* **2015**, *34*, 26-34.
[295] R. M. Steinman, G. Kaplan, M. D. Witmer, Z. A. Cohn, Identification of a novel cell type in peripheral lymphoid organs of mice. V. Purification of spleen dendritic cells, new surface markers, and maintenance in vitro, *J. Exp. Med.* **1979**, *149*, 1-16.
[296] F. Alexis, E. Pridgen, L. K. Molnar, O. C. Farokhzad, Factors affecting the clearance and biodistribution of polymeric nanoparticles, *Mol. Pharm.* **2008**, *5*, 505-515.
[297] D. E. Amacher, Serum transaminase elevations as indicators of hepatic injury following the administration of drugs, *Regul. Toxicol. Pharm.* **1998**, *27*, 119-130.
[298] J. Ozer, M. Ratner, M. Shaw, W. Bailey, S. Schomaker, The current state of serum biomarkers of hepatotoxicity, *Toxicology* **2008**, *245*, 194-205.

[299] I. V. Zhigaltsev, N. Belliveau, I. Hafez, A. K. Leung, J. Huft, C. Hansen, P. R. Cullis, Bottom-up design and synthesis of limit size lipid nanoparticle systems with aqueous and triglyceride cores using millisecond microfluidic mixing, *Langmuir.* **2012**, *28*, 3633-3640.

[300] A. K. Leung, I. M. Hafez, S. Baoukina, N. M. Belliveau, I. V. Zhigaltsev, E. Afshinmanesh, D. P. Tieleman, C. L. Hansen, M. J. Hope, P. R. Cullis, Lipid Nanoparticles Containing siRNA Synthesized by Microfluidic Mixing Exhibit an Electron-Dense Nanostructured Core, *J. Phys. Chem. C Nanomater. Interfaces* **2012**, *116*, 18440-18450.

[301] G. Wang, J. J. Wang, F. Li, S. S. To, Development and Evaluation of a Novel Drug Delivery: Pluronics/SDS Mixed Micelle Loaded With Myricetin In Vitro and In Vivo, *J. Pharm. Sci.* **2016**, *105*, 1535-1543.

[302] D. Danon, L. Goldstein, Y. Marikovsky, E. Skutelsky, Use of cationized ferritin as a label of negative charges on cell surfaces, *J. Ultrastruct. Res.* **1972**, *38*, 500-510.

[303] J. Heyes, L. Palmer, K. Bremner, I. MacLachlan, Cationic lipid saturation influences intracellular delivery of encapsulated nucleic acids, *J. Controlled Release* **2005**, *107*, 276-287.

[304] C. A. Alabi, K. T. Love, G. Sahay, H. Yin, K. M. Luly, R. Langer, D. G. Anderson, Multiparametric approach for the evaluation of lipid nanoparticles for siRNA delivery, *Proc. Natl. Acad. Sci. USA* **2013**, *110*, 12881-12886.

[305] M. Jayaraman, S. M. Ansell, B. L. Mui, Y. K. Tam, J. Chen, X. Du, D. Butler, L. Eltepu, S. Matsuda, J. K. Narayanannair, K. G. Rajeev, I. M. Hafez, A. Akinc, M. A. Maier, M. A. Tracy, P. R. Cullis, T. D. Madden, M. Manoharan, M. J. Hope, Maximizing the potency of siRNA lipid nanoparticles for hepatic gene silencing in vivo, *Angew. Chem. Int. Ed.* **2012**, *51*, 8529-8533.

[306] R. S. Burke, S. H. Pun, Extracellular Barriers to in Vivo PEI and PEGylated PEI Polyplex-Mediated Gene Delivery to the Liver, *Bioconjugate Chem.* **2008**, *19*, 693-704.

[307] H. E. Gottlieb, V. Kotlyar, A. Nudelman, NMR Chemical Shifts of Common Laboratory Solvents as Trace Impurities, *J. Org. Chem.* **1997**, *62*, 7512-7515.

[308] A. V. Delgado, F. Gonzalez-Caballero, R. J. Hunter, L. K. Koopal, J. Lyklema, Measurement and interpretation of electrokinetic phenomena, *J. Colloid Interface Sci.* **2007**, *309*, 194-224.

[309] B. Carrillo-Conde, E. H. Song, A. Chavez-Santoscoy, Y. Phanse, A. E. Ramer-Tait, N. L. Pohl, M. J. Wannemuehler, B. H. Bellaire, B. Narasimhan, Mannose-functionalized "pathogen-like" polyanhydride nanoparticles target C-type lectin receptors on dendritic cells, *Mol. Pharm.* **2011**, *8*, 1877-1886.

[310] A. D. Duong, S. Sharma, K. J. Peine, G. Gupta, A. R. Satoskar, E. M. Bachelder, B. E. Wyslouzil, K. M. Ainslie, Electrospray encapsulation of toll-like receptor agonist resiquimod in polymer microparticles for the treatment of visceral leishmaniasis, *Mol. Pharm.* **2013**, *10*, 1045-1055.

6.5 Supplemental Data

6.5.1 Additional Data

Table 34: Size measurement (DLS) of lyophilized Sp-Ac-DEX nanoparticles after resuspension in PBS. Particles were lyophilized with different amounts (% in m/m) of cryoprotectants.

Cryoprotectant		PDI	Size average / d.nm	Peak	Intensity		Number	
					Size / d.nm	Intensity / %	Size / d.nm	Intensity / %
No Cryo-protectant	0%	0.453	255.0	1	387.5	75.9	78.4	100.0
				2	100.0	22.3		
				3	5281.0	1.8		
PVA	3%	0.579	274.9	1	515.4	69.3	85.5	99.2
				2	118.5	30.3	528.3	0.8
				3	5537.0	0.4		
Glucose	1%	0.236	154.0	1	158.6	92.8	97.6	100.0
				2	4526.0	3.7		
				3	1536.0	3.5		
	5%	0.535	244.7	1	153.0	57.1	94.3	99.7
				2	843.3	40.1	748.7	0.3
				3	5238.0	2.8		
	10%	0.328	166.9	1	178.0	93.4	88.4	100.0
				2	5102.0	3.9	1012.0	
				3	1148.0	2.7		
	20%	0.491	236.8	1	217.9	81.8	92.9	100.0
				2	719.2	17.9		
				3	5560.0	0.4		
	40%	0.218	143.7	1	155.1	96.9	88.0	100.0
				2	4790.0	3.1		

Cryoprotectant		PDI	Size average / d.nm	Peak	Intensity		Number	
					Size / d.nm	Intensity / %	Size / d.nm	Intensity / %
Sucrose	1%	0.542	226.2	1	174.5	69.4	99.8	100.0
				2	794.5	22.7		
				3	4869.0	7.9		
	5%	0.373	188.8	1	244.1	95.2	85.4	100.0
				2	4859.0	4.8		
	10%	0.265	158.2	1	167.5	93.1	90.3	100.0
				2	3691.0	6.9		
	20%	0.261	156.8	1	167.0	94.7	86.5	100.0
				2	3402.0	5.3		
	40%	0.164	137.8	1	148.4	98.7	95.7	100.0
				2	4939.0	1.3		
Trehalose	1%	0.247	147.6	1	156.0	91.9	87.0	100.0
				2	3070.0	8.1		
	5%	0.299	156.9	1	166.1	94.6	85.3	100.0
				2	4702.0	5.4		
	10%	0.297	159.4	1	174.9	93.5	80.1	100.0
				2	2060.0	3.8		
				3	4880.0	2.6		
	20%	0.212	147.9	1	163.3	97.0	89.2	100.0
				2	4624.0	3.0		
	40%	0.203	150.1	1	164.4	97.3	93.3	100.0
				2	4795.0	2.7		
Dextran 1 kDa	1%	0.523	318.7	1	346.3	70.4	331.4	1.3
				2	105.1	29.6	81.8	98.7
	5%	0.297	168.5	1	245.5	97.6	90.2	100.0
				2	4882.0	2.4		
	10%	0.269	157.4	1	164.5	93.1	92.6	100.0
				2	4571.0	5.7		
				3	1278.0	1.2		
	20%	0.309	167.4	1	191.5	96.5	88.5	100.0
				2	5038.0	3.5		
	40%	0.175	144.2	1	155.9	98.5	98.4	100.0
				2	5011.0	1.5		

Table 35: Surface potential of particles with different cryoprotective additives after resuspension determined by zeta potential

Cryoprotectant		Zeta Potential average (mV)	Zeta Potential deviation (mV)
No Cryoprotectant	0%	12.77	1.20
PVA	3%	11.96	1.85
Glucose	1%	11.45	0.64
	5%	10.53	2.47
	10%	13.00	0.78
	20%	9.50	0.92
	40%	10.8	0.79
Sucrose	1%	9.80	2.34
	5%	10.90	2.62
	10%	10.55	0.21
	20%	9.03	1.77
	40%	12.95	0.21
Trehalose	1%	16.50	1.73
	5%	13.60	1.13
	10%	11.86	3.37
	20%	13.20	2.40
	40%	13.77	0.64
Dextran 1 kDa	1%	12.90	0.42
	5%	13.00	1.13
	10%	12.17	1.19
	20%	13.85	1.77
	40%	11.14	1.45

Table 36: Size measurement of surface modified particles by NTA technology. Particles were incubated in PBS or DMEM up to 3 days. Particle sizes are described by the mean (bold) value and SD (in brackets).

Particle Modification		Sp-Ac-DEX NPs	DEXylated NPs		PEGylated NPs	
			3.5 kDa	5 kDa	2 kDa	5 kDa
Particle size measured in PBS / d.nm	0 h	**155.6** (48.6)	**215.1** (87.1)	**193.1** (76.1)	**208.6** (94.0)	**178.3** (78.4)
	15 h	**160.6** (59.3)	**216.4** (83.4)	**205.4** (78.2)	**178.4** (81.9)	**180.5** (79.3)
	22 h	**225.2** (94.6)	**213.9** (120.7)	**183.8** (89.6)	**178.8** (87.8)	**176.7** (74.0)
	40 h	**181.0** (112.3)	**207.9** (101.7)	**226.5** (117.8)	**198.2** (85.9)	**179.6** (77.2)
	3 d	**174.9** (89.3)	**155.1** (73.1)	**196.7** (99.7)	**251.5** (134.2)	**195.6** (86.6)
Particle size measured in DMEM / d.nm	0 h	**210.3** (85.9)	**347.6** (195.3)	**265.9** (122.1)	**214.6** (113.5)	**244.1** (166.6)
	15 h	**212.0** (98.2)	**388.7** (237.8)	**420.7** (319.1)	**210.5** (97.6)	**241.7** (138.6)
	22 h	**250.5** (96.9)	**386.6** (233.9)	**408.4** (268.1)	**202.4** (104.9)	**238.5** (155.4)
	40 h	**206.3** (101.6)	**385.7** (213.4)	**366.3** (258.7)	**224.8** (111.6)	**264.8** (136.5)
	3 d	**206.6** (89.0)	**366.0** (221.7)	**300.7** (216.0)	**219.4** (102.3)	**220.4** (127.6)

[a]Particle size in d.nm of modified Sp-Ac-DEX NPs measured by NTA in PBS and DMEM

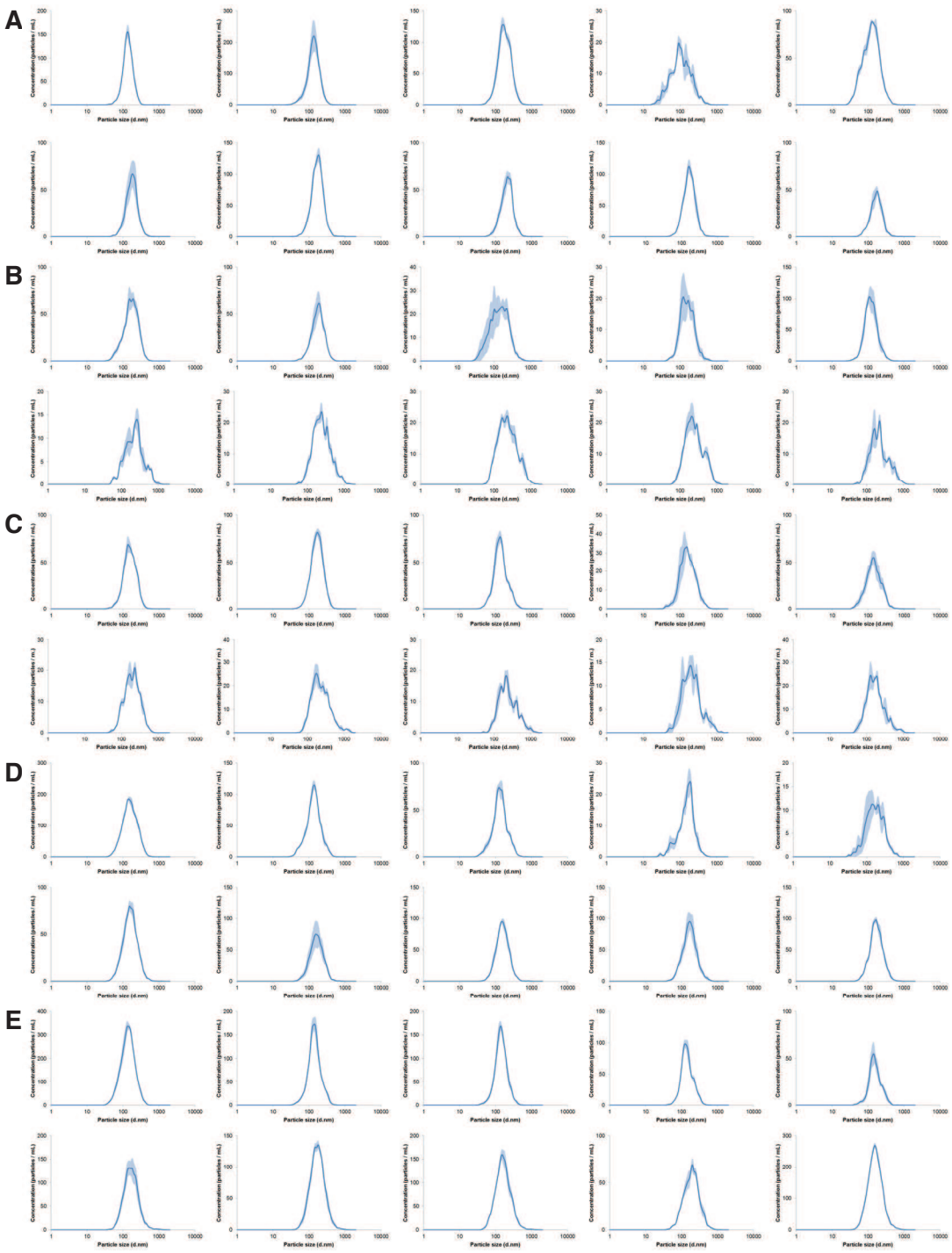

Figure 84: NTA measurements of surface-modified particles in PBS (top) or DMEM (bottom) with 10% FCS after 0 hours, 15 hours, 22 hours, 40 hours, and 3 days. (A) Non-modified, (B) DEXylated 3.5 kDa, (C) DEXylated 5 kDa, (D) PEGylated 2 kDa, and (E) PEGylated 5 kDa Sp-Ac-DEX particles.

6.5.2 ^{1}H-NMR Spectra

Acetalated Polysaccharides

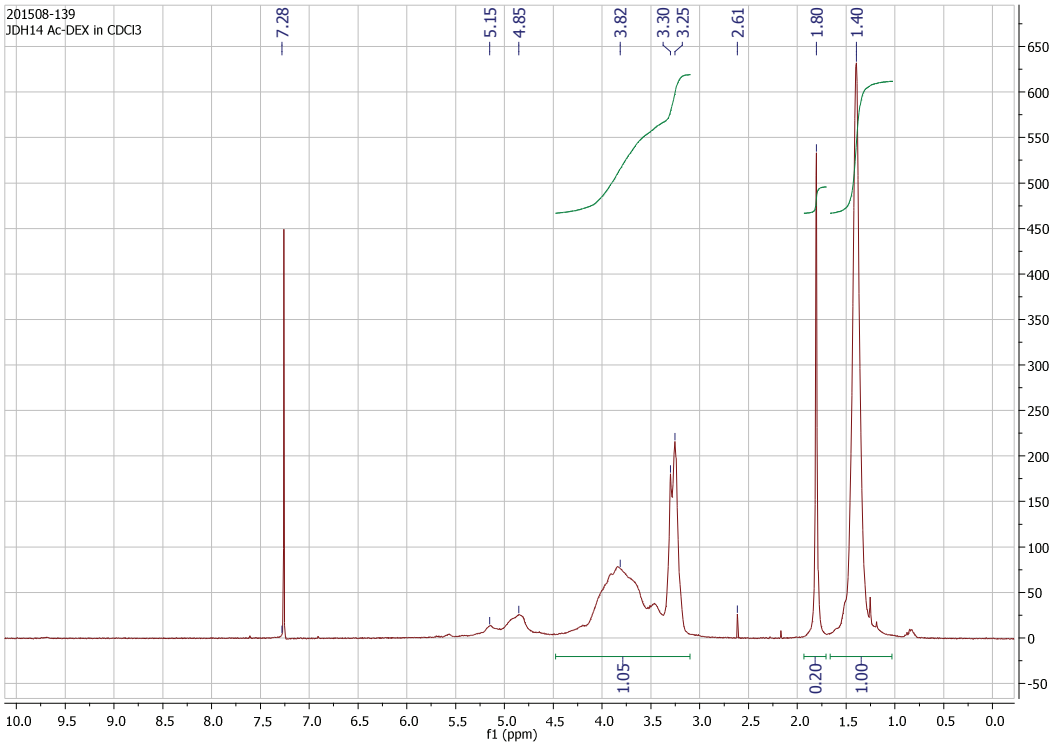

Figure 85: ^{1}H-NMR of Ac-DEX in $CDCl_3$.

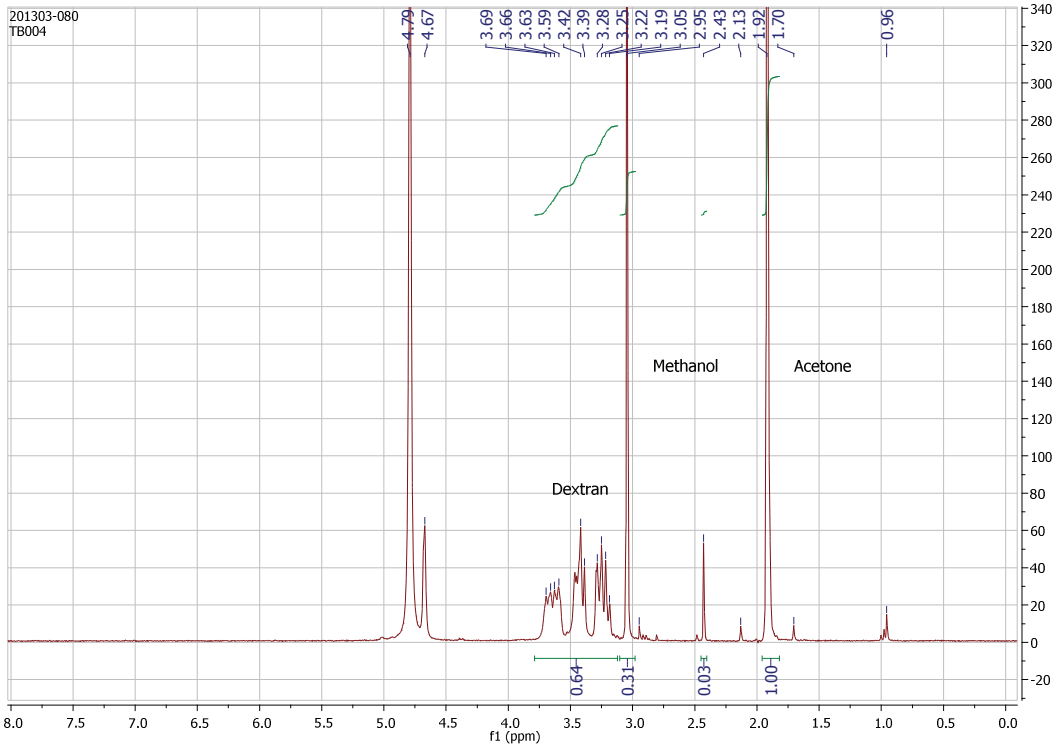

Figure 86: ^{1}H-NMR of Ac-DEX in D_2O/DCl.

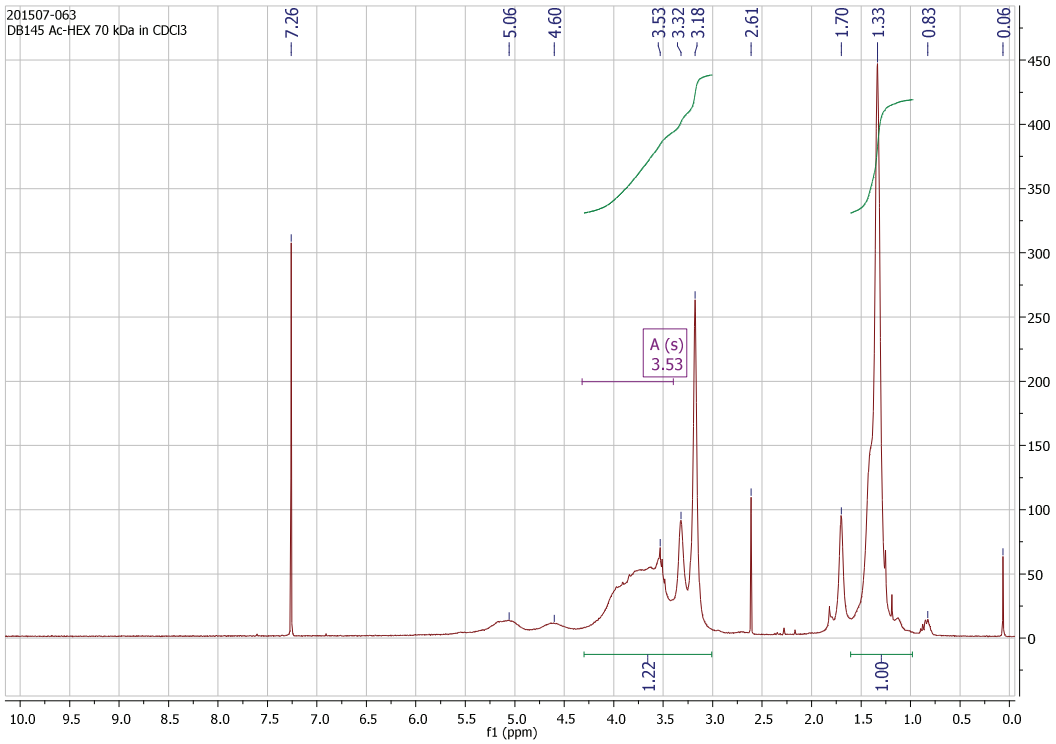

Figure 87: ^{1}H-NMR of Ac-HES 70 kDa in $CDCl_3$.

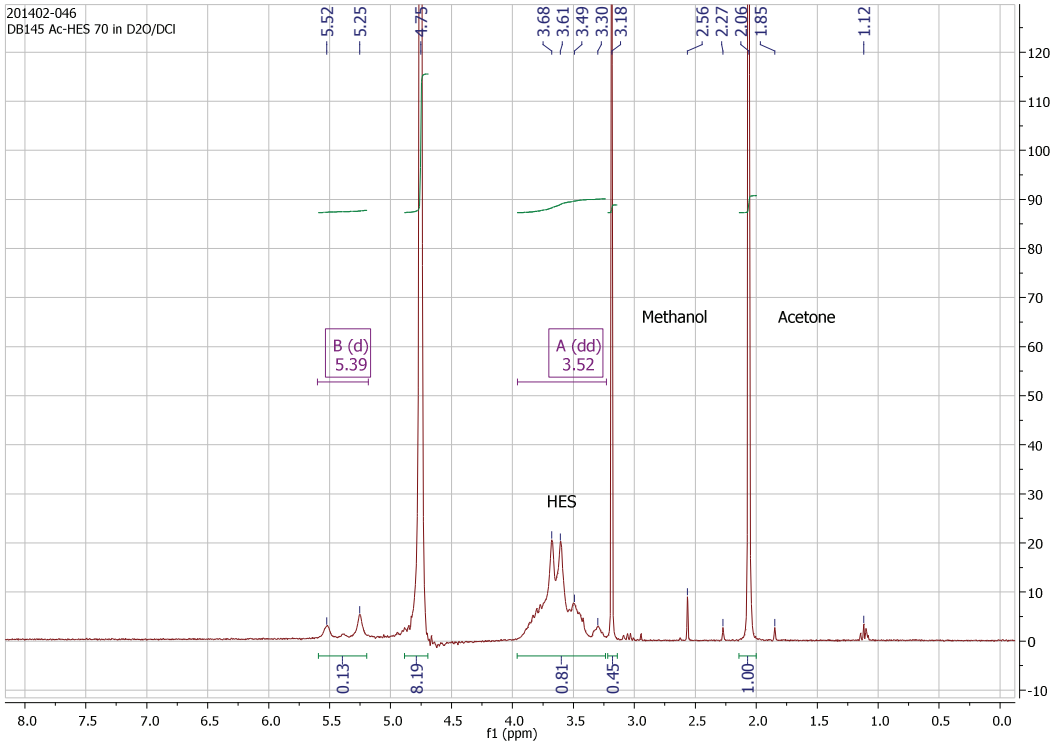

Figure 88: ^{1}H-NMR of Ac-HES 70 kDa in D_2O/DCl.

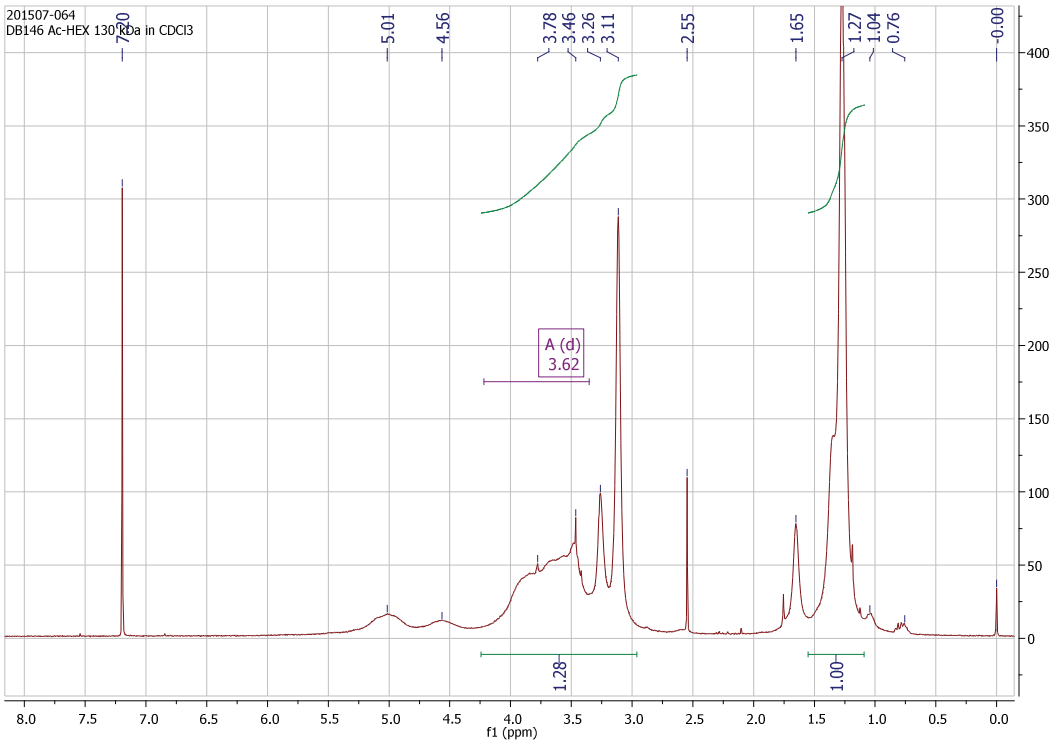

Figure 89: ^{1}H-NMR of Ac-HES 130 kDa in $CDCl_3$.

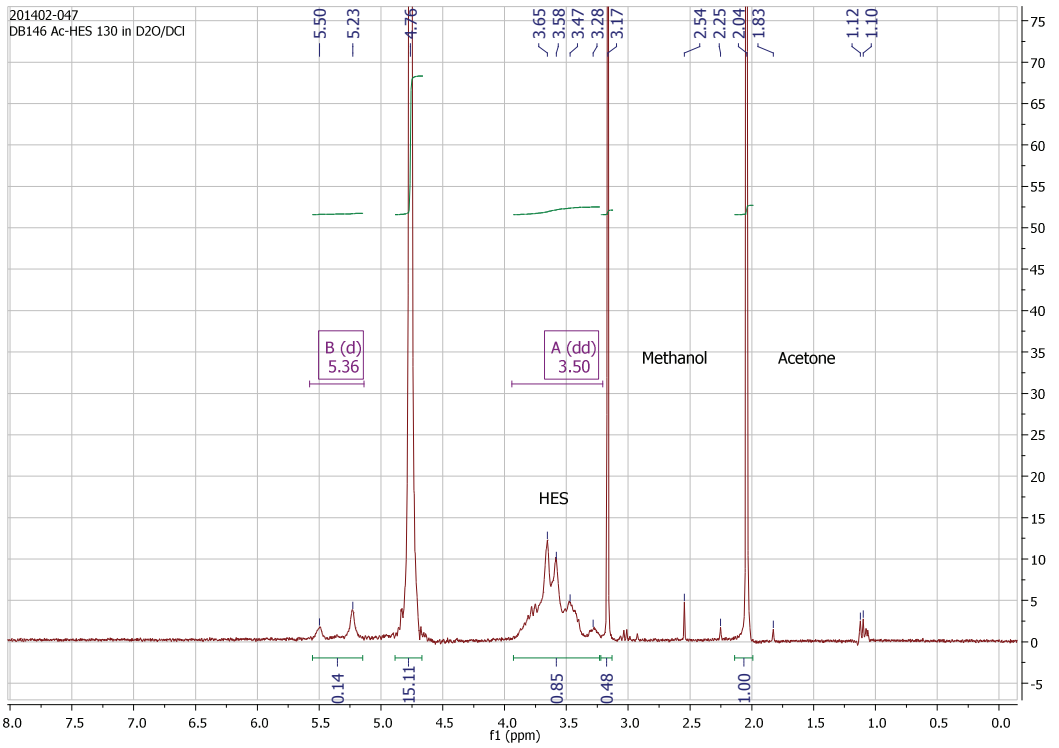

Figure 90: ^{1}H-NMR of Ac-HES 130 kDa in D_2O/DCl.

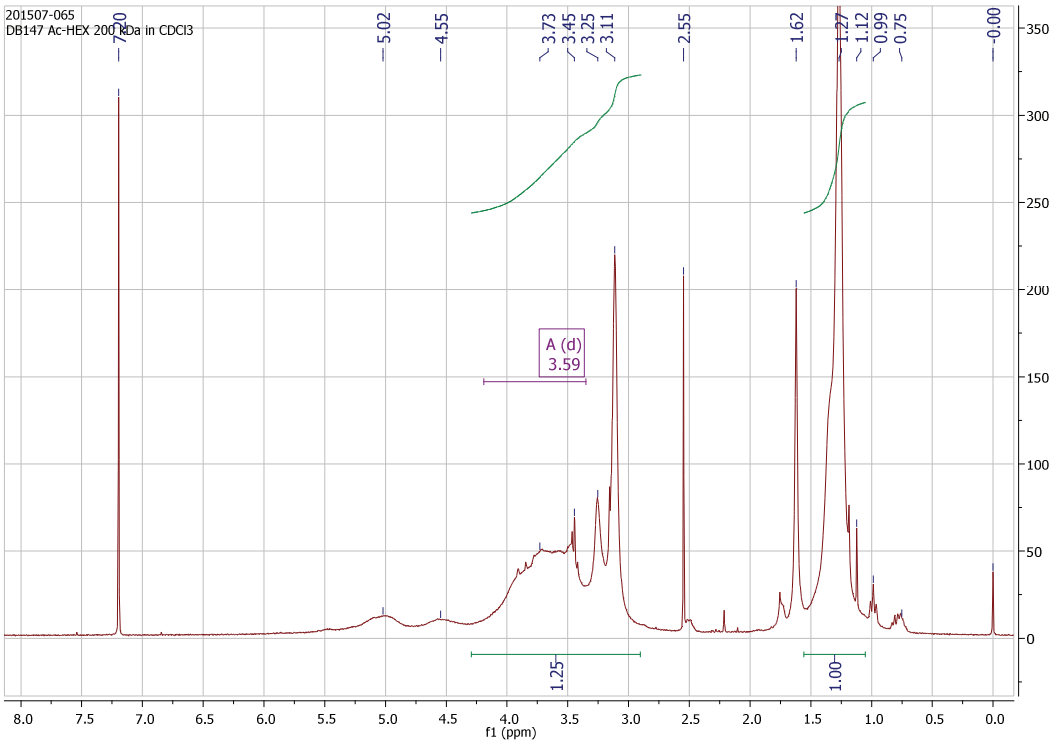

Figure 91: ^{1}H-NMR of Ac-HES 200 kDa in $CDCl_3$.

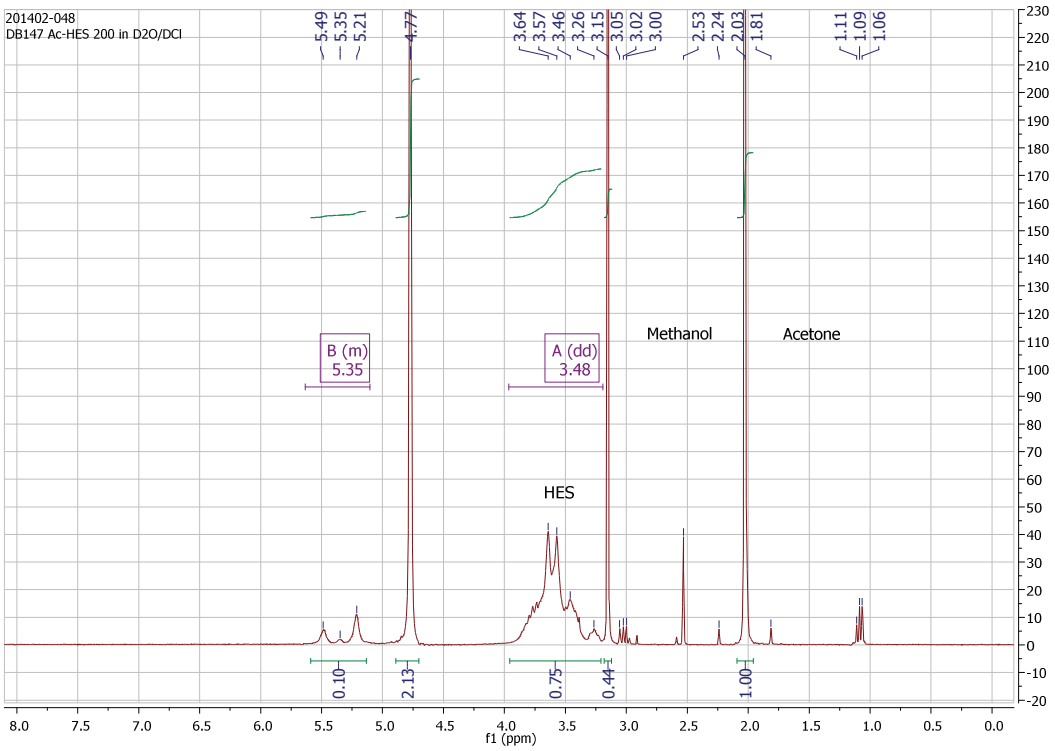

Figure 92: ^{1}H-NMR of Ac-HES 200 kDa in D_2O/DCl.

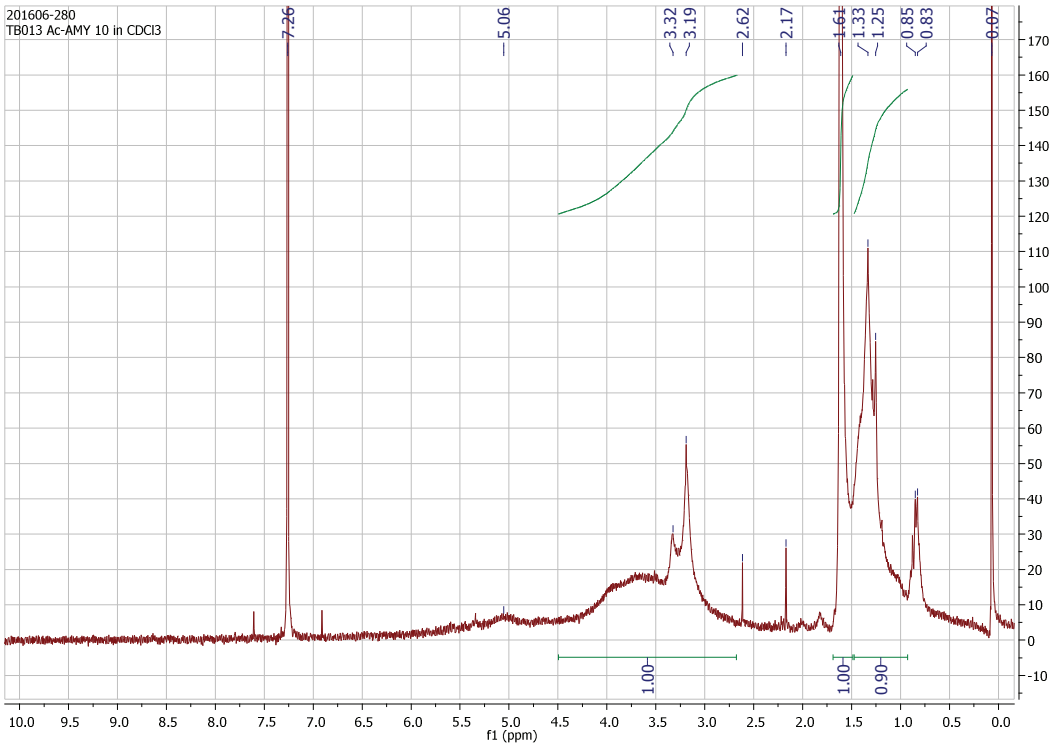

Figure 93: ^{1}H-NMR of Ac-AMY 10 min. in $CDCl_3$.

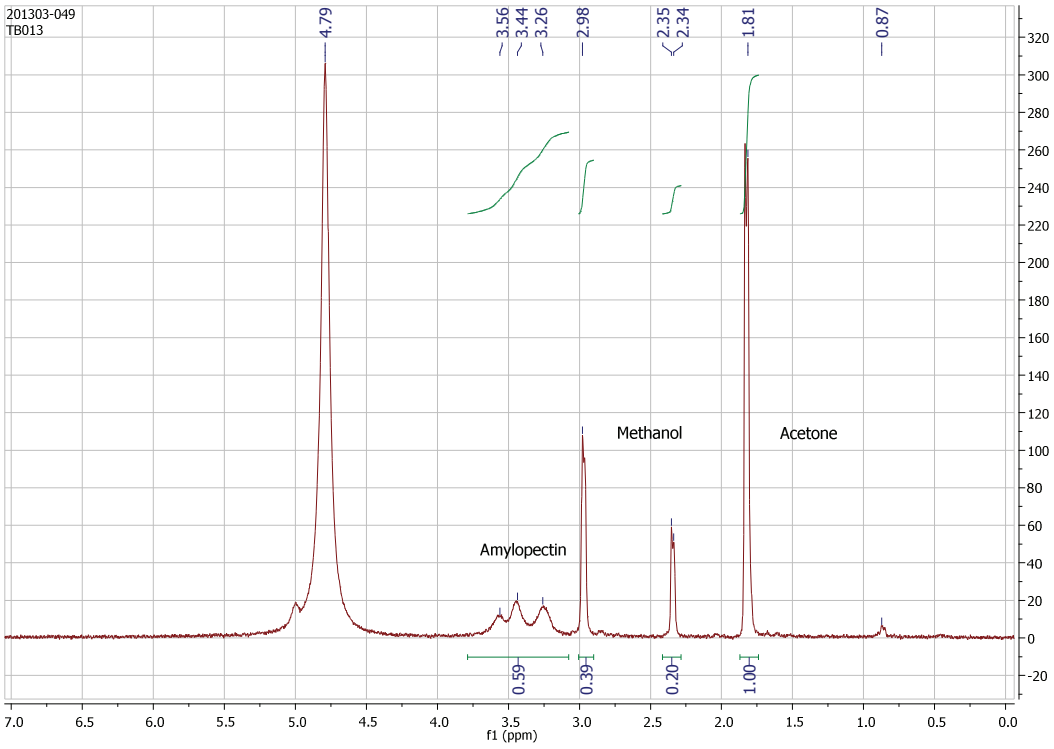

Figure 94: ^{1}H-NMR of Ac-AMY 10 min. in D_2O/DCl.

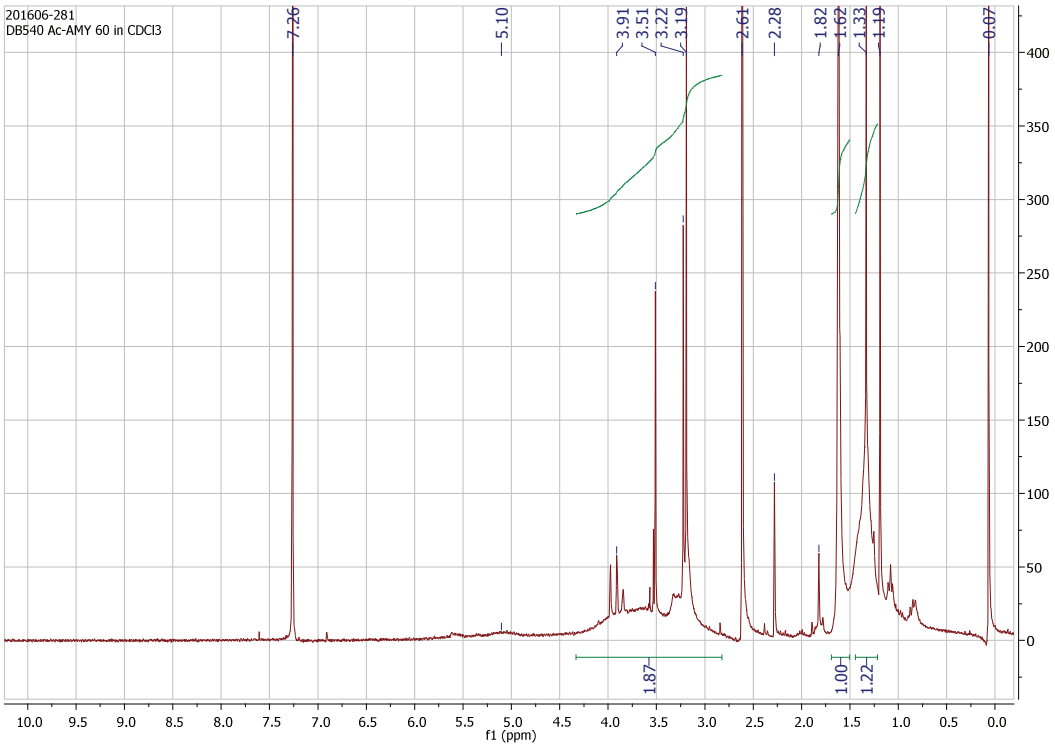

Figure 95: ^{1}H-NMR of Ac-AMY 60 min. in $CDCl_3$.

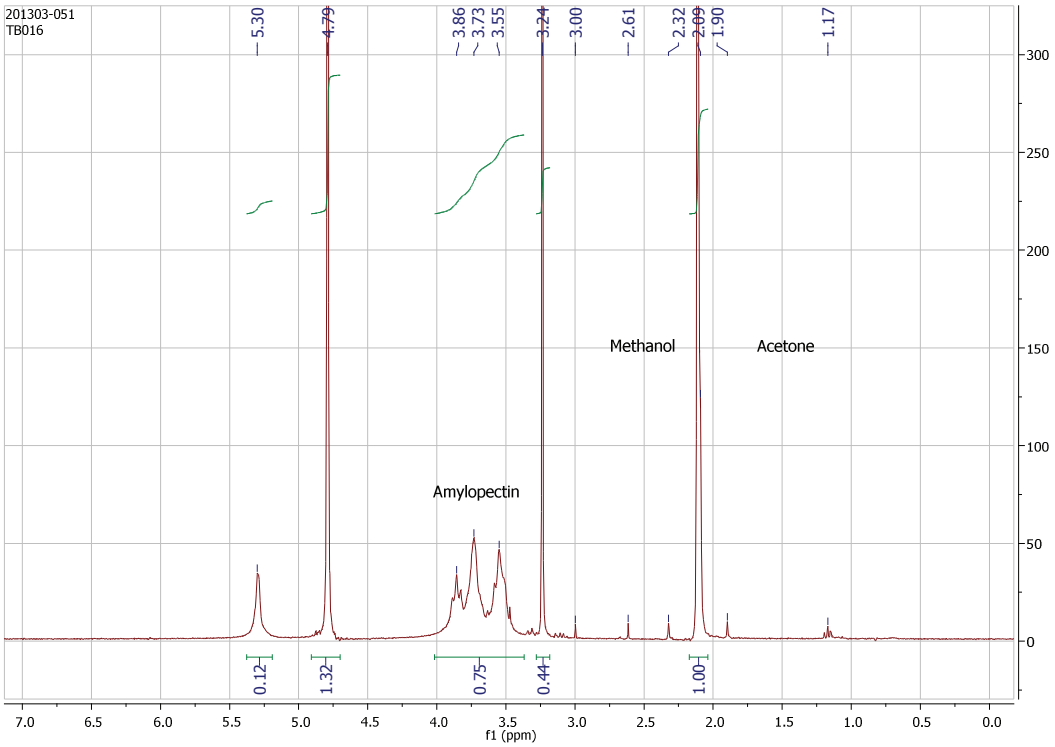

Figure 96: ^{1}H-NMR of Ac-AMY 60 min. in D_2O/DCl.

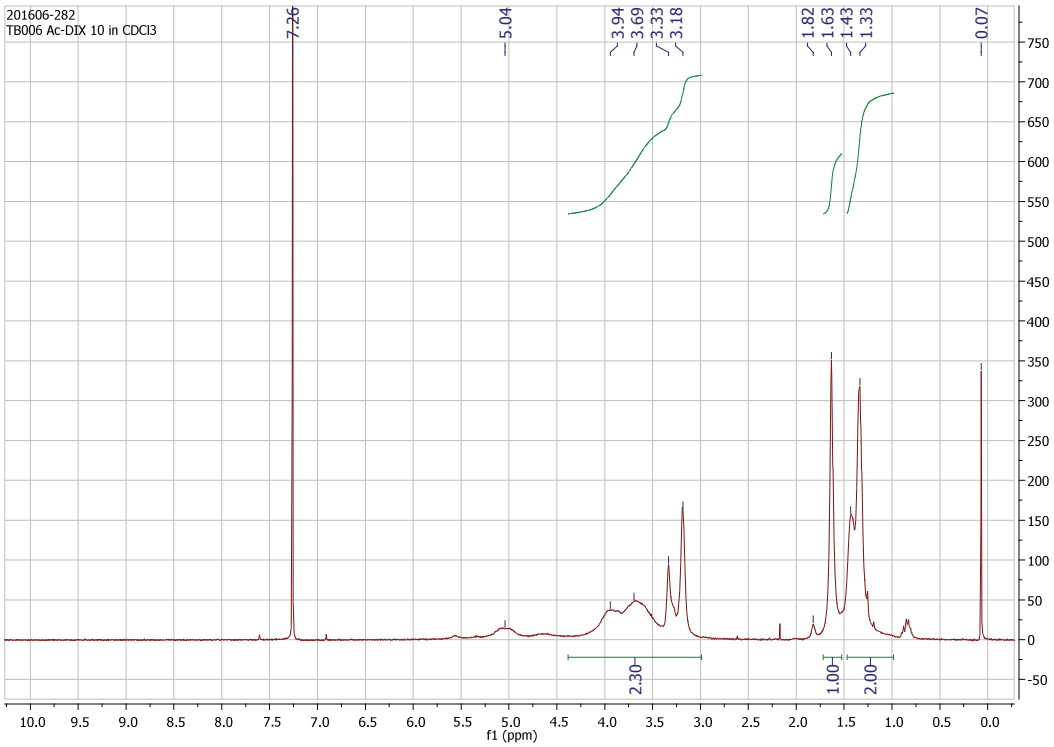

Figure 97: ^{1}H-NMR of Ac-DIX 10 min. in $CDCl_3$.

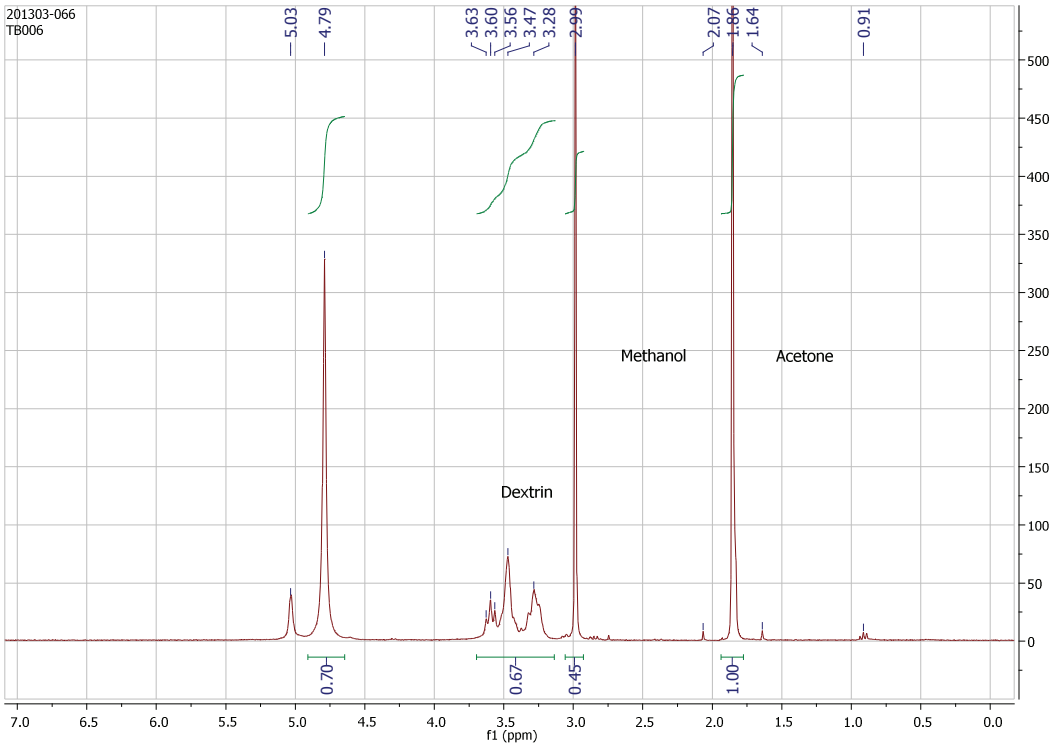

Figure 98: ^{1}H-NMR of Ac-DIX 10 min. in D_2O/DCl.

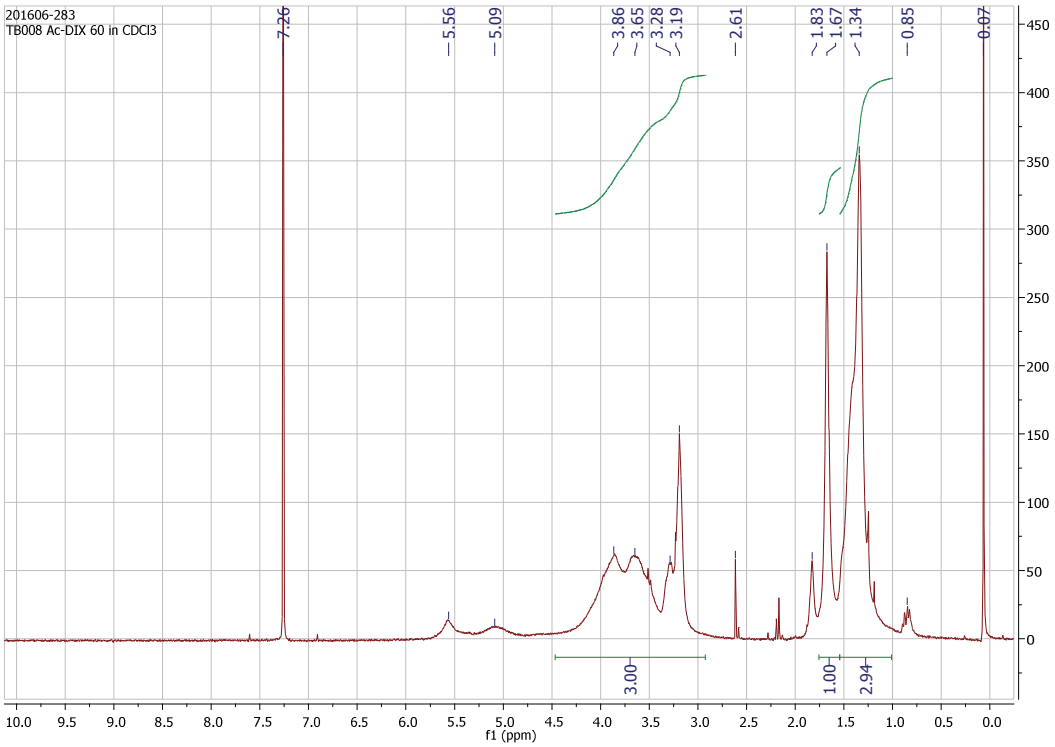

Figure 99: ^{1}H-NMR of Ac-DIX 60 min. in $CDCl_3$.

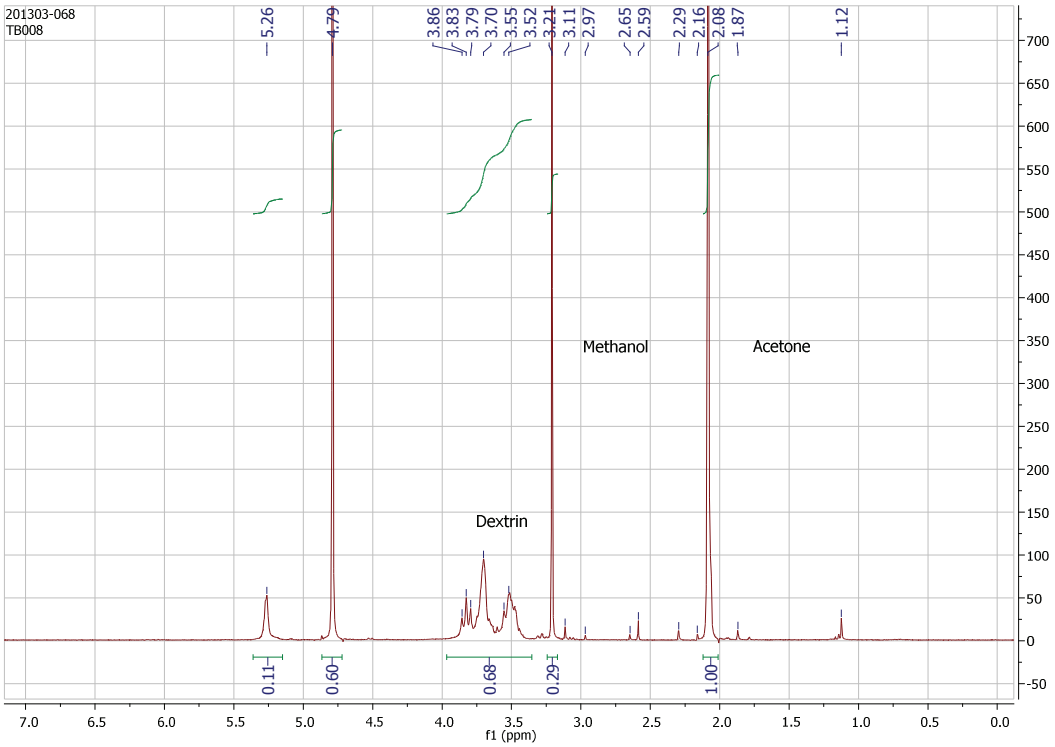

Figure 100: ^{1}H-NMR of Ac-DIX 60 min. in D_2O/DCl.

Partially Oxidized and Acetalated Polysaccharides

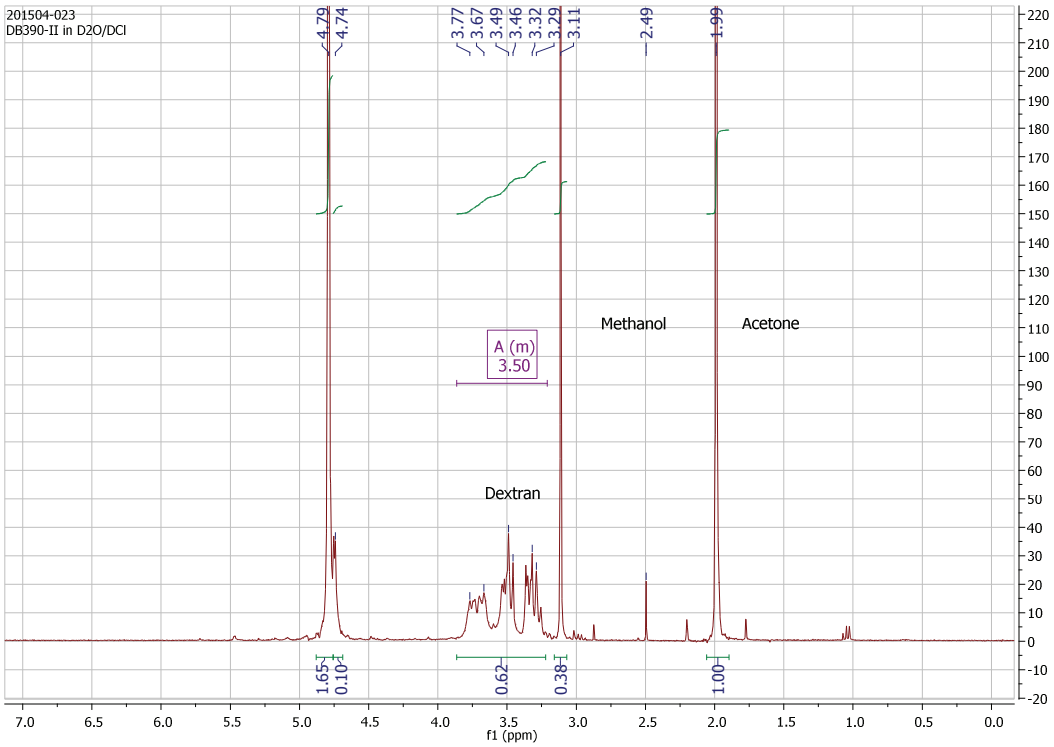

Figure 101: ^{1}H-NMR of Ac-ox-DEX in D_2O/DCl.

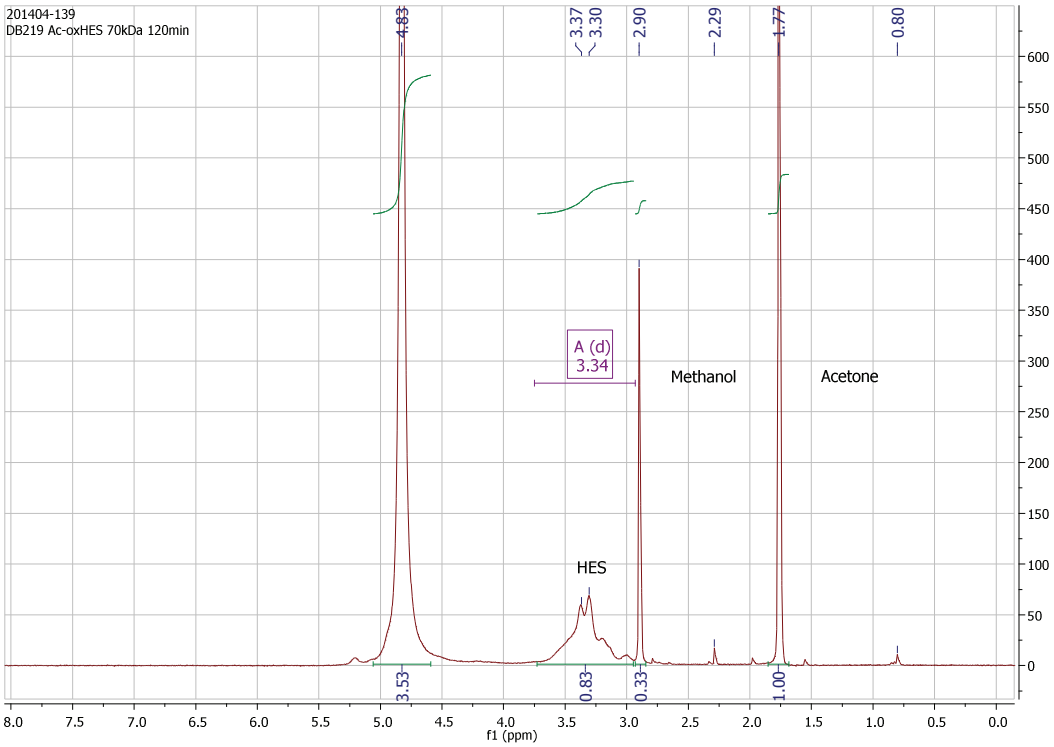

Figure 102: ^{1}H-NMR of Ac-ox-HES 70 kDa in D_2O/DCl.

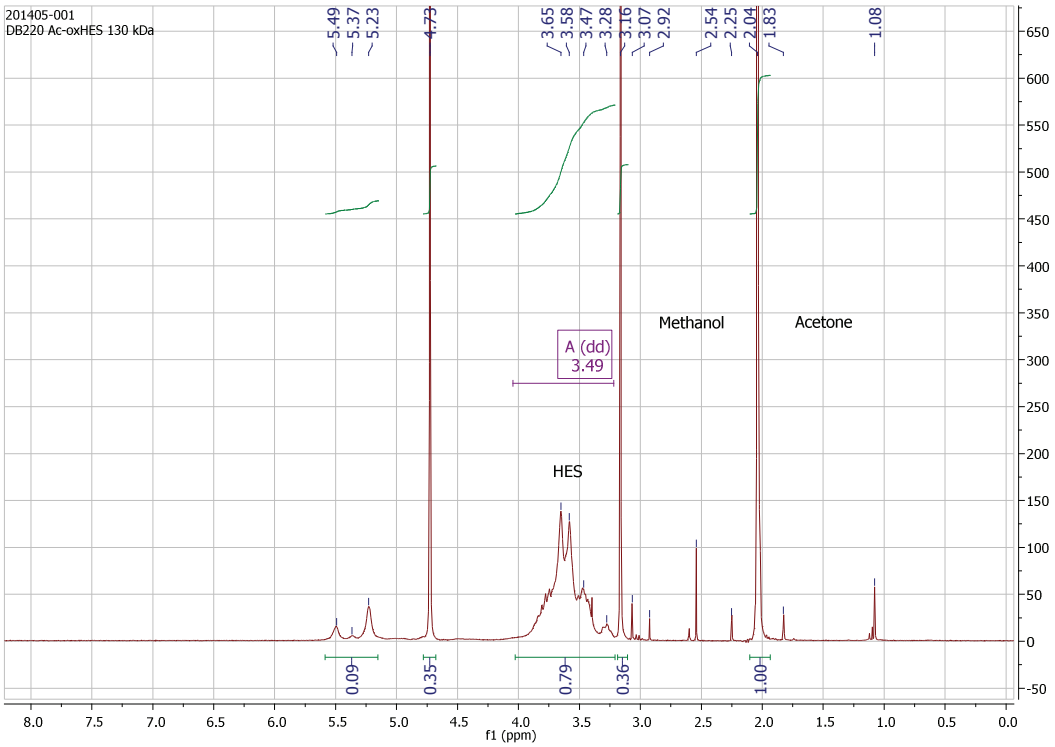

Figure 103: ^{1}H-NMR of Ac-ox-HES 130 kDa in D_2O/DCl.

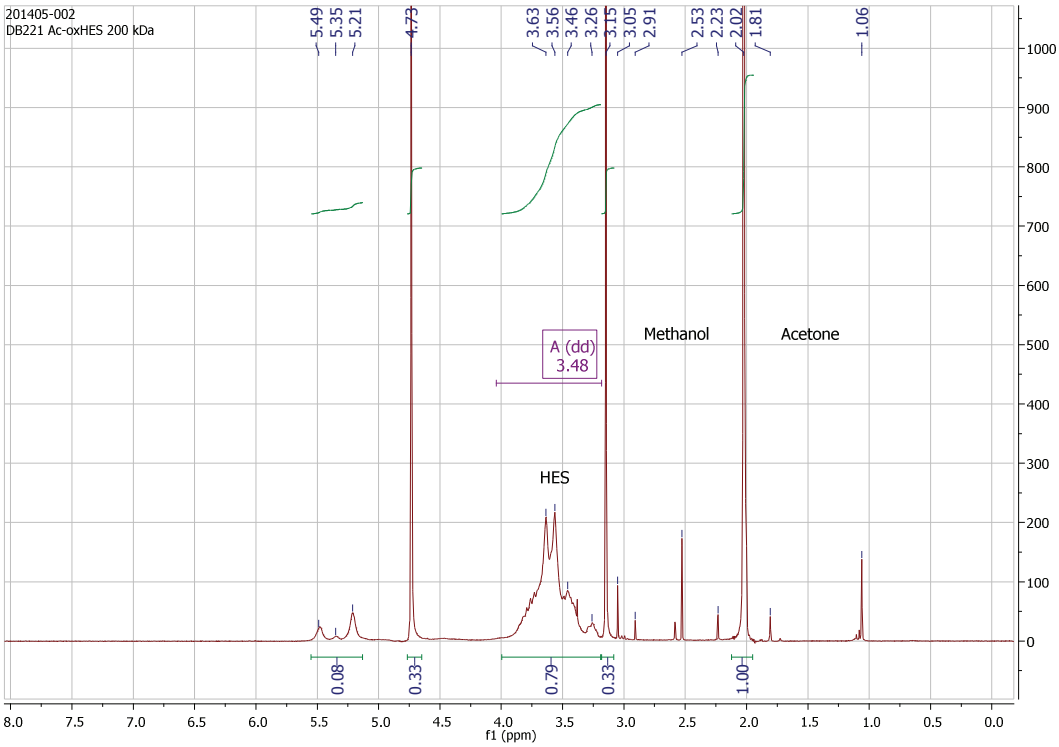

Figure 104: ^{1}H-NMR of Ac-ox-HES 200 kDa in D_2O/DCl.

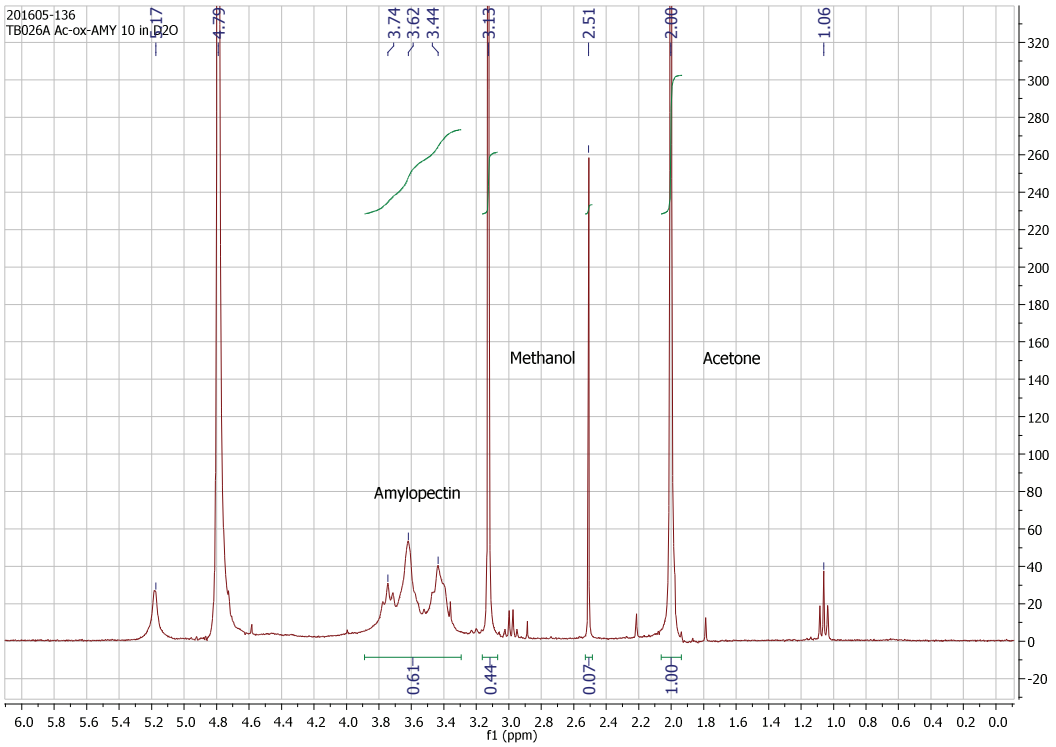

Figure 105: ^{1}H-NMR of Ac-ox-AMY 10 min. in D_2O/DCl.

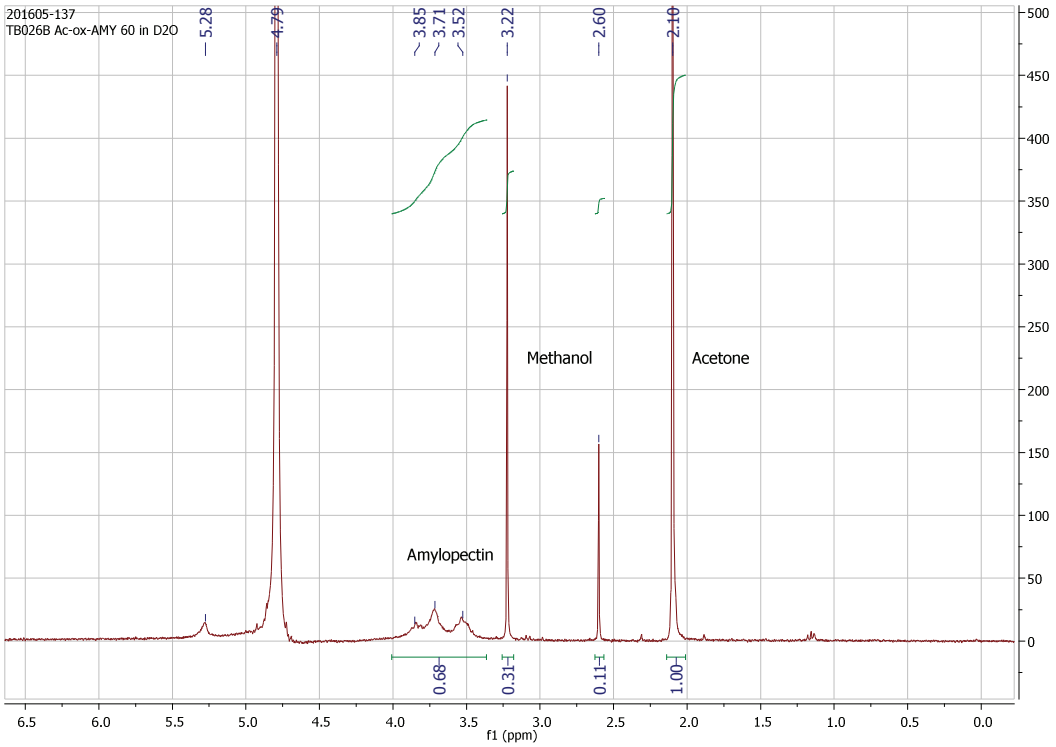

Figure 106: ^{1}H-NMR of Ac-ox-AMY 60 min. in D_2O/DCl.

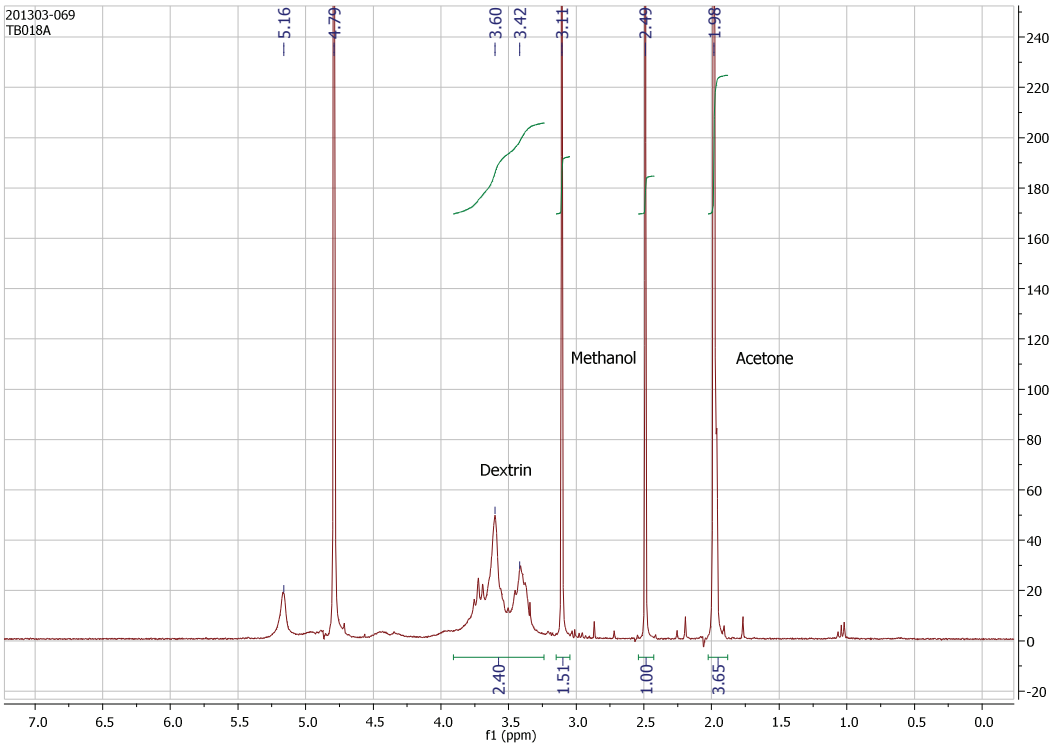

Figure 107: ^{1}H-NMR of Ac-ox-DIX 10 min. in D_2O/DCl.

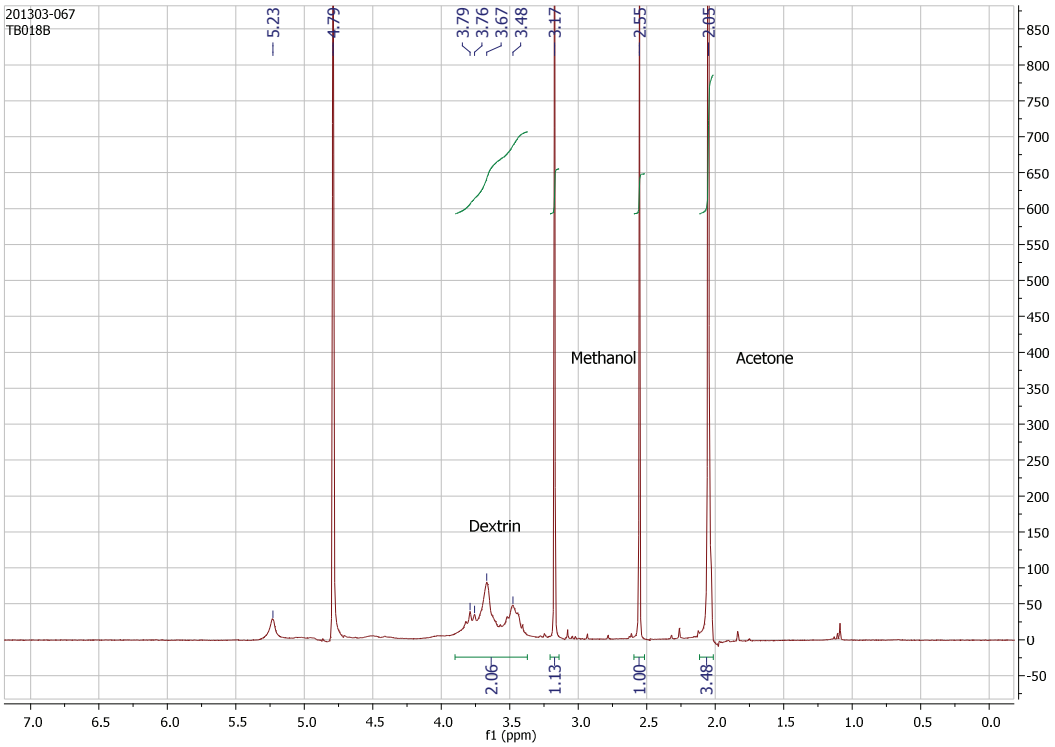

Figure 108: ^{1}H-NMR of Ac-ox-DIX 60 min. in D_2O/DCl.

Spermine-Functionalized Ac-Polysaccharides

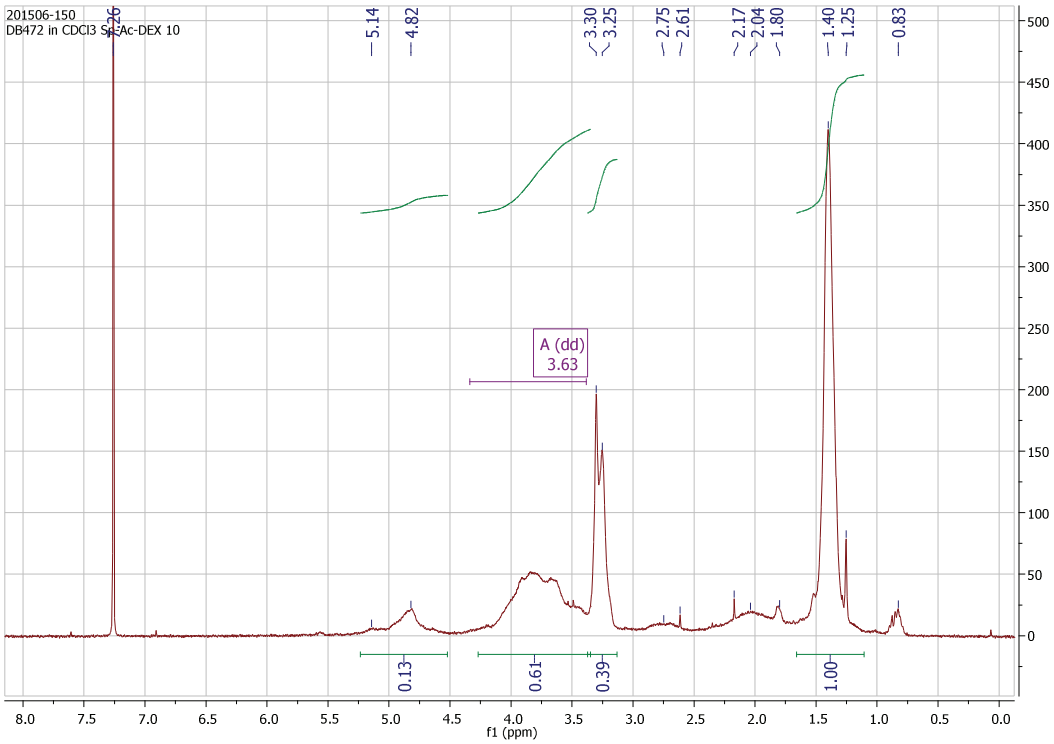

Figure 109: ^{1}H-NMR of Sp-Ac-DEX in $CDCl_3$.

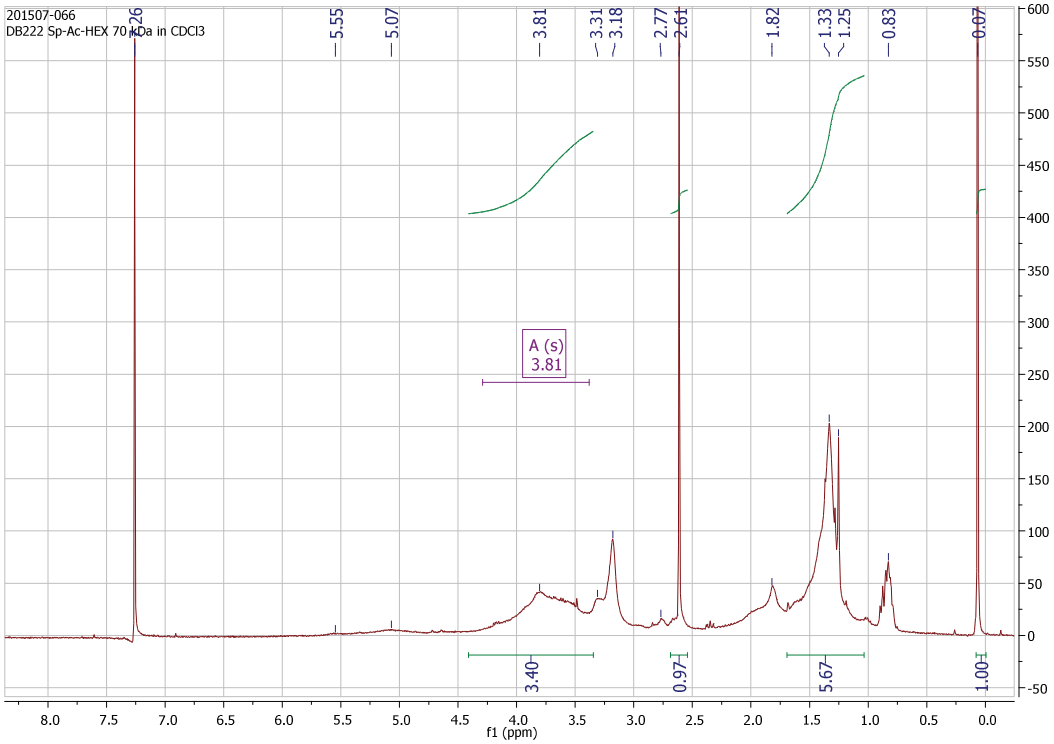

Figure 110: ^{1}H-NMR of Sp-Ac-HES 70 kDa in $CDCl_3$.

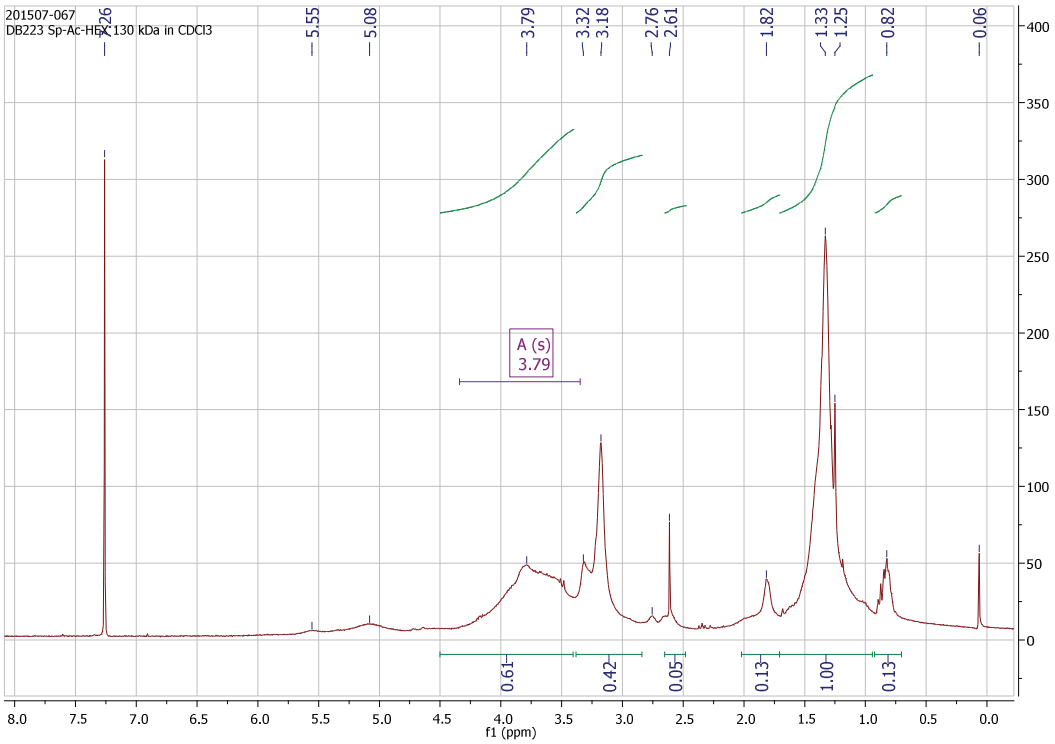

Figure 111: ^{1}H-NMR of Sp-Ac-HES 130 kDa in $CDCl_3$.

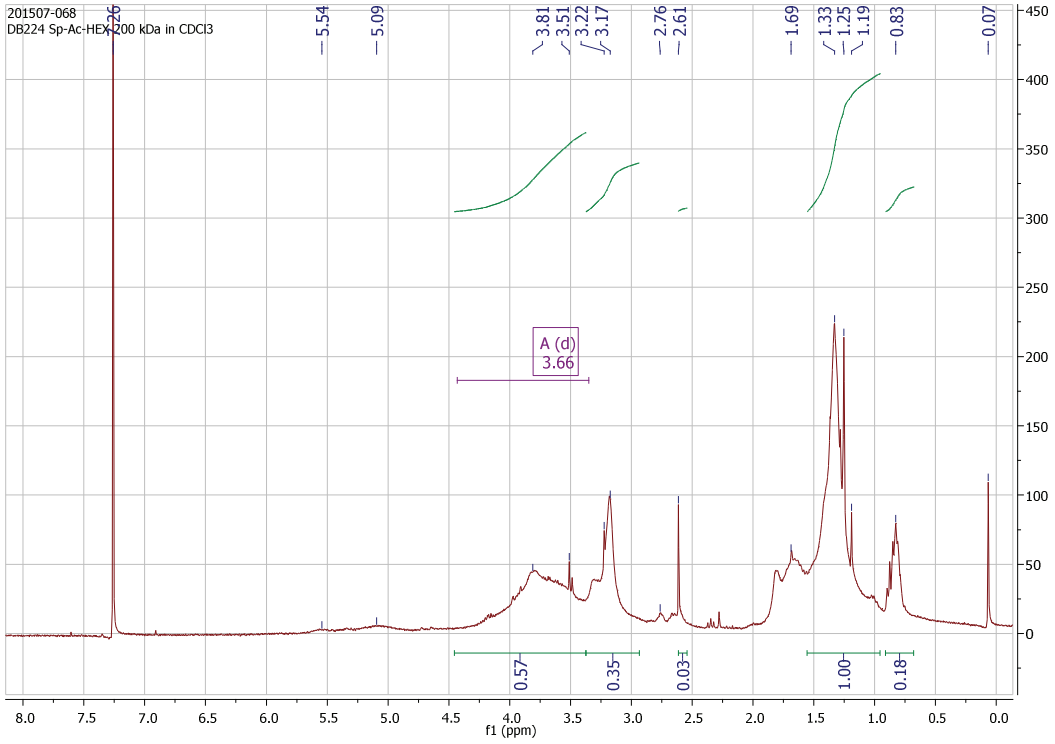

Figure 112: ^{1}H-NMR of Sp-Ac-HES 200 kDa in $CDCl_3$.

Other NMR Spectra

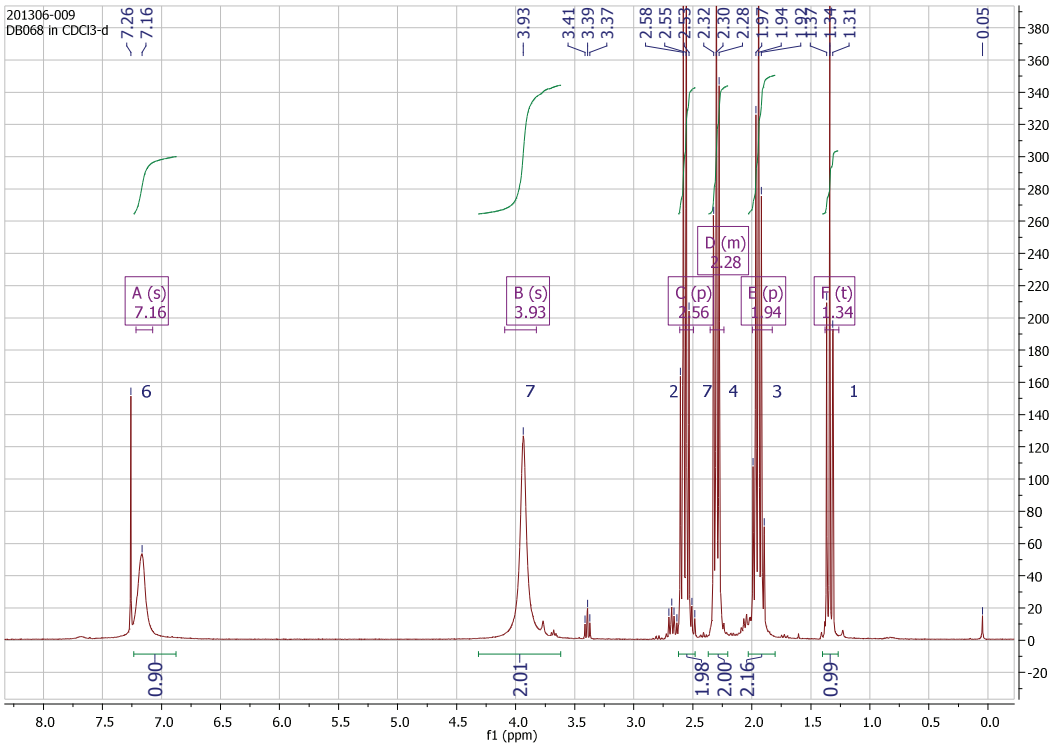

Figure 113: [1]H-NMR of 4-mercaptobutanehydrazide (thiol linker) in MeOH.

6.5.3 ESI-MS Spectra

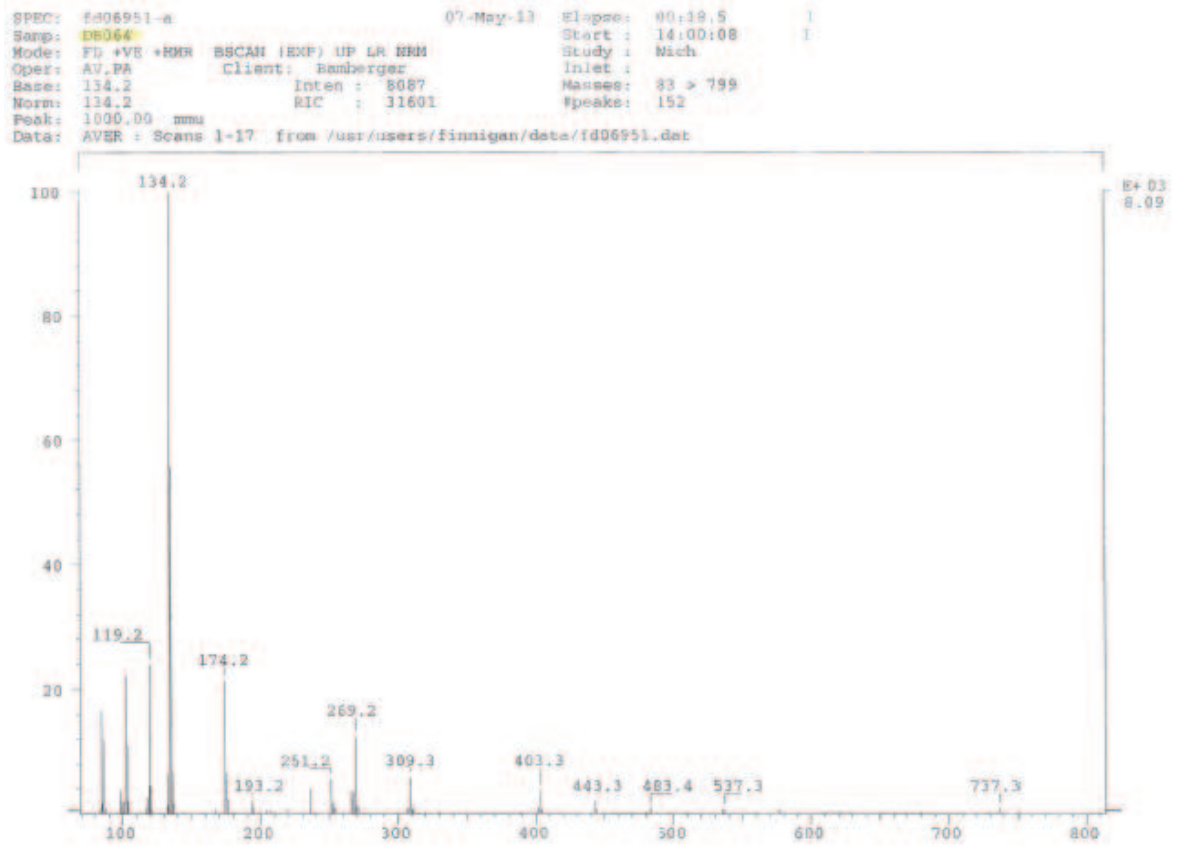

Figure 114: ESI-MS of 4-mercaptobutanehydrazide (thiol linker).

6.5.4 IR Spectra

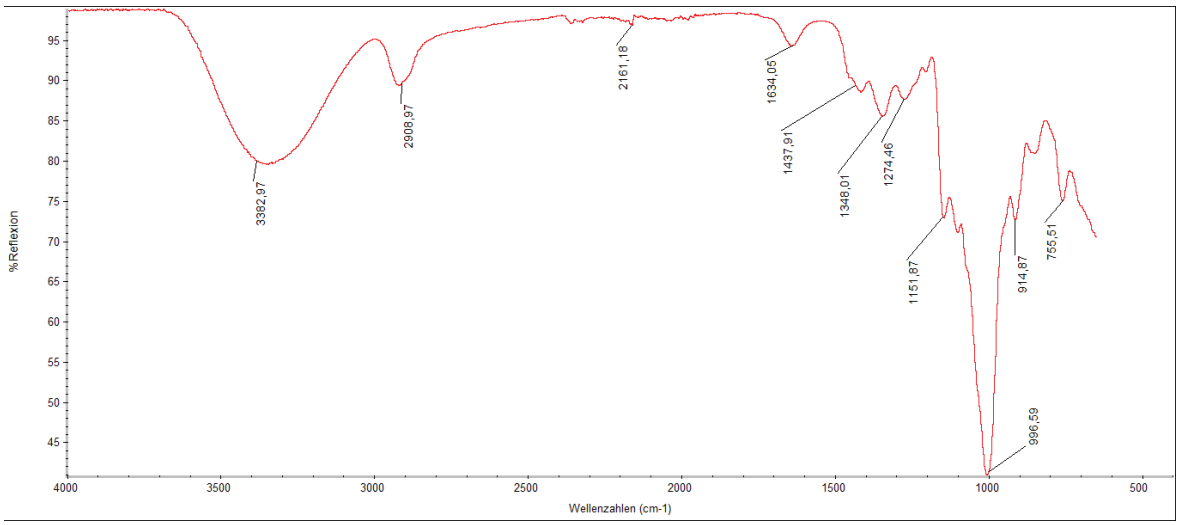

Figure 115: IR spectrum of partially oxidized dextran (ox-DEX).

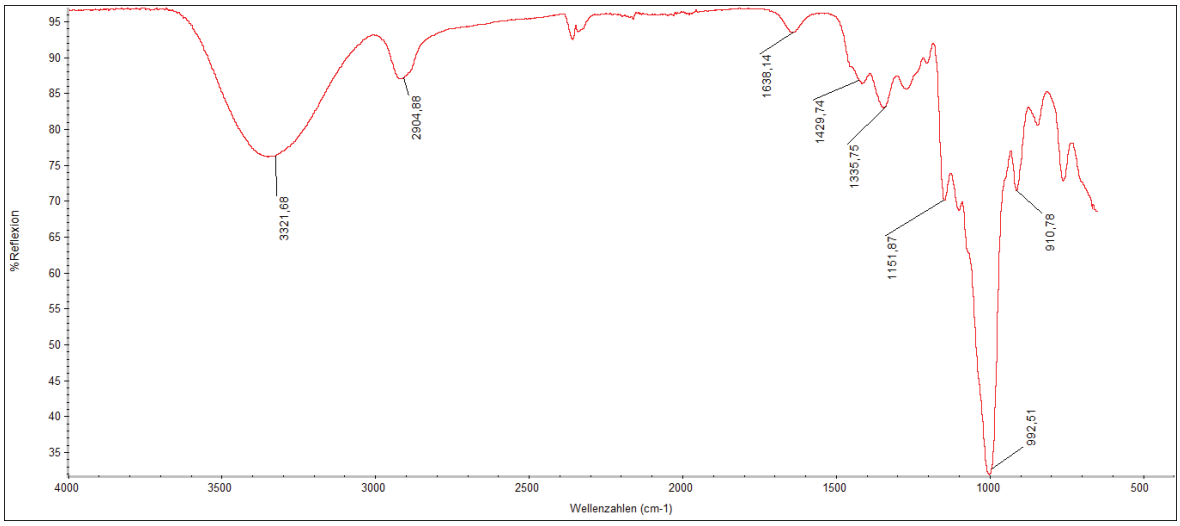

Figure 116: IR spectrum of dextran 10 kDa.

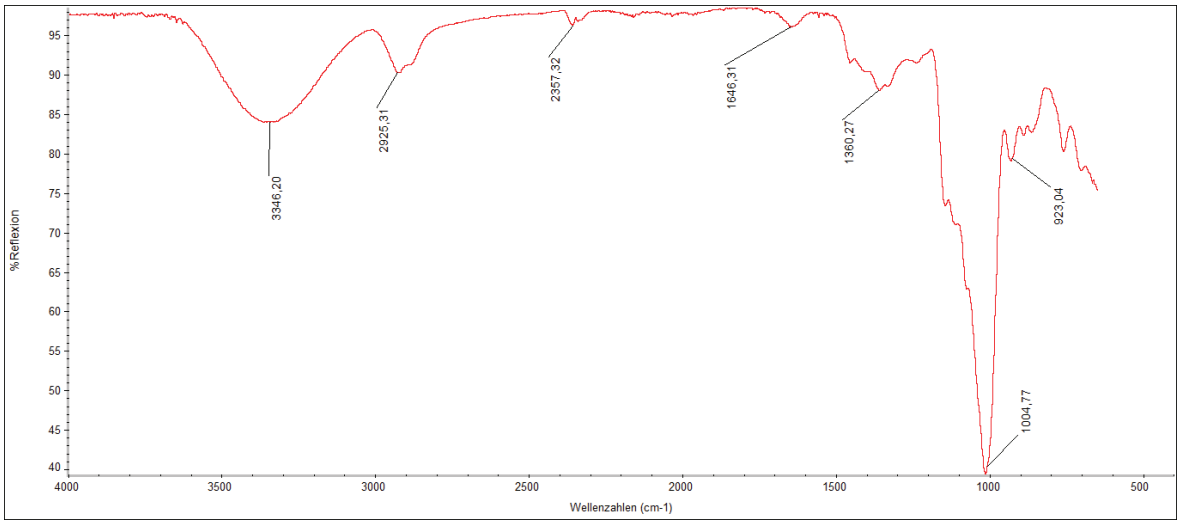

Figure 117: IR spectrum of partially oxidized HES 70 kDa (ox-HES).

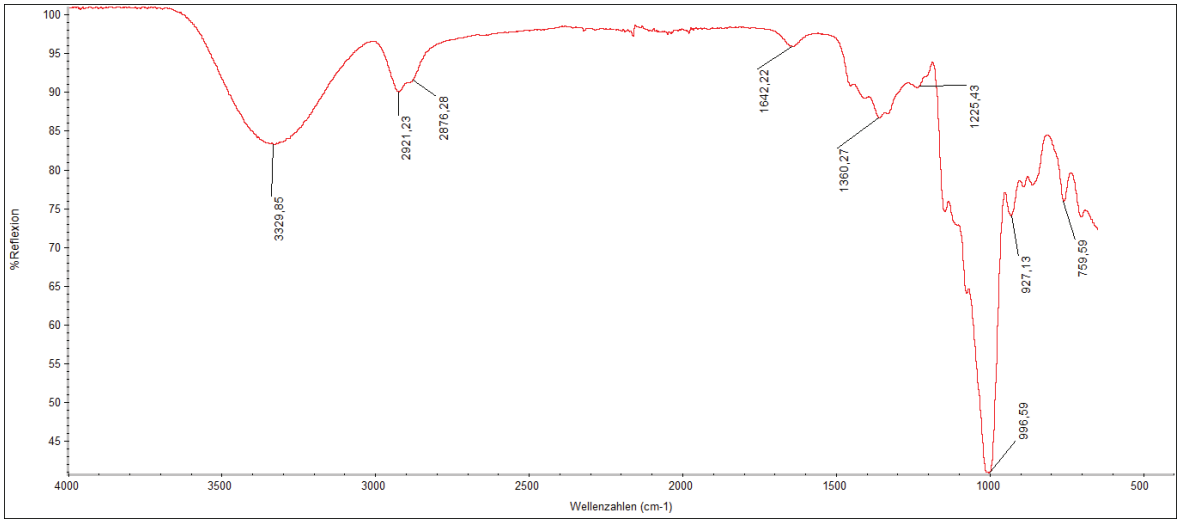

Figure 118: IR spectrum of HES 70 kDa.

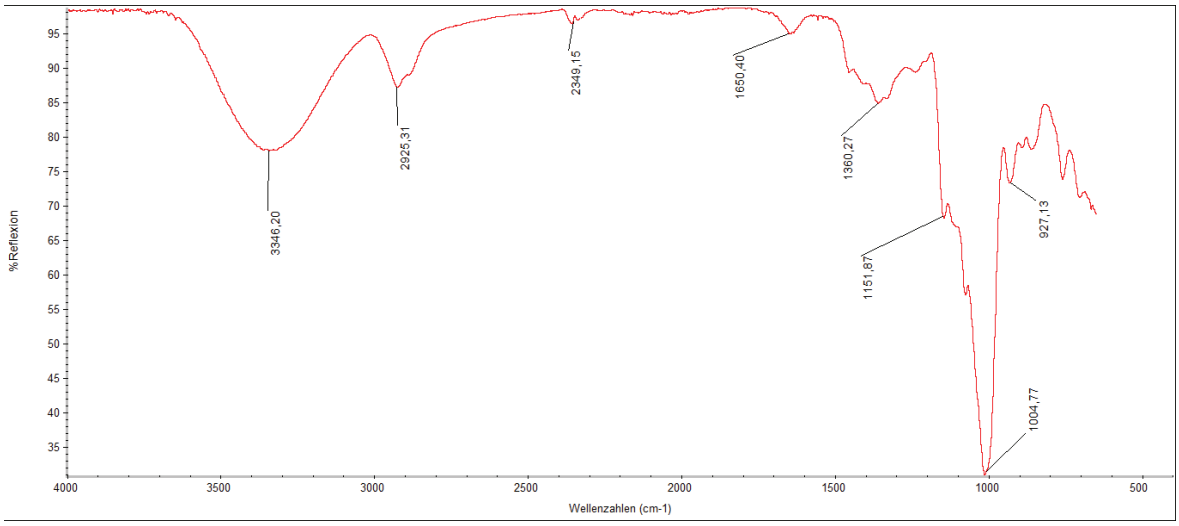

Figure 119: IR spectrum of partially oxidized HES 130 kDa (ox-HES).

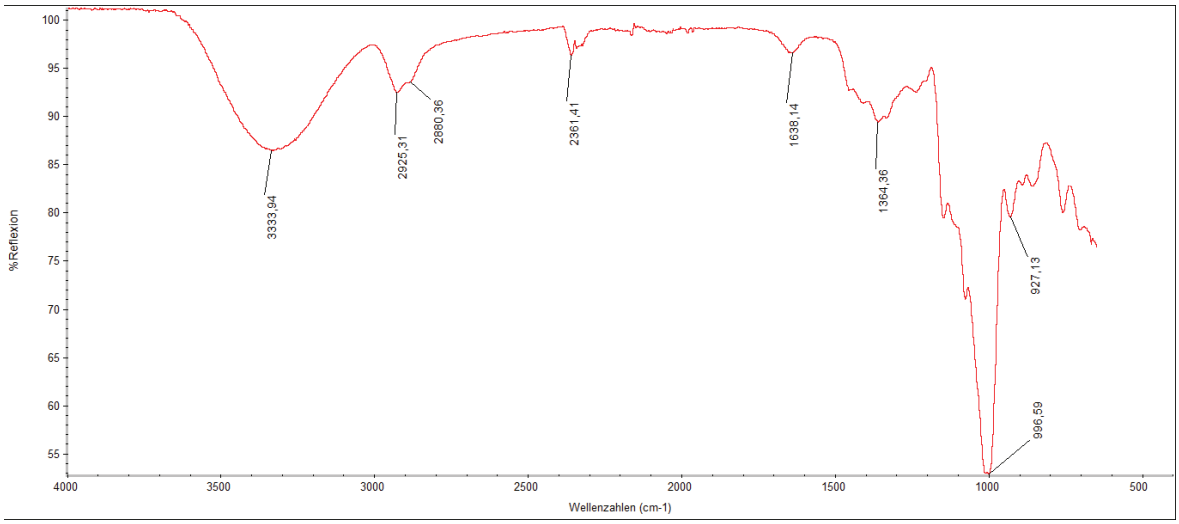

Figure 120: IR spectrum of HES 130 kDa.

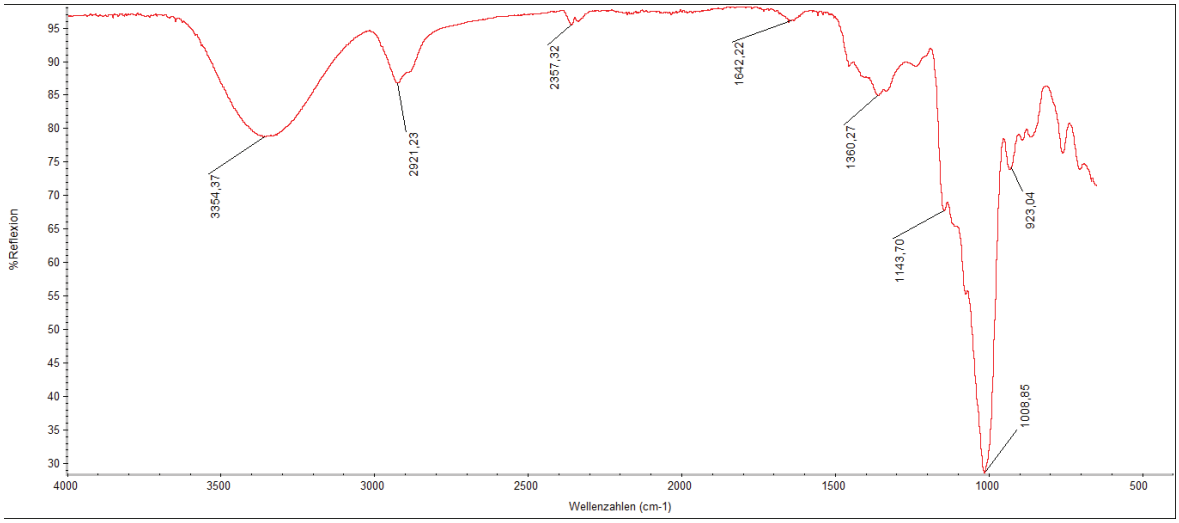

Figure 121: IR spectrum of partially oxidized HES 200 kDa (ox-HES).

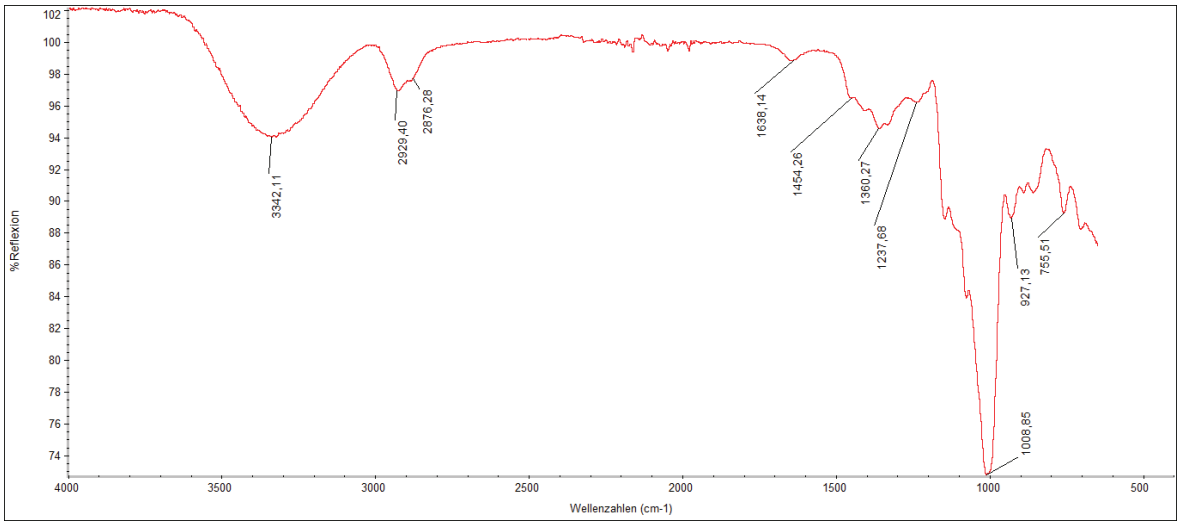

Figure 122: IR spectrum of HES 200 kDa.

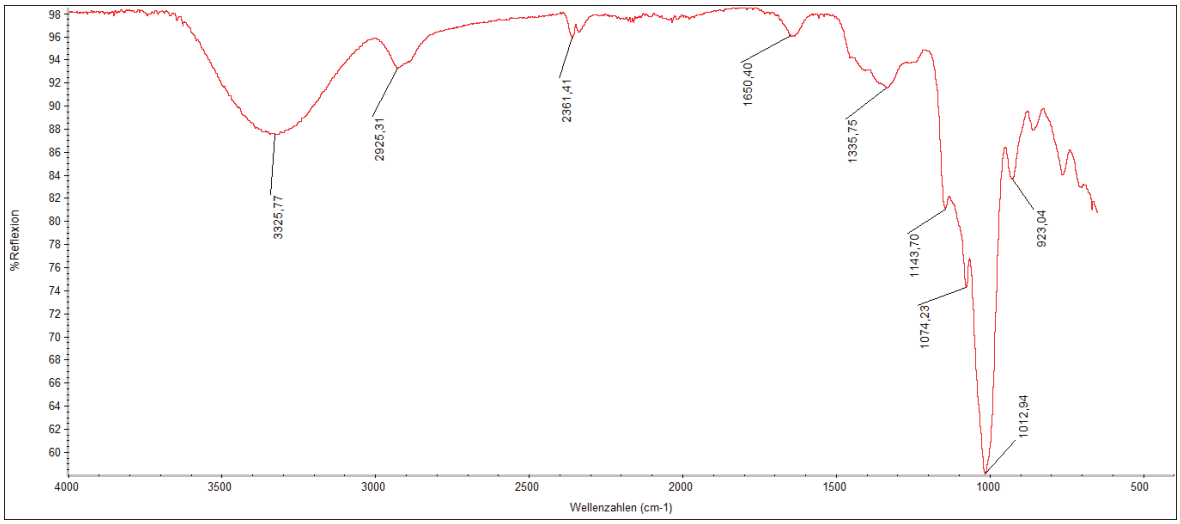

Figure 123: IR spectrum of partially oxidized amylopectin (ox-AMY).

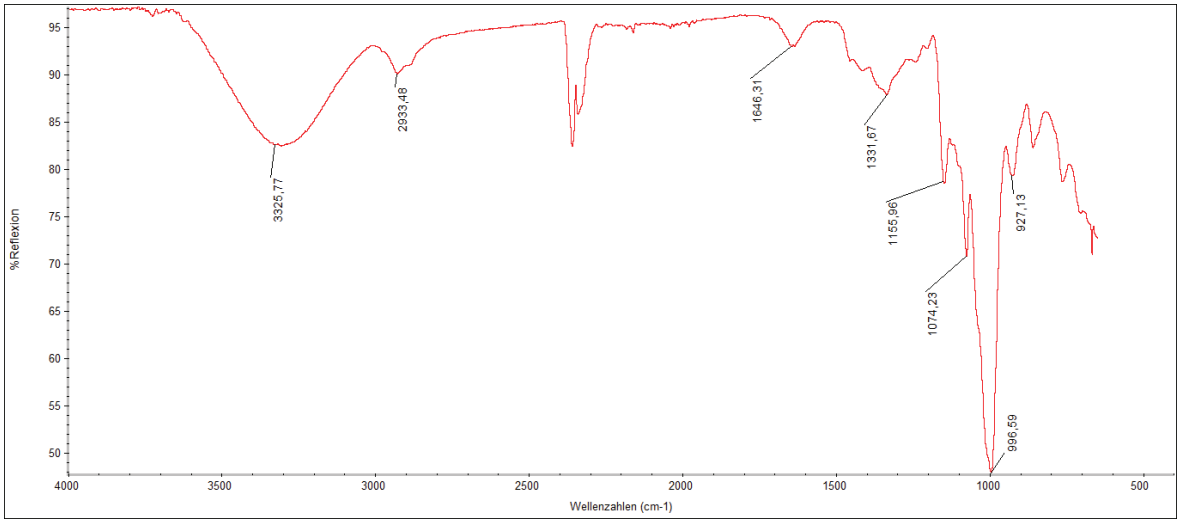

Figure 124: IR spectrum of amylopectin.

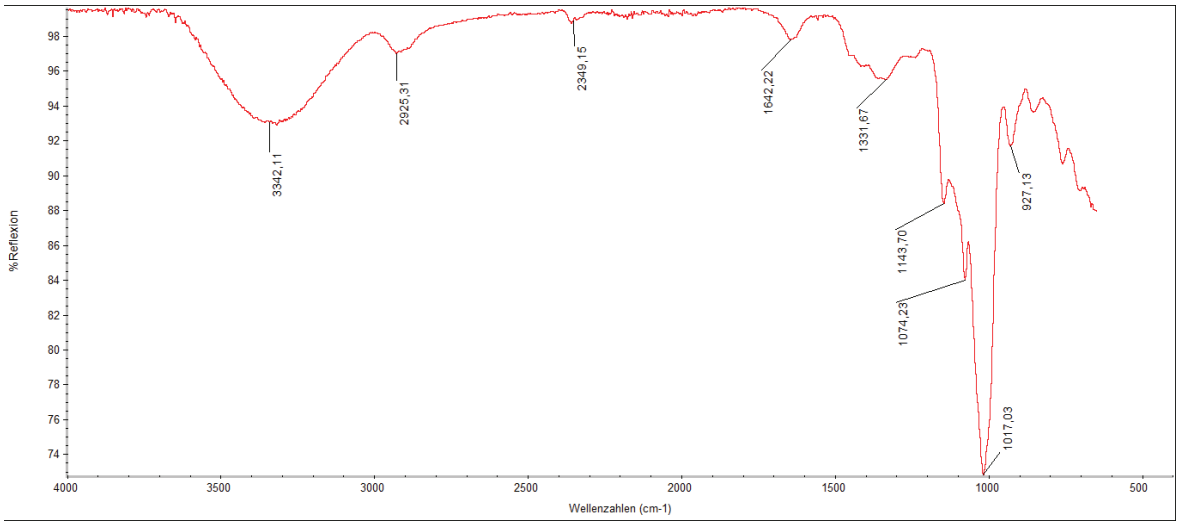

Figure 125: IR spectrum of partially oxidized dextrin (ox-DIX).

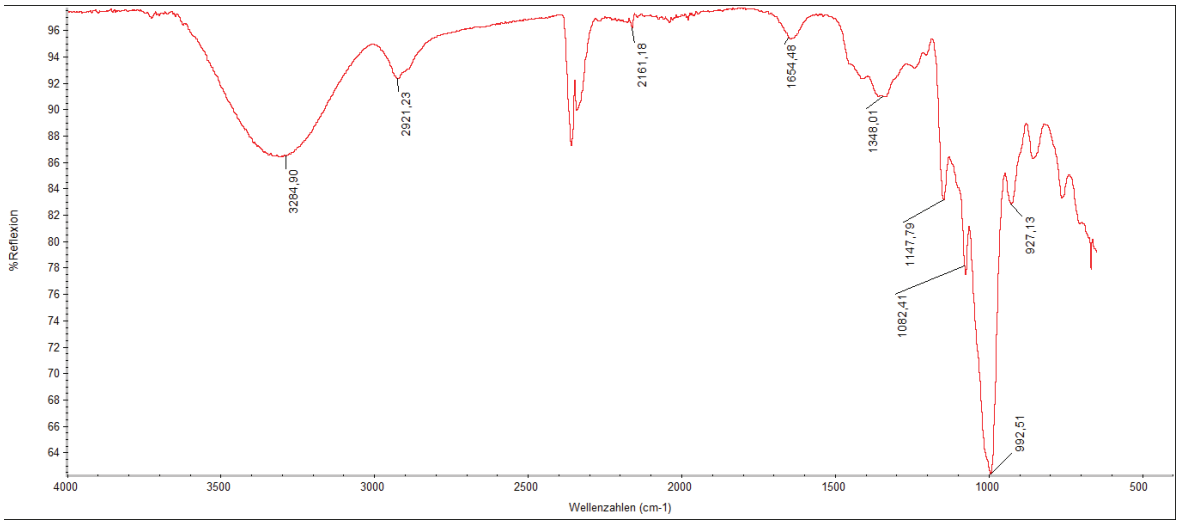

Figure 126: IR spectrum of dextrin.

6.5.5 Graphs of Standard Curves

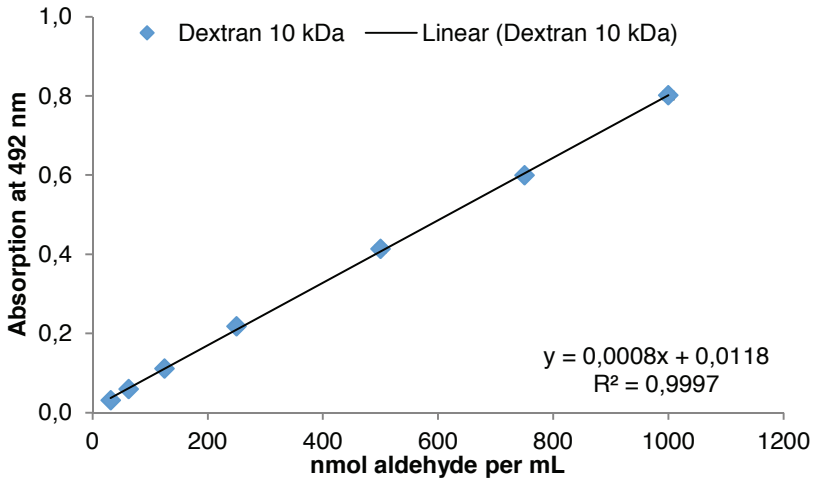

Figure 127: Standard curve of dextran 10 kDa for the PCA assay.

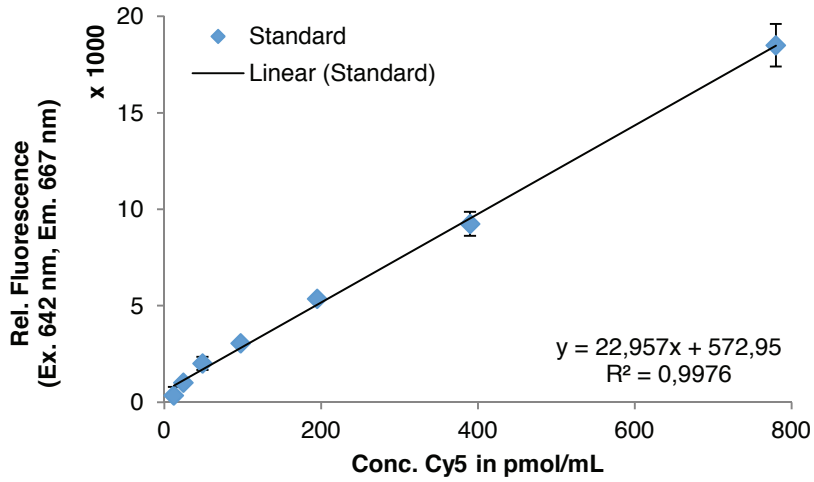

Figure 128: Standard curve of sulfo-Cy5-NHS for the determination of conjugated fluorescent dye to the particle surface.

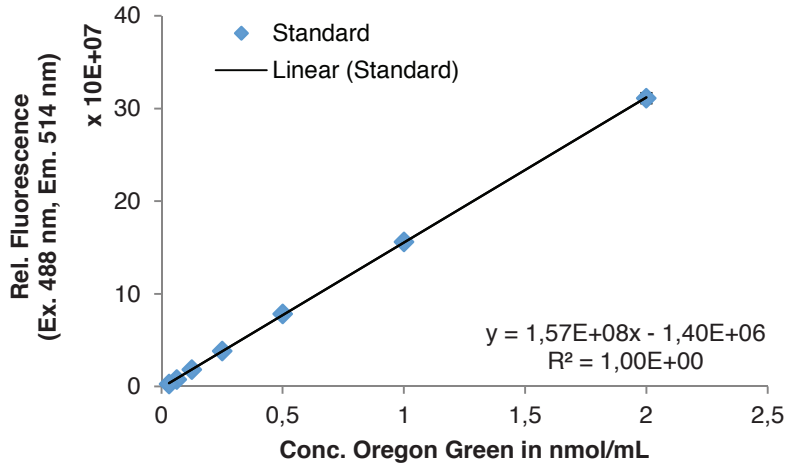

Figure 129: Standard curve of Oregon Green® 488-NHS for the determination of conjugated fluorescent dye to the particle surface.

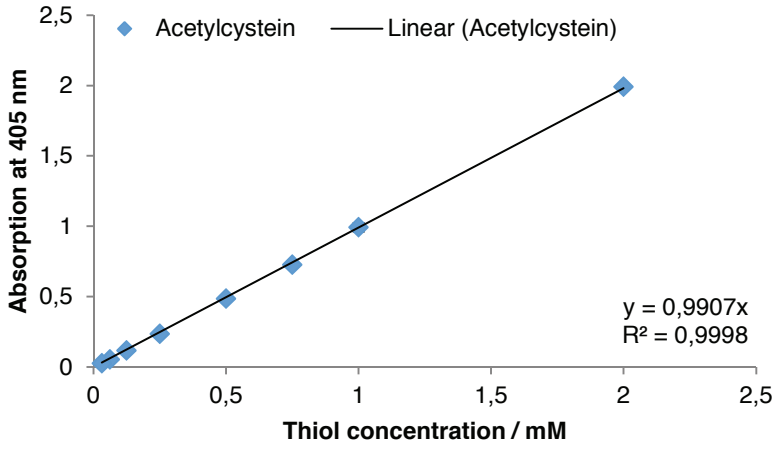

Figure 130: Standard curve of *N*-acetyl-*L*-cysteine for Ellman's assay.

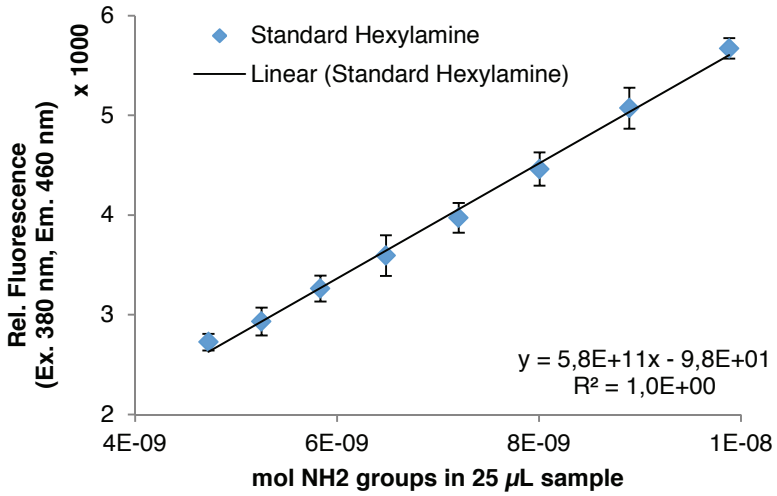

Figure 131: Standard curve of hexylamine for fluorescamine assay.

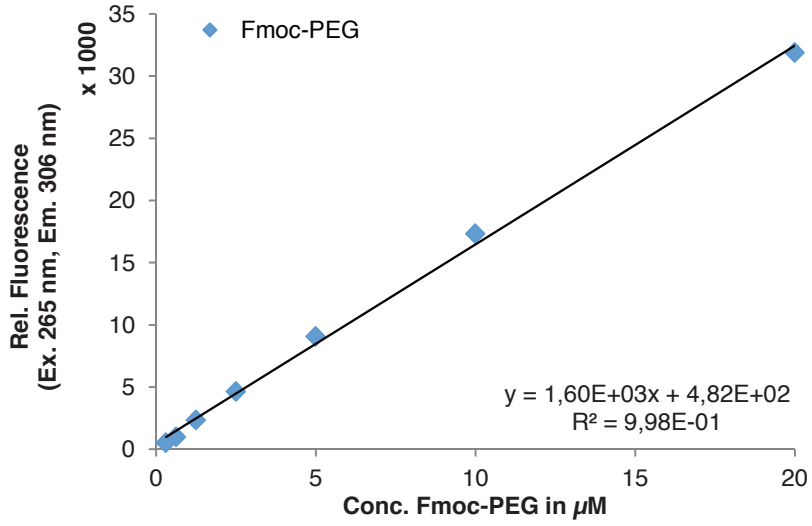

Figure 132: Standard curve of Fmoc-PEG-NHS for the determination of conjugated PEG to the particle surface.

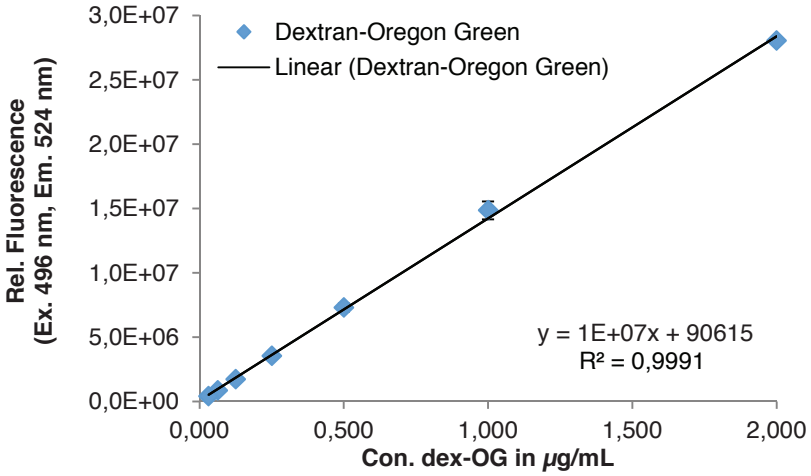

Figure 133: Standard curve of dextran-Oregon Green® 488 for the determination of the encapsulation efficiency of dex-OG488 in the particles.

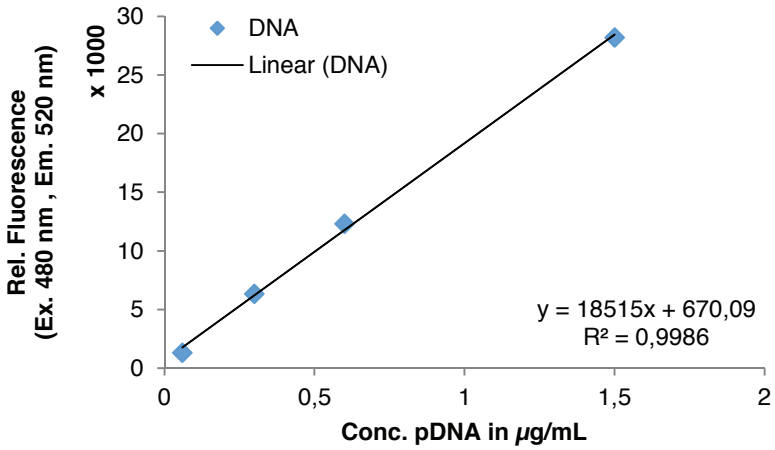

Figure 134: Standard curve of pDNA for the determination of encapsulated DNA in nanoparticles with the Pico Green® assay.

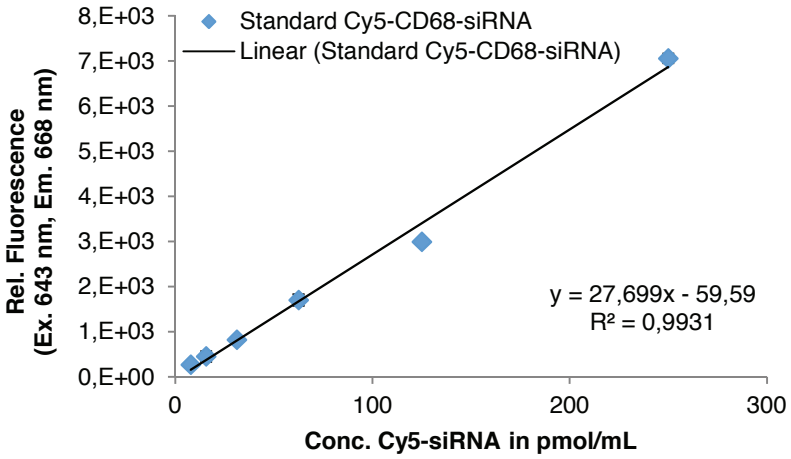

Figure 135: Standard curve of Cy5-siRNA for the determination of encapsulated siRNA in nanoparticles by fluorescence measurement.

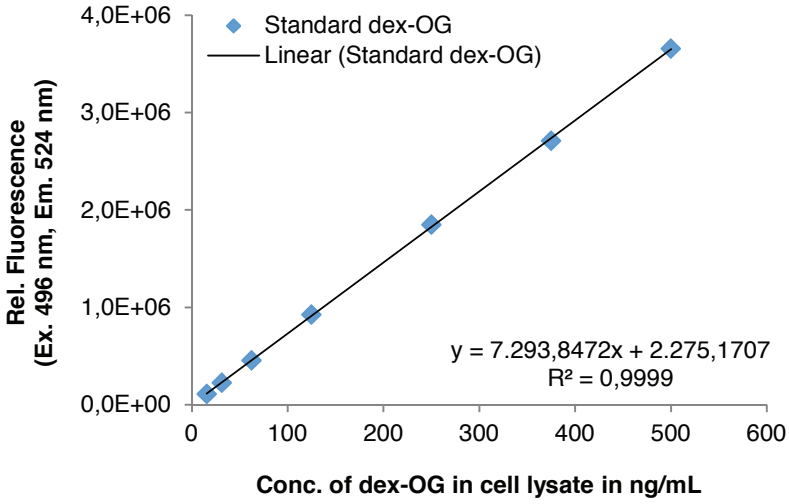

Figure 136: Standard curve of dextran-Oregon Green® 488 in cell lysate for the determination of nanoparticles taken up by HeLa cells.

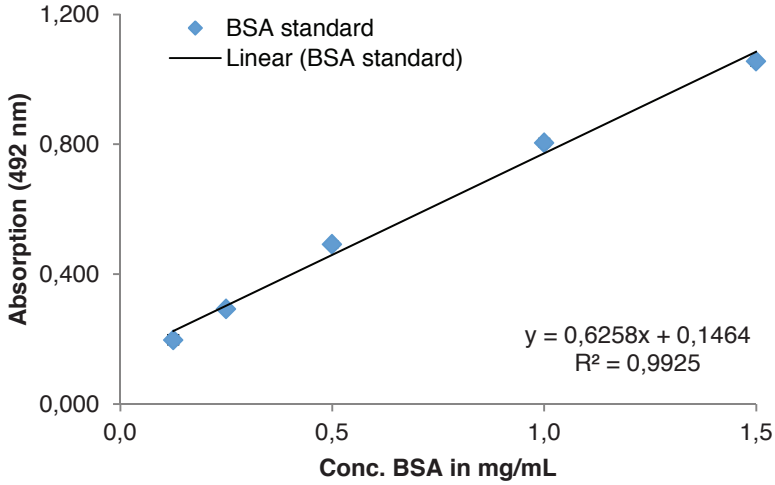

Figure 137: Standard curve of BSA in cell lysate for the determination of HeLa cells per well by PCA assay.

CURRICULUM VITAE

PERSONAL DATA

Name:	Denise Nadine Bamberger
Birth date and place:	[redacted]
Nationality:	German
Contact:	[redacted]
E-Mail:	[redacted]

EDUCATION

[redacted]

PHD STUDIES

07/2012–08/2016	PhD thesis in pharmaceutical chemistry at the Institute for Pharmacy and Biochemistry, Johannes Gutenberg-Universität Mainz, Germany [redacted]
10/2015–04/2016	Research stay at the UT Southwestern Medical Center, Cancer Center, Dallas, Texas, USA [redacted]

WORK EXPERIENCE

[redacted]

Conferences and Meetings

09/2013	GDCh-Wissenschaftsforum Chemie 2013, Darmstadt, Germany Poster presentation
08/2014	Gordon Research Seminar and Conference, Drug Carriers in Medicine and Biology, Waterville Valley, New Hampshire, USA Talk and poster presentation
09/2014	Summer School SFB 1066, Stromberg, Germany Talk and poster presentation
07/2015	Summer School SFB 1066, Nomborn, Germany
04/2016	PBP World Meeting, Glasgow, United Kingdom Poster presentation

Awards and Grants

09/2013–08/2015	PhD scholarship from the Stipendienstiftung Rheinland-Pfalz, Germany
07/2014	Travel award from the Akademie der Wissenschaften, Mainz, Germany
07/2014	Travel award from DAAD, Germany
08/2014	Invitation for a young investigator talk at GRC and travel grant
10/2015	Research grant from the Klaus Tschira Stiftung, Germany